INTRODUCTION

1.Transient Receptor Potential (TRP) channels

The transient receptor potential (TRP) superfamily consists of more than 30 cation channels which are largely non-selective channels permeable to both monovalent and bivalent cations, including potassium (K^+), sodium (Na^+), magnesium (Mg^{2+}), and calcium (Ca^{2+}). Their primary function is to contribute to changes in intracellular Ca^{2+} concentration by providing Ca^{2+} entry channels, adjusting the driving force for Ca^{2+} entry, and also supplying intracellular pathways for Ca^{2+} release from organelles. Cell membrane depolarization, muscular contraction, transmitter release, cell proliferation, gene transcription, and cell death are all influenced by cytosolic Ca^{2+} concentration changes [1]. TRP channels are widely expressed in a variety of tissues and cell types, both excitable and non-excitable, and are activated by a variety of triggers such as intracellular and extracellular messengers, chemical, mechanical, visual, and thermal stimuli, oxidative and osmotic stress, and possibly some by the filling state of the channel.

1.1 History

TRP channels are evolutionarily conserved integral membrane proteins from nematodes to humans [2]. In 1969, the first *Trp* gene was discovered by Cosens and Manning in a spontaneous mutant with defective vision of *Drosophila melanogaster*. They located this mutation on the third chromosome of *Drosophila* genome and they further found that the mutant flies behave as though were blind under bright illumination [3] [4].

Based on the mutant's electrophysiological characteristics, Minke et al. were the first to refer to it as a "transient receptor potential" (trp) in 1975 [5]. Despite the absence of clues about its biological function the analysis of the inferred amino acid sequence revealed that *Trp* gene encoded a cation channel [6].

The *Trp* gene was successfully cloned in 1989 by Montell et al. and Wong et al., who identified it as a transmembrane protein. The connection between *Trp* mutants and Ca^{2+} was established by Minke's group by demonstrating that trp protein is a plasma membrane component that oscillates between Ca^{2+}-transporting and non-transporting states [7] [8]. The theory that TRP was a Ca^{2+} channel was consolidated by the *in vivo* analysis of a TRP isoform with a specific acidic residue (Asp621) mutation in the pore [9].

After the 1990s, TRPs were described in a large number of cell types [10] [11] and TRP channels became a field in 1995 with the discovery of human TRP proteins [12]. The field augmented with the discovery of "thermoTRPs" and the realization that TRPs are global sensors of sensory input [13].

1.2 Classification and structure of TRP channels

TRPs are classified into seven subfamilies based on amino acid sequence homology: TRPC (Canonical), TRPV (Vanilloid), TRPM (Melastatin), TRPA (Ankyrin), TRPML (Mucolipin), TRPN (no mechanoreceptor potential or NOMPC-like) and TRPP (Polycystic) [13] . The seven TRP subfamilies are broadly divided into groups 1 and 2. The group number 1 of TRPs consists of five subfamilies: TRPC, TRPM, TRPV, TRPA, and TRPN, which have the highest sequence homology to the founding member of the superfamily, the *Drosophila* TRP. The two subfamilies TRPP and TRPML are distantly related to the group 1 TRPs and represent the group 2 TRPs (**Figure 1**). In yeast, the eighth TRP family has been recently discovered and denominated as TRPY [14] [15] .

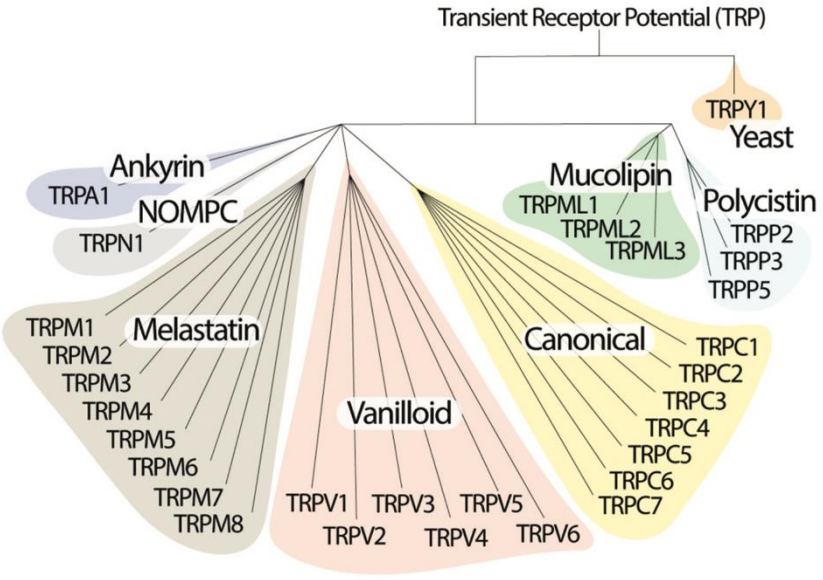

Figure 1. Phylogenetic tree of the eukaryote TRP ion channels superfamily [16].

All TRPs are permeable to Ca^{2+} with the exceptions of TRPM4 and TRPM5, which are only permeable to monovalent cations. Most Ca^{2+}-permeable TRP channels are poorly selective for Ca^{2+}, with permeability ratio relative to Na^{+} (PCa/PNa) in the range between 0.3 and 10. As opposite, TRPV5 and TRPV6 are two highly Ca^{2+}-selective TRP channels with PCa/PNa > 100. Most TRPs are expressed in the plasma membrane, where they

control ion influx. Nevertheless, some TRPs have been reported to function as intracellular Ca^{2+} release channels and they have been named as "plasmalemmal" TRP channels (e.g., TRPV1 and TRPM8). Also their localization on intracellular membranes has been described [17]. Their structure is similar to other ion channels [18]: a six-transmembrane helix domains (S1 through S6) with a reentrant loop between S5 and S6 forming the pore region and with the C-terminus and N-terminus regions located in the intracellular portion [19]. This transmembrane *core* is composed as follows: a voltage sensor–like domain comprising the first four segments (S1–S4; VSLD) and a pore domain formed by the last two segments (S5 and S6) which form the lower gate that regulates cation entry into the channel by opening and closing. The S4-S5 linker, a short amphipathic helix that runs almost parallel to the inner membrane connect these two modules [20]. A 25-amino acid motif, named TRP domain, in the sixth segment of the C-terminus, is poorly conserved among TRPs except for TRPA1, TRPMLs and TRPPs [21].The TRP box, a sequence of 6-amino acids within the TRP domain is highly conserved among TRPCs (EWKFAR), but less conserved in TRPMs and TRPVs. The TRP domain forms an α-helical structure able to interact with the N-terminus and the membrane that may be involved in channel gating. The N-terminus possesses variable number of ankyrin repeats (33-residue motifs consisting of two antiparallel α-helices connected by β-hairpin motifs) which distinguish the different TRP subfamilies: 14 to 15 in TRPA, around 29 in TRPN, 6 in TRPV and 3 to 4 in TRPC. Ankyrin repeats which normally act as a scaffold for protein-protein interactions may contribute to the regulation of TRP channels and to subunit assembly in tetramers and also to the interaction with ligands and protein partners [22] [23, 24] [25, 26].

TRPs may contain other specific domains and motifs: including coiled coils and lipid-interaction domains, calmodulin-binding sites, calcium-binding EF-hand-like and helix-loop-helix motifs that can bind calcium ions, C-terminal PDZ-binding domains (TRPC4/C5), serine/threonine kinases (TRPM6/M7), and a Nudix hydrolase domain (TRPM2) or phosphorylation sites which control channel functions [27]. (**Figure 2**)

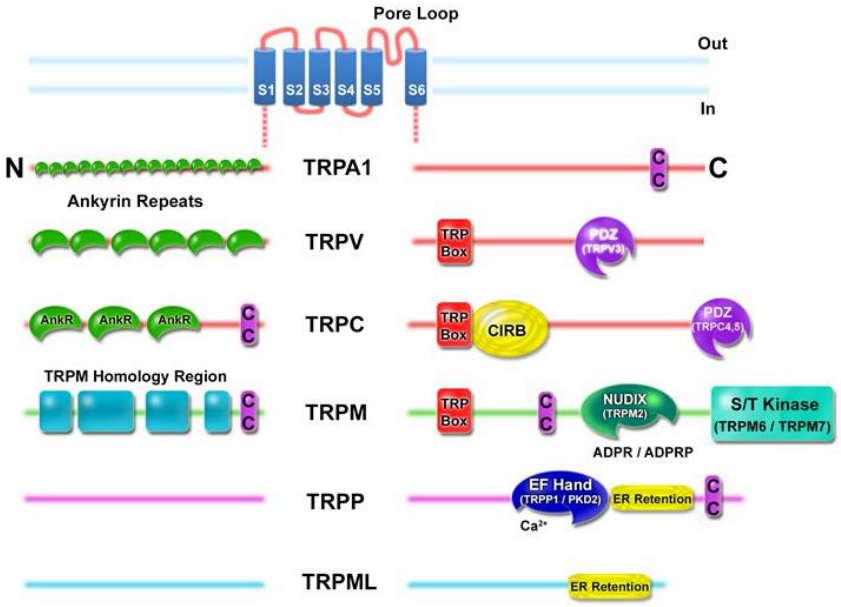

Figure 2. Schematic representation of TRP channels domains.
https://www.guidetopharmacology.org/GRAC/FamilyIntroductionForward?familyId=78

It has been described that four subunits (with 6 transmembrane domains each) can assemble in homo- and/or hetero- tetramers, to form the functional channel, where each subunit contribute to assemble a shared selectivity filter and ion-conducting pore [28]. Members of the same or different subfamilies have been discovered to form heteromultimeric channels, thus suggesting the existence of a wide spectrum of channels with different functions [29].

1.3 Function and activation of TRP channels

TRP channels are widely expressed in many tissues (nearly all cells tested express at least one member of the superfamily) and they are necessary for all senses in animals contributing to a plethora of physiological functions. These include the senses of sight, smell, taste, hearing, and a variety of touches, including the capability to detect temperature changes [6]. These features highlight TRPs' extraordinary diversity of physiological roles, as well as their classification as polymodal sensors. TRP channels are extremely diverse, with low sequence homology, despite their general membrane structure and cation permeability. Nevertheless, they can be activated by exogenous chemical substances, lipids, oxidative stress, acids, pheromones, osmolarity, mechanical stimulation, light, temperature, and others. TRPs contribute to several physiological processes, including homeostatic functions (including renal, bone, muscle function), biological processes within the cardiovascular, endocrine, immune, and central nervous

system and pure sensory functions (chemo-, thermo- or mechano- sensation). Their function is not limited to play key roles in the responses to various classes of external stimuli (sound, light, temperature, chemicals, and touch) but they also confer to cells the ability to sense local environmental changes. Despite the heterogeneity among TRP channels, three main general modes of activation have been identified: a) direct activation by ligands, which encompass exogenous small organic molecules, including synthetic compounds and natural products, such as capsaicin, icilin, allyl isothiocyanate (AITC) and endogenous lipids or products of lipid metabolism (diacylglycerol (DAG), phosphoinositides, eicosanoids, endocannabinoids, oxidative stress byproducts, and others) b) direct activation due to changes in environmental temperature (such as for vanilloid receptors) and to application of mechanical forces (as for cell swelling by hypoosmotic stimuli) [30] c) indirect activation through G protein-coupled receptors (GPCRs) and receptor tyrosine kinases stimulation thereby stimulating phospholipases C (PLC) with a subsequent liberation of Ca^{2+} from intracellular stores.

1.4 TRPs and diseases

TRPs are also involved in a large number of pathological conditions due to their expression in many different tissues, organs and cell types, and due to the fundamental functions, that they mediate. Mutations in many TRP channels result in disease, including a variety of sensory impairments [15] and channelopathies, a group of disorders caused by impaired channel function as a result of either genetic or acquired factors. Many pathogenic mutations (both, gain- and loss-of-function) in TRP genes have been described including splicing defects, nonsense, missense or in-frame mutations, frameshift, deletions/insertions. Since TRP channel signaling often causes changes in intracellular Ca^{2+} concentrations, aberrant activity induced by inherited mutations is likely to interfere with Ca^{2+}-dependent cellular functions or cause hazardous Ca^{2+} overload. *Trpc6*, *Trpm6*, *Trpp2*, *Trpml1*, and *Trpml2* are among the *Trp* genes frequently mutated, which result in a variety of human hereditary channelopathies, including focal segmental glomerulosclerosis, hypomagnesemia with secondary hypocalcemia, autosomal dominant polycystic kidney disease and mucolipidosis type IV. In nociceptors, a specialized subset of peripheral sensory neurons that mediate pain when stimulated by mechanical, chemical or thermal noxious stimuli, TRP channels represent the major class of detectors and transducers [31, 32]. Nociception is the sensory process that involves noxious and pain-producing stimuli perception. Although under physiological conditions,

the activation of nociceptive molecular detectors and transducers by specific noxious stimuli is crucial for nociception and pain sensation, the altered modulation of detectors' activity, is highly critical for nociception and pain under pathophysiological conditions [33]. Abnormal TRPs activation in nociceptors has important implications such as hyperalgesia, allodynia and chronic pain, thus leading to pathological conditions including inflammatory pain, neuropathic pain, visceral pain, migraine and cancer pain [34].

1.5 TRPV subfamily

TRPV "Vanilloid" subfamily has six mammalian members. TRPVs are classified into two types. TRPV1-TRPV4 are all heat-activated channels that also function as chemosensors for a variety of endogenous and synthetic compounds. They are also non-cation selective (very slightly permeable to Ca^{2+}). Furthermore, TRPV4 has recently been identified as being activated in response to cell swelling [35]. TRPV5 and TRPV6 have slightly different features. Their temperature sensitivity is lower than the other ones, but they are the only TRP family channels that are extremely Ca^{2+}-selective, and they are both tightly controlled by intracellular Ca^{2+} [36]. TRPV5 and TRPV6 function as gatekeepers in epithelial Ca^{2+} transport and selective Ca^{2+} influx routes in non-excitable cells [37]. The TRPV1 channel is also known as the "capsaicin receptor." Camphor, allicin [38], nitric oxide (NO), and spider toxins [39], as well as ethanol [40], can activate it. It can also be controlled by extracellular cations. Inflammatory mediators may enhance TRPV1 expression levels in the membrane [41, 42], stimulate TRPV1 phosphorylation by protein kinases [43], or produce phosphatidil 4,5-bisphophate inhibition of TRPV1 [44]. TRPV1 is not only involved in the acute pain that is induced by chemicals and mild heat, but it also makes a significant contribution to peripheral sensitization. Numerous drugs have been created to modulate TRPV1 activity to reduce pain due to the role that it plays in pain perception.

TRPV4 is another essential member of the TRPV subfamily. This polymodal receptor has a diverse expression pattern as well as a wide range of physiological activities [45].

TRPV4 is found in a variety of non-nervous tissues and cells, including the urinary bladder, kidney, vascular endothelium, keratinocytes, cochlear hair cells, and Merkel cells [43] [46], but it is also expressed in trigeminal ganglion (TG) and dorsal root ganglion (DRG) sensory neurons, where once activated it triggers substance P (SP) and calcitonin gene-related peptide (CGRP) release, resulting in neurogenic inflammation

[47]. TRPV4 was first shown to be an osmo-transducer that is activated by a decrease in osmolarity, pointing to its potential function in controlling cell swelling. Later research revealed that TRPV4 is also triggered by endocannabinoids, arachidonic acid (AA) metabolites, low pH, citrate, shear stress, harmless warmth (27–35 °C) [48] and (NO). Two transduction mechanisms, the PLC/ DAG pathway and the PLA2/AA pathway, have been proposed to explain the mechanism of mechanical stress-mediated activation of TRPV4 [49]. Based on previous studies, TRPV4 is not directly triggered by mechanotransduction, and is instead phosphorylated by Src-family of tyrosine kinase in response to hypotonicity [49]. Src family kinase-dependent tyrosine phosphorylation of TRPV4 on TYR-253 mediates its response to hypotonic stress. Since prostaglandin E2 (PGE2) and serotonin can work together to engage this receptor in mechanical and osmotic stimuli-evoked hyperalgesia through cAMP/ protein kinase A (PKA) and PKC, the TRPV4 channel also plays a significant role in mechanical hyperalgesia produced by inflammatory mediators (132). Additionally, the activation of protease-activated receptor 2 (PAR_2) by proteases produced during inflammation may sensitize TRPV4 by activating a number of second messenger pathways, including PKA, PKC, PKD, and PLC (122, 133).

2.TRPA1

Transient receptor potential ankyrin 1 (TRPA1) subtype, was firstly described in 1999 in lung fibroblasts by Jaquemar et al., as an ankyrin-like protein with transmembrane domains protein 1 (ANKTM1). Successively the protein was recognized as a TRP channel for its homology with several members of the same superfamily and it is the sole member of the TRPA mammalian subfamily [50]. Since its discovery, TRPA1 has been found to be expressed in both mammals and invertebrates, including rat, mouse, dog, chicken, fruit fly, *Danio rerio,* and *Caenorhabditis elegans* [6].

TRPA1 is a non-selective cation channel permeable to Na^+, K^+, with a predilection for Ca^{2+} due to its conductance ranging from ~70 pS to ~110 pS in the inward and outward directions. TRPA1 is widely expressed in neuronal and in non-neuronal cells such as epithelial, endothelial, colon and hair cells. Recently, its expression has been discovered in Schwann cells [51]. TRPA1 acting as a cellular sensor can be triggered by a wide spectrum of external stimuli (mechanical, chemical and thermal), many of which we are exposed to in daily life, as well as by endogenous signals related to inflammation

and cell damage. Due to its expression in nociceptive neurons most of TRPA1 agonists promote pain sensation, thus contributing to the pathophysiology of almost all organ systems [52, 53].

2.1 Structure of TRPA1

Trpa1 gene encodes a 1100 amino acids protein (1119 aa in human, 1125 aa in rat, 1115 aa in mouse), with a molecular mass of 120 to 130 kDa. In humans, the *Trpa1* gene consists of 27 exons and spans 55,701 base pairs of the human chromosome 8q13 [53]. TRPA1 monomer has a TRP superfamily conserved transmembrane *core* composed of six transmembrane α-helices with a pore-forming loop (with a size of 11.0 Å) between TM5 and TM6. The pore can enlarge in the presence of TRPA1 activators, increasing Ca^{2+} permeability and enabling even larger charged molecules to pass through the membrane [54]. The N- and C- termini are cytoplasmatic, with the N-terminus accounting for 64% of the total protein and the C- terminus accounting for just 14% (**Figure 3**). The most distinguishing feature of TRPA1 channel, from which its name derives, is the presence of 14 in mouse and 16 in human ankyrin repeat domains in the N-terminal portion of the protein. Ankyrin repeat domains, as mentioned above, plays important roles in inter-subunit interactions, ligand and protein-protein interactions, elasticity, channel trafficking and formation of molecular springs.

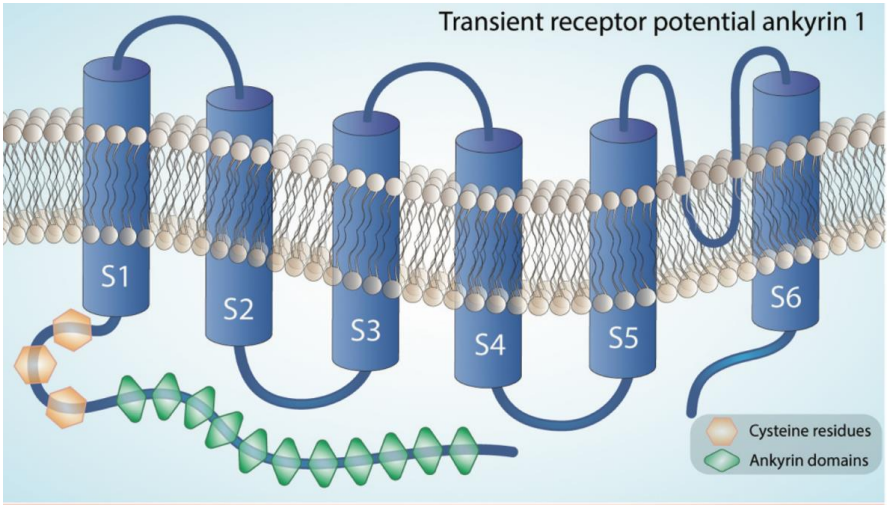

Figure 3. Structure of the TRPA1 channel [16].

This component, like most members of the TRP channel superfamily, contributes to homo- or heterotetrameric cation channels formation. In primary sensory neurons, TRPA1 often co-localizes with Transient receptor potential vanilloid 1 (TRPV1) channel,

thus assembling into hetero-tetramers to adjust the single channel biophysical features. Particularly, the complex formed by the proteins TRPA1 and TRPV1 appears to be the source of the direct contact between TRPA1 and TRPV1 and the control of TRPA1 intrinsic properties by TRPV1 [55]. Increased intracellular Ca^{2+} concentration may activate TRPA1 and amplify its sensitivity to various agonists through interaction with the EF hand Ca^{2+}-binding motif predicted inside ankyrin repeat 12. Another putative Ca^{2+}-binding domain important for TRPA1 regulation is found in the distal C-terminal region, constituted by residues E1077, D1080, D1081, and D1082, and it is necessary also for Ca^{2+}-dependent channel inactivation [56]. Calmodulin is also responsible for Ca^{2+}-mediated regulation of TRPA1, since it binds directly to the C-terminus of the channel, both potentiating and inhibiting TRPA1 [57]. Moreover, changes in extracellular Ca^{2+} can activate TRPA1 and enhance the current generated by TRPA1 agonists.

2.2 Localization of TRPA1

In a subpopulation of primary sensory neurons in DRG, TG and vagal (VG) ganglia, TRPA1 protein is highly expressed. Unmyelinated C- and sparsely myelinated Aδ-fibres, and rarely big myelinated fibers, are found in TRPA1-expressing neurons [58]. However, recent research showing that TRPA1 co-localizes with markers of non-peptidergic neurons, such as the purinergic P2X3 receptor, isolectin B4 (IB4), or the Na(V)1.8 channel, has cast doubt on the original hypothesis that TRPA1 expression is restricted to peptidergic nociceptors [59]. SP, neurokinin A (NKA), and CGRP, which are released from peripheral nerves and mediate neurogenic inflammatory reactions, are the neuropeptides expressed by TRPA1-positive nociceptors.

In the central nervous system, TRPA1 is expressed in oligodendrocytes, where it may play a role in ischemia and neurodegeneration, in astrocytes, where it may contribute to resting intracellular Ca^{2+} levels and regulate inhibitory synapses by modulating the extracellular concentration of γ- aminobutirric acid (GABA), and in hippocampal neurons, where it may be linked with the cannabinoid receptor CB1. Additionally, TRPA1 has been found in several tissues composed of extra-neuronal cells. These include vascular endothelial cells, where it modulates vessel tone, keratinocytes, and skin fibroblasts, where it mediates secretion of eicosanoids like PGE2 and leukotriene B4 (LTB4), thereby promoting mechanical transduction, and dental pulp fibroblasts, where it enhances the perception of noxious cold. It is also expressed in taste cells, where it interacts with the bitter taste receptor TAS2R60. More recently, in 2017, TRPA1

expression was detected also in Schwann cells [51]. In the same study was observed that, in a mouse model of neuropathic pain secondary to partial sciatic nerve ligation, TRPA1 silencing in nociceptors attenuated mechanical allodynia without affecting macrophage infiltration and oxidative stress. Schwann cell TRPA1 generated a spatially constrained gradient of oxidative stress, which maintained macrophage infiltration to the injured nerve, and sent paracrine signals to activate TRPA1 of ensheathed nociceptors to sustain mechanical allodynia [51].

2.3 Activation, modulation of TRPA1

TRPA1 is a cellular sensor which detects chemical, mechanical, and thermal stimuli. A peculiarity of this channel is its ability to be triggered by a large variety of chemicals, many of which are present in everyday life such as irritants, natural molecules environmental toxins and common pharmaceuticals, as well as endogenous reactive mediators, derived from both metabolism and oxidative stress [56]. TRPA1 agonists of exogenous and endogenous nature can be classified into two major groups: electrophilic and non-electrophilic activators.

Electrophilic agonists

These agonists covalently modify the channel after binding it. This interaction is mediated by the thiol group of three cysteine residues (C621, C641, C665), and by a lysine residue (K710) situated in the N-terminus. Many TRPA1 agonists are carbon or sulfur-reactive electrophiles that interact with nucleophilic groups (such as cysteine residues). Another activation mechanism is the oxidation of thiol groups, which results in the formation of disulfide bonds [60]. AITC, a pungent substance found in mustard oil, wasabi (TRPA1 is also known as the “wasabi receptor”), and horseradish, allicin (found in garlic and onions), cinnamaldehyde (found in cinnamon), methyl salicylate (found in wintergreen), gingerol (found in ginger), and eugenol (found in cloves) are among the natural compounds included in this first group of activators. Industrial chemicals, laboratory chemicals like formalin, volatile irritants such as acrolein and crotonaldehyde, and general anesthetics (e.g., isoflurane, lidocaine, propofol) are able to activate TRPA1 channel [56] [16]. Recent studies have shown that also endogenous bioproducts are able to covalently modify TRPA1. In fact, reactive carbonyl species (RCS, such as unsaturated aldehydes and prostaglandin J2, mediating cysteine carbonylation), reactive oxygen species (ROS, causing cysteine oxidation), reactive nitrogen species (RNS, mediating *S*-

nitrosylation) behave as TRPA1 activators [61]. Due to its capacity to release protons when hydrated to carbonic acid, carbon dioxide (CO_2) is one of the metabolic products that can indirectly trigger TRPA1 channel [62]. Oxidized phospholipids can alter the cysteine residues in TRPA1 under oxidative stress conditions, thus activating the channel. NO acts in both the central nervous system *via* a cGMP pathway and in the periphery on sensory neurons by direct activation of TRPA1 *via* formation of adducts with free thiols of cysteine residues [63]. Hydrogen peroxide (H_2O_2), which oxidizes cysteine residues to produce either cysteine sulfenic acids or disulfides, acts as TRPA1 activator. It is significant to note that TRPA1 and these reactive chemicals' interactions are essential for detecting tissue damage, especially when inflammatory events take place.

Non-electrophilic agonists

Non-electrophilic modulators are compounds incapable of inducing covalent modifications of the channel protein. These non-reactive agonists commonly interact with TRPA1 by a reversible and transient interconnection within a conventional binding region in the receptor [64]. Numerous herbal and plant derivatives are listed in this category, including nicotine, menthol, Δ^9-tetrahydrocannabinol (the psychoactive ingredient in marijuana contained in *Cannabis sativa*), thymol (found in thyme and oregano), and carvacrol (found in oregano). Common pharmaceuticals including clotrimazole, nifedipine, and nonsteroidal anti-inflammatory drugs (such as diclofenac and acyl-glucuronide ibuprofen) are additional non-electrophilic activators [56] [16]. Menthol has an unusual bimodal effect on mouse TRPA1, activating the channel at lower doses and inhibiting it at higher ones [65]; in contrast, menthol activate the human isoform of the channel at all concentrations. This highlights the important role played by species differences in TRPA1 [64].

GPCRs may modify TRPA1 function through second-messenger signalling cascades. Thus, TRPA1 activation can occur either directly or indirectly as a result of intracellular signaling pathways started by bradykinin, prostaglandins, histamine, trypsin, and CGRP [66] [67]. PLC, generating diacylglycerol DAG and inositol triphosphate (IP3), and PKA, which can upregulate membrane TRPA1 expression in trigeminal neurons *via* increased channel trafficking, promote TRPA1 sensitization [68]. According to Meents et al. [69], TRPA1 possesses unique phosphorylation sites for PKA, including four residues in the N-terminal domain (S86, S317, and S428) and one at the C-terminus (S972).

Temperature modulation

In addition, TRPA1 activity may be influenced by a large variety of stimuli. TRPA1, was initially described as a sensor of noxious cold (<15°C) [70], however the role of TRPA1 as a temperature sensor has been debated for a long time. By now, it has been accepted that TRPA1 activity can be modulated by temperature with species-specific temperature sensitivity, recent findings appear to suggest a direct activation of TRPA1 by cold temperatures. Further research is required to determine the precise function of TRPA1 in noxious cold thermosensitivity.

Ca^{2+} modulation

Ca^{2+} can modify the TRPA1 channel either intracellularly or extracellularly. This can promote secondary events that increase cytosolic Ca^{2+} levels. On the other hand, TRPA1 activity can be desensitized by extremely elevated intracellular Ca^{2+} [71]. Taken together, several studies on Ca^{2+}-dependent regulation demonstrate that Ca^{2+} induces a rapid potentiation of the channel followed by a slow but strong inactivation.

Mechanical modulation

Another feature attributed to TRPA1 is mechanosensation and, particularly, mechanical hypersensitivity. At the beginning TRPA1 was proposed to be a mechanosensor. Infact, the ankyrin repeats of its structure, were supposed to serve as a spring to gate TRPA1 in response to mechanical stimuli, due to their expression in inner-ear hair cells and due to the mechanotransducer function of TRP channels of invertebrates [72] [73]. The TRPA1 worm orthologue is sensitive to mechanical pressure and to several amphipathic molecules (trinitrophenol and chlorpromazine) that produce a membrane curvature that leads to TRPA1 activity modulation. To date, the mechanosensory role of TRPA1 remains to be further investigated. Contradictory results were obtained when mechanical stimulation was applied to TRPA1-deficient mice; while some studies indicated that the intensity of acute mechanical nociceptive pain remained constant [74], other works reported that it significantly decreased as a result of the channel's absence [73, 75]. It is reasonable to assume that TRPA1 channel has a role in mechanotransduction, even though it is not a key mechanosensor, as well as in mechanical allodynia and hypersensitivity in rodent models of both inflammatory and neuropathic pain.

Chemical modulation

It is indisputable that TRPA1 exhibits remarkable sensitivity to a wide range of chemical substances, making it the ideal chemosensor. Other mechanisms that control TRPA1 activity include phosphorylation, voltage, ROS-dependent and membrane-delimited protein-protein interactions, modulation by metals, many of which have stimulatory effects (e.g., Zn^{2+}, Cd^{2+}, and Cu^{2+}) and activation by UV light (human TRPA1 can be activated by near UV light in a wavelength-dependent manner) [53]. Positive intracellular potential can activate this TRP subtype even though TRPA1's voltage dependence is weaker than that of other TRP channels [76]. The voltage-sensing domain is assumed to be located within the COOH-terminal tail of TRPA1 since the TM4 lacks any charged residues, which typically serve as voltage sensors in voltage-sensitive ion channels.

2.4 Inhibition of TRPA1

TRPA1 has recently been considered as a highly interesting target for the development of analgesic and anti-inflammatory medicines due to its critical function in many painful and inflammatory disorders. Unfortunately, differences between human and rodent TRPA1 homologues complicate TRPA1-targeted drug discovery. Compounds that seem to be human TRPA1 antagonists can act as agonists or show no activity when examined in the rat and mouse homologues. As mentioned above, menthol can both inhibit or activate TRPA1 depending on the species and concentration [65]. There is a wide range of naturally occurring antagonists for TRPA1, many of which function as mild agonists or inhibitors. Camphor, basil, wormwood, rosemary, 1,8-cineole (eucalyptol), lemon eucalyptus, and sage are further natural antagonists. Gadolinium, amiloride, gentamicin, and ruthenium red are examples of nonselective antagonists that can block a variety of TRP channels [77]. To date, a number of selective inhibitors have been created with the aim of offering efficient methods to treat TRPA1-related disorders, such as aliments that cause pathological pain.

Xanthine derivatives, such as HC-030031 (by Hydra Biosciences in 2007) and its derivative Chembridge-5861528, 10 times more potent, were the first TRPA1 antagonists identified [78] [79]. HC-030031 reduced the nociceptive response typical of both the first and second phases of the formalin test, a crucial model of inflammatory pain, in addition to inhibiting responses by recognized TRPA1 agonists, such as AITC. Chemically, HC-

030031 is a low potency TRPA1 activator with a core of xanthine alkaloid similar to that of caffeine. It also covalently binds to the receptor. Since its discovery, HC-030031 has been extensively used as a pharmacological tool to investigate the function of TRPA1 channel in numerous physiological processes and disease models [78].

Other potent antagonists are the oxime derivatives: AP18, A-967079 and V948 [24], and 3-(4,5-diphenyl-1,3-oxazol-2-yl) propanol oxime (SZV-1287). AP18, was identified in the same year of HC-030031 [74] and it covalently binds to the channel. The first use of this compound shed light on the role of TRPA1 in mechanical hyperalgesia, as AP18 reverted complete Freund adjuvant-induced mechanical hyperalgesia in mice [74].

A-967079, for which has been described a putative binding pocket within the channel pore composed by residues S873, T874, L881, F909, F944, showed, for the first time, that TRPA1 antagonism does not affect body temperature or noxious cold sensation [80]. In a rodent model of diabetic neuropathy, Chembridge-5861528, a derivative of HC-030031, was successfully used [81]. It decreased pain-related behavior and hypersensitivity [82].

The trichloro(sulfanyl)ethylbenzamides, such as AMG5445 [83], and the thioaminal-containing compounds CMP1, CMP2, and CMP3, are two more groups that are known to potently block TRPA1.

It has been determined that certain plant extracts used to alleviate pain or migraines are TRPA1 agonists. These substances have also been described as partial agonists that desensitize the channel and the sensory nerve terminal that mediate pain and neurogenic inflammation, even though this activity would be in opposition to the positive effects of these substances [84]. Parthenolide, tanacetum’s active ingredient, is a partial TRPA1 agonist with the ability to compete with endogenous full channel agonists in the treatment of migraine [85].

The TRPA1 channel as well as the dual function of primary sensory neurons (neurogenic inflammatory and nociceptive responses) were both prolonged desensitized by parthenolide. Ligustilide, a natural drug used to treat pain and headaches, is present in high amounts in herbal medicines and, like parthenolide, activates TRPA1 to promote nociceptor desensitization. Due to its outstanding safety profile, acetaminophen (paracetamol), a commonly used painkiller, is administered to children and expectant mothers to treat pain. Its therapeutic activity's mode of action, however, remains unknown. The main toxic effects of an APAP overdose are caused by N-acetyl-p-

benzoquinone imine (NAPQI), the principal metabolite of acetaminophen. NAPQI likely targets TRPA1 due to its exceptional responsiveness, desensitizing the channel and preventing pain signals from reaching relay sites in the dorsal spinal cord [86]. More significantly, antipyrine, propyphenazone, and dipyrone (metamizole), older analgesics that are still used successfully in clinical practice, but whose mechanism of action is still debated, are potent and selective TRPA1 antagonists at concentrations completely compatible with human plasma levels, and by this mechanism inhibit inflammatory and neuropathic pain [87].

Until now, despite the large number of selective TRPA1 antagonists, only five molecules have been tested in clinical trials for pain treatment or other TRPA1 related conditions. Among these: GRC 17536, tested for painful diabetic neuropathy; CB-189625, investigated in a phase-1 clinical trial for acute surgical pain; GDC-0334, tested in a phase-1 trial for asthma treatment; HX-100, for painful diabetic neuropathy and allergic asthma; ODM-108, studied for the treatment of neuropathic pain, but without positive outcome [16].

2.5 TRPA1 and PAIN

According to the International Association for the Study of Pain (IASP) the definition of pain is: “An unpleasant sensory and emotional experience associated with, or resembling that associated with, actual or potential tissue damage.” (IASP taxonomy. https://www.iasp-pain.org/terminology?navItemNumber=576 2019) According to this definition, pain is a subjective sensation that is affected at different degrees by psychological, biological, and also social factors. Anatomical position, intensity, duration (acute if it resolves quickly, chronic if it lasts a long time, episodic, or end of dose pain), etiology (malignant or non-malignant), or the pathophysiological mechanism involved (nociceptive, inflammatory, or pathological pain) are all criteria used to classify pain [16, 88].

Nociceptive pain, also known as "physiological pain," is a type of pain simply derived by the perception of noxious or harmful stimuli and it serves to warn and protect the organism against potential or actual damage caused by external stimuli.

Inflammatory pain is both protective and adaptive. It occurs as a result of infection or cellular and tissue injury once the immune system has been activated. This type of pain aims to encourage healing by inducing hypersensitivity, which prevents physical contact and movement of the wounded body part, hence lowering the chance of further harm. The

third form of pain lacks the physiological aim of protection and is referred to as "pathological pain" and it represents a disease condition of the nervous system rather than a symptom of some disorder.

Neuropathic pain is the pathological pain induced by a disease or lesion of the somatosensory nerve system, whereas dysfunctional pain occurs in the absence of such damage or inflammation [89, 90] [16]. Nociceptors are a subgroup of sensory neurons that respond to painful and harmful stimuli due to the presence of a wide range of receptors and ion channels in the plasma membrane across the soma and fibers, allowing them to convert noxious inputs to electrical impulses, which are then transferred to the central nervous system (CNS) to communicate pain. The TRP family is the most common type of detector and transducer found in nociceptive neurons [33]. Among these, TRPA1 plays a crucial role in pain sensation, which is strongly due to its high expression in primary sensory neurons and its ability to sense a large variety of harmful and unpleasant stimuli.

2.6 TRPA1 and inflammatory pain

A wide range of inflammatory substances and mediators are endowed with a pivotal role in the onset and maintenance of pain. Protons, nucleosides, nucleotides, oxidative stress byproducts, proteases, prostaglandins, histamine, norepinephrine, serotonin, cytokines, chemokines, neurotrophins, and other peptides including bradykinin and endothelin are a few of these [91]. The theory that TRPA1 significantly contributes to the hypersensitivity to chemical, thermal, and mechanical stimuli that characterizes a number of models of neuropathic pain, including nerve injury, diabetic neuropathy, and neuropathy brought on by chemotherapeutic agents (CIPN), is solidly gaining support. The activation of GPCRs by transmitters like bradykinin, adenosine triphosphate (ATP), nerve growth factor (NGF), CGRP, and prostaglandins can result in the phosphorylation of TRPA1 and TRPV1 at multiple sites via PKC and PKA, which can lead to sensitization [69] [53]. Two aspects of TRPA1 channel's function in inflammatory pain should be considered. Proinflammatory substances use TRPA1 to activate and/or sensitize nociceptors. The proinflammatory neuropeptides SP/Neurokinin A (NKA) and CGRP, on the other hand, are typically released in response to stimulation of TRPA1 and orchestrate a sort of feedforward proinflammatory mechanism by encouraging vasodilation, plasma protein leak, and stimulatory effects on immune cells [67]. In cellular studies, TRPA1 was found to contribute to the excitatory effects of bradykinin via a PLC/Ca^{2+} signaling

pathway [92]. This finding provided the first evidence for the role of TRPA1 in inducing inflammatory hypersensitivity [93]. First evidence of TRPA1's function in inflammatory pain models were obtained in rodents that received intradermal or intra-articular injections of complete Freund's adjuvant (CFA). According to Obata et al. [94] and Dunham et al. [95], TRPA1 up-regulation in DRG neurons and sensitization of TRPA1-expressing neurons were related to CFA-induced cold and mechanical hyperalgesia. These preliminary data were supported by pharmacological studies, which showed that HC-030031 or AP-18 significantly decreased CFA-evoked mechanical and cold hypersensitivity [96] [97] [74].

Recent evidence suggests that TRPA1 channel contribute to the maintenance of nociceptor hypersensitivity, despite the well-documented role of it in the establishing acute hyperalgesia associated with an early inflammatory response. TRPA1 was discovered to mediate hypersensitivity associated with chronic inflammation even days or weeks after the adverse stimulus was administered, when the damaging substances were withdrawn, or the inflammation seemingly resolved. In osteoarthritis models induced by CFA, carrageenan, monosodium iodoacetate, and monosodium urate [96] [97] neuronal sensitization was decreased by TRPA1 gene deletion or selective antagonism. In particular, the ability of TRPA1 antisense mRNA to inhibit carrageenan-induced inflammatory hyperalgesia implies that channel activation is essential for both the onset and maintenance of this phenomena [98]. However, the underlying molecular mechanisms which, under inflammatory circumstances, result in a TRPA1-driven chronic painful phenotype, are not completely known.

2.7 TRPA1 and neuropathic pain

Recent findings in many animal models have suggested that TRPA1 is involved in various patterns of neuropathic pain, a clinically relevant pain syndrome most frequently due to peripheral nerve injury (PNI). The main feature of neuropathic pain is an aberrant transmission of sensory impulses to the CNS and [99]. The most frequently reported causes of damage to the CNS and peripheral nervous system (PNS) include brain and spinal cord injuries, nerve compression and trauma, neurodegenerative diseases, autoimmune disorders, channelopathies, diabetes, HIV and VZV infection, leprosy, chemotherapeutics, and alcohol abuse [100].The findings of numerous investigations

highlighted TRPA1's role in fostering neuropathic pain and the sensory hypersensitivity its related sensory hypersensitivity.

2.7.1 TRPA1 and nerve injury

A down-regulation of TRPA1 expression in L5/DRG has been seen in a model of lumbar spinal nerve ligation, which is where the contribution of TRPA1 channel to neuropathic pain was originally examined [94].

In additional nerve damage models, such as sciatic nerve injury by chronic constriction or transection, both dysregulation and adaptation of TRPA1 receptor in DRG neurons have been further documented [101].

TRPA1 antagonists reduced the hypersensitivity in these models, and in particular diminished mechanical allodynia. Similar outcomes from genetic channel deletion were obtained, highlighting the critical part that TRPA1 channel plays in mechanical hypersensitivity following nerve damage [102] [103]. First, after spinal nerve ligation in rats, decreased cold responsiveness emerged due to antisense suppression of TRPA1. Second, oral administration of HC-030031 corrected the mechanical hypersensitivity that was discovered six weeks after surgery in a rat model of L5/L6 nerve ligation (Eid et al., 2008). These findings were further supported by the use of the selective receptor antagonist A-967079, which in nerve injury models reduced post-injury cold hypersensitivity without affecting baseline cold perception.

2.7.2 TRPA1 and diabetes painful neuropathy

Diabetes mellitus frequently results in peripheral neuropathic pain referred as Peripheral Diabetic Neuropathy (PDN) and it is described as a superficial burning pain associated with mechanical and thermal hypersensitivity. By activating the TRPA1 channel, oxidative stress and glucose metabolic byproducts, such as 4-hydroxy-2-nonenal (4-HNE) and methylglyoxal, sustain and contribute to pain and hyperalgesia in diabetes mellitus. TRPA1 suppression lessens mechanical allodynia and hypersensitivity in mouse models of streptozotocin-induced diabetes [104] [81].

According to a more recent theory [105] [106], reactive compounds produced by diabetes induce a sustained activation of nociceptive nerve fibers *via* the TRPA1 channel, leading to pain hypersensitivity and a subsequent loss of cutaneous nerve fiber function, which is what causes the harmful long-term effect.

2.7.3 TRPA1 and CIPN

Additionally, taking anticancer medications is a circumstance that causes the creation of ROS and the activation of TRPA1, which results in cold and mechanical allodynia. It has been suggested that the TRPA1 channel has a role in neuropathic pain syndromes that do not originate from mechanical damage, such as the pain brought on CIPN [81].

CIPN is defined by a persistent pain state and functional handicap, which significantly impacts the quality of life of a significant number of treated patients, and frequently leads to therapy withdrawal [107]. Paresthesias and dysesthesias of the extremities, sudden pain and mechanical and thermal hypersensitivity are some of the most typical sensory signs of CIPN. CIPN is a significant dose-limiting adverse reaction of chemotherapy drugs, these include platinum-based compounds (e.g., cisplatin and oxaliplatin), taxanes (e.g., paclitaxel), vinca alkaloids (e.g., vincristine), the first-in-class proteasome inhibitor, bortezomib and the aromatase inhibitors exemestane, letrozole, and anastrozole. The potential of chemotherapeutic medicines to cause oxidative stress is regarded as an additional and collective trait that, although on the one hand helps to explain why these drugs have an anticancer effect, on the other hand, it appears to be the cause of serious adverse events, such as CIPN. According to this theory, it has been shown that antioxidants like acetyl-L-carnitine, a-lipoic acid, or vitamin C can reduce the pain caused by oxaliplatin-induced mechanical hyperalgesia, heat- and cold-evoked allodynia, and other painful conditions in rats [108].

The first example of the involvement of a TRP channel was obtained by studying cisplatin in a rodent model of CIPN. TRPV1 was paradoxically discovered to protect against mechanical allodynia since channel deletion increased cisplatin-induced neurotoxicity [109]. TRPA1 is ideally adapted to contribute to CIPN because of its primary location in nociceptive sensory neurons and its nociceptive function as a sensor of oxidative stress [110]. In fact, a single dosage of oxaliplatin causes mechanical and cold hypersensitivity in either rats or mice that develop quickly and over time. A TRPA1 channel blocker (HC-030031), a ROS scavenger (α-lipoic acid), and TRPA1 gene deletion have all been shown to improve protection from hypersensitivity or its reversion in CIPN animal models [111] [82, 112].The role of TRPA1 in mechanical hypersensitivity does not appear to be limited to oxaliplatin, since TRPA1-deficient mice also had a significant decrease in mechanical allodynia following treatment of the

chemically comparable medication, cisplatin. These initial series of events may happen quickly after oxaliplatin delivery, but there is indirect evidence that oxidative stress may persist for days following exposure to oxaliplatin. In fact, when given on the fifth day following oxaliplatin treatment, the antioxidants acetyl L-carnitine, α-lipoic acid, and vitamin C dramatically attenuated oxaliplatin-evoked mechanical hyperalgesia [108].
Although common, TRPA1 does not appear to have an exclusive function in models of CIPN. Mechanical hyperalgesia is caused in part by the activation of the TRPV4 channel in a mouse model of paclitaxel-induced neuropathy [113]. However, TRPA1 alone is wholly responsible for mediating both cold allodynia and the TRPV4-resistant mechanical hyperalgesia induced by paclitaxel [114]. Additionally, paclitaxel dramatically increased cold hyperalgesia in a rat model of diabetes as compared to normoglycemic paclitaxel-treated control animals [115]. Paclitaxel therapy was associated with accumulation of atypical mitochondria and an increase in mitochondrial ROS generation in diabetic and control rats [115]. Increased mitochondrial ROS generation and inadequate radical detoxification may combine to cause paclitaxel potentiation of cold hyperalgesia in diabetes [115]. The finding that pretreatment with antioxidant molecules or TRPA1 antagonists prevented the sensory hypersensitivity induced by paclitaxel [115] [116] supports the theory that the common final pathway activated by chemically distinct chemotherapeutics produces notable oxidative stress [108], which in turn activates and sensitizes the TRPA1 channel.

Recent studies have shown that a single dosage of oxaliplatin or bortezomib is effective and the onset of mechanical and cold symptoms occurs 1-3 days after intake. Trevisan et al [112], describe hypersensitivity that lasts 11-15 days. Platinum-derived medicines, such as paclitaxel and bortezomib, do not directly target TRPA1, and there is evidence that cisplatin and oxaliplatin gate the channel by creating ROS from cells other than primary sensory neurons [111]. When hypersensitivity develops, the antioxidant α-lipoic acid or the TRPA1 antagonist HC-030031 completely reverse it [111] [112]. When chemotherapeutic drugs were delivered to TRPA1 deleted animals, hypersensitivity was completely absent [111] [112]. This finding suggests that TRPA1 is both required and sufficient for producing a prolonged (10-days) hypersensitive condition that does not outlive the presence of the chemotherapeutic drug in plasma and/or tissues.
Transient (1-6 hours) treatment with oxaliplatin or bortezomib raised an oxidative stress marker, implying that both events (increased oxidative stress and ability to target TRPA1) are required to produce the hypersensitive condition. The following experiment

confirmed this theory. Mice were totally and permanently protected from developing hypersensitivity by receiving treatment with a TRPA1 antagonist or ROS scavenger before and for 6 hours after oxaliplatin or bortezomib administration [117]. The findings collectively shed light on the unifying theory that oxidative stress byproducts generated systemically or close to sensory neurons as a result of exposure to chemotherapeutic agents activate/sensitize TRPA1 to cause a chronic hypersensitivity condition [111] [112]. In this scenario, TRPA1 might be a unique pharmaceutical target for cancer patients who, regrettably, acquire CIPN while receiving chemotherapy.

2.7.4 TRPA1 and migraine pain

Migraine pain represent a major medical need due to its widespread incidence in the general population. Although the underlying mechanism causing migraine pain is unknown, the use of monoclonal antibodies against CGRP or CGRP receptor (CGRP-R) and small molecules that target the CGRP-R in clinical practice suggests that the neuropeptide plays a significant role in this disease [118] [119]. One of the key mechanisms of migraine headaches appears to be the component of neurogenic inflammation induced by CGRP released from the terminals of trigeminal neurons.

Migraine attacks may be triggered by stimuli that, by acting on various receptors or channels, activate peptidergic nociceptors to release CGRP. TRPA1 is now emerging as a key migraine contributor and a novel target for the creation of migraine medications. TRPA1's involvement in migraine pathophysiology is supported by its sensitivity to exogenous and endogenous agents known to release CGRP from TG neurons and trigger migraine, as well as the inhibition or desensitization of this channel by specific analgesic and antimigraine agents [119]. TRPA1 is specifically expressed in a subset of TRPV1-expressing peptidergic neurons in the trigeminal ganglia, coexisting with neuropeptides such as CGRP and SP. TRPA1 agonists stimulate meningeal vasodilation by eliciting CGRP production from trigeminal neurons and dural tissue in the trigeminovascular system [120] [121]. Acrolein, an irritating chemical found in cigarette smoke and also created endogenously by plasma membrane peroxidation due to oxidative stress, is one of the TRPA1 activators relevant for migraine. Acrolein causes TRPA1 dependent CGRP production when administered to the nasal mucosa, which improves meningeal blood flow and causes neurogenic inflammation in cranial regions. As a result, it has been suggested that acrolein mediates neurogenic inflammation and headache induced by toxic environmental irritants, such as smoking [120]. In mice, cigarette smoke triggers a

neurogenic inflammatory response in the airways that is fully driven by TRPA1 activation [122]. In line with these findings, it has been demonstrated that applying acrolein, to the rat nasal mucosa causes a TRPA1-dependent and CGRP-mediated increase in meningeal blood flow [120]. Due to its ability to stimulate TRPA1, acrolein, which is also included in car exhaust and tear gas, may be responsible for the irritating responses elicited by tear gas, which include headache in addition to cough, chest pain, and dyspnea. Ammonium chloride [110] and formalin (formaldehyde) [78] are two more TRPA1 agonists that have long been known as migraine or cluster headache provoking drugs.

NO, a vasodilator gaseous compound, is released glyceryl trinitrate (GTN), which has been shown to cause migraine attacks in patients [119], and its analogues have been shown to have cardioprotective effects, and cause pain-like responses *via* TRPA1 [78]. By activating TRPA1 NADPH oxidase (NOX1/2) in the soma of trigeminal nociceptors and causing the production of ROS and CGRP, GTN causes periorbital allodynia [123]. One potential explanation for the frequent unpleasant reaction caused by nitroglycerine and its analogs is thought to be intra- and extracranial vasodilatation. The ability of sumatriptan to reverse nitroglycerine-induced headaches and migraines, which are likely caused by a direct vasoconstrictor effect via activation of the serotonin 5-HT1B receptor [124], supports the theory that cranial artery vasodilatation caused by NO plays a significant pro-headache role. *In vitro* [125] and *in vivo* [126], nitroglycerine/NO have been shown to produce CGRP, and more recently, NO has been discovered to behave as a TRPA1 agonist [63].

Umbellulone, the major volatile constituent of the California Bay Laurel, *Umbellularia californica,* which is also known as the ‘head-ache tree’ due to the ability of its scent to cause headache attacks, directly activates TRPA1 by reacting with thiols of cysteine channel’s residues [127] [128]. Indeed, umbellulone gated TRPA1, thereby releasing CGRP. Intranasal administration of umbellulone elicited neurogenic meningeal vasodilation and trigeminovascular system activation similar to acrolein tests [127]. Inhibitors of CGRP, CGRP-R, or TRPA1 totally reversed the effects of acrolein and umbellulone on meningeal arteries [120].

Interestingly, parthenolide, a bioactive component of feverfew, and isopetasin, the main ingredient in butterbur, have been found to have antimigraine effects that are connected to partial TRPA1 agonism and chronic desensitization of TRPA1 [85] [129].

2.7.5 TRPA1 and cancer pain

About 70–90% of cancer patients experience pain, which is a frequent and debilitating symptom of the disease that frequently worsens quality of life more than cancer itself and may have a substantial negative impact on adherence to therapy and satisfaction with care [130] [131]. In terms of disability, suffering, health care, and social and economic costs the burden of cancer-related pain is considerable [132] [133]. In fact, it can make patients less able to carry out daily activities and it is frequently accompanied by sleeplessness, anxiety, exhaustion, and sadness [134] [135]. Patients who have unrelieved pain may also become socially and familiarly reclusive, which can contribute to feelings of loneliness and emotional distress [135].

When pain is more severe or lasts longer, the risk of falling into depression rises [136]. Concomitant depression might deteriorate with pain, thus significantly lowering quality of life [137]. Numerous studies have revealed that many patients' pain is still poorly managed, even though up to 90% of cancer patients can have significant pain relief [132] [138]. Cancer-related pain represnts a significant financial burden on healthcare systems, and the inability to effectively manage pain can have a negative impact on quality of life [133]. Cancer patients may experience pain due to the tumor itself, or to diagnostic and/or therapeutic procedures, or to adverse reactions after treatment [139]. Neuropathic pain affects about 20% of cancer patients, but if patients who also experience mixed pain with a neuropathic component are included, the number of patients afflicted by neuropathic pain rises to about 40% [140]. The prevalence of cancer-related pain is higher in palliative care or pain management clinics rather than in other clinical settings, and some malignancies (such as the lung, prostate, or breast) are linked to this [137].

Cancer management treatment value is significantly influenced by the evaluation, effective control, and management of cancer-related pain. For patients, healthcare professionals, payers, and health systems, cancer-related pain treatment consequently gains new significance. A multimodal approach that often includes pharmacologic medicines and psychosocial support is necessary to achieve the aim of cancer-related pain treatment, which include enhancing patient comfort, functionality, and safety [141]. As the disease spreads, the tumor microenvironment (TME), which consists of cancer cells, immunological, inflammatory, and structural cells, gradually invades the surrounding tissues and releases certain chemical signals, aiding in the creation of a proalgesic neural environment [142] [143]. The interaction between TME and the peripheral sensory nerve

terminals that are nearby or integrated into the TME is crucial for starting and maintaining cancer-associated pain, even though it is impossible to rule out the possibility that cancer may communicate with distant sites to elicit pain. However, cancer pain remains incompletely understood and poorly managed, thus representing a major unmet medical need. It has been proposed that the activation of ion channels in primary sensory neurons can contribute to the initial processing of cancer pain [135].

Other murine models have contributed to clarify the central and peripheral pathogenic mechanisms involved in the development and maintenance of cancer and neuropathic pain [144]. This comprises a variety of neuropathological processes such as pathological sensory neuronal development and signaling, algogenic compounds generated by tumors and associated immune cells, dysregulated activity of bone cells close to the tumor, and various neuropathological substances [145] [146]. The characteristics that have led to the classification of cancer pain as a distinct pain state with both nociceptive and neuropathic aspects are a result of this broad and complicated pathological milieu [147]. Until recently, the role of the TRPA1 channel and oxidative stress in cancer-related pain was unknown. Antoniazzi et al. [148] demonstrated that mechanical and cold allodynia associated with tumor growth are entirely due to oxidative stress-dependent activation of nociceptor TRPA1 in a model of cancer pain obtained by the inoculation of a mouse melanoma cell line in the hind paw in mice. These results were confirmed by both pharmacological (by selective TRPA1 antagonists and antisense oligonucleotides) and genetic (*Trpa1*$^{-/-}$ deleted mice) tools, which did not show the development of thigmotaxis behavior, or mechanical or cold allodynia [148]. Thus, a noteworthy analogy is emerging between a variety of neuropathic pain models and a model of cancer pain, underlining the general role of oxidative stress and the TRPA1 channel to sustain chronic pain.

2.7.6 TRPA1 and other pain syndromes

According to studies on visceral inflammatory illnesses, TRPA1 is expressed in the viscera, and it is involved in the development of visceral pain. Particularly, it was discovered that TRPA1 mediates mechanical hypersensitivity in chemically induced colitis at the level of the gastrointestinal tract. The release of SP and subsequent neuropeptide-mediated neurogenic inflammation occur as a result of colon cells TRPA1 sensitization in dextran sulfate sodium (DSS) triggered colitis [149] [150]. Additionally, research on pancreatic involvement show that TRPA1 causes chronic pancreatic inflammation and pain. Compared to wild type animals, TRPA1 knockout mice

experience a milder form of pancreatitis induced by the administration of trinitrobenzene sulfonic acid (TNBS) into the pancreatic duct [151].

Osteoarthritis, a chronic degenerative disease characterized by the degradation of joint cartilage and periarticular bone remodeling causing stiffness, joint pain, and decreased movement, is another illness that causes inflammatory pain. Pharmacological or genetic TRPA1 inhibition decreased mechanical hypersensitivity in mice models of osteoarthritis induced by administration of monosodium iodoacetate. Additionally, it was observed that under specific experimental circumstances, osteoarthritis-related inflammation was reduced [97] [152].

Additional examples of pain conditions involving pathological TRPA1 activity include allergic contact dermatitis, postoperative pain, inflammatory pain brought on by bacterial infection, back pain, temporomandibular disorder and fibromyalgia. Given the limited therapeutic options currently available for pain management and the range of pain states in which TRPA1 has been implicated, this cation channel represents a viable therapeutic target for the creation of novel analgesic drugs.

3. Schwann cells

Two broad categories of cells form the nervous system: neurons, whose function is to generate and propagate electrical and chemical signals, and glial cells. Glial cells, also known as glia or neuroglia, are a diverse group of cell types with unique morphologies, functions, and locations throughout the nervous system. Astrocytes, oligodendrocytes, microglia, ependymal cells, and radial glia are among the five types of glial cells found in the CNS. In the PNS, three types of glial cells have been found: Schwann cells, enteric glial cells, and satellite cells [153]. Since its discovery in the mid-1800s glia was assumed to have merely a passive function, providing support, protection, and nutrition to the neurons around it, as well as enabling conduction. Hower, recently the role of glia has been revised, and it has become clear that these cells play crucial roles in the growth and development of the nervous system. Schwann cells, or neurilemma cells, are the main glial cells in the PNS. They form the myelin sheath (like oligodendrocytes in the CNS) that insulates an axon by tightly winding their membranous processes around the axon in a spiral. It is known that they also provide support to nerve cells by contributing to damage repair after an injury (**Figure 4**).

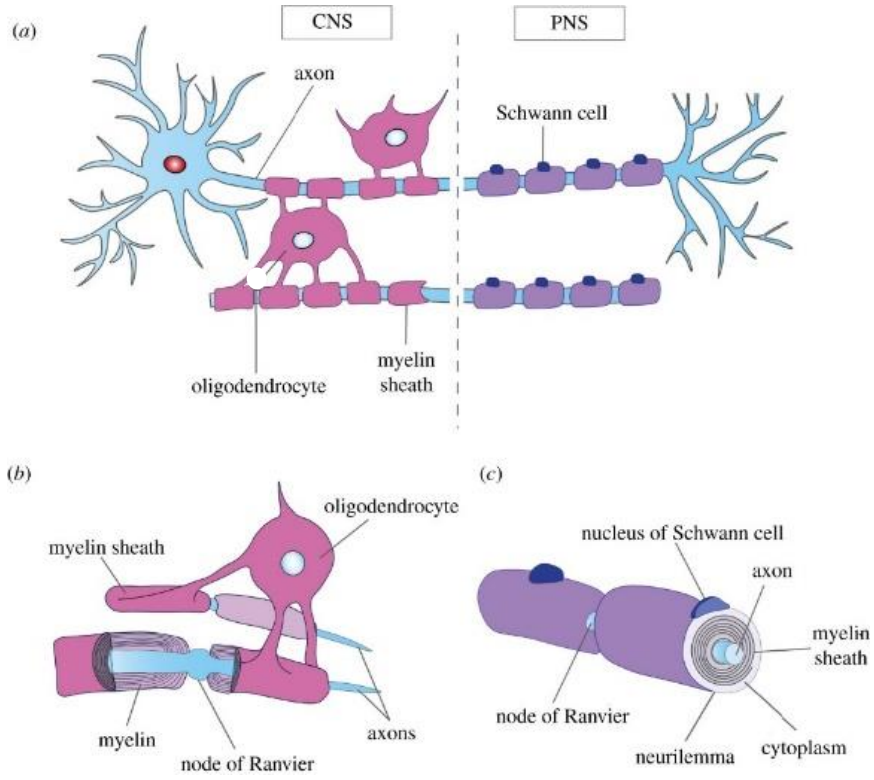

Figure 4. Comparison of central and peripheral myelination. (a) Each oligodendrocyte in the CNS can extend cytoplasmic projections to form multiple, multi-layered myelin sheaths (pink) around different axons, whereas each Schwann cell in the PNS completely wraps around a single axon by laying down multiple layers of cell membrane, of which the innermost layers constitute the myelin sheath (purple). (b) There is typically one oligodendrocyte between two nodes of Ranvier, which is not covered by plasma membrane to allow action potentials to jump from node to node. (c) Compared to oligodendrocytes, Schwann cell myelinated axons possess thicker myelin sheaths. Schwann cells also have an enlarged non-axonal domain due to the extra presence of the cytoplasm and nuclei, which is covered by the outermost layer, called the neurilemma [154].

They originate from neural crest cells, which undergo a first developmental transition turning into Schwann cell precursors associating themselves with the first growing axons. Secondly, Schwann cell precursors give rise to immature Schwann cells, which finally differentiate into myelin or non-myelin-forming Schwann cell [155] (**Figure 5**).

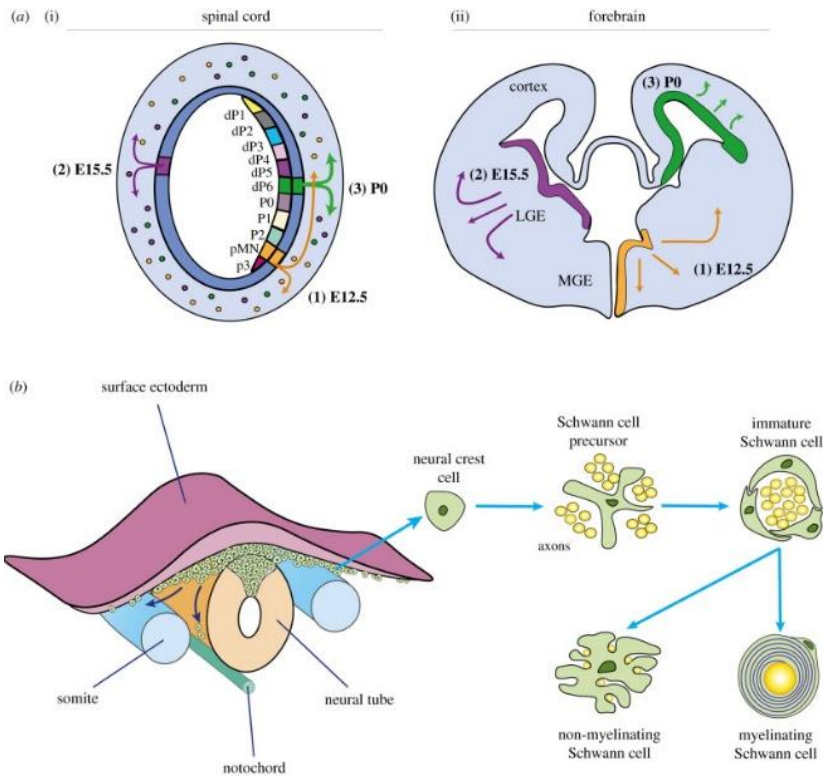

Figure 5. Origins, migration and development of oligodendrocyte progenitor cells (OPCs) and Schwann cells. (a) In the rodent spinal cord, OPCs originate from the pMN domain in the ventral ventricular zone at approximately embryonic (E)12.5. This is followed by a second wave of progenitors in more dorsal regions, which then migrate throughout the spinal cord to myelinate white matter tracts. Similarly, in the rodent telencephalon, the first wave of OPCs arise from ventral progenitor cells in the medial ganglionic eminence (MGE) at E12.5. Subsequently, a second wave of OPCs is generated several days later at about E15.5 by dorsal progenitor cells in the lateral ganglion eminence (LGE). After birth, cortex-derived progenitors give rise to the final wave of OPCs. (b) During the formation of the neural tube, neural crest cells arise from the tips of the neural folds. Neural cells initially form and accumulate at the dorsal surface of the tube, but soon migrate along with different pathways to differentiate into Schwann cell precursor cells, as well as progenitors of melanocytes, autonomic neurons, dorsal root sensory glia, chromaffin cells and other peripheral glia). Schwann cell precursor cells then transition into immature Schwann cells upon neuregulin-1 (NRG1), fibroblast growth factor 2 (FGF2) and Notch signalling. While all immature Schwann cells are thought to possess myelinating potential, only immature Schwann cells in close association with large-diameter axons differentiate into myelinating Schwann cells. By contrast, Schwann cells that associate with smaller-diameter axons form bundles of non-myelinating Remak cells [154].

Prior to myelination, Schwann cells and axon create a 1:1 ratio as development progresses, with Schwann cells arranged side by side along axonal projections [156]. The transcription of myelin-specific genes and the down-regulation of immature Schwann cell genes by myelin-forming Schwann cells signal the beginning of axon myelination. As a result, a group of molecules that serve as adhesives are produced, enabling the

development of myelin, a compact structure made of successive layers of plasma membrane wrapped around an axon with the intention of protecting it. P0 glycoprotein (the main myelin membrane protein in the mammalian PNS), MBP, PMP22kd (PMP-22), MAG, cyclic nucleotide protease (CNPase), and PLP are examples of myelin-specific proteins found only in Schwann cells. Notably, oligodendrocytes also express MBP, MAG, and primarily PLP [153]. On the other hand, non-myelinating Schwann cells either migrate toward the neuromuscular junctions to become terminal Schwann cells [157] or associate with small diameter axons in a way that causes one Schwann cell to enfold numerous axons to create a Remak bundle. This class of Schwann cells continues to express genes comparable to those of immature cells, such as GFAP, low-affinity NGFR, NCAM, and GAP-43 [158]. They do not express any myelin-specific markers.

3.1 Schwann cells function

These glial cells perform a variety of essential roles to ensure proper PNS development and the maintenance of its homeostasis, in addition to their role in accelerating conduction velocity in all large-diameter peripheral axons by providing myelin ensheathment. Schwann cells play a number of roles in promoting axonal expansion during the development of peripheral neurons, including the production of growth factors including brain-derived neurotrophic factor (BDNF), glial cell line-derived neurotrophic factor (GDNF), and NGF [159]. Schwann cell-secreted neurotrophic factors play a crucial role in promoting neuronal survival. The idea that Schwann cells serve as a first line of defense for axonal neuroprotection is consistent with this [160]. Schwann cells serve a crucial function in maintaining a balance between regeneration and degeneration in the PNS after nerve damage and axon degeneration because they lose their differentiated shape. By producing a variety of regenerative factors, survival factors, and inflammatory mediators, as well as by removing cellular and myelin waste, Schwann cells can develop a repair immature-like phenotype that supports nerve regeneration. By directing axons back to their destinations, these actions aim to recover brain function. Schwann cells ensheath the regenerated axons and differentiate again to generate myelin or non-myelinating Schwann cells in order to complete the repair process [161] [155].

3.2 Schwann cells and pain

Schwann cells function is not restricted to the physiological and pro-regenerative processes, indeed they are also implicated in sustaining chronic pain. Primary sensory neurons become sensitized and hyperexcitable after a peripheral nerve lesion, which results in neuropathic pain. It has been demonstrated that non-neuronal cells, particularly glial cells, play active roles in mediating painful feelings in addition to non-neuronal cells. Particularly glial cells, have been found to have active roles in mediating painful feelings in addition to changes in the activity of neuronal systems, thus interacting with nociceptive neurons to modulate pain *via* neuroactive signaling molecules secretion [162]. Schwann cells, which can detect nerve injury and initiate the response among neuroglia, are increasingly recognized as being critical in the onset and maintenance of neuropathic pain [159]. Schwann cells change in how their receptors and channels are expressed and/or activated in various neuropathic pain conditions. This modulation of intracellular pathways causes the release of glial mediators, such as cytokines, chemokines, and growth factors, which are linked to dysregulated pain signaling.

P2X receptors are a type of GPCR that is activated by nucleotides like ATP. P2X receptors, like the other ATP receptors P2Y, are present in Schwann cells and have been demonstrated to be important in the regulation of neuropathic pain. The P2X4 receptor subtype, in particular, is significantly upregulated in Schwann cells of damaged nerves. The development of pain hypersensitivity is inhibited in P2X4 receptor mutant mice after nerve damage. The development of pain hypersensitivity is inhibited in P2X4 receptor mutant mice after nerve damage. Thus, ATP plays an important role in the regulation of neuropathic pain by acting on neurons as well as Schwann cells, which produce mediators such as proinflammatory cytokines and chemokines [159]. Notably, Schwann cells themselves release ATP. Toll-like receptors (TLRs), of which TLR2 is strongly associated with the activation of Schwann cells and production of proinflammatory molecules [163], LDL receptor-related protein 1 (LRP1), which serves as a Schwann cell survival factor after peripheral nerve injury [164], and lysophosphatidic acid (LPA)1 receptor, which is upregulated in Schwann cells after sciatic nerve injury are additional receptors upregulated in Schwann cells following sciatic nerve injury and they are suggested as crucial in the initiation of neuropathic pain [165]. Hydroxyl carboxylic acid receptor type 2 (HCAR2), was found to be upregulated in the sciatic nerve and in the DRG neurons of neuropathic mice and it has been proposed as a new receptor for the

regulation of neuropathic pain [159]. Additionally, Schwann cells develop the ability to express major histocompatibility complex (MHC-II) under inflammatory and traumatic conditions so that they can deliver antigens to T helper lymphocytes. These cells consequently become activated and promote post traumatic axon loss and consequent neuropathic pain [166]. Chemokines and proinflammatory cytokines like tumor necrosis factor α (TNF-α), interleukin-1 (IL-1), and IL-6, which are all upregulated after peripheral nerve injury and contribute to axonal damage and enhanced nociceptor activity, are among the soluble mediators secreted by activated Schwann cells as well as by the infiltrating macrophages. The main mediator of hyperalgesia is TNF-α, which is produced by Schwann cells. Indeed, neuropathic pain states are induced by direct TNF- α injection into healthy nerves [164]. Simultaneously, Schwann cells release anti-inflammatory molecules that are crucial for neuropathic pain regulation because they counteract against the action of proinflammatory mediators. Erythropoietin (EPO) and its receptor EpoR are also both increased in Schwann cells following nerve damage. By binding to its receptor, EPO can prevent Schwann cells from producing TNF-α, this event prevents axonal degradation and facilitates recovery from chronic pain conditions [167] [164]. Therefore, a potential target for therapeutic intervention in the future is the balance between inflammatory and anti-inflammatory mediators. Additionally, sensory problems and neuropathic pain may result from physiologic changes in Schwann cells without severe myelin degradation or axonopathy [164].

3.2.1 Schwann cells TRPA1 and pain

TRPA1 channel is mainly expressed in small-diameter unmyelinated C- fibers or thinly myelinated Aδ-fibers, which are highly sensitive to noxious stimulation, of sensory ganglia, including DRG, TG and nodose ganglia (NG) [70] [168]. TRPA1 is expressed at several locations throughout the CNS in addition to its localization in nociceptive neurons of the PNS. In human brain TRPA1 has been identified in the hippocampus, cortex, substantia nigra, caudate nucleus, globus pallidus, cerebellum, putamen, hypothalamus, and amygdala [169]. Many studies have found TRPA1 in the striatum, amygdala, brainstem, hippocampus, and brainstem of rats [170] [16].TRPA1's function in the CNS is still not fully known, yet. Recent research has shown that glial cells such astrocytes, oligodendrocytes, and Schwann cells express TRPA1, which may play a role in maintaining chronic pain and hyperalgesia [171] [51] [172].

TRPA1 expression in Schwann cells was detected in 2017, in a mouse model of partial sciatic nerve ligation, where it promotes and maintains neuroinflammation and the consequent neuropathic pain [173]. Indeed, TRPA1 silencing in nociceptors attenuated mechanical allodynia without affecting macrophage infiltration and oxidative stress, whereas TRPA1 silencing in Schwann cells reduced both allodynia and neuroinflammation. It has been hypothesized that Schwann cell TRPA1 activates TRPA1 on nociceptor nerve fibers to cause allodynia by causing persistent oxidative stress via NOX1, which keeps macrophage infiltration into the damaged nerve in a spatially constrained manner [173]. An explanation to this phenomenon was given by the evidence that the oxidative stress provoked by the macrophages infiltrated within the site of injury activates TRPA1 in Schwann cells, without directly targeting TRPA1 in the nociceptors ensheated. Activation of Schwann cell TRPA1 and Ca^{2+} influx lead to the release of H_2O_2 in a NOX1-dependent manner, to amplify and sustain the oxidative stress signal as a consequence. This, in turn, mediates a dual function: an outwardly directed oxidants release maintains macrophage recruitment inside the injured nerve trunk, whereas an inwardly directed oxidative stress targets nociceptor TRPA1 to sustain mechanical allodynia [51] (**Figure 6**). Therefore, this feed-forward mechanism, that involves invading macrophages, oxidative stress, and Schwann cell TRPA1, was shown to be fundamental to sustain mechanical allodynia in mouse models of neuropathic pain.

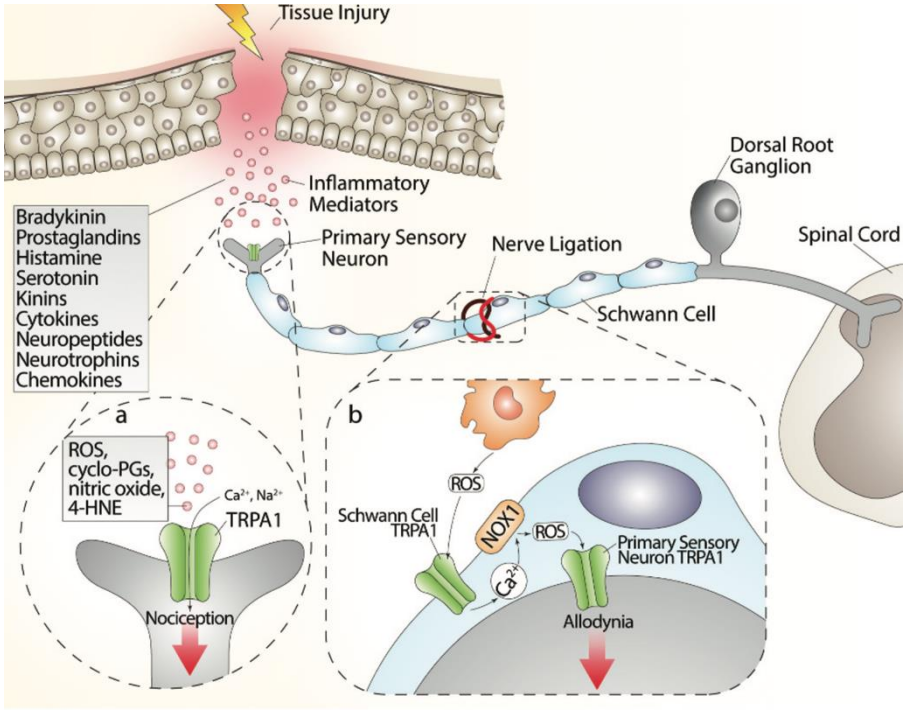

Figure 6. (a) Tissue injury induces the release of multiple inflammatory mediators, such as reactive oxygen (ROS), nitrogen (nitric oxide) and carbonylic (4-HNE) species, bradykinin, prostaglandins, histamine, serotonin, kinins, cytokines, neuropeptides, neurotrophins and chemokines. Some of these molecules directly activate TRPA1 in primary sensory neurons, whereas others modulate its activity indirectly, thus triggering electrical signal transmission to the CNS to generate acute pain. (b) The injured nerve trunk releases proinflammatory agents, including chemokines, which recruit macrophages within the lesioned area. The oxidative stress produced by activated macrophages targets TRPA1 in Schwann cells, which evokes a Ca^{2+}-dependent, NOX1-mediated amplification of oxidative stress byproducts release, which in turn targets nociceptor TRPA1 to signal mechanical allodynia [16].

Additionally, Schwann cell TRPA1 is necessary for macrophage invasion in the endoneurial area in a mouse model of complex regional pain syndrome type I (CRPS-I) induced by ischemia and reperfusion of a rat hind limb in order to promote and maintain allodynia [174]. In the CRPS-I model, the initial burst of oxidative stress after reperfusion sets off a feed-forward mechanism that causes the damaged nerve's resident macrophages and Schwann cell TRPA1 to sustain chronic neuroinflammation and allodynia. Mice that have Schwann cell TRPA1 selectively deleted showed reduced increases in macrophage infiltration, 4-HNE, mechanical allodynia, and cold allodynia [175]. The painful alcoholic neuropathy has also been linked to the TRPA1 channel. In a mouse model of ethanol-evoked neuropathic pain, acute ethanol administration led to delayed mechanical allodynia, and it has been suggested that Schwann cells expressing the nociceptive channel TRPA1 may be responsible for this poorly known process [176]. Schwann cell TRPA1 by producing oxidative stress in a macrophage-independent manner, maintains mechanical allodynia. Alcohol dehydrogenase-2 (ADH-2) does, in fact, convert ethanol into acetaldehyde, which, in an autocrine manner, targets Schwann cell TRPA1 to produce the burst of oxidative stress required to maintain persistent pain and neuroinflammation. This suggests that the involvement of active macrophages is not always necessary for the activation of the proalgesic Schwann cell TRPA1 pathway [177]. The role prominent role of Schwann cells in maintaining neuroinflammation in peripheral nerves and sustaining prolonged allodynia has recently been reported in a mouse model of periorbital mechanical allodynia (PMA). CGRP-mediated neuronal/ Schwann cell pathway mediates allodynia associated with neurogenic inflammation, contributing to the algesic action of CGRP. CLR/RAMP1activation in human and mouse Schwann cells generated long-lasting signals from endosomes that evoke cAMP-dependent formation of

NO. NO, by gating SC TRPA1, releases ROS, which in a feed-forward manner sustain allodynia *via* nociceptor TRPA1 [67].

AIM

Acute pain is a frequent and evolutionary conserved survival mechanism. Chronic pain, which can last for years, is linked to inflammatory disorders, peripheral and central neuropathies and cancer and it is a debilitating painful syndrome that affects 25% of European people. Pain, a common symptom of cancer that can reduce quality of life more than the disease itself, affects around 70% of cancer patients. It becomes more frequent and debilitating in the presence of bone metastases, which is a common consequence of many primary tumors, including breast cancer [178]. Thus, the burden of chronic pain is considerable in terms of health care, disability, and of both social and economic cost. Furthermore, chronic pain is expected to increase in the near future. The current medications for treating neuropathic pain are frequently ineffective. Identifying the mechanisms in the peripheral and central neural systems that maintain chronic pain (allodynia/hyperalgesia) is a major challenge in pain research.

Patients with cancer may have symptoms such as breakthrough pain, different types of spontaneous non-evoked pain, and augmented sensitivity to harmless or unpleasant stimuli (hyperalgesia), which may be brought on by a variety of mediators. However, little is known about the mechanisms driving both evoked and non-evoked (allodynia/hyperalgesia) cancer pain. Finding the fundamental mechanisms that underlie cancer pain as well as the molecular targets in the peripheral and central nervous systems for novel therapeutic therapies is a significant problem in pain research. To develop better and safer pain medications, it is crucial to identify such mechanisms and targets. However, it is essential to establish the cellular and molecular mechanisms involved in cancer-related pain before suggesting such a route as a good target for the discovery of new medications for cancer pain.

A key component of various models of inflammatory and neuropathic pain is the non-selective cation channel TRPA1, which is expressed by TRPV1-positive neurons and functions as a multisensor for a variety of unpleasant external and endogenous stimuli. The finding that TRPA1 is a target for a novel class of chemically diverse molecules, including those produced by oxidative stress, raises the possibility of a novel route combining TRPA1 and oxidative stress for creating neurogenic inflammation and for sensing pain. Among the TRP channels expressed in primary sensory neurons, TRPV4 has been connected to animal models of CIPN-evoked allodynia. Recent studies have also

emphasized the critical function of this channel in models of cancer pain and neuropathic pain. Furthermore, an expanding branch of studies demonstrates that ROS maintain pain hypersensitivity in a variety of neuropathic pain models, including as alcohol related peripheral neuropathy, diabetic neuropathy, peripheral nerve injury, and CIPN.

The primary goal of this three-year project was to identify the cellular and molecular mechanisms that, from cancer growth and treatment result in a chronic pain condition.

First, we aimed to study the mechanism underlying the CIPN-related pain symptoms caused by some chemotherapeutic drugs, such thalidomide and its derivatives. Thalidomide, an anti-emetic and sedative that was used in the past to treat nausea and vomiting but later banned for its potential to cause birth defects in humans, is now used to treat leprosy and a number of tumors, including multiple myeloma, myelodysplastic syndrome, and various solid tumors. Pomalidomide and lenalidomide, two thalidomide derivatives, also show anticancer activity in patients with multiple myeloma who relapse or are resistant to previous anticancer therapies. Unfortunately, thalidomide and its derivatives create a painful peripheral polyneuropathy that frequently ends in extreme discomfort or even the withdrawal of medication, just as other chemically unrelated chemotherapeutic medicines (platinum-based medications, taxanes, and bortezomib). According to a number of preclinical studies, antioxidants can reduce the mechanical and thermal hypersensitivity that chemotherapy-induced rodents experience. This is consistent with the idea that ROS contribute to CIPN. First, we questioned whether mice would have pain-like reactions to thalidomide, lenalidomide, and pomalidomide. Then we investigated the involvement of oxidative stress and TRPA1 and TRPV4 channels sensitive to oxidants in the mechanical and thermal hypersensitivities induced by thalidomide, lenalidomide, and pomalidomide since it is known that thalidomide administration causes oxidative stress in mice, rats, and humans.

In the second part of the project we aimed at deciphering the role of different mediators and the interplay between macrophages/microglia and Schwann cells/oligodendrocytes in the development and maintenance of cancer pain is focusing on morphological, biochemical and molecular changes that underline the shift from a normal to a hyperalgesic phenotype. In two mouse models of cancer pain, we first explored the implication of macrophages MΦs in mechanical allodynia. Then, we investigated the role of Schwann cell TRPA1 in the MΦ-dependent allodynia. In addition to revealing an

essential function of sciatic nerve resident macrophages (rMΦs), results obtained after B16-F10 melanoma cell inoculation revealed the role of Schwann cell TRPA1 to release M-CSF, which sustains rMΦ expansion, and to generate the oxidative stress that targets the neuronal TRPA1 to signal pain.

And then we studied a model of bone cancer pain. In the third part of the present project, we hypothesized that osteoclast-dependent osteolysis mediators target Schwann cells to elicit metastatic bone cancer pain. To address this hypothesis, we used adeno-associated virus (AAV)-mediated cell-specific IGF-1R silencing in Schwann cells or DRG neurons in a mouse model of metastatic bone cancer pain obtained by E0771 breast carcinoma cell inoculation into the mammary gland [179, 180]. Insulin growth factor-1 (IGF-1), an osteoclast-dependent osteolysis biomarker, contributes to metastatic bone cancer pain, but the underlying mechanism is poorly understood. In mice, the femur metastasis caused by intramammary inoculation of breast cancer cells resulted in IGF-1 increase in femur and sciatic nerve, and IGF-1-dependent stimulus/non-stimulus-evoked pain-like behaviors. Treatment of metastatic bone cancer pain represents a major medical challenge, as current therapies are insufficient, resulting in psychological distress, anxiety, and significantly reduced quality of life. The mechanism of metastatic bone cancer pain involves several interactions between tumor and bone cells, activated inflammatory cells, and bone-innervating neurons [181] [182]. Although bone resorption associated with the invasion of cancer cells has been considered as the primary cause of metastatic bone cancer pain [183], knowledge of the cellular and molecular mechanisms underlying metastatic bone cancer pain is limited.

Clarifying the involvement of Schwann cells-TRPA1 and oxidative stress in cancer-related pain is crucial since it may also have clinical implications for patients. The creation of novel therapeutic approaches that use the delivery of certain antagonists that specifically target TRPA1 channel could alleviate cancer-related pain and the neuropathy caused by the use of anticancer medications, improving the patients' quality of life.

RESULTS

4. Oxidative stress mediates thalidomide-induced pain by targeting peripheral TRPA1 and central TRPV4

4.1 Methods

Animals

In vivo experiments and tissue collections were carried out according to the European Union (EU) guidelines for animal care procedures and the Italian legislation (DLgs 26/2014) application of the EU Directive 2010/63/EU. Studies were conducted under the University of Florence research permit #204/2012-B. Sprague-Dawley rats (male, 75-100 g, 4-5 weeks) C57BL/6J mice (male, 20-25 g, 5 weeks) (Harlan Laboratories), wild-type (*Trpa1*$^{+/+}$) and TRPA1-deficient (*Trpa1*$^{-/-}$; B6129P-Trpa1$^{tm1Kykw/J}$; Jackson Laboratories) mice (25-30 g, 6-8 weeks) [184], wild-type (*Trpv4*$^{+/+}$) and TRPV4-deficient (*Trpv4*$^{-/-}$) mice (25-30 g, 5-8 weeks) [185], wild-type (*Trpv1*$^{+/+}$) and TRPV1-deficient (*Trpv1*$^{-/-}$; B6129X1-Trpv1$^{tm1Jul/J}$, Jackson Laboratories) mice (25-30 g, 5-8 weeks) generated by heterozygous mice on a C57BL/6J background, were used.

Study design

Group size of n=6 animals for behavioral experiments was determined by sample size estimation using G*Power (v3.1) [186] to detect size effect in a post-hoc test with type 1 and 2 error rates of 5 and 20%, respectively. Allocation concealment of mice to vehicle(s) or treatment(s) group was performed using a randomization procedure (http://www.randomizer.org/). Mice were housed in a temperature- and humidity-controlled vivarium (12 h dark/light cycle, free access to food and water). Behavioral experiments were done in a quiet, temperature-controlled (20-22 °C) room between 9 am and 5 pm and were performed by an operator blinded to genotype and drug treatment. Animals were anesthetized with a mixture of ketamine and xylazine (90 mg/kg and 3 mg/kg, respectively, intraperitoneal, i.p.) and euthanized with inhaled CO_2 plus 10-50% O_2.

C57BL/6J, *Trpa1*$^{+/+}$ or *Trpa1*$^{-/-}$, *Trpv4*$^{+/+}$ or *Trpv4*$^{-/-}$ and *Trpv1*$^{+/+}$ or *Trpv1*$^{-/-}$ mice were treated with thalidomide (1, 10, 50 and 100 mg/kg, i.p.) pomalidomide (1 mg/kg, i.p.) and lenalidomide (5 mg/kg, i.p.) or their vehicle. No weight loss was observed in mice

after the treatment throughout the duration of the experiments. The mechanical and thermal (hot and cold) allodynia of thalidomide, pomalidomide, and lenalidomide were monitored for 40 days starting 3 hours after drug administration.

Systemic (i.p.) HC-030031 (100 mg/kg), HC-067047 (10 mg/kg), phenyl-α-tert-butyl nitrone (PBN, 100 mg/kg) and capsazepine (4 mg/kg) and local (intraplantar, i.pl., 20 µl/site) and intrathecal (i.th., 5 µl/site) HC-030031 (100 µg), HC-067047 (100 µg) and PBN (100 µg) were administered at day 7 after thalidomide, pomalidomide or lenalidomide injection. The vehicle for drugs was 4% dimethyl sulfoxide, DMSO and 4% Tween80 in 0.9% NaCl.

Reagents

If not otherwise indicated, all reagents were from Sigma-Aldrich. HC-030031 (2-(1,3-Dimethyl-2,6-dioxo-1,2,3,6-tetrahydro-7H-purin-7-yl)-N-(4-isopropylphenyl) acetamide) was provided by Prof Delia Preti (University of Ferrara, Italy). HC-067047 was from Tocris Bioscience.

Behavioral studies

Rota-rod test. The locomotor function, coordination, and sedation of mice was assessed after drug administration. The animals were trained on a rotarod apparatus (Ugo Basile) at 8 rpm 24 hours before the test. The day of the experiment the number of falls was recorded. The cut-off time was 240 seconds [117].

Von Frey test. Mechanical allodynia was measured by using the up-and-down paradigm [187]. The mechanical threshold was determined before (basal level) and after drug administration. The 50% mechanical paw withdrawal threshold (g) response was calculated.

Acetone test. Cold allodynia was assessed as previously described [117]. Briefly, a droplet (50 µl) of acetone was gently applied to the plantar surface of the mouse hind paw, and the time spent in elevation and licking of the plantar region was recorded over a 60 second period. Acetone was applied three times at a 10-15 minute interval, and the average elevation/licking time was calculated. Nociception to the acetone test was detected before (basal) and after treatments.

Hot plate test. Mice were placed on a hot plate (Ugo Basile) set at 50 ± 0.1 °C. The latency to the first hind paw licking/withdrawal was taken as an index of the nociceptive threshold and detected before (basal) and after treatments. Cut-off time was set at 30 seconds.

Cell culture and isolation of primary sensory neurons

Human embryonic kidney (HEK293) cells stably transfected with the cDNA for human TRPA1 (hTRPA1-HEK293), or with the cDNA for human TRPV4 (hTRPV4-HEK293) and naive untransfected HEK293 cells (#RL-1573, American Type Culture Collection, ATCC) were cultured as previously described [188]. HEK293 and hTRPA1-HEK293 but not hTRPV4-HEK293 were further authenticated. Primary DRG neurons were isolated from rats or *Trpa1*$^{+/+}$ and *Trpa1*$^{-/-}$ mice. Briefly, lumbosacral (L5-S2) ganglia were enzymatically digested using 2 mg/ml of collagenase type 1A with 1 mg/ml of trypsin for rats or with 1 mg/ml of papain for mice in Hanks' Balanced Salt solution (HBSS, 35 minutes, 37 °C). Ganglia were then transferred to warmed Dulbecco's Modified Eagle Medium (DMEM) containing 10% fetal bovine serum (FBS), 10% horse serum, 2 mM L-glutamine, 100 U/ml penicillin and 100 mg/ml streptomycin and mechanically dissociated in single cells. Neurons were filtered, centrifuged (6 minutes, x1.200 rpm) at room temperature (RT) and resuspended in DMEM with added 100 ng/ml mouse-nerve growth factor and 2.5 mM cytosine-b-D-arabino-furanoside free base. The resuspended cells were plated on glass coverslips coated with Poly-L-Lysine (8.3 µM) and laminin (5 µM) and cultured for 3-4 days (37 °C) before calcium imaging or whole-cell patch-clamp recordings.

Cellular recordings

Intracellular calcium was measured as previously reported [188]. Cells were exposed to H_2O_2 (30 µM-10 mM) or its vehicle (0.9% NaCl). HC-030031 (30 µM), HC067047 (10 µM), or their vehicles (3% and 1.5% DMSO, respectively), dithiothreitol (DTT, 10 mM) and 2-mercaptoethanol (β-ME, 50 mM) or their vehicles (0.9% NaCl) were applied 10 minutes before the stimuli. Results were expressed as the percentage of increase of ratio$_{340/380}$ ($R_{340/380}$) over the baseline normalized to the maximum effect induced by ionomycin (5 µM) added at the end of each experiments. Whole-cell patch-clamp recordings were performed as reported [188]. Currents were evoked in the voltage-clamp mode at a holding potential of -60 mV; signals were sampled at 1 kHz and low-pass filtered at 10 kHz. Cells were stimulated with thalidomide, pomalidomide and lenalidomide (all, 100 µM) or their vehicle (1% DMSO), allyl isothiocyanate (AITC, 100 µM), capsaicin (CPS, 1 µM) and the TRPV4 agonist, 4α-phorbol 12,13-didecanoate (4-alpha-PDD, 100 µM) or their vehicle (0.1% DMSO). Peak currents were normalized to

cell membrane capacitance and expressed as mean of the current density (pA/pF) in averaged results.

H_2O_2 measurement

The H_2O_2 content was determined in the tissues by using the Amplex Red® assay (Invitrogen). Tissues were collected and placed into modified Krebs/HEPES buffer containing (in mM): 99.01 NaCl, 4.69 KCl, 2.50 $CaCl_2$, 1.20 $MgSO_4$, 1.03 KH_2PO_4, 25.0 $NaHCO_3$, 20.0 Na-HEPES, and 5.6 glucose, pH 7.4, minced, and incubated with Amplex Red (100 μM) and horseradish peroxidase (HRP, 1 U/ml) (1 hour, 37 °C) protected from light. Fluorescence excitation and emission were at 540 and 590 nm, respectively. H_2O_2 production was calculated using H_2O_2 standard and expressed as μmol/l/mg of dry tissue.

Immunofluorescence

Mice were anesthetized, transcardially perfused with PBS (phosphate buffer saline), followed by 4% paraformaldehyde, and tissues were collected, post-fixed for 24 hours, and paraffin embedded. Antigen retrieval was performed in sodium citrate buffer (10 mM sodium citrate, 0.05% Tween 20, pH 6.0) (20 minutes, 98 °C). The slides were then incubated with the 4-HNE primary antibody (#ab48506, HNEJ-2, mouse monoclonal, 1:40, Abcam) diluted in fresh blocking solution (PBS, pH 7.4, 2.5% normal goat serum) 1 hour at RT, followed by a fluorescent polyclonal secondary antibodies Alexa Fluor 594 (1:600; Invitrogen) 1 hour at RT, and cover-slipped with mounting medium with 4′,6-diamidino-2-phenylindole (DAPI, #ab228549, Abcam). Fluorescence images were obtained using an AxioImager 2 microscope (Carl Zeiss). The fluorescence intensity of 4-HNE staining was evaluated by the image processing module of ZEN Pro (Carl Zeiss).

Statistical analysis

Data are presented as mean ± SEM. For behavioral experiments with repeated measures, a two-way mixed model was used to compare the control and treated groups of mice at each time point tested, using the Bonferroni's correction for multiple time points. The one-way ANOVA followed by the Bonferroni's correction was used for comparison between multiple groups. Agonist potency was expressed as half maximal effective concentration (EC_{50}). Statistical analyses were performed on raw data using Prism 8

GraphPad software (GraphPad Software Inc.). P<0.05 was considered statistically significant.

4.2 Results

4.2.1 Thalidomide evokes mechanical and cold hypersensitivity mediated by TRPA1 and TRPV4

To explore whether thalidomide elicited sensory hypersensitivities in mice, we administered a single i.p. injection of increasing doses (1, 10, 50 and 100 mg/kg) of the drug, or its vehicle, in C57BL/6J mice. We observed a dose-dependent, early (3 hours after administration) and prolonged (~35 days) mechanical and cold allodynia (**Fig.7A** and **7B**). In contrast, any dose of thalidomide failed to evoke hypersensitivity to thermal (hot) stimuli (**Fig.7C**). Further mechanistic studies were performed in mice treated with a single dose (50 mg/kg, i.p.) of thalidomide, which, after the man to mouse conversion [189], approximates the dose used in patients [190].

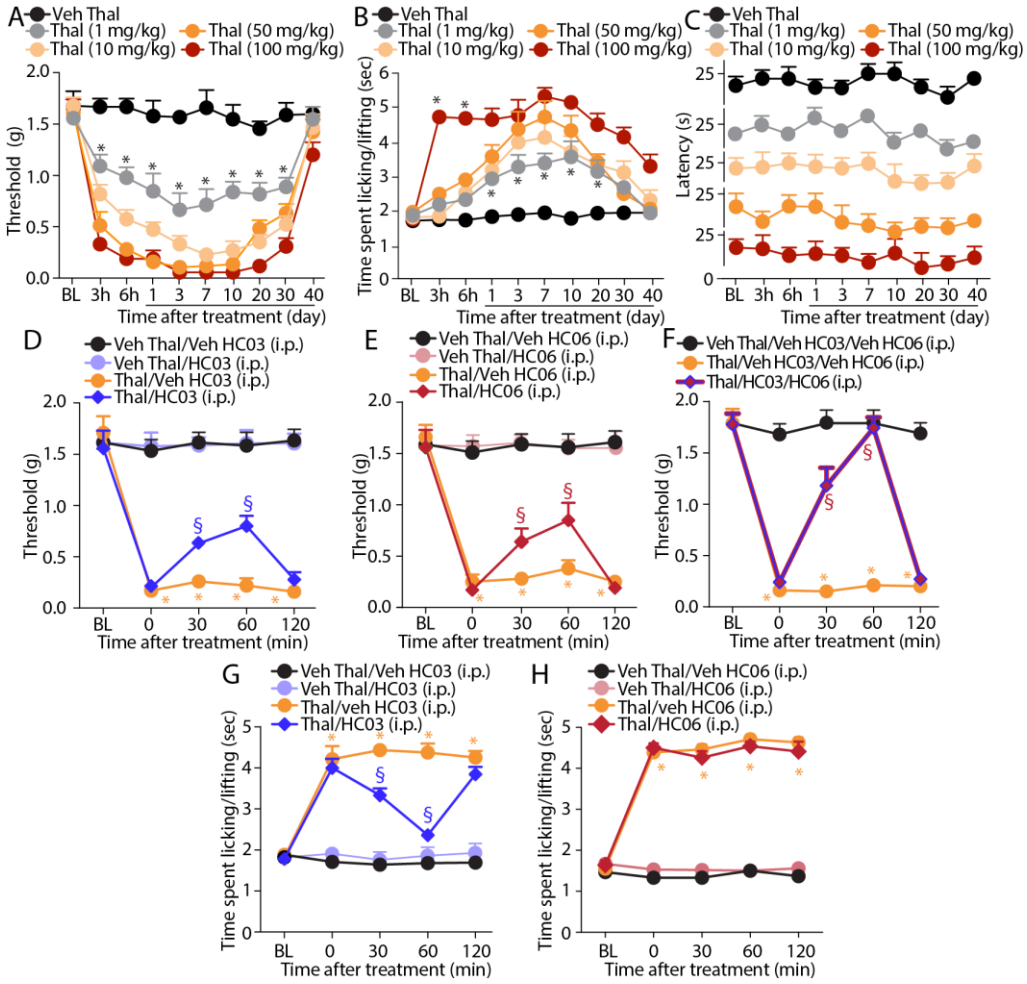

Figure7. Thalidomide elicits mechanical and cold, but not heat, hypersensitivity that is dependent on TRPA1 and TRPV4. **A-C**, Dose- and time- dependent mechanical and cold allodynia and heat hypersensitivity following intraperitoneal (i.p.) injection of thalidomide (Thal, 1, 10, 50 and 100 mg/kg) or Veh. **D-F**, Mechanical allodynia at day 7 following Thal (50 mg/kg, i.p.) and Veh and after the administration of HC-030031 (HC03, 100 mg/kg, i.p.), HC-067047 (HC06, 10 mg/kg, i.p.), a combination of HC03 (100 mg/kg, i.p.) and HC06 (10 mg/kg, i.p.) or Veh. **G-H**, Cold allodynia at day 7 following Thal (50 mg/kg, i.p.) or Veh and after the administration of HC03 (100 mg/kg, i.p.), HC-067047 (HC06, 10 mg/kg, i.p.) or Veh. BL, baseline. Data are mean ± SEM, n = 6 mice. **P*<0.05 *vs.* Veh Thal or Veh Thal/Veh HC03/Veh HC06; §*P*<0.05 *vs.* Thal/Veh HC03/Veh HC06. Two-way ANOVA followed by Bonferroni's post hoc test.

To test the implication of TRP channels, both pharmacological and genetic tools were used. Seven days after thalidomide administration, when the allodynia plateaued, systemic (i.p.) administration of the selective TRPA1 antagonist, HC-030031 (100 mg/kg) [78], partially reversed mechanical allodynia (**Fig.7D**), without affecting the basal threshold value in naive animals (**Fig.7D**). Because of the incomplete inhibition produced by TRPA1 antagonism, the role of TRPV4 and TRPV1 was explored. The TRPV1 antagonist, capsazepine (4 mg/kg, i.p.), given at day 7 after thalidomide or vehicle, failed to affect mechanical allodynia (**Fig.8A**). Conversely, systemic (i.p.) administration of the selective TRPV4 antagonist, HC-067047 (10 mg/kg, at day 7 after thalidomide or vehicle) [191], which did not affect the baseline threshold value in vehicle-treated animals (**Fig. 7E**), partially attenuated mechanical allodynia (**Fig.7E**). However, a combination of TRPA1 and TRPV4 antagonists completely reversed thalidomide-evoked mechanical allodynia (**Fig.7F**). Cold allodynia, induced by thalidomide, resulted to be exclusively dependent on TRPA1 as HC-030031 administered at day 7 after thalidomide completely attenuated the response to the cold stimulation, while administration of HC-067047 or capsazepine was ineffective (**Fig.7G** and **7H** and **Fig. 8B**).

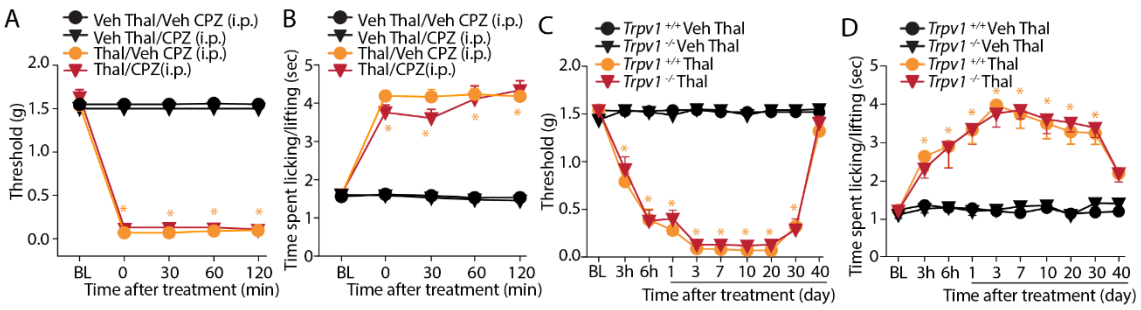

Figure 8. Genetic deletion or pharmacological blockade of TRPV1 does not affect mechanical and cold hypersensitivity evoked by thalidomide. **A** and **B**, Mechanical and

cold allodynia at day 7 following intraperitoneal (i.p.) injection of thalidomide (Thal, 50 mg/kg) or Veh and after the administration of capsazepine (CPZ, 4 mg/kg, i.p.) or Veh. **C** and **D,** Time-dependent mechanical and cold allodynia following Thal (50 mg/kg, i.p.) or Veh in *Trpv1*$^{+/+}$ or *Trpv1*$^{-/-}$ mice. BL, baseline. Data are mean ± SEM, n = 6 mice. **P*<0.05 *vs.* Veh Thal/Veh CPZ or *Trpv1*$^{+/+}$/Veh Thal. Two-way ANOVA followed by Bonferroni's post hoc test.

To further prove the contribution of TRP channels, mice with genetic deletion of TRPA1, TRPV4 or TRPV1 were used. *Trpa1*$^{+/+}$, *Trpv4*$^{+/+}$ and *Trpv1*$^{+/+}$ mice developed mechanical and cold hypersensitivity with time courses similar to those observed in C57BL/6J mice, starting 3 hours and lasting ~35 days after thalidomide administration (**Fig.9A** and **9B** and **Fig.8C**). While *Trpv1*$^{-/-}$ mice showed unchanged mechanical hypersensitivities (**Fig.8C**), in *Trpa1*$^{-/-}$ and *Trpv4*$^{-/-}$ mice, thalidomide-evoked mechanical allodynia was significantly, but not completely, reduced (**Fig.9A** and **9B**). The relative contribution of TRPA1 and TRPV4 to thalidomide-evoked mechanical allodynia was further investigated by evaluating the combined effect of channel pharmacological antagonism and genetic deletion. Thus, mechanical allodynia at day 7 after thalidomide injection was completely attenuated in *Trpa1*$^{-/-}$ treated with HC-067047 (10 mg/kg, i.p.) and in *Trpv4*$^{-/-}$ mice treated with HC-030031 (100 mg/kg, i.p.) (**Fig.9C** and **9D**). Cold allodynia observed in *Trpa1*$^{+/+}$, *Trpv4*$^{+/+}$ and *Trpv1*$^{+/+}$ was completely abolished in *Trpa1*$^{-/-}$ mice and unaffected in both *Trpv4*$^{-/-}$ and *Trpv1*$^{-/-}$ mice (**Fig.9E** and **9F** and **Fig.8D**).

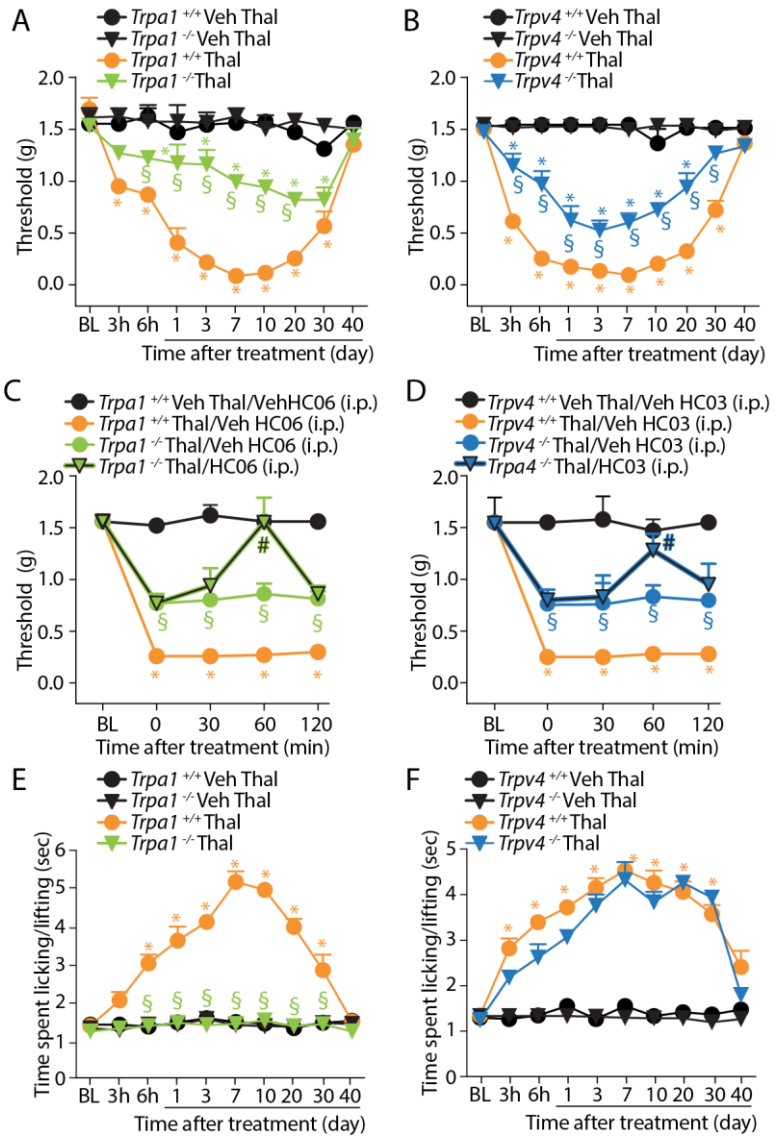

Figure 9. Genetic deletion of TRPA1 and TRPV4 attenuates mechanical and cold hypersensitivity evoked by thalidomide. **A** and **B,** Time-dependent mechanical allodynia following intraperitoneal (i.p.) injection of thalidomide (Thal, 50 mg/kg) or Veh in *Trpa1*$^{+/+}$, *Trpa1*$^{-/-}$, *Trpv4*$^{+/+}$ and *Trpv4*$^{-/-}$ mice. **C,** Mechanical allodynia in *Trpa1*$^{+/+}$ and *Trpa1*$^{-/-}$, *Trpv4*$^{+/+}$ and *Trpv4*$^{-/-}$ mice at day 7 following Thal (50 mg/kg, i.p.) or Veh and after the administration of HC-067047 (HC06, 10 mg/kg, i.p.) or Veh in *Trpa1*$^{-/-}$ mice and HC-030031 (HC03, 100 mg/kg, i.p.) or Veh in *Trpv4*$^{-/-}$ mice. **E** and **F**, Time-dependent cold allodynia following Thal (50 mg/kg, i.p.) or Veh in *Trpa1*$^{+/+}$, *Trpa1*$^{-/-}$, *Trpv4*$^{+/+}$ or *Trpv4*$^{-/-}$ mice. BL, baseline. Data are mean ± SEM, n = 6 mice. **P*<0.05 *vs.* *Trpa1*$^{+/+}$/Veh Thal or *Trpv4*$^{+/+}$/Veh Thal or *Trpa1*$^{+/+}$/ Veh Thal/ Veh HC06or *Trpv4*$^{+/+}$/Veh Thal/Veh HC03; §*P*<0.05 *vs.* *Trpa1*$^{+/+}$/ Thal or *Trpv4*$^{+/+}$/ Thal or *Trpa1*$^{+/+}$/ Thal/Veh HC06 or *Trpv4*$^{+/+}$/Thal/Veh HC03; $^{\#}$*P*<0.05 *vs.* *Trpa1*$^{-/-}$/Thal/Veh HC06 or *Trpv4*$^{-/-}$/Thal/Veh HC03. Two-way ANOVA followed by Bonferroni's post hoc test.

4.2.2 Pomalidomide and lenalidomide evoke mechanical and cold allodynia similar to thalidomide

The two newer derivatives of thalidomide, pomalidomide and lenalidomide, used for the treatment of multiple myeloma and other hematological conditions [192], have been reported to evoke CIPN [193, 194]. Thus, the ability of pomalidomide and lenalidomide to induce mechanical and thermal hypersensitivity was explored in mice. Systemic administration of amounts of pomalidomide (1 mg/kg, i.p.) and lenalidomide (5 mg/kg, i.p.), equivalent in mice to the respective therapeutic doses, induced a time-dependent mechanical and cold allodynia that initiated 3 hours and lasted 35 days after drug administration (**Fig.10A** and**10B**). The two drugs did not affect the threshold value to heat stimuli (**Fig.10C**). Seven days after pomalidomide and lenalidomide administration, treatment with HC-030031 (100 mg/kg, i.p.) or HC-067047 (10 mg/kg, i.p.) partially reversed mechanical allodynia (**Fig.10D** and **10E**), which was, however, completely attenuated in mice receiving a combination of HC-030031 and HC-067047 (**Fig.10F**). Cold allodynia evoked by pomalidomide and lenalidomide was entirely inhibited by HC-030031, whereas HC-067047 was ineffective (**Fig.10H-10J**). Thalidomide, pomalidomide and lenalidomide did not affect motor coordination in mice, evaluated by using the rotarod test, as no falls were observed in mice receiving the drugs, nor did they exhibit writhing or stereotypic behaviors, such as freezing or hyperactivity, curling, grooming or biting/licking, after thalidomide injection. Present pharmacological and genetic findings indicate that TRPA1 and TRPV4 channels contribute to the mechanical allodynia induced by thalidomide and its derivatives, but only TRPA1 mediates cold hypersensitivity caused by these drugs.

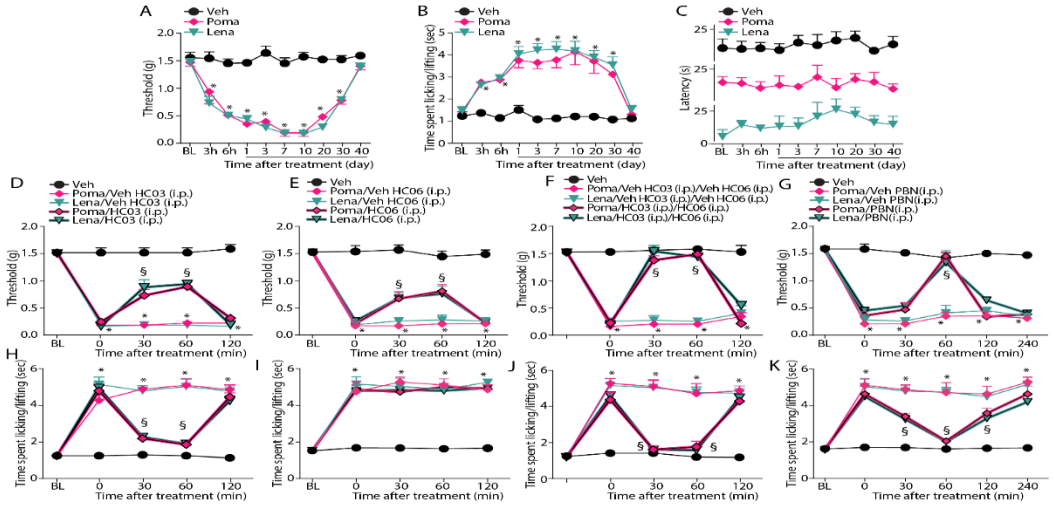

Figure.10 Pomalidomide and lenalidomide evoke mechanical and cold allodynia**. A-C,** Dose- and time- dependent mechanical, cold and heat hypersensitivity following intraperitoneal (i.p.) pomalidomide (Poma, 1 mg/kg), lenalidomide (Lena, 5 mg/kg) or Veh. **D**-**F**, Mechanical allodynia at day 7 following Poma (1 mg/kg, i.p.) and Lena (5 mg/kg, i.p.) or Veh and after the administration of HC-030031 (HC03, 100 mg/kg, i.p.), HC-067047 (HC06, 10 mg/kg, i.p.) or a combination of HC03 (100 mg/kg, i.p.) and HC06 (10 mg/kg, i.p.) or Veh. **H-J**, Cold allodynia at day 7 following Poma (1 mg/kg, i.p.) and Lena (5 mg/kg, i.p.) or Veh and after the administration of HC03 (100 mg/kg, i.p.), HC06 (10 mg/kg, i.p.) or a combination of HC03 (100 mg/kg, i.p.) and HC06 (10 mg/kg, i.p.) or Veh. **G** and **K**, Mechanical and cold allodynia at day 7 following Poma (1 mg/kg, i.p.) and Lena (5 mg/kg, i.p.) or Veh and after the administration of phenyl-α-tert-butyl nitrone (PBN, 100 mg/kg, i.p.). Data are mean ± SEM, n = 6 mice. **P*<0.05 *vs.* Veh; §*P*<0.05 *vs.* Poma/Lena/Veh HC03/Veh HC06 or Poma/Lena/Veh PBN. Two-way ANOVA followed by Bonferroni's post hoc test.

4.2.3 Thalidomide and its derivatives elicit hypersensitivity *via* oxidative stress generation that targets TRPA1 and TRPV4

To test the hypothesis that thalidomide and its derivatives directly activate both the TRPA1 and TRPV4 receptors, we studied the ability of the drugs to elicit an inward current in cultured rat DRG neurons. Thalidomide, pomalidomide and lenalidomide (all 100 μM) failed to evoke any inward current in capsaicin sensitive DRG neurons (**Fig.11A**), which otherwise responded to the TRPA1 and TRPV4 agonist, AITC (100 μM) and 4-αPDD (100 μM), respectively. Like other anticancer drugs, thalidomide and its derivatives are known to generate oxidative stress [195, 196]. Thus, we hypothesized that oxidative stress burst, and its reactive byproducts generated by thalidomide, pomalidomide and lenalidomide, could be implicated in mechanical and cold allodynia evoked by the anticancer drug. Systemic (i.p.) administration of the ROS scavenger, PBN (100 mg/kg), at day 7 after the administration of the three drugs abated mechanical and cold allodynia (**Fig.11B** and **11C** and **Fig.10G** and **10K**), thus supporting a role of oxidative stress. PBN did not affect the basal threshold value in naive animals.

While strong evidence has been accumulated on the ability of H_2O_2 to activate TRPA1 [197], only H_2O_2-mediated activation of TRPV4 was reported in human and rodent (rat and mouse) lung microvascular endothelial cells [198] and indirectly in rat brain slices [199]. Here, we show that H_2O_2 elicited concentration-dependent Ca^{2+} responses in hTRPV4-HEK293 cells, with an EC_{50} (5 mM) 10 times higher than that observed in hTRPA1-HEK293 cells (EC_{50} = 500 μM) (**Fig.11D**). The Ca^{2+} response evoked by a lower H_2O_2 concentration (500 μM) in hTRPA1-HEK293 was inhibited in the presence of HC-030031, but not of HC-067047, (**Fig.11E**). However, the Ca^{2+} response evoked by

H_2O_2 (5 mM) in hTRPV4-HEK293 was attenuated by HC-067047, but not by HC-030031. H_2O_2 (500 µM or 5 mM) was ineffective in untransfected HEK293 cells (**Fig.11E**). Considering that H_2O_2 caused TRPA1 activation *via* the oxidization of cysteine residues [197], we tested the hypothesis that oxidation by H_2O_2 of TRPV4 implicates cysteine residues. In hTRPV4-HEK293, exposure to two cysteine-reducing agents, DTT and β-ME [197] attenuated the Ca^{2+} response evoked by H_2O_2 in hTRPV4-HEK293 cells (**Fig. Fig.11F**). Finally, we tested low (500 µM) and high (5 and 10 mM) H_2O_2 concentrations in cultured mouse DRG neurons taken from *Trpa1*$^{+/+}$ and *Trpa1*$^{-/-}$ mice. The lower H_2O_2 concentration (500 µM) elicited a Ca^{2+} response in neurons from *Trpa1*$^{+/+}$ mice, but not in those from *Trpa1*$^{-/-}$ mice (**Fig.11G**). The residual calcium response to a higher concentration of H_2O_2 (10 mM) observed in DRG neurons from *Trpa1*$^{-/-}$ mice was abated in the presence of HC-067047 (**Fig.11G**). Thus, *in vitro* data confirmed the ability of H_2O_2 to target the TRPV4 channel, provided that the concentration/dose of H_2O_2 is sufficiently high.

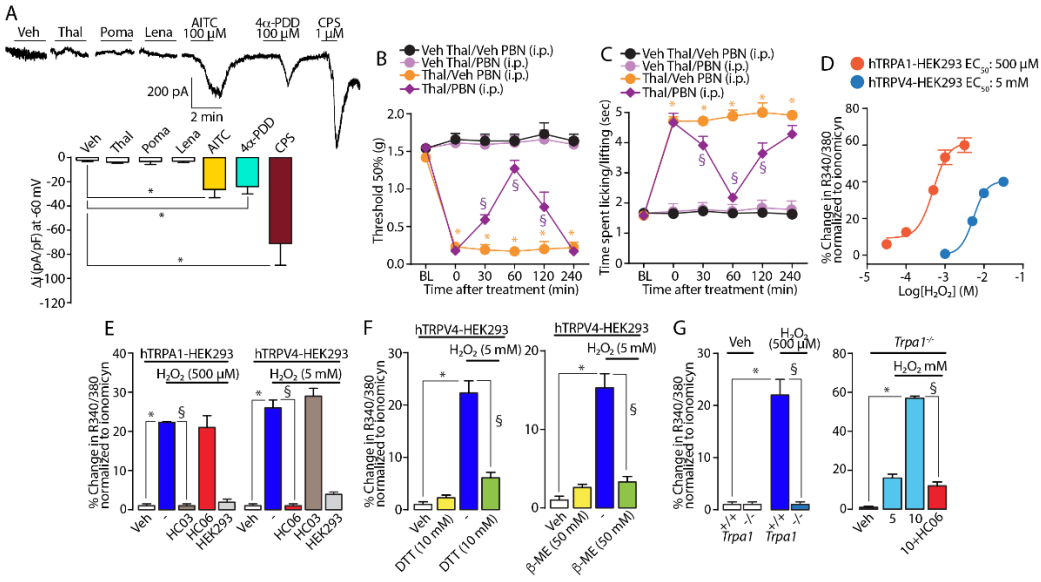

Figure 11. Oxidative stress targets TRPA1 and TRPV4. **A**, Typical traces and pooled data of patch-clamp inward currents elicited by thalidomide (Thal), pomalidomide (Poma) and lenalidomide (Lena) (all, 100 µM), allyl isothiocyanate (AITC, 100 µM), 4α-phorbol 12,13-didecanoate (4α-PDD, 100 µM), capsaicin (CPS, 1 µM) or Veh in mouse dorsal root ganglion (DRG) neurons. Data are mean ± SEM, n = 4-5 cells. **P*<0.05 *vs.* Veh. One-way ANOVA followed by Bonferroni's post hoc test. **B** and **C**, Mechanical and cold allodynia at day 7 following the intraperitoneal (i.p.) injection of thalidomide (Thal, 50 mg/kg) or Veh, and after the administration of phenyl-α-tert-butyl nitrone (PBN, 100 mg/kg, i.p.) or Veh. Data are mean ± SEM, n = 6 mice. **P*<0.05 *vs.* Veh Thal/Veh PBN; §*P*<0.05 *vs.* Thal/Veh PBN. Two-way ANOVA followed by Bonferroni's post hoc test. **D**, Concentration response (Ca^{2+}-mobilization)-curve to H_2O_2 in cultured hTRPA1-HEK293 and hTRPV4-HEK293 transfected cells. **E**, Pooled data of Ca^{2+}-response to

H_2O_2 (500 µM and 5 mM) or Veh in untransfected HEK293 or hTRPA1-HEK293, hTRPV4-HEK293 cells in presence of HC-030031 (HC03, 30 µM) or HC-067047 (HC06, 10 µM). **F**, Pooled data of the Ca^{2+}-response to H_2O_2 (5 mM) in hTRPV4-HEK293 cells in the presence of dithiothreitol (DTT, 10 mM) or 2-mercaptoethanol (β-ME, 50 mM). **G**, Pooled data of the Ca^{2+}-response to H_2O_2 (500 µM) in DRG neurons from *Trpa1*$^{+/+}$ and *Trpa1*$^{-/-}$ mice and H_2O_2 (5 and 10 mM) in DRG neurons from *Trpa1*$^{-/-}$ mice in presence of HC06 (10 µM). Data are mean ± SEM, n = 20-25 neurons or 80-100 cells. **P*<0.05 *vs.* Veh; §*P*<0.05 *vs.* H_2O_2 (500 µM, 5 mM or 10 mM). One-way ANOVA followed by Bonferroni's post hoc test.

4.2.4 Peripheral and central (spinal) TRPA1 and TRPV4 activation differentially contributes to thalidomide-induced mechanical allodynia

One major issue raised by the present data is that, while oxidative stress inhibition completely attenuated mechanical allodynia, TRPA1 or TRPV4 pharmacological antagonism or gene deletion provided partial reduction, and total reduction was attained solely by the simultaneous inhibition of both channels. A recent study reported that oxidative stress generated at central or peripheral sites may contribute differently to cisplatin and paclitaxel-evoked hypersensitivity [200]. Thus, we hypothesized whether oxidative stress activates TRPA1 and TRPV4 at different anatomical sites to mediate thalidomide-evoked mechanical allodynia. To test this hypothesis, we measured two oxidative stress biomarkers, H_2O_2 and the more stable peroxidation product of plasma membrane phospholipid peroxidation, 4-HNE [104]. H_2O_2 levels (**Fig.12A**) and 4-HNE staining (**Fig.12B**) were increased in homogenates or tissues slices, respectively, of the hind paw, sciatic nerve and lumbar spinal cord, taken from mice at day 7 after thalidomide, compared to its vehicle. Systemic treatment with a dose of PBN that reversed thalidomide-evoked allodynia reduced H_2O_2 levels and 4-HNE staining in all three tissues (**Fig.12A** and **12B**). Thus, while oxidative stress produced at each site may potentially contribute to thalidomide-evoked mechanical allodynia, the role of centrally *vs.* peripherally generated oxidative stress is unknown.

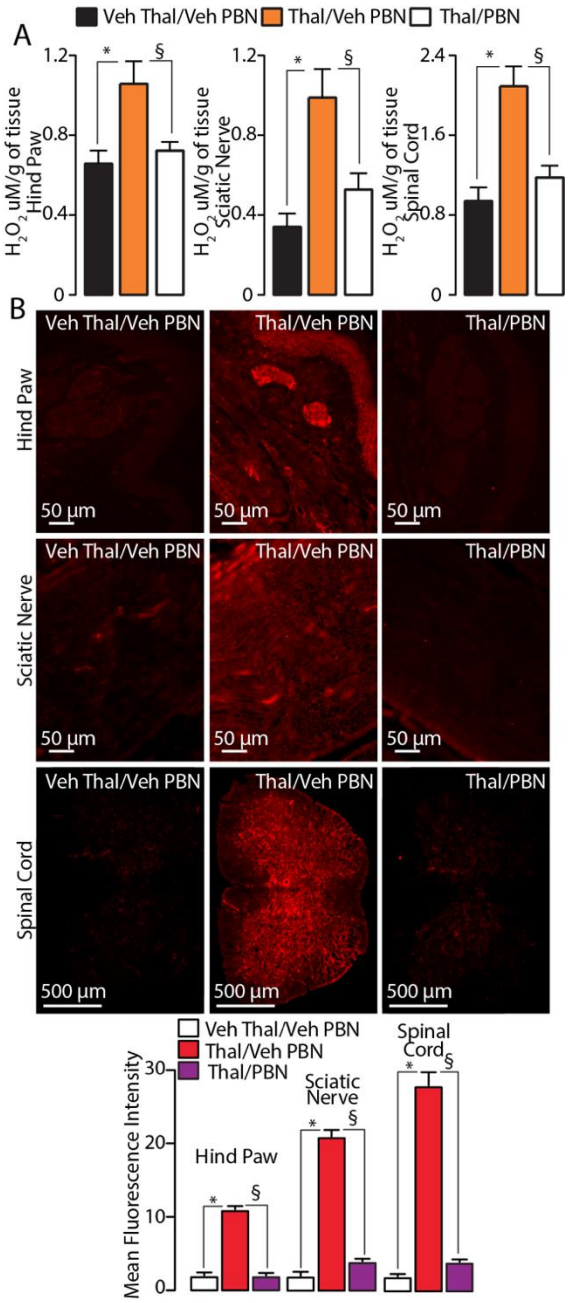

Figure 12. Thalidomide increases oxidative stress in the hind paw, sciatic nerve and spinal cord. **A,** H_2O_2 levels in the hind paw, sciatic nerve and spinal cord at day 7 following intraperitoneal (i.p.) injection of thalidomide (Thal, 50 mg/kg) or Veh and 60 minutes after the administration of phenyl-α-tert-butyl nitrone (PBN, 100 mg/kg, i.p.) or Veh. **B** and **C,** Representative images and mean fluorescence 4-HNE staining in the hind paw, sciatic nerve and spinal cord at day 7 following Thal (50 mg/kg, i.p.) and 60 minutes after the administration of PBN (100 mg/kg, i.p.) or Veh. Data are mean ± SEM (n = 6 mice). **P*<0.05 *vs.* Veh Thal/Veh PBN; §*P*<0.05 *vs.* Thal/Veh PBN. One-way ANOVA followed by Bonferroni's post hoc test.

To explore this hypothesis, we investigated the implication of peripheral *vs.* central TRPA1 and TRPV4 in thalidomide-induced mechanical allodynia, by injecting channel

antagonists locally in the hind paw or intrathecally in the brain. We found that, at day 7 after thalidomide, mechanical allodynia was partially reversed by the i.pl. injection of HC-030031 (100 µg), but not of HC-067047 (100 µg) (**Fig.13A**). In contrast, i.th. HC-067047 (100 µg), but not HC-030031 (100 µg), partially reversed thalidomide-induced mechanical allodynia (**Fig.13B**). Neither i.th. nor i.pl. HC-030031 and HC-067047 affect the basal threshold value in naive animals. These results implicated the engagement of peripheral TRPA1 and central TRPV4 in the thalidomide-induced mechanical allodynia. To further support this hypothesis, at day 7 after thalidomide injection, we tested the ability of a combination of i.pl. HC-067047 and i.th. HC-030031, or *vice versa*, to attenuate thalidomide-evoked mechanical allodynia. While a combination of i.pl. HC-067047 and i.th. HC-030031 failed to affect allodynia (**Fig.13C**), a combination of i.pl. HC-030031 and i.th. HC-067047 provided complete reversal of the pain-like response (**Fig.13D**), thus supporting the view that TRPA1 mediates the peripheral, and TRPV4 the central, component of thalidomide-evoked mechanical allodynia.

To understand how the increased oxidative stress could engage the peripheral TRPA1 and the central TRPV4, PBN was given to mice by either i,pl. or i.th. administration. At day 7 after thalidomide, i.pl. (100 µg) or i.th. (100 µg) PBN injection partially inhibited mechanical allodynia (**Fig.13E** and **13F**), while a combination of i.pl. and i.th. PBN completely attenuated the response (**Fig.13G**). However, cold allodynia, which is entirely TRPA1-dependent, was completely reversed by i.pl. PBN (**Fig.13H**). PBN (i.pl. or i.th.) did not affect the basal threshold value in vehicle treated mice. We also found that i.th. PBN, while partially reversing mechanical allodynia in *Trpa1*$^{+/+}$ and *Trpv4*$^{+/+}$ mice (**Fig.13I** and **13J**), did not affect the residual mechanical allodynia in *Trpv4*$^{-/-}$ (**Fig.13I**), and completely reversed the response in *Trpa1*$^{-/-}$ mice (**Fig.13J**). Altogether, these data indicate that selective ROS scavenging at either the peripheral or central levels inhibits the correspondent TRPA1 and TRPV4 component, respectively. Only simultaneous inhibition of the oxidative stress that targets both ion channels warrants complete attenuation of the mechanical allodynia.

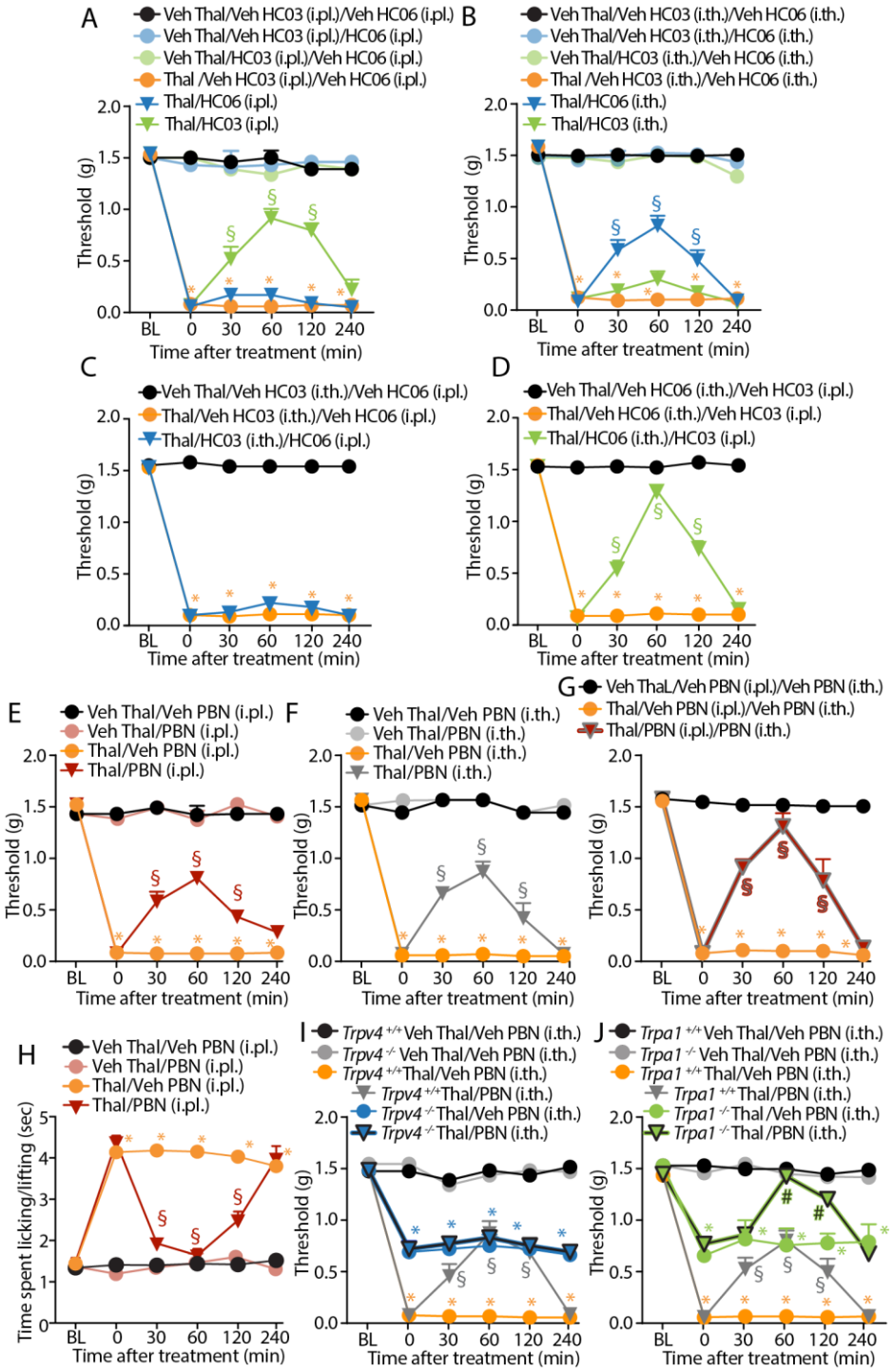

Figure 13. Peripheral TRPA1 and central TRPV4 contribute to thalidomide-induced mechanical allodynia. **A** and **B,** Mechanical allodynia at day 7 following intraperitoneal (i.p.) thalidomide (Thal, 50 mg/kg) or Veh and after the administration of intraplantar (i.pl., 20 µl) or intrathecal (i.th., 5 µl) HC-030031 (HC03, 100 µg), HC-067047 (HC06, 100 µg) or Veh. **C** and **D**, Mechanical allodynia at day 7 following Thal (50 mg/kg, i.p.) or Veh and after the administration of a combination of HC03 (100 µg, i.th.) and HC06 (100 µg, i.pl.) or HC06 (100 µg, i.th.) and HC03 (100 µg, i.pl.) or Veh. **E-G**, Mechanical allodynia at day 7 following Thal (50 mg/kg, i.p.) or Veh and after the administration of i.pl. or a combination of i.pl. and i.th phenyl-α-tert-butyl nitrone (PBN, 100 µg) or Veh. **H**, Cold allodynia at day 7 following Thal (50 mg/kg, i.p.) or Veh and after the

administration of i.pl. PBN (100 µg) or Veh. **I** and **J**, Mechanical allodynia in *Trpv4*$^{+/+}$, *Trpv4*$^{-/-}$, *Trpa1*$^{+/+}$ and *Trpa1*$^{-/-}$ mice at day 7 following Thal (50 mg/kg, i.p.) or Veh and after the administration of i.th. PBN (100 µg) or Veh. Data are mean ± SEM, n = 6 mice. **P*<0.05 *vs.* Veh Thal/Veh HC03/Veh HC06 or veh Thal/Veh PBN; §*P*<0.05 *vs.* Thal/Veh HC03/Veh HC06 or Thal/Veh PBN; $^{\#}$*P*<0.05 *vs. Trpa1*$^{-/-}$/Thal/Veh PBN. Two-way ANOVA followed by Bonferroni's post hoc test.

5. Peripheral Nerve Resident Macrophages and Schwann cells Mediate Cancer Induced Pain

5.1 Methods

Study design

The group size of n = 6 animals for behavioral experiments was determined by sample size estimation using G*Power (v3.1) [201] to detect size effect in a post-hoc test with type 1 and 2 error rates of 5 and 20%, respectively. Allocation concealment of mice to vehicle(s) or treatment(s) group was performed using a randomization procedure (http://www.randomizer.org/). The assessors were blinded to the identity (genetic background or allocation to treatment group) of the animals. Identity of the animals was unmasked to assessors only after data collection. No animals were excluded from experiments. Outliers were included in the analyses.

All experiments and sample collections were carried out according to the European Union (EU) guidelines for animal care procedures and the Italian legislation (DLgs 26/2014) application of the EU Directive 2010/63/EU. Studies were conducted under University of Florence research permits (#579/2017-PR). The behavioral studies followed the animal research reporting *in vivo* experiment (ARRIVE) guidelines.

Animals

Adult C57BL/6J (male and female 20-25 g, 5-6 weeks), littermate wild type (*Trpa1*$^{+/+}$) and TRPA1-deficient (*Trpa1*$^{-/-}$) mice (male, 25-30 g, 6-8 weeks), generated by heterozygotes on a C57BL/6J background (B6.129P-*Trpa1*^{tm1Kykw}/J; RRID:IMSR_JAX:006401 Jackson Laboratories) [51], were used. To generate mice in which the *Trpa1* gene was conditionally silenced in Schwann cells/oligodendrocytes, homozygous 129S-Trpa1^{tm2Kykw}/J (*floxed TRPA1, Trpa1*$^{fl/fl}$, Stock No: 008649, RRID:IMSR_JAX:008649 Jackson Laboratories), were crossed with hemizygous B6.Cg-Tg(Plp1-CreERT)3Pop/J mice (Plp1-CreERT, Stock No: 005975, RRID:IMSR_JAX:005975 Jackson Laboratories), expressing a tamoxifen-inducible Cre in myelinating cells (Plp1, proteolipid protein myelin 1) [51]. The progeny (*Plp1-Cre*;*Trpa1*$^{fl/fl}$) was genotyped by standard PCR for *Trpa1* and *Plp1-Cre*^{ERT}. Mice negative for *Plp1-Cre*^{ERT} (*Plp1-Cre*$^{-}$;*Trpa1*$^{fl/fl}$) were used as control. Both positive and negative mice to *Cre*^{ERT} and homozygous for floxed *Trpa1* (*Plp1-Cre*^{ERT};*Trpa1*$^{fl/fl}$ and *Plp1-Cre*$^{ERT-}$;*Trpa1*$^{fl/fl}$, respectively) were treated with tamoxifen (i.p., 1 mg/100 µl in corn oil,

once a day, for 5 consecutive days) [51], resulting in Cre-mediated ablation of *Trpa1* in PLP-expressing Schwann cells/oligodendrocytes. Successful Cre-driven deletion of TRPA1 mRNA was confirmed by RT-qPCR [51]. To selectively delete the *Trpa1* gene in primary sensory neurons, 129S-Trpa1$^{tm2Kykw/J}$ mice (*floxed Trpa1*, *Trpa1$^{fl/fl}$*, Stock No: 008649; Jackson Laboratories), which possess loxP sites on either side of the S5/S6 transmembrane domains of the *Trpa1* gene, were crossed with hemizygous *Advillin-Cre* male mice [202, 203]. The progeny (*Adv-Cre*;*Trpa1$^{fl/fl}$*) were genotyped by standard PCR for *Trpa1* and *Advillin-Cre*. Mice negative for *Advillin-Cre* (*Adv-Cre^{-}*;*Trpa1$^{fl/fl}$*) were used as control. Successful *Advillin-Cre* driven deletion of TRPA1 mRNA was confirmed by RT-qPCR. To evaluate the involvement of MΦs, MaFIA (stock No: 005070, Jackson Laboratories) mice were used.

Mice were housed in a temperature- and humidity-controlled *vivarium* (12 hours dark/light cycle, free access to food and water, 5 animals per cage). At least 1 hour before behavioral experiments, mice were acclimatized to the experimental room and the evaluations were performed between 9:00 AM and 5:00 PM. Animals were anesthetized with a mixture of ketamine and xylazine (90 mg/kg and 3 mg/kg, respectively, i.p.) and euthanized with inhaled CO_2 plus 10-50% O_2.

Cancer cell inoculation

Naïve (CRL-6475; RRID:CVCL_0159 American Type Culture Collection, ATCC) and green fluorescent protein (GFP) expressing B16-F10 murine melanoma and Lewis lung carcinoma (LLC1, CRL-1642, RRID:CVCL_4358 ATCC) cells were cultured in Dulbecco's Modified Eagle Medium (DMEM) containing 10% fetal bovine serum (FBS) and 1% penicillin-streptomycin (10000 U/100 µg/mL) at 37 ºC with 5% CO_2 in a humidified atmosphere and were used without further authentication. For inoculation, 20 µl of B16-F10 melanoma (2 x 10^5 cells) or LLC1 (5 x 10^5 cells) cells were suspended in phosphate buffer saline (PBS) and injected into the plantar region of the mouse right hindpaw [148, 204]. Control groups (sham) were injected with 20 µl of PBS containing B16-F10 melanoma (2 x 10^5 cells) or LLC1 (5 x 10^5 cells) cells killed by quickly freezing and thawing them twice without cryoprotection.

Treatment protocols

MaFIA mice were treated with systemic (2 mg/kg, i.p.) or local (60 μg/6 μl, i.pl.) B/B-HmD (AP20187) or their vehicle (10% PEG-400, 1.7% tween 80 in 0.9% NaCl) for 5 consecutive days (daily, from day 10 to day 14 for B16-F10 melanoma and from day 4 to day 8 for LLC1 cells) [205, 206] after cancer cell inoculation. In another set of experiments, AP20187 or its vehicle were administered by perineural (p.n., 60 μg/6 μl) injection at three adjacent sites (each at a distance of 2 mm) of the sciatic nerve trunk (from ~10 to ~16 mm from the paw surface) for 5 consecutive days (daily, from day 10 to day 14) after B16-F10 melanoma cell inoculation. To transiently deplete the monocyte/MΦ population, C57BL/6J mice received liposome-encapsulated clodronate (LCL, 5 mg/ml i.p., Clodronate Liposomes.com) or vehicle (liposome-encapsulated PBS) one day before and 14 consecutive days (daily, from day 1 to day 14) after B16-F10 melanoma cell inoculation. A neutralizing anti-CCL2 monoclonal antibody (40 μg/200 μl, i.p.) (#AF-479-NA, Mouse CCL2/JE/MCP-1, R&D system) or its vehicle (IgG2B, isotype control) were administered every 2 days (from day 8 to day 14) after B16-F10 melanoma cell inoculation. A neutralizing anti-M-CSF (#BE0204, clone 5A1, RRID:AB_10950309 BioxCells), anti-G-CSF (#MAB414, Clone 67604, RRID:AB_2085954 R&D system) and anti-GM-CSF (#BE0259, clone MP1-22E9, RRID:AB_2687738) monoclonal antibody (all, 300 μg/200 μl, i.p.) or their vehicle (IgG2B, isotype control) were administered at day 3, 7, 10 and 13 after B16-F10 melanoma cell inoculation. PLX3397 (40 mg/kg, i.p.) (#S7818, Selleckchem) or its vehicle (4% dimethyl sulfoxide, DMSO, 4% tween 80 in 0.9% NaCl) were administered for 7 consecutive days (daily, from day 8 to day 14) after B16-F10 melanoma cell inoculation. A-967079 (100 mg/kg, i.p.), PBN (100 mg/kg, i.p.), or their vehicle (4% DMSO, 4% tween 80 in 0.9% NaCl) were given at day 14 after B16-F10 melanoma cell inoculation.

M-CSF (1, 10 and 100 ng), G-CSF and GM-CSF (both, 100 ng) or their vehicle (0.9% NaCl) were i.pl. (20 μl) administered. A neutralizing anti-M-CSF monoclonal antibody (#BE0204, clone 5A1, BioxCells) (300 μg/200 μl, i.p.) or its vehicle (IgG2B, isotype control), A-967079 (100 mg/kg, i.p.), PBN (100 mg/kg, i.p.), or their vehicle (4% DMSO, 4% tween 80 in 0.9% NaCl), were administered 30 minutes and 1 hour before M-CSF (100 ng/20 μl, i.pl.). Peritoneal MΦs (up to 250×10^6 cells per ml) were harvested from naïve C57BL/6J mice by peritoneal lavage with 10 ml of warm PBS, 4 days after thioglycolate (3%, 2 ml/mice, i.p.) injection. For inoculation, 20 μl of MΦs (3×10^4 cells) were

suspended in PBS and injected (i.pl.) in the hindpaw of MΦ-depleted tumor-bearing MaFIA mice at day 14 after cancer cell inoculation. Unless otherwise indicated, reagents were purchased from Sigma-Aldrich.

Mechnical allodynia

Mechanical allodynia was assessed before (baseline) and after the various pharmacological interventions at different time points. The measurement of mechanical paw-withdrawal threshold was carried out using von Frey filaments of increasing stiffness (0.02-2 g) applied to the plantar surface of the mouse hindpaw, according to the up-and-down paradigm [187]. The 50% mechanical paw-withdrawal threshold (g) response was then calculated from the resulting scores.

Cell cultures

Human Schwann cells (HSC, #P10351, Innoprot) were cultured in Schwann cell medium (#P60123, Innoprot) according to the manufacturer's protocol. All cells were used when received without further authentication. Mouse Schwann cells were isolated from sciatic nerves of C57BL/6J mice. Briefly, the *epineurium* was removed, and nerve explants were divided into 1 mm segments and dissociated enzymatically using collagenase (0.05%) and hyaluronidase (0.1%) in Hank's Balanced Salt Solution (HBSS, 2 hours, 37 °C). Cells were collected by centrifugation (800 rpm, 10 minutes, room temperature) and the pellet was resuspended and cultured in DMEM containing: 10% fetal calf serum, 2 mM L-glutamine, 100 U/ml penicillin, 100 mg/ml streptomycin. Three days later, cytosine arabinoside (10 mM) was added to remove fibroblasts. All cells were cultured in an atmosphere of 95% air and 5% CO_2 at 37 °C.

H_2O_2 assay

H_2O_2 level was assessed in sciatic nerve tissue at day 14 after cancer cell inoculation and 60 minutes after A-967079, PBN or their vehicle, by using the Amplex Red® assay (Invitrogen). Briefly, tissue was rapidly removed and placed into modified Krebs/HEPES buffer (composition in mmol/l: 99.01 NaCl, 4.69 KCl, 2.50 $CaCl_2$, 1.20 $MgSO_4$, 1.03 KH_2PO_4, 25.0 $NaHCO_3$, 20.0 Na-HEPES, and 5.6 glucose [pH 7.4]). Samples were minced and incubated with Amplex red (100 μM) and HRP (1 U/ml) (1 hour, 37 °C) in modified Krebs/HEPES buffer protected from light. Fluorescence excitation and emission were at 540 and 590 nm, respectively. H_2O_2 production was calculated using H_2O_2 standard and expressed as μmol/l of mg of dry tissue.

Multi-analyte ELISA assay

A series of chemokines and cytokines including IL-1α, IL-1β, IL-2, IL-4, IL-6, IL-10, IL-12, IL-17A, IFN-γ, TNF-α, TGF-1β, CCL2, CCL3, CCL4, M-CSF, G-CSF, and GM-GSF was assessed in the tumor and sciatic nerve tissue homogenates at day 14 after cancer cell inoculation in C57BL/6J mice using a multi-analyte ELISA array kit (#336161, Qiagen) according to the manufacturer's protocol. Samples were assayed in triplicate. The raw data obtained from the absorbance (optical density, OD 450 nm) readings were normalized to the mg of tissue.

M-CSF ELISA assay

M-CSF assay in mouse tissue. M-CSF was assayed in the tumor and sciatic nerve tissue homogenates at day 14 after cancer cell inoculation in C57BL/6J mice using a single-analyte ELISA array kit (#ab199084, Abcam) according to the manufacturer's protocol. Samples were assayed in triplicate. Data were expressed as pg/mg of proteins.
M-CSF assay in cultured cells. HSC were plated in 96-well clear bottom black ($5x10^5$ cells/well) and maintained in 5% CO_2 and 95% O_2 (24 hours, 37°C). The cultured medium was replaced and added with A967079 (30 µM), PBN (50 µM) or vehicle (0.5% DMSO) for 20 min at room temperature. HSC were then stimulated with H_2O_2 (100 nM), PF-4840154 (50 nM) or vehicle (PBS) for 16 hours in 5% CO_2 and 95% O_2. The cell supernatant was assayed for M-CSF content using a single-analyte ELISA array kit (#ab245714, Abcam) according to the manufacturer's protocol. Data were expressed pg/ml.

Immunofluorescence

The tumor and sciatic nerve tissues were dissected at day 14 after B16-F10 melanoma cells, day 8 after LLC1 cell inoculation or sham and 60 minutes after A-967079, PBN, or their vehicle, from anesthetized and transcardially perfused with PBS, followed by 4% paraformaldehyde, mice. The sciatic nerve and the hindpaw were postfixed for 24 hours, and paraffin embedded. Immunofluorescence staining was performed according to standard procedures. Briefly, after antigen retrieval (Ethylenediaminetetraacetic acid, EDTA, solution pH 9.0, Dako) for 20 minutes at 98 °C, sections (5 µm) were incubated with the following primary antibodies: F4/80 [1:50, MA516624, rat monoclonal (Cl:A3-1), RRID:AB_2538120 Thermo Fisher Scientific] diluted in antibody diluent (Roche Diagnostics) 1 hour at room temperature. Sections were then incubated for 2 hours in the

dark with a fluorescent secondary antibody polyclonal, Alexa Fluor® 488, (1:600, Invitrogen). Sections were coverslipped using a water-based mounting medium with 4'6'-diamidino-2-phenylindole (DAPI, Abcam). The analysis of negative controls (non-immune serum) was simultaneously performed to exclude the presence of non-specific immunofluorescent staining, cross-immunostaining, or fluorescence bleed-through. For histological evaluation, sections were stained with hematoxylin/eosin and, based on the morphology, the boundaries of the nerve trunk corresponding to the *epineurium* were identified and reported in adjacent immunofluorescence images with dashed lines. The number of $F4/80^+$ cells was counted in 10^4 μm^2 boxes in the sciatic nerve trunk.

Sciatic nerve explant culture

Sciatic nerve from naïve MaFIA mice was removed under aseptic conditions and cut into six segments of about 5 mm in length. Tissues were placed into culture dishes and maintained free-floating in DMEM containing: 10% fetal calf serum, 2 mM L-glutamine, 100 U/ml penicillin, 100 mg/ml streptomycin, in an atmosphere of 95% air and 5% CO_2 at 37 °C. Explant cultures were exposed to H_2O_2 (100 nM) in presence of A967079 (30 μM), PBN (50 μM), PLX3397 (1 μM) or their vehicle (0.03%, 0.05% and 0.001% DMSO, respectively) for 3 days. Tissues were then harvested, washed in PBS and fixed in 4% paraformaldehyde before being transferred to 30% sucrose overnight, frozen and cryosectioned at 20 μm in glass slide. Sections were coverslipped using a water-based mounting medium with DAPI (Abcam). The number of $F4/80^+$ cells was counted in 10^4 μm^2 boxes in the sciatic nerve trunk.

Real-Time PCR

RNA was extracted from human and mouse Schwann cells. Total RNA was extracted using the RNeasy Mini kit (Qiagen SpA), according to the manufacturer's protocol. RNA concentration and purity were assessed spectrophotometrically by measuring the absorbance at 260 nm and 280 nm. Reverse transcription was performed with the Qiagen QuantiTect Reverse Transcription Kit (Qiagen SpA) following the manufacturer's protocol. For mRNA relative quantification, rt-PCR was performed on Rotor Gene® Q (Qiagen SpA). The sets of probes for human cells were as follow: ACTB (β-actin): Primer1, CCT TGC ACA TGC CGG AG: Primer2, ACA GAG CCT CGC CTT TG: Probe, /56-FAM/TCA TCC ATG /ZEN/GTG AGC TGG CGG /3IABkFQ/ (NCBI Ref Seq: NM_001101); CSF1 (csf1) Primer1, TCT TTC AAC TGT TCC TGG TCT AC:

Primer2, TGT CGG AGT ACT GTA GC CA: Probe, /56-FAM/ACA GTC AGA/ZEN/TGG AGA CCT CGT GC/31ABkFQ/ (NCBI Ref Seq: NM_172212). The sets of probes for mouse cells were as follow: ACTB (β-actin): Primer 1, GAC TCA TCG TAC TCC TGC TTG; Primer 2, GAT TAC TGC TCT GGC TCC TAG; Probe, /56-FAM/CTG GCC TCA /ZEN/CTG TCC ACC TTC C/3IABkFQ/ (NCBI ref. seq. NM_007393); CSF1 (csf1): Primer1, CTT CAT GCC AGA TTG CCT TTG; Primer2, CGC ATG GTC TCA TCT ATT ATG TCT; Probe, /56-FAM/CAG CTG GAT/ZEN/GAT CCT GTT TGC TAC CT/3IABkFQ/ (NCBI Ref Seq: NM_001113529).

Statistical analysis

Results are shown as the mean and standard error of the mean (SEM). The statistical significance of differences between groups was assessed using Student's t-test, one-way or two-way analysis of variance (ANOVA) followed by Bonferroni post hoc where appropriate. Statistical analyses were performed on raw data using Prism 8 (GraphPad Software Inc.). P values less than 0.05 ($P<0.05$) were considered significant.

5.2 Results

5.2.1 Neural resident macrophages mediate cancer pain

Intraplantar (i.pl.) inoculation of B16-F10 melanoma cells into the hindpaw of C57BL/6J mice induced a time-dependent increase in paw thickness, mainly due to tumor growth (**Fig.14A** and **14B**). Tumor progression was associated with a parallel increase in mechanical allodynia in the ipsilateral paw (**Fig.14B**) and in the number of $F4/80^+$ monocytes and MΦs within the tumor and the adjacent tissue (tMΦs) (**Fig.14C**) and inside the ipsilateral sciatic nerve trunk (rMΦs) (**Fig.14D**). Since no sex differences in cancer growth and mechanical hypersensitivity were observed (**Fig.15A**), male mice were used in subsequent experiments. Control (sham) mice, inoculated with killed cells, developed neither the increase in paw volume, nor mechanical allodynia (Figure 1B). To explore the role of MΦs in cancer-evoked allodynia, cancer cells were inoculated in MΦ Fas-Induced Apoptosis (MaFIA) transgenic mice, which express a green fluorescent protein (GFP) reporter and a drug-inducible Fas suicide gene under control of the M-CSF receptor promoter. The inoculation of cancer cells in MaFIA mouse hindpaw induced a time-dependent increase in paw thickness and mechanical allodynia, like those observed in C57BL/6J mice (**Fig.14E** and **14F**). After inoculation, MaFIA mice received daily injections (day 10-14) of the B/B homodimerizer agent AP20187 (2 mg/kg,

intraperitoneal, i.p.) to induce apoptosis in the entire MΦ population. After AP20187-treatment, MaFIA mice exhibited a marked reduction in the number of $GFP^+/F4/80^+$ cells in both the tumor and sciatic nerve (**Fig.14G**) and in mechanical allodynia (**Fig.14F**).

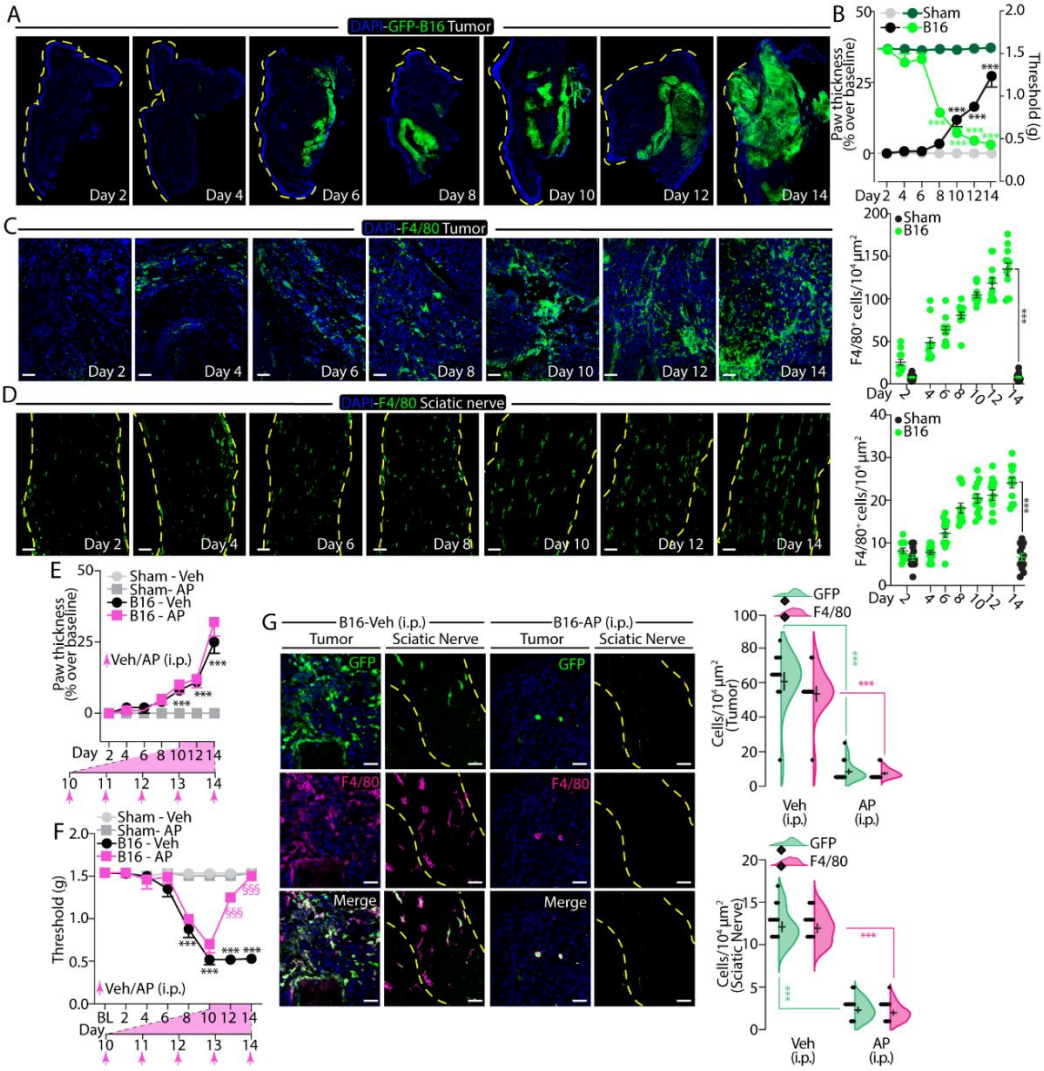

Figure 14. Mechanical allodynia and neuroinflammation induced by B16-F10 melanoma cell inoculation in mouse hindpaw**.** (**A**) Typical whole slide images of the time-dependent expansion of GFP^+-B16-F10 melanoma cell after inoculation in C57BL/6J mouse hindpaw. (**B**) Time-dependent paw thickness, mechanical allodynia and numbers of $F4/80^+$ cells in the tumor (**C**) and sciatic nerve (**D**) after B16-F10 melanoma (B16) cell inoculation or sham in C57BL/6J mice. Time-dependent paw thickness (**E**), mechanical allodynia (**F**), typical images and numbers of GFP^+ and $F4/80^+$ cell in tumor and sciatic nerve (**G**) after B16 cell inoculation or sham in MaFIA mice treated with AP12087 (AP) or Veh (i.p.). BL, baseline. Pink arrows: time of treatment with Veh/AP. Yellow dashed line delimits hindpaw epidermis (A) and *epineurium* (**D**, **G**). Scale bar 50 µm. N=6 mice. ***$P < 0.001$ to Sham, Sham-Veh, GFP Veh, F4/80 Veh; §§§$P < 0.001$ to B16-Veh. Data are presented as mean ± SEM, data points overlaid (**C**, **D**, **G**). Two-way and one-way ANOVA and Bonferroni post hoc test.

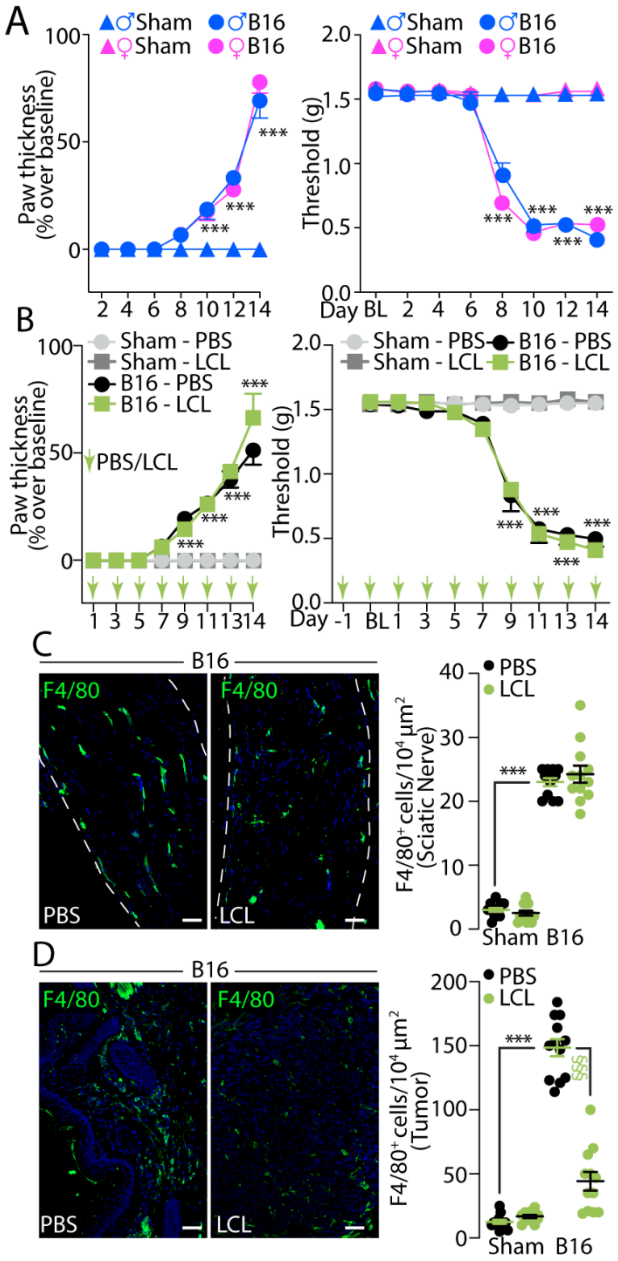

Fig. 15. (**A**) Time-dependent increase in paw thickness and mechanical allodynia after B16-F10 melanoma (B16) cell inoculation or sham in male and female C57BL/6J mice. (**B**) Time-dependent increase in paw thickness and mechanical allodynia after B16 cell inoculation or sham in C57BL/6J mice treated with liposome-encapsulated clodronate (LCL) or PBS (i.p.). Representative images and pooled data of F4/80^{+} cell in ipsilateral sciatic nerve (**C**) and tumor (**D**) at day 14 after B16 cell inoculation or sham in C57BL/6J mice, treated with LCL or PBS (i.p.). BL, baseline. Green arrows indicate the time of treatment with PBS or LCL (i.p.). Dashed line delimits the *epineurium*. Scale bar 50 µm. N = 6 mice. ***P < 0.001 to Sham, Sham-PBS; §§§P < 0.001 to B16-PBS. Two-way (**B**) and one-way (**C**) ANOVA and Bonferroni post hoc test. Two-way (**A**, **B**) and one-way (**C**, **D**) ANOVA and Bonferroni post hoc test.

To determine whether tMΦs or rMΦs contribute to cancer-evoked allodynia, MΦ-depleted MaFIA mice with an established melanoma were used. MΦ-depleted tumor-bearing MaFIA mice were inoculated (day 14) in the hindpaw with $F4/80^+$ cells harvested from the peritoneum of naïve C57BL/6J mice to reconstitute the tMΦ population. This intervention, while repopulated $F4/80^+$ cells within the tumor microenvironment, failed to repopulate the number of $F4/80^+$ cells within the sciatic nerve trunk (**Fig.16A**) and to restore mechanical allodynia (**Fig.16B**). In other experiments, tumor-bearing MaFIA mice received a local injection (60 µg, 6 µl, i.pl.) of AP20187 for 5 consecutive days (day 10-14). This treatment depleted the tumor $GFP^+/F4/80^+$ (tMΦ) cells but did not diminished the increased number of sciatic nerve $GFP^+/F4/80^+$ (rMΦ) cells (**Fig.16C**) and mechanical allodynia (**Fig.16D**). Together, these data suggest that the sciatic nerve rMΦ subpopulation is necessary and sufficient to mediate cancer-evoked allodynia.

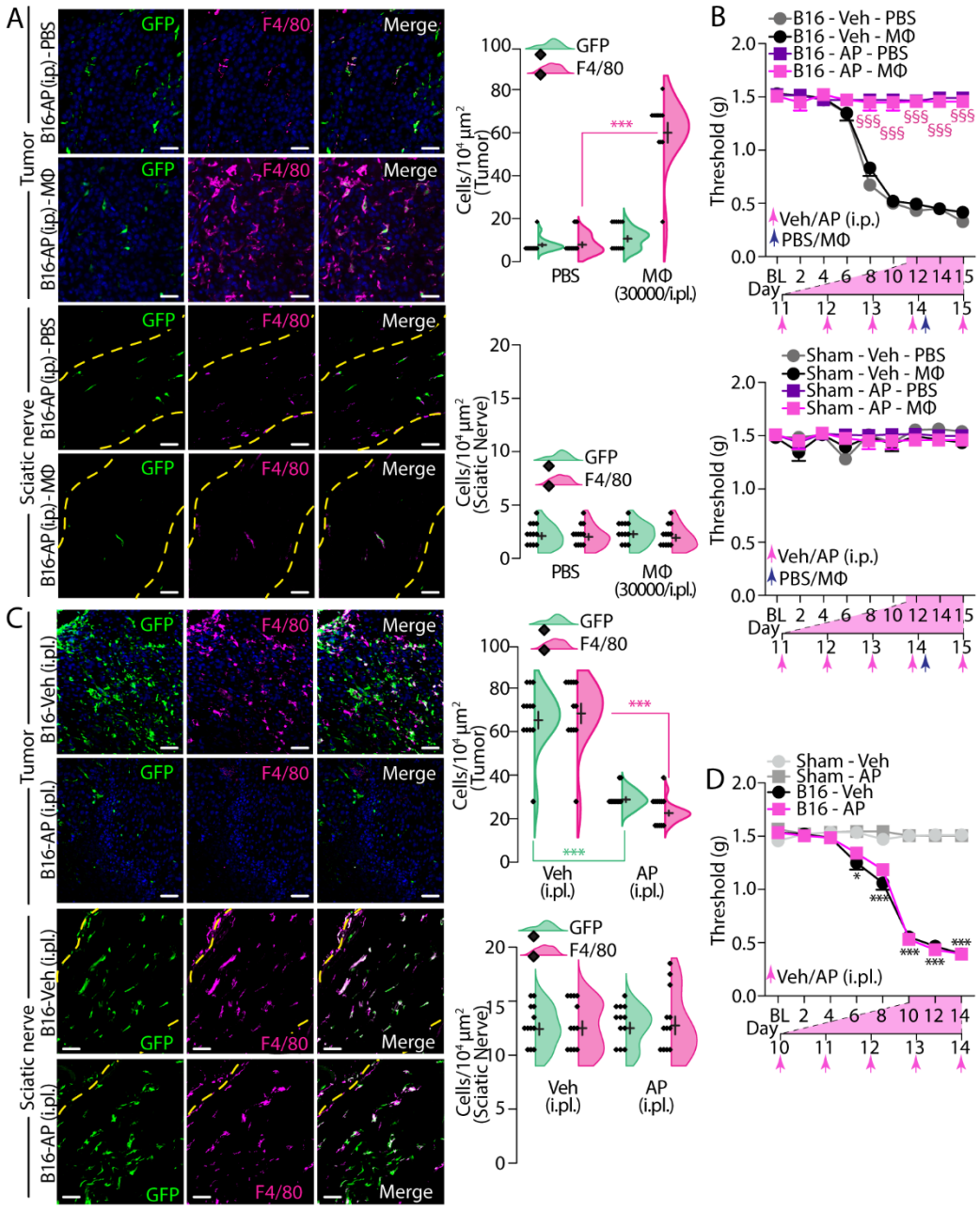

Figure. 16. Resident macrophages are responsible for cancer-evoked allodynia. (**A**) Typical images and data of GFP^+ and $F4/80^+$ cells in the tumor and ipsilateral sciatic nerve and (**B**) time-dependent mechanical allodynia, after B16-F10 melanoma (B16) cell inoculation or sham in MaFIA mice, treated with AP12087 (AP) or Veh (i.p.) and inoculated (i.pl., at day 14) with MΦs or PBS. (**C**) Typical images and data of GFP^+ and $F4/80^+$ cells in the tumor and sciatic nerve and (**D**) time-dependent mechanical allodynia after B16 cell inoculation or sham in MaFIA mice treated with AP or Veh (i.pl.). BL, baseline. Pink arrows: days of treatment; blue arrow: day of MΦ/PBS inoculation. Yellow dashed line delimits the *epineurium*. Scale bar 50 µm. N=6 mice. $^*P < 0.05$, $^{***}P < 0.001$ to F4/80 PBS, F4/80 Veh, GFP Veh, Sham-Veh; $^{§§§}P < 0.001$ to B16-Veh- MΦ. Data are presented as mean ± SEM, data points overlaid (A, C). Two-way and one-way ANOVA and Bonferroni post hoc test.

In a model of neuropathic pain evoked by partial sciatic nerve ligation, we and others have shown that the MΦs responsible for the allodynia quickly accumulate inside the injured sciatic nerve trunk [51, 205, 207-209]. This fast recruitment was eliminated by treatment with liposome-encapsulated clodronate (LCL), which rapidly depletes circulating monocytes [210] and attenuates the number of MΦs recruited at the site of the injury [51]. However, in the present model of cancer pain, daily LCL (i.p., one day before and day 1-14 after cancer cell inoculation), while markedly reducing tumor F4/80$^+$ cells, did not affect sciatic nerve F4/80$^+$ cells, paw thickness, or mechanical allodynia (**Fig.15B-15D**). These findings further support the role of the expanded sciatic nerve rMΦs, but not hematogenous MΦs which accumulate from the blood stream into the tumor microenvironment, to sustain cancer-evoked allodynia.

5.2.2 M-CSF promotes macrophage expansion and cancer-evoked allodynia

Next, we investigated the mechanisms underlying the rMΦ expansion responsible for cancer-evoked mechanical allodynia. We used a multiplex array to profile chemokines and cytokines in the tumor and sciatic nerve at day 14 after cancer cell inoculation in C57BL/6J mice. Except for IL-1α, IL-6, IL-10, IL-12, transforming growth factor-1β (TGF-1β, and granulocyte-CSF (G-CSF) which were unchanged in tumor homogenates, the other mediators, including IL-1β, IL-2, IL-4, IL-17A, interferon-γ (IFN-γ, TNF-α, CCL2, CCL3, CCL4, M-CSF, and GM-GSF, were increased both in tumor and sciatic nerve homogenates (**Fig.17A**). In neuropathic pain models, chemokines, including CCL-2 or M-CSF, augment MΦ number in injured nerves [202, 207]. In contrast to the role of CCL2 in MΦs recruitment and allodynia after nerve injury [51, 207, 211], this chemokine does not contribute to cancer pain as treatment with a neutralizing anti-CCL2 monoclonal antibody (mAb) did not affect tumor growth, mechanical allodynia (**Fig.18A**) and the number of either tMΦs or rMΦs (**Fig.18B** and **18C**).

In some neuropathic pain models [202, 212-214], M-CSF has been shown to mediate both MΦ increase and allodynia. In the present model of cancer-evoked pain, we found that M-CSF levels were markedly increased in both tumor and sciatic nerve homogenate at day 14 after B16-F10 melanoma cell inoculation (**Fig.17B**). Targeting the M-CSF signal with the M-CSF receptor (M-CSFR) antagonist, PLX3397, or a neutralizing anti-M-CSF mAb, which did not affect tumor growth (**Fig.17C** and **17H**), markedly attenuated the number of both tMΦs and rMΦs (**Fig.17F**, **17G**, **17K** and **17L**) and mechanical allodynia

(**Fig.17D** and **17I**). Accumulation of $F4/80^+$ cells in the sciatic nerve was associated with a robust increase in oxidative stress (H_2O_2), which was reduced by PLX3397 (**Fig.17E**) or an anti-M-CSF mAb (**Fig-17J**). Thus, M-CSF mediates cancer-evoked rMΦ expansion and the ensuing allodynia.

5.2.3 M-CSF induces allodynia and neuroinflammation *via* TRPA1

In addition to M-CSF, the CSF family includes G-CSF and GM-CSF, which were found to regulate tumor-nerve interactions, remodeling of peripheral nerves, and sensitization of damage-sensory neurons [215]. G-CSF and GM-CSF levels were increased in sciatic nerve trunk homogenates at day 14 after cancer cell inoculation (**Fig. 17A**).

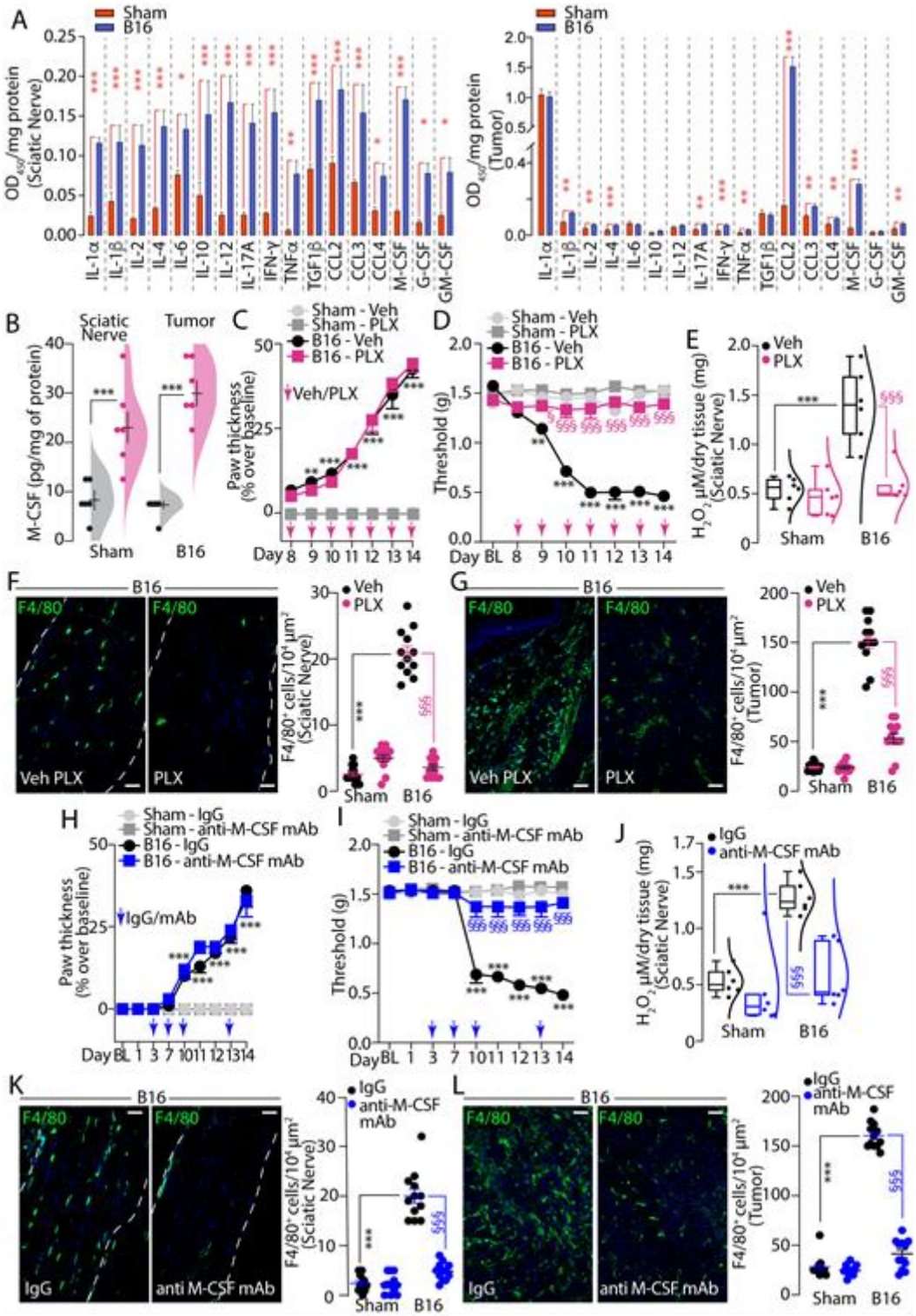

Figure 17. M-CSF promotes macrophage expansion and cancer-evoked allodynia. (**A**) Cytokines/chemokines array profile, (**B**) M-CSF content in sciatic nerve and tumor after B16-F10 melanoma (B16) cell inoculation or sham in C57BL/6J mice. Time-dependent paw thickness (**C**), mechanical allodynia (**D**), H_2O_2 content (**E**) and typical images and data of F4/80$^+$ cells in sciatic nerve (**F**) and tumor (**G**) after B16 cell inoculation or sham in C57BL/6J mice after PLX3397 (PLX) or Veh (i.p.). Time-dependent paw thickness (**H**) and mechanical allodynia (**I**), H_2O_2 content (**J**) and typical images and data of F4/80$^+$ cell in sciatic nerve (K) and tumor (L) after B16 cell inoculation

or sham in C57BL/6J mice treated with an anti-M-CSF mAb or IgG2B (IgG) (i.p.). Assays were performed at day 14 from B16 cell inoculation or sham. BL, baseline. Pink arrows: treatment with PLX/Veh; blue arrow: treatment with anti-M-CSF mAb/IgG. Dashed line delimits the *epineurium.* Scale bar 50 μm. N=6 mice. **P* < 0.05, ***P* < 0.01, ****P* < 0.001 to Sham, Sham-Veh, Sham-IgG; $^{§}P$ < 0.05, $^{§§§}P$ < 0.001 to B16-Veh and B16-IgG. Data are presented as mean ± SEM, data points overlaid (**B**, **F**, **G**, **K**, **L**). (**E**, **J**) Box plots 25th and 75th percentile, min and max values and data points overlaid. Student's t-test; Two-way and one-way ANOVA and Bonferroni post hoc test.

However, in contrast to M-CSF, neutralizing anti-G-CSF or anti-GM-CSF mAbs did not affect cancer-evoked mechanical allodynia (**Fig.18D** and **18E**), reinforcing the pivotal role of M-CSF in cancer-induced pain.

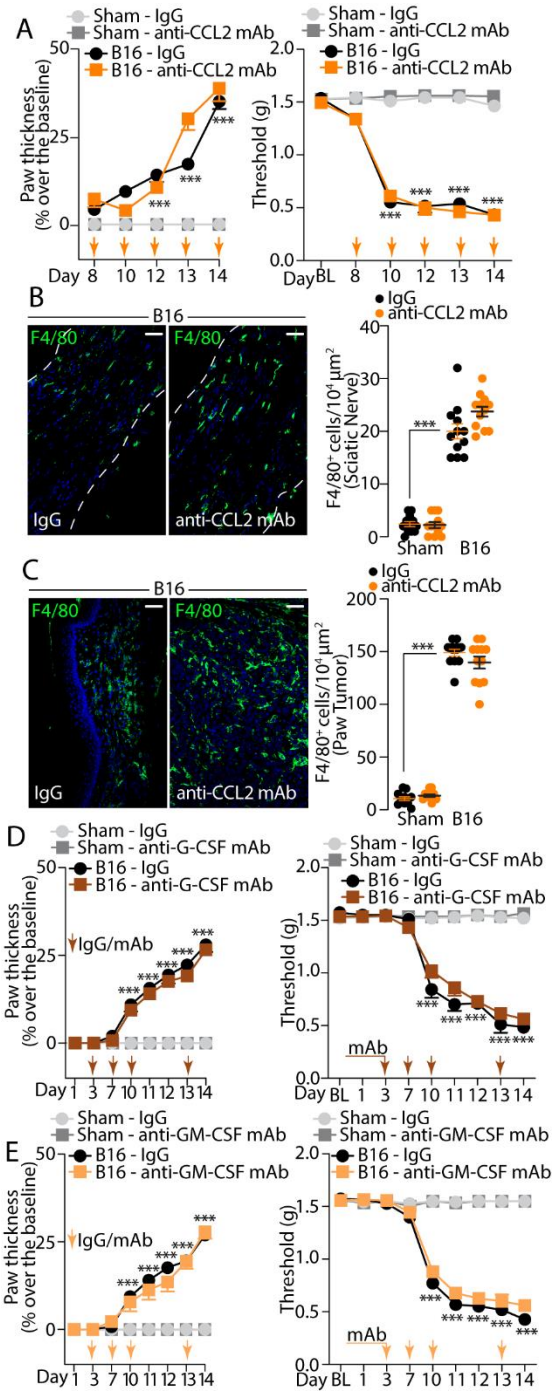

Fig. 18. (**A**) Time-dependent increase in paw thickness and mechanical allodynia after B16-F10 melanoma (B16) cell inoculation or sham in C57BL/6J mice treated with an mAb anti-CCL2 or IgG2B (IgG) (i.p.). Representative images and pooled data of F4/80$^+$ cells in ipsilateral sciatic nerve (**B**) and tumor (**C**) at day 14 after B16 cell inoculation or sham in C57BL/6J mice treated with a mAb anti-CCL2 or IgG (i.p.). Time-dependent increase in paw thickness and mechanical allodynia after B16 cell inoculation or sham in C57BL/6J mice, treated with a mAb anti-G-CSF or IgG (i.p.) (**D**) and a monoclonal mAb anti-GM-CSF or IgG (i.p.) (**E**). BL, baseline. Arrows indicate the time of treatments. Dashed line delimits the *epineurium*. Scale bar 50 µm. N = 6 mice. ***$P < 0.001$ to Sham-IgG. Two-way (A, B, E, F) and one-way (C, D) ANOVA and Bonferroni post hoc test.

We next studied the mechanism by which M-CSF causes mechanical allodynia and neuroinflammation. Local injection of M-CSF (1-100 ng, 20 μl, i.pl.) induced a dose-dependent mechanical allodynia lasting for 6 hours (**Fig.19A**). Pretreatment with an anti-M-CSF mAb prevented the development of mechanical allodynia and the increase in $F4/80^+$ cells in the ipsilateral sciatic nerve trunk (**Fig. 19B** and **19C**). The involvement of MΦs in the M-CSF-induced nociception was shown by using MΦ-depleted MaFIA mice, in which the M-CSF injection failed to induce mechanical allodynia (**Fig.19D**), whereas G-CSF and GM-CSF still elicited allodynia (**Fig.19E** and **19F**). We previously reported that cancer-evoked allodynia induced by B16-F10 melanoma cell inoculation was absent in *Trpa1*$^{-/-}$ mice [148]. To investigate the role of TRPA1 in M-CSF-induced mechanical allodynia and neuroinflammation, M-CSF was injected in *Trpa1*$^{+/+}$ and *Trpa1*$^{-/-}$ mice. In *Trpa1*$^{-/-}$ mice, M-CSF failed to increase mechanical allodynia and $F4/80^+$ cells in the sciatic nerve (**Fig.19G** and **19H**). In contrast, allodynia evoked by G-CSF and GM-CSF was unaffected by TRPA1 deletion (**Fig.19I**).

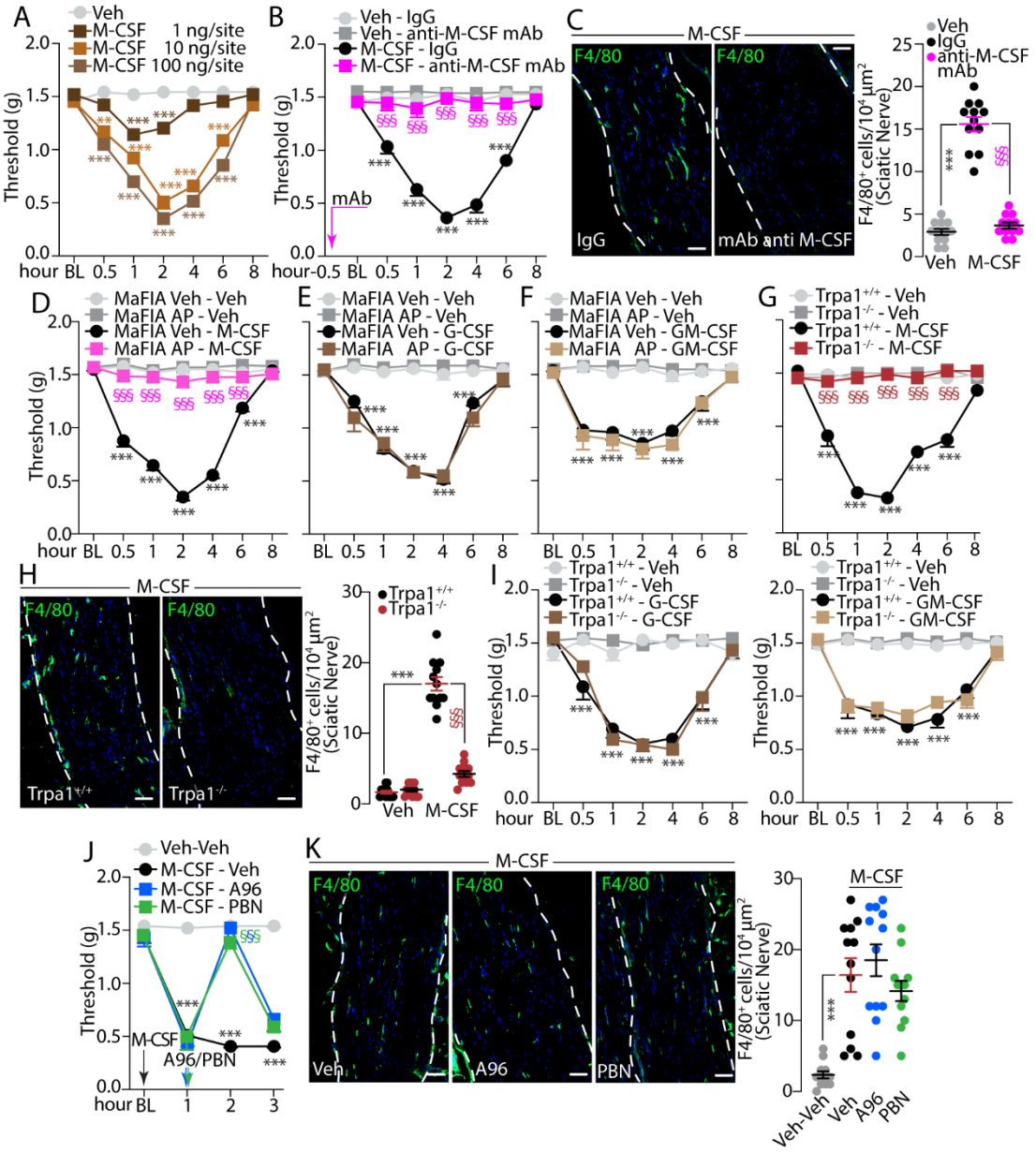

Figure 19. M-CSF induces allodynia and neuroinflammation *via* TRPA1**.** (**A**) Time- and dose-dependent mechanical allodynia in C57BL/6J mice after M-CSF or Veh (i.pl.) and (**B**) pretreated with an anti-M-CSF mAb or IgG2B (IgG) (i.p.). (**C**) Typical images and data of F4/80$^+$ cell in sciatic nerve of C57BL/6J mice after M-CSF (i.pl.) and pretreated with an anti-M-CSF mAb or IgG (i.p.). Time-dependent mechanical allodynia induced by M-CSF (**D**), G-CSF (**E**) and GM-CSF (**F**) or Veh (i.pl.) in MaFIA mice treated with AP12087 (AP) or Veh (i.p.). (**G**) Time-dependent mechanical allodynia, (**H**) typical images and data of F4/80$^+$ cell in sciatic nerve after M-CSF or Veh (i.pl.) in *Trpa1*$^{+/+}$ and *Trpa1*$^{-/-}$ mice. (**I**) Time-dependent mechanical allodynia after G-CSF, GM-CSF or Veh (i.pl.) in *Trpa1*$^{+/+}$ and *Trpa1*$^{-/-}$ mice. (**J**) Mechanical allodynia, (**K**) typical images and data of F4/80$^+$ cell in sciatic nerve after M-CSF or Veh (i.pl.) in C57BL/6J mice treated with A967079 (A96), PBN or Veh (i.p.). BL, baseline. Dashed line delimits the *epineurium*. Scale bar 50 µm. N=6 mice. $^{**}P < 0.01$, $^{***}P < 0.001$ to Veh, Veh-IgG, MaFIA Veh-Veh, *Trpa1*$^{+/+}$-Veh, Veh-Veh; $^{§§§}P < 0.001$ to M-CSF-IgG, MaFIA Veh-M-CSF, *Trpa1*$^{+/+}$-M-CSF, M-CSF-Veh. Data are presented as mean ± SEM, data points overlaid (C, H, K). Two-way and one-way ANOVA and Bonferroni post hoc test.

5.2.4 M-CSF from Schwann cells sustains allodynia

As monocytes are known to release M-CSF [216, 217], we tested whether the M-CSF in the paw and sciatic nerve originated from MΦs. M-CSF was measured in the tumor and sciatic nerve from tumor-bearing and MΦ-depleted MaFIA mice. AP12087 treatment, while reducing both tMΦs and rMΦs, left unchanged the M-CSF content in the ipsilateral sciatic nerve and tumor homogenates (**Fig.20A**). Schwann cells, which ensheath nerve fibers and represent 90% of the nucleated cells of nerve fibers are known to release M-CSF [218, 219]. We confirmed that both human and mouse cultured Schwann cells express M-CSF mRNA (**Fig. 20B**). We then explored the mechanism of M-CSF release from Schwann cells. TRPA1 stimulation has been reported to promote oxidative stress [51, 220] and oxidants may release members of the CSF family [221]. Exposure of cultured human Schwann cells to the non-reactive (PF-4840154) or reactive (H_2O_2) agonists increased M-CSF levels in the cell supernatant, responses that were attenuated by the TRPA1 antagonist, A967079, and PF-4840154-evoked release of M-CSF was reduced by PBN (**Fig.20C**). This finding implicates an autocrine pathway that upon Schwann cell TRPA1 activation elicits M-CSF release mediated by ROS generation.

To further explore the contribution of Schwann cell and neuronal TRPA1 in M-CSF release in sciatic nerve, we used *Plp1-Cre^{ERT+};Trpa1$^{fl/fl}$* and *Adv-Cre^{+};Trpa1$^{fl/fl}$* mice, which harbor a selective deletion of TRPA1 in the Schwann cell /oligodendrocyte lineage and in primary sensory neurons, respectively. At day 14 after cancer cell inoculation, M-CSF levels in the ipsilateral sciatic nerve, but not in the tumor, of *Plp1-Cre^{ERT+};Trpa1$^{fl/fl}$* mice, were reduced, while in *Adv-Cre^{+};Trpa1$^{fl/fl}$* they were preserved in both the sciatic nerve and tumor, compared to control (*Plp1-Cre^{ERT-}/Trpa1$^{fl/fl}$* and *Adv-Cre^{-};Trpa1$^{fl/fl}$*) mice (**Fig. 20D** and **20E**). This finding suggests that Schwann cell TRPA1 is a major driver of neural M-CSF released in tumor-bearing mice. To further support the role of M-CSF released by Schwann cell TRPA1 in rMΦ expansion, we used an *ex vivo* sciatic nerve explant culture. In sciatic nerve explant culture from naïve MaFIA mice, the exposure to H_2O_2 for 3 days increased the number of GFP^+ cells (**Fig.20F**), an effect that was attenuated by the TRPA1 antagonist, A967079, the antioxidant, phenyl-N-tert-butylnitrone (PBN), and the M-CSF receptor antagonist, PLX3397 (**Fig.20F**).

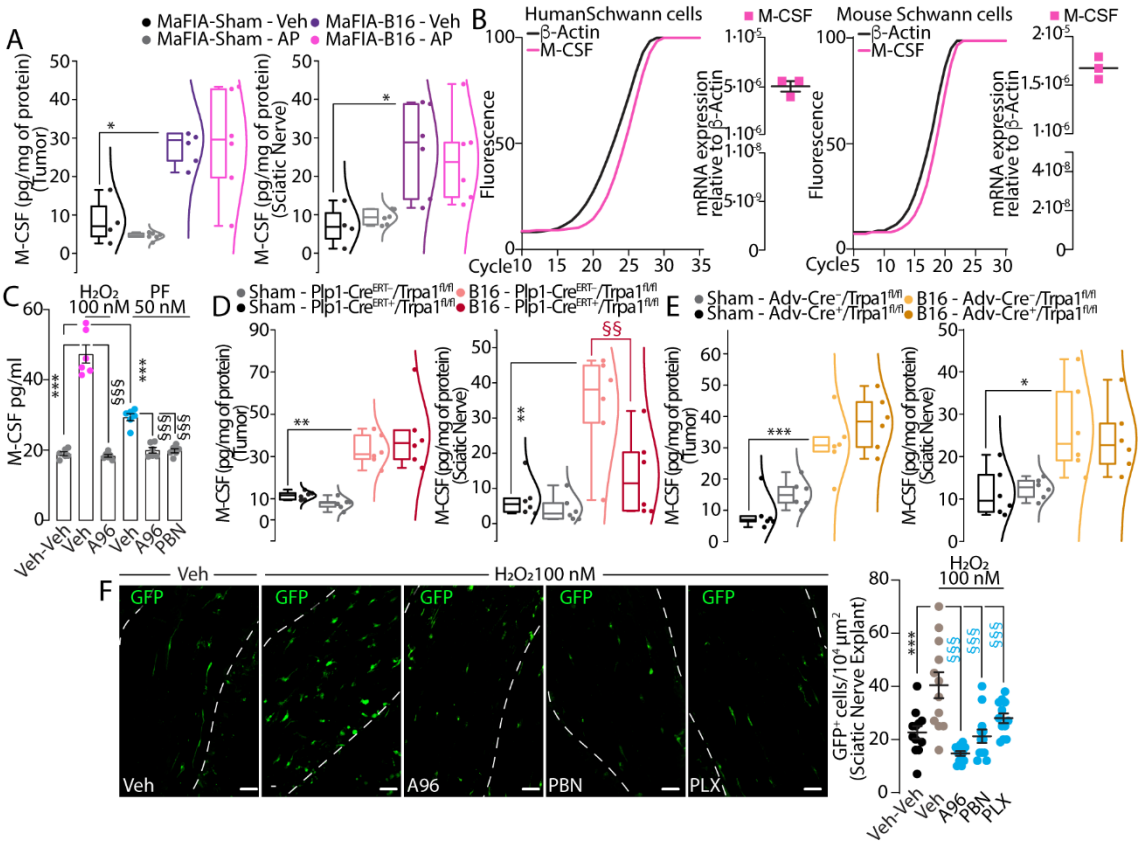

Figure 20. M-CSF is released from Schwann cell TRPA1. (**A**) M-CSF content in tumor and sciatic nerve after B16-F10 melanoma (B16) cell inoculation or sham in MaFIA mice after AP12087 (AP) or Veh (i.p.). (**B**) M-CSF mRNA relative expression in human and mouse Schwann cells. (**C**) M-CSF content in human Schwann cells stimulated with H_2O_2, PF-4840154 (PF) or Veh in presence of A967079 (A96), PBN or Veh. M-CSF content in tumor and sciatic nerve at day 14 after B16 cell inoculation or sham in *Plp1-Cre$^{ERT-/ERT+}$/Trpa1$^{fl/fl}$* (**D**) and *Adv-Cre^{-}/Cre^{+}Trpa1$^{fl/fl}$* (**E**). (F) Typical images and data of GFP^{+} cells in sciatic nerve explant from MaFIA mice after H_2O_2 or Veh exposure, in the presence of A96, PBN, PLX or Veh. Dashed line delimits the *epineurium.* Scale bar 50 µm. N=6 mice (**A**, **D**, **E**), N=3 experiments (**B**, **C**, **F**). **P* < 0.05, ***P* < 0.01, ****P* < 0.001 to MaFIA-Sham-Veh, Veh-Veh, Sham-*Plp1-Cre^{ERT-}/Trpa1$^{fl/fl}$*, Sham-*Adv-Cre^{-} /Trpa1$^{fl/fl}$*; §§*P* < 0.01, §§§*P* < 0.001 to Veh H_2O_2 and B16-*Plp1-Cre^{ERT-}/Trpa1$^{fl/fl}$*. (**A**, **D**, **E**) Box plots 25th and 75th percentile, min and max values and data points overlaid. (**B**, **C**, **F**) Data are presented as mean ± SEM, data points overlaid. One-way ANOVA and Bonferroni post hoc test.

5.2.5 Schwann cell TRPA1 mediates neuroinflammation, which sustains cancer allodynia

TRPA1 is implicated in cancer pain [148]. However, the underlying mechanism by which TRPA1 sustains chronic cancer allodynia is unknown. Our results show that cancer pain entails rMΦ expansion in the sciatic nerve and the release of M-CSF, which elicits TRPA1-dependent mechanical allodynia and neuroinflammation. We investigated

whether TRPA1 promotes the cancer-evoked neuroinflammation that causes chronic allodynia. B16-F10 melanoma cell inoculation in *Trpa1*$^{-/-}$ mice did not induce cancer-evoked mechanical allodynia (**Fig.21A**). The increased number of rMΦs in *Trpa1*$^{+/+}$ mice was markedly reduced in *Trpa1*$^{-/-}$ mice (**Fig. 21B**), while the number of tMΦs remained equally elevated in both mouse strains (**Fig.22A**). In addition, we found that the high levels of the oxidative stress marker, H_2O_2, detected in ipsilateral sciatic nerve homogenates of *Trpa1*$^{+/+}$ mice, were absent in *Trpa1*$^{-/-}$ mice (**Fig.21C**). In partial contrast with this observation, a single injection (i.p. day 14 after inoculation) of the TRPA1 antagonist A967079, or the antioxidant PBN, transiently and completely reversed mechanical allodynia and the increase in H_2O_2 levels (**Fig.21D**, **21G**, **21F** and **21I**), but failed to affect the number of rMΦs (**Fig.21E** and **21H**) and tMΦs (**Fig.22B** and **22C**). Accordingly, a single injection (i.p. 1 h post M-CSF) of A967079 and PBN transiently reversed mechanical allodynia (**Fig.19J**) without decreasing the number of rMΦs (**Fig.19K**). This observation indicates that a short-term inhibition of the TRPA1 channel or oxidative stress, while efficiently abating allodynia, is not sufficient to attenuate the cellular neuroinflammatory response.

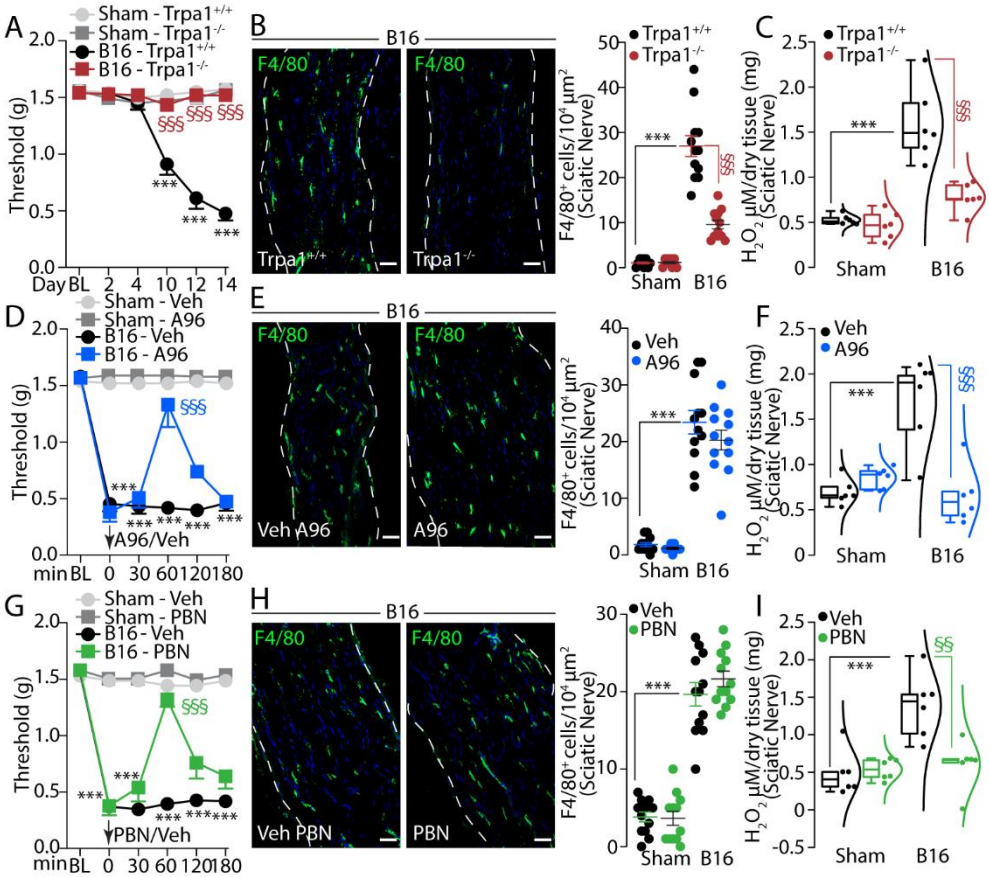

Figure 21. TRPA1 mediates neuroinflammation and cancer-evoked allodynia. (**A**) Time-dependent mechanical allodynia, (**B**) typical images and data of F4/80^{+} cells and, (**C**) H_2O_2 content in sciatic nerve after B16-F10 melanoma (B16) cell inoculation or sham in *Trpa1*$^{+/+}$ and *Trpa1*$^{-/-}$ mice. (**D**) Mechanical allodynia, (**E**) typical images and data of F4/80^{+} cells and (**F**) H_2O_2 content in sciatic nerve in C57BL/6J mice at day 14 after B16 cells inoculation or sham and after A967079 (A96) or Veh (i.p.). (**G**) Mechanical allodynia, (**H**) typical images and data of F4/80^{+} cell and (I) H_2O_2 content in sciatic nerve in C57BL/6J mice at day 14 after B16 cell inoculation or sham and after PBN or Veh (i.p.). BL. Baseline. Dashed line delimits the *epineurium*. Scale bar 50 µm. N=6 mice. ***P < 0.001 to Sham-*Trpa1*$^{+/+}$, Sham-Veh; $^{§§}P$ < 0.01, $^{§§§}P$ < 0.001 to B16-*Trpa1*$^{+/+}$, B16-Veh. Data are presented as mean ± SEM, data points overlaid (B, E, H). (C, F, I) Box plots 25th and 75th percentile, min and max values and data points overlaid. Two-way and one-way ANOVA and Bonferroni post hoc test.

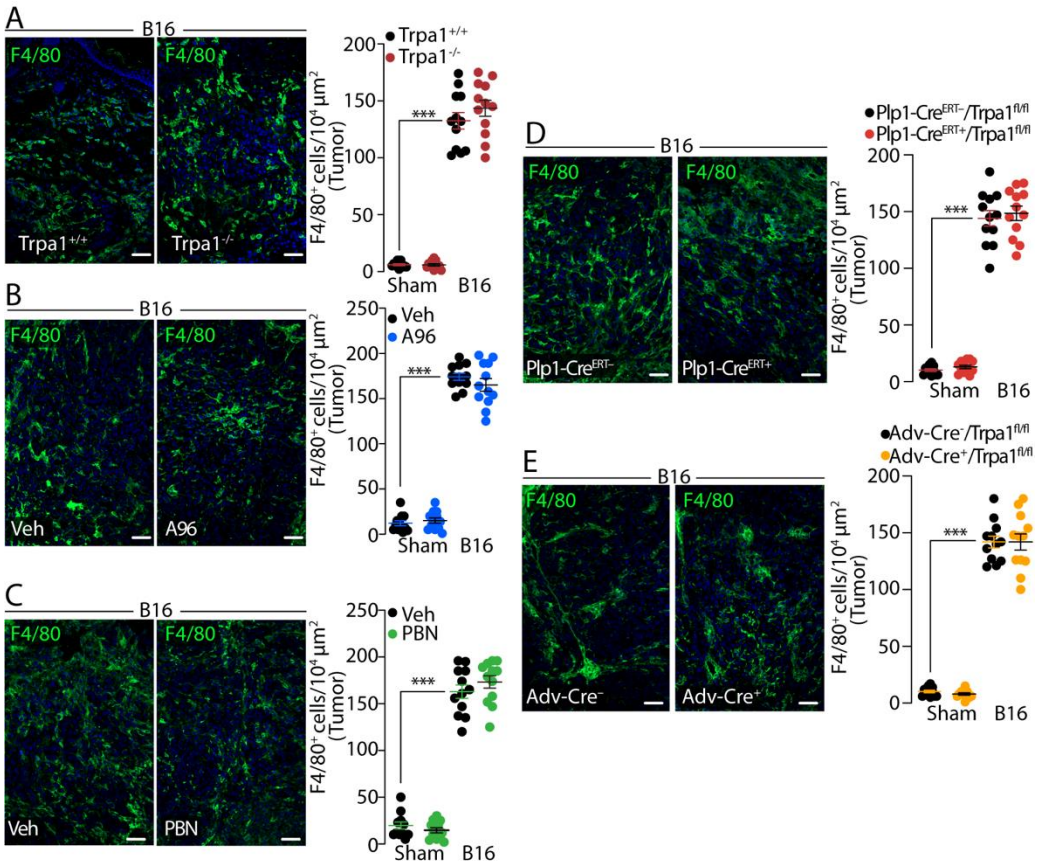

Figure 22. Representative images and pooled data of F4/80^{+} cells in tumor at day 14 after B16-F10 melanoma (B16) cell inoculation or sham in the following conditions: (**A**) *Trpa1*$^{+/+}$ and *Trpa1*$^{-/-}$ mice; C57BL/6J mice, 60 minutes after A967079 (A96) or Veh (i.p.) (**B**) and PBN or Veh (i.p.) (**C**); (**D**) *Plp1-Cre*$^{ERT-}$*/Trpa1*$^{fl/fl}$ and *Plp1-Cre*$^{ERT+}$*/Trpa1*$^{fl/fl}$ mice, and; (**E**) *Adv-Cre*$^{-}$*/Trpa1*$^{fl/fl}$ and *Adv-Cre*$^{+}$*/Trpa1*$^{fl/fl}$ mice. Scale bar 50 µm. N = 6 mice. ***P < 0.001 to Sham. One-way ANOVA and Bonferroni post hoc test.

We then investigated the role of Schwann cell TRPA1 in orchestrating mechanical allodynia and neuroinflammation. After B16-F10 melanoma cell inoculation, *Plp1-Cre^{ERT+}/Trpa1$^{fl/fl}$* mice showed a markedly attenuated mechanical allodynia, number of rMΦs, (**Fig.23A** and **23B**) and H_2O_2 levels in the ipsilateral sciatic nerve compared to *Plp1-Cre^{ERT-}/Trpa1$^{fl/fl}$* (**Fig.23C**). The number of tMΦs was unchanged in both mouse strains (**Fig.22D**). To investigate the contribution of neuronal TRPA1, we studied *Adv-Cre^{+};Trpa1$^{fl/fl}$*. In these mice, while mechanical allodynia was attenuated (**Fig.23D**), the number of rMΦs (**Fig.23E**), tMΦs (**Fig.22E**) and the H_2O_2 levels in the sciatic nerve (**Fig.23F**) were unaffected compared to *Adv-Cre^{-}/Trpa1$^{fl/fl}$*. Thus, in contrast to the Schwann cell TRPA1, the channel expressed by nociceptors signals pain, but does not contribute to neuroinflammation.

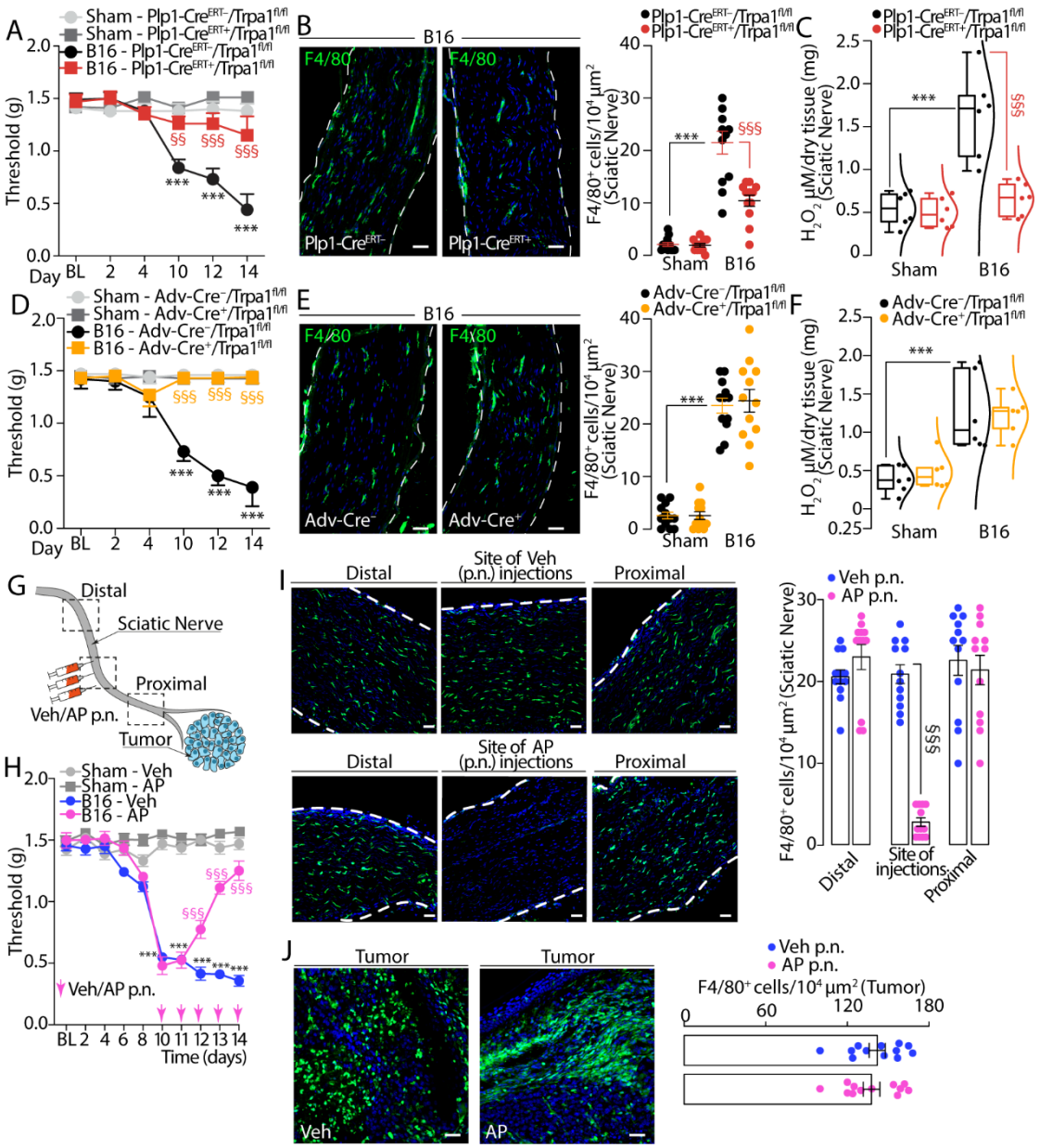

Figure 23. Schwann cell TRPA1 mediates neuroinflammation and cancer allodynia and segmental resident macrophages depletion switches off allodynia. Time-dependent mechanical allodynia after B16-F10 melanoma (B16) cell inoculation or sham in *Plp1-Cre$^{ERT-/ERT+}$/Trpa1$^{fl/fl}$* (**A**) or *Adv-Cre^{-}/Cre^{+}/Trpa1$^{fl/fl}$* mice (**D**). Typical images and data of F4/80^{+} cells (**B**, **E**) and H_2O_2 content (**C**, **F**) in sciatic nerve after B16 cell inoculation or sham in *Plp1-Cre$^{ERT-/ERT+}$/Trpa1$^{fl/fl}$* or *Adv-Cre^{-}/Cre^{+}/Trpa1$^{fl/fl}$* mice. (**G**) Illustration of three local perineural (p.n.) injections of AP12087 (AP) or Veh in sciatic nerve after B16 cell inoculation in MaFIA mice. (**H**) Time-dependent mechanical allodynia, typical images and data of F4/80^{+} cell in sciatic nerve (**I**) and tumor (**J**) after B16 cell inoculation or sham in MaFIA mice treated with AP or Veh (p.n.). BL. Baseline. Pink arrows: treatment with Veh/AP. Dashed line delimits the *epineurium.* Scale bar 50 µm. N=6 mice. ***P < 0.001 to Sham-*Plp1-Cre^{ERT-}/Trpa1$^{fl/fl}$*, Sham-*Adv-Cre^{-}/Trpa1$^{fl/fl}$*, Sham-Veh; §§P < 0.01, §§§P < 0.001 to B16-*Plp1-Cre^{ERT-}/Trpa1$^{fl/fl}$*, B16-*Adv-Cre^{-}/Trpa1$^{fl/fl}$*, B16-Veh. Data are presented as mean ± SEM, data points overlaid (**B**, **E**, **I**, **J**). (**C**, **F**) Box plots 25th and 75th percentile, min and max values and data points overlaid. Two-way and one-way ANOVA and Bonferroni post hoc test.

5.2.6 rMΦs and Schwann cell TRPA1 mediates allodynia in a second cancer pain model

To obtain further evidence on the role of rMΦ and the Schwann cell TRPA1 channel in cancer-related mechanical allodynia, we used another model of cancer pain by using LLC1 cells. Inoculation of these cells, but not killed cells, into the hindpaw of C57BL/6J mice, elicited a progressive and rapid cancer growth that was associated to temporarily similar increases in mechanical allodynia (**Fig.24A** and **24B**) and in the number of tMΦs of rMΦs (**Fig.24C** and **24D**). No sex differences in cancer growth and mechanical hypersensitivity were observed (**Fig.24A** and **24B**). Thus, also in this case, male mice were used in subsequent experiments. The MΦ role was confirmed by using MaFIA mice, which after intraplantar inoculation of LCC1 cells developed a time-dependent increase in paw thickness and mechanical allodynia similar to that observed in C57BL/6J mice (**Fig.24E** and **24F**). However, MaFIA mice receiving daily injections (day 4-8) of AP20187 exhibited a normal cancer growth (**Fig.24E**) but a markedly reduced mechanical allodynia (**Fig.24F**) and $GFP^+/F4/80^+$ cells in both the sciatic nerve and tumor (**Fig.24G** and **24H**). Robust evidence of the key role of TRPA1 derived from the observation that *Trpa1*$^{-/-}$ mice inoculated with LLC1 cells showed normal tumor growth (**Fig.24I**) and increased number of tMΦs (**Fig.24L**) comparable to *Trpa1*$^{+/+}$ mice. However, in *Trpa1*$^{-/-}$ mice, mechanical allodynia (**Fig.24J**) and rMΦ expansion (**Fig.24K**) were remarkably reduced. Similar results were obtained with *Plp1-Cre*$^{ERT+}$*/Trpa1*$^{fl/fl}$ mice, in which mechanical allodynia (**Fig.24N**) and increase in rMΦ number (**Fig.24O**), but not increase in paw thickness (**Fig. 24M**) and tMΦ number (**Fig.24P**), were attenuated as compared to *Plp1-Cre*$^{ERT-}$*/Trpa1*$^{fl/fl}$. Reported data strengthen the hypothesis that rMΦs and Schwann cell TRPA1 are a common mechanism to sustain neuroinflammation and pain in different types of mouse cancer.

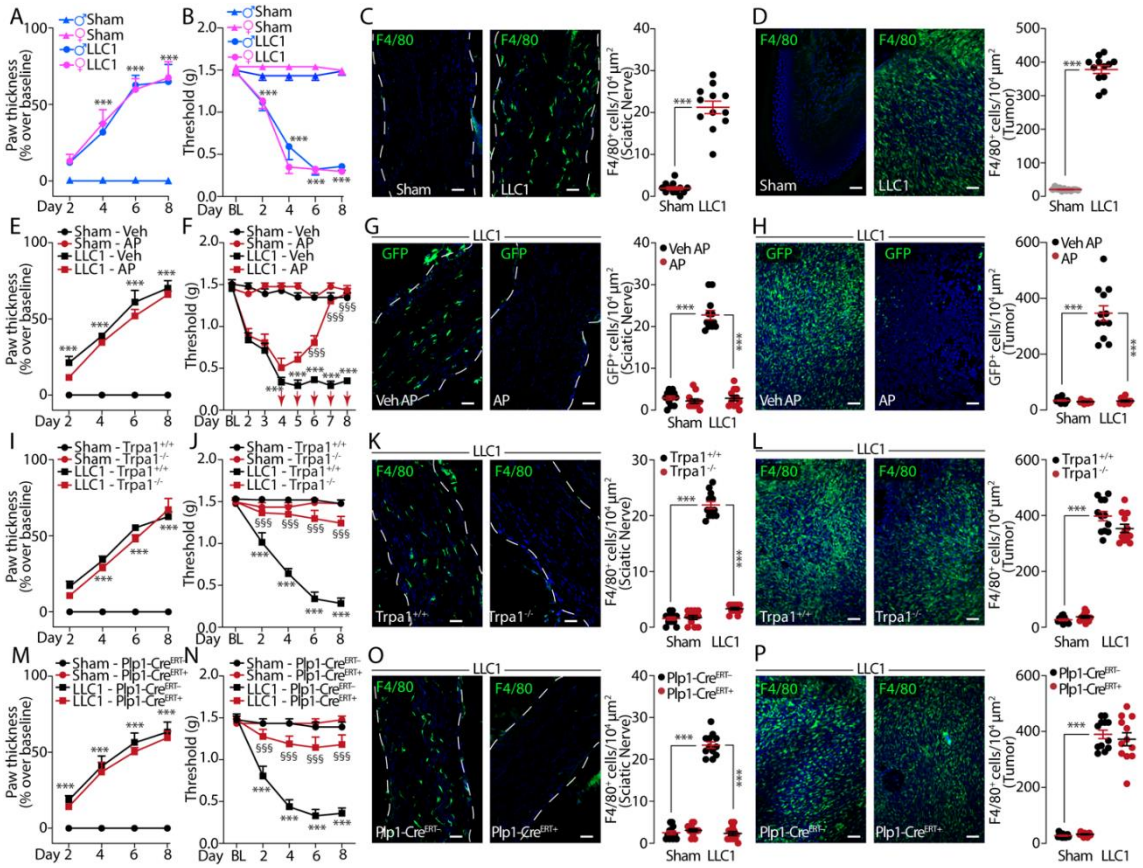

Figure 24. Mechanical allodynia and neuroinflammation induced by LLC1 cells inoculation in mouse hindpaw. Time-dependent increase in paw thickness (**A**) and mechanical allodynia (**B**) after LLC1 cells inoculation or sham in C57BL/6J male and female mice. Representative images and pooled data of F4/80^{+} cells in ipsilateral sciatic nerve (**C**) and tumor (**D**) after LLC1 cell inoculation or sham in C57BL/6J mice. Time-dependent increase in paw thickness (**E**) and mechanical allodynia (**F**) and representative images and pooled data of GFP^{+} cell in ipsilateral sciatic nerve (**G**) and tumor (**H**) after LLC1 cell inoculation or sham in MaFIA mice treated with AP12087 (AP) or Veh (i.p.). Time-dependent increase in paw thickness (**I**) and mechanical allodynia (**J**) and representative images and pooled data of F4/80^{+} cells in ipsilateral sciatic nerve (**K**) and tumor (**L**) after LLC1 cell inoculation or sham in *Trpa1*$^{+/+}$ and *Trpa1*$^{-/-}$ mice. Time-dependent increase in paw thickness (**M**) and mechanical allodynia (N) and representative images and pooled data of F4/80^{+} cells in ipsilateral sciatic nerve (**O**) and tumor (**P**) after LLC1 cells inoculation or sham in *Plp1-Cre*$^{ERT-}$*/Trpa1*$^{fl/fl}$ and *Plp1-Cre*$^{ERT+}$*/Trpa1*$^{fl/fl}$ mice. Immunofluorescence was performed at day 8 from LLC1 cell inoculation or sham. BL, baseline. Red arrows indicate the time of treatment with AP or Veh. Dashed line delimits the *epineurium.* Scale bar 50 µm. N = 6 mice. ***$P < 0.001$ to sham, Sham-Veh, Sham-*Trpa1*$^{+/+}$, Sham-*Plp1-Cre*$^{ERT-}$*/Trpa1*$^{fl/fl}$; §§§$P < 0.001$ to LLC1-veh, LLC1-*Trpa1*$^{+/+}$, LLC1-*Plp1-Cre*$^{ERT-}$*/Trpa1*$^{fl/fl}$. Two-way (A, B, E, F, I, J, M, N) and one-way (C, D, G, H, K, L, O, P) ANOVA and Bonferroni post hoc test.

5.2.7 The site where resident macrophages mediate allodynia

Experiments with MΦ-depleted MaFIA mice highlighted the key role of rMΦs to sustain allodynia. However, the precise anatomical site where rMΦs mediate allodynia remains unknown. To address this issue, we used MΦ-depleted tumor-bearing MaFIA mice. Mice received AP20187 for 5 days (daily, day 10-14) by perineural injection at three adjacent sites (each at a ~2 mm distance) of the ipsilateral sciatic nerve trunk (from ~10 to ~14 mm from the paw surface) (**Fig.23G**). Perineural treatment elicited a substantial reduction in mechanical allodynia (**Fig.23H**) and a marked decrease in the number of GFP^+ cells in the portion corresponding to the sciatic nerve segment that had been treated with AP20187 (**Fig.23I**). The number of GFP^+ cells in both the distal and proximal portion to that treated with AP20187 was similar in MaFIA mice that received either the dimerizing agent or its vehicle (**Fig.23I**). The number of GFP^+ cells in the paw (tMΦs) was similar in mice treated with AP20187 or vehicle (**Fig.23J**). These data indicate that depletion of rMΦs in a limited portion of the ipsilateral sciatic nerve is necessary and sufficient to interrupt the signaling pathway that entails MΦs and Schwann cell interaction to mediate allodynia.

6. Schwann cell Insulin-like Growth Factor Receptor Type-1 Mediates Metastatic Bone Cancer Pain in Mice

6.1 Methods

Animals

Female mice were used throughout (25–30 g, 5–8 weeks old). The following strains of mice were used: C57BL/6 J (Charles River, RRID: IMSR_JAX:000664), wild-type (*Trpa1*$^{+/+}$), and TRPA1-deficient (*Trpa1*$^{-/-}$; B6129P-Trpa1^{tm1Kykw}/J; RRID: IMSR_JAX:006401, Jackson Laboratory) mice [184]. Genetically modified mice were maintained as heterozygotes on the C57BL/6 J background. To generate mice in which the Trpa1 gene was conditionally silenced in Schwann cells, homozygous 129S-Trpa1$^{tm2Kykw/J}$ (floxed Trpa1, *Trpa1*$^{fl/fl}$, RRID:IMSR_JAX: 008649 Jackson Laboratory) were crossed with hemizygous B6.Cg-Tg(Plp1-CreERT)3Pop/J mice (Plp-Cre^{ERT}, RRID: IMSR_JAX:005975 Jackson Laboratory) expressing a tamoxifen-inducible Cre in their Schwann cells (Plp1, proteolipid protein myelin 1) [51]. The progeny (Plp-Cre^{ERT};

Trpa1$^{fl/fl}$) was genotyped using PCR for Trpa1 and Plp-Cre^{ERT}. Mice that were negative for Plp1-Cre^{ERT} (Plp-Cre^{ERT-}; *Trpa1*$^{fl/fl}$) were used as controls. Both positive and negative mice for Cre^{ERT} and homozygous floxed Trpa1 (Plp-Cre^{ERT+}; *Trpa1*$^{fl/fl}$ and Plp-Cre^{ERT-}; *Trpa1*$^{fl/fl}$, respectively) were treated with i.p. 4-OHT (1 mg/100 µL in corn oil) once a day consecutively for 3 d. This treatment resulted in the Cre-mediated ablation of Trpa1 in Schwann cells expressing Plp. To selectively delete Trpa1 in primary sensory neurons, *Trpa1*$^{fl/fl}$ mice were crossed with hemizygous Advillin-Cre mice (Adv-Cre) [51, 203]. Mice that were positive or negative for Cre and homozygous for floxed Trpa1 (Adv-Cre^{+}; *Trpa1*$^{fl/fl}$ and Adv-Cre^{-}; *Trpa1*$^{fl/fl}$, respectively) were used. The successful Cre-driven deletion of TRPA1 mRNA was confirmed using reverse transcription quantitative real-time PCR (RT-qPCR).

To evaluate the involvement of macrophages, transgenic Macrophage Fas-Induced Apoptosis (MaFIA) mice (C57BL/6-Tg(Csf1r-EGFP-NGFR/FKBP1A/TNFRSF6)2Bck/J, stock No: 005070, RRID:IMSR_JAX:005070, Jackson Laboratories) were used. These transgenic mice express a mutant human FK506 binding protein 1A, 12kDa (FKBP12)-Fas inducible suicide/apoptotic system, driven by the mouse Csf1r promoter conjugated with a green fluorescent protein (GFP), which preferentially binds the B/B dimerizing agent (B/B-HmD, AP20187) (Diatech Labline s.r.l.). Treatment of mice with AP20187 induces the dimerization of the suicide protein to activate the cytoplasmic FKBP12-Fas fragments, leading to the apoptosis of transgene-expressing cells and consequent macrophage depletion [222].

The group size of n = 6 mice for behavioral experiments was determined by sample size estimation using G Power [v3.1; [201]] to detect the size effect in a *post-hoc* test with type 1 and 2 error rates of 5% and 20%, respectively. Allocation concealment of mice into the vehicle(s) or treatment groups was performed using a randomization procedure (http://www.randomizer.org/). The assessors were blinded to the identity of the animals (genetic background or allocation to treatment groups). None of the animals were excluded from the study. Behavioral studies followed Animal Research: Reporting of *In Vivo* Experiments (ARRIVE) guidelines [223]. Animal experiments and sample collections were carried out according to the European Union (EU) guidelines for animal care procedures and Italian legislation (DLgs 26/2014) application of the EU Directive 2010/63/EU.

All animal studies were approved by the Animal Ethics Committee of the University of Florence and the Italian Ministry of Health (permit no. 1146/2020-PR). The use of FFPE sections of human cutaneous tissues was approved by the Local Ethics Committee of the Florence University Hospital (Area Vasta Toscana Centro) (18271_bio/2020), according to the Helsinki Declaration, and informed consent was obtained.

Cell Lines

Human Schwann cells (HSC) (#P10351; Innoprot, Derio, Spain) were grown and maintained in Schwann cell medium (#P60123, Innoprot) at 37 °C with 5% CO_2 and 95% O_2. Cells were passaged at 90% confluence and discarded after 12 passages [51].

Naïve E0771 (CRL-6475; RRID: CVCL_0159, American Type Culture Collection [ATCC]) murine breast carcinoma cells were cultured in Dulbecco's modified Eagle medium (DMEM) containing fetal bovine serum (FBS, 10%) and penicillin–streptomycin (10,000 U/100 mg/mL) at 37 °C with 5% CO_2 in a humidified atmosphere.

GFP-expressing E0771 cells were generated by lentiviral transduction. Briefly, human embryonic kidney 293 cells (HEK293T; #CRL3216™; ATCC, Manassas, VA, USA) were grown in DMEM containing FBS (10%) and L-glutamine (2 mM) and transfected when a confluence of approximately 6×10^5 cells was reached in a 100 mm petri dish. The transfection mix contained reduced serum medium (1 mL) (#11058021 Opti-MEM™; Thermo Fisher Scientific, Waltham, MA, USA), 9.5 µg/mL packaging plasmid (#12260 psPAX2; Addgene, Watertown, MA, USA), 5 µg/mL envelope plasmid (#35616, pCAG-VSVG; Addgene), 15 µg/mL EF1a- gfp-2a-puro (#129443; Addgene), and 45 µg/mL polyethylenimine (PEI) (#23966; Polysciences, Warrington, PA, USA). After overnight incubation, 10 mL of fresh medium was added to the cell culture. The transfected cells were maintained at 37 °C in 5% CO_2 and 95% O_2 for a further 48 h. Then, the supernatant was collected and filtered using a 0.45 µm polyethersulfone filter (PES) and used to infect E0771 cells previously plated (50% of confluency) on a 100-mm petri dish for 24 h. Finally, the medium containing the lentivirus was discarded and a fresh medium with puromycin (1 µg/mL) was added to the cell culture to select E0771 GFP^+ cells.

Human breast cancer cells, MDA-MB-231 (#HTB-26™; ATCC), and the murine macrophage cell lineage, RAW 264.7 (#TIB-71™; ATCC), were grown in DMEM supplemented with FBS (10%), L-glutamine (2 mM), penicillin (100 U/mL), and streptomycin (100 mg/mL) at 37 °C in 5% CO_2 and 95% O_2. To induce osteoclast

differentiation, RAW 264.7 cells were cultured at a density of 2×10^5 cells/mL and treated with lipopolysaccharide (LPS; Lipopolysaccharide from *Escherichia coli* O55:B5 L6529) (100 ng/mL) for 3 d [224]. The human monocytic U937 cell line (#CRL-1593.2™; ATCC) was maintained at 37 °C, 5% CO_2, and 95% O_2 in RPMI-1640 medium supplemented with heat-inactivated FBS (10%), L-glutamine (2 mM), 4-(2-hydroxyethyl)-1-piperazineethanesulfonic acid (HEPES; 10 mM), and sodium pyruvate (1 mM). Osteoclast differentiation of U937 cells was induced by stimulation with phorbol 12-myristate 13-acetate (48 nM) for 2 d and then with 1,25-dihydroxyvitamin D3-13C3 (10 nM) for another 3 d [225]. All cells were used when received without further authentication.

Cancer cell inoculation

For inoculation, 20 µL of E0771 breast carcinoma cells (2×10^5 cells) were suspended in PBS and injected into the fourth right mammary fat pad of the mouse. Control groups were injected with 20 µL of PBS containing E0771 breast carcinoma (2×10^5 cells) killed by quick freezing and thawing (twice) without cryoprotection. E0771 cell lines were syngeneic with the C57BL/6J mouse strain. The mammary thickness was measured using a digital caliper and the tumor volume was calculated according to the formula $V = 0.52 \times \text{width}^2 \times \text{length}$, where width is the smaller of the two measurements [226].

Treatment protocols

If not otherwise indicated, the reagents were obtained from Merck Life Science SRL (Milan, Italy). C57BL/6J (E0771 inoculated or control mice) were treated with: picropodophyllin (PPP) (20 mg/kg, i.p.) and Ro32-0432 (1 mg/kg, i.p.) or their vehicle (4% DMSO, 4% Tween 80 in 0.9% NaCl) twice a day from 17 to 20 d after cell inoculation; N-tert-butyl-alpha-phenylnitrone (PBN) (100 mg/kg, i.p.), cPTIO (0.6 mg/kg i.p.), L-NAME (50 mg/kg, i.p.), Akti-1/2 (50 mg/kg, i.p.), reparixin (5 mg/kg i.p.), AP20187 (2 mg/kg i.p.), and Pexidartinib (PLX-3397) (40 mg/kg i.p.) or their vehicle (4% DMSO, 4% Tween 80 in 0.9% NaCl) once a day from 10 to 20 d after cell inoculation; NT157 (50 mg/kg, i.p.) or its vehicle (4% DMSO, 4% Tween 80 in 0.9% NaCl) every 2 d from 10 to 20 d after cell inoculation; neutralizing anti-IL-6 (200 µL, 1 mg/mL, i.p.) (#BE0046, clone MP5-20F3, RRID:AB_1107709 Bio X Cell, Lebanon, NH, USA), anti-TGF-β (200 µL, 1 mg/mL, i.p.) (#BE0057, clone 1D11.16.8, RRID:AB_1107757, Bio X Cell), and anti-IGF-1 monoclonal antibodies (mAb) [#05-

172, clone Sm1.2, RRID: AB_309643; Millipore, Burlington, MA, USA; i.th. (5 µL) or p.n. (5 µL) (50 µg/mL)] or their vehicle (IgG1, isotype control, #BE0083, clone MOPC-21, RRID: AB_1107784; Bio X Cell) every 2 d from 10 to 20 d after cell inoculation.
Plp-CreERT^{+} or Plp-CreERT$^{–}$ were treated with an intrasciatic (i.e., 5 µL) injection of pAAV[FlexOn]-CMV-EGFP-mIGF1R[shRNA]-mCherry viral vector (2×10^{10} VG/mL) two weeks before E0771 cell inoculation. Adv-Cre^{+} or Adv-Cre$^{–}$ mice were treated with an i.th. (5 µL) injection of pAAV[FlexOn]-CMV-EGFP-mIGF1R[shRNA]-mCherry viral vector (2×10^{10} VG/mL) two weeks before E0771 cell inoculation. At 20 d after E0771 cell inoculation, mice were euthanized (ketamine 200 mg/kg and xylazine 20 mg/kg, i.p.) and the sciatic nerve and DRGs were harvested for analysis. Viral infection was confirmed by immunofluorescence analysis. Only the infected cells (mCherry) were fluorescent upon examination with a red filter.
In another set of experiments, IGF-1 (0.1, 0.5, and 1 nmol) or its vehicle (0.9% NaCl) (10 µL) was then injected (i.pl.). PPP (120 nmol), Ro32-0432 (20 nmol), PBN (670 nmol), cPTIO (200 nmol), L-NAME (1 µmol), Akti-1/2 (100 nmol), NT157 (100 nmol), and PitStop2 (500 pmol) or their vehicle (4% DMSO, 4% Tween 80 in 0.9% NaCl) were administered (10 µL, i.pl.) 30 min before IGF-1 (1 nmol, i.pl.).

Behavioral assays

Mechanical allodynia

The mechanical paw-withdrawal threshold was measured using von Frey filaments of increasing stiffness (0.02–2 g) applied to the plantar surface of the mouse hind paw, according to the up-and-down paradigm [187]. The 50% mechanical paw-withdrawal threshold (g) response was then calculated from the resulting scores.

Cold response

Cold sensitivity was assessed by measuring the acute nocifensive response to acetone-evoked evaporative cooling as previously described [227]. Briefly, mice were placed in a wire mesh floor cage and, after habituation, a droplet (50 µL) of acetone, formed on the flat-tip needle of a syringe, was gently touched to the plantar surface of the hind paw, and the time spent in elevation and licking of the plantar region over a 60-s period was measured. Acetone was applied three times at 10- to 15-min intervals and the average elevation/licking time was calculated.

Acute nociception

Immediately after i.pl. injection, mice were placed inside a plexiglass chamber, and spontaneous nociception was assessed for 10 min by measuring the time (seconds) that the animal spent licking/lifting the injected paw.

Open field test

The mice were acclimated to the room for 1 h before recording. Mice were introduced into individual activity transparent acrylic chambers (30.48×30.48×30.48 cm) aligned horizontally or vertically, with each chamber housing a single mouse for analysis. The mice were placed in the chamber and their activity was recorded for 10 min with a digital camera. Videotapes were analyzed using an open-source video tracking system [228]. Spontaneous locomotor activity, measured as the cumulative distance traveled, and time spent in the inner zone in the open field apparatus was analyzed. The inner zone is defined as a square comprising the inner 50% of the area.

Rota-rod test

For the locomotor function assessment animals were trained on a rotarod apparatus (Ugo Basile) 24 h before the test. The day of the experiment, each mouse was individually placed on the apparatus, which accelerated from 4 to 40 rpm over the trial time of 300 seconds. Latency to fall was evaluated and recorded for three trials.

Virus Generation

The AAV plasmid for stable RNAi of mouse IGF1R was obtained by choosing Cre-lox conditional shRNA expression based on the FLEX switch system [229]. The construct pAAV[FlexOn]-CMV-EGFP-mIGF1R[shRNA]- mCherry (#VB210916-1096bqm) was obtained using VectorBuilder (mIGF1R shRNA; 5′ AAGCTGTGTGTCTCCGAAATTTTACATCTGTGGCTTCACTAAAATTTCGGAG ACACACAGCTG -3′). Viral particles were produced by transfecting AAVPro-HEK293T cells (Takara, Shiga, Japan) with the plasmid for RNAi of mouse IGF-1R, the packaging plasmid expressing the Rep/Cap gene (AAV2/8 and AAV2/9n, #112864 and #112865; Addgene), and a helper plasmid (#112867, Addgene). To produce viral particles capable of selectively infecting Schwann cells, the packaging plasmid AAV2/8 was used (#112864; Addgene)[230], according to the manufacturer's protocol. The viral titer obtained using the RT-qPCR kit assay (#6233; Takara) was 2×10^{10} VG/mL in a volume

of 600 µL. To obtain viral particles capable of selectively infecting primary sensory neurons, the packaging plasmid AAV2/9n (#112865; Addgene) was used[231], according to the manufacturer's protocol. The viral titer obtained was 2 x 10^{10} VG/mL in a volume of 600 µL, tested using a RT-qPCR kit assay (#6233; Takara).

AAV production and cell lysis

AAVPro-HEK293T cells were cultured in DMEM supplemented with FBS (10%), Pen/Strep (1%), and L-glutamine (2%). Three days before transfection, cells were seeded in a CellBIND Polystyrene CellSTACK 2 Chamber (#3310, Corning, Corning, NY, USA) for 48 h to reach 80% confluence. Then, cells were detached using PBS plus Trypsin-EDTA 0.05% (EuroClone, Milan, Italy) and collected to be seeded in a CellBIND Polystyrene CellSTACK 2 Chamber (#3310; Corning) for 24/36 h, until 80% of confluence. For transfection, 2.5 mg of total DNA from the Rep/cap, pHelper, and pAAV[FlexOn]-CMV-EGFP-mIGF1R[shRNA]-mCherry vectors were used. Considering the total number of base pairs for each plasmid, the total µg/bp required to obtain a molar ratio of 1:1:1 for each plasmid was calculated. For transfection, 176 mL of Opti-MEM (Thermo Fisher Scientific) with DNA was mixed, and PEI (1:3 DNA to PEI ratio) was added. After 15 min of incubation, the mix of OptiMEM + DNA + PEI was combined with 350 mL of DMEM supplemented with FBS (2%). The 2 Chamber medium was replaced with the prepared transfection medium, covering all five layers of the chamber, and incubated for 72 to 96 h depending on the serotype (the AAV2 serotype was incubated for 48–72 h, while the other serotypes were incubated for 96 h). The cells and medium were then harvested. Cells were transferred into 50 mL conical tubes and centrifuged at 1000 × *g* for 10 min at 4 °C. Supernatants and pellets were processed separately. The supernatant was filtered through 0.45-µm PES membranes, and 25 mL of PEG solution (400 g of 40% polyethylene glycol + 24 g of NaCl in ddH_2O to a final volume of 1.000 mL) was added to every 100 mL of supernatant. The entire solution was stirred slowly at 4 °C for 1 h and then kept at 4 °C for 3 h without stirring to allow precipitation. The sample was then centrifuged at 2.800 × *g* for 15 min at 4 °C, the supernatant was discarded, and the virus (small pellet) was resuspended in PBS (10 mL), Pluronic F68 (0.001%), and NaCl (200 mM). The cell pellet was resuspended and lysed in 10 mL of PBS + Pluronic F68 (0.001%) + NaCl (200 mM), sonicated (4 × 1 s pulse with a 15 min interval between each pulse 50% amplitude) in ice, then centrifuged at 3.200 × *g* for 15 min at 4 °C. The lysate obtained was added to the resuspended virus after

processing the supernatant. The viral suspension was incubated with benzonase (50 UI/mL) at 37 °C for 45 min. Then, it was centrifuged at 2.400 × *g* for 10 min at 4 °C. The clarified supernatant was transferred to new tubes and was kept overnight at 4 °C before purification.

Iodixanol-based purification protocol

Purification using a gradient of iodixanol was prepared as previously described[232] with a few modifications. Starting with a 60% iodixanol solution (OptiPrep; STEMCELL Technologies, Vancouver, Canada), a gradient was prepared with a 15% solution [4.5 mL of iodixanol (60%) + 13.5 mL of NaCl/PBS-MK buffer (1M)], a 25% solution [5 mL of iodixanol (60%) + 7 mL of PBS-MK buffer (1×) + 30 µL of phenol red], a 40% solution [6.7 mL of iodixanol (60%) + 3.3 mL of PBS-MK buffer (1×)], and a 60% solution [10 mL of iodixanol (60%) + 45 µL of phenol red]. Each solution was added into a 39-mL Quick-Seal tube (Beckman Coulter, Brea, CA, USA) using an 18 G needle in the following order: 8 mL of the iodixanol solution (15%), 6 mL of the iodixanol solution (25%), 5 mL of the iodixanol solution (40%), and 5 mL of the iodixanol solution (60%). Then, 5 mL of the clarified supernatant was added to the top of the gradient. After sealing the tubes, they were centrifuged in a Type 70 Ti rotor (Beckman Coulter) at 350.000 x g at 10 °C for 90 min and then pierced with a 16 G needle on top and an 18 G needle at the interface between the 60% and 40% iodixanol gradients. Viral particles contained in the 40% iodixanol layer were collected in 1.5 mL microcentrifuge tubes. The collected fractions were concentrated using Amicon Ultra-15 centrifugal filter units (molecular weight cut-off, 100 kDa; Merck Millipore). The membrane was covered with 15 mL of Pluronic F68 PBS (49.5 mL PBS + 500 µL Pluronic F68) for 10 min, then it was discarded, and 15 mL of Pluronic F68 PBS (0.01%) (45 mL PBS + 5mL of 0.1% Pluronic F68 PBS) was added. The tubes were centrifuged at 3.000 rpm for 5 min at 4 °C. The supernatant was discarded, and 15 mL of Pluronic F68 (0.001%) + NaCl PBS (200 mM) was added and centrifuged at 3.000 rpm for 5 min at 4 °C. The sample was then added and centrifuged at 3.500 rpm for 8 min at 4 °C. After several centrifugation steps, viral particles were concentrated to a final volume of 500 µL. The viral titer was quantified using RT-qPCR, and the sample was stored at –80 °C.

Primary culture of mouse Schwann cells (MSC).

MSC were isolated from the sciatic nerve of C57BL/6J mice, as previously described [51]. Briefly, the sciatic nerve was dissected, the epineurium was removed, and nerve explants were divided into 1 mm segments and dissociated enzymatically using collagenase (0.05%) and hyaluronidase (0.1%) in Hank's balanced salt solution (HBSS) (2 h, 37 °C). Cells were collected by centrifugation (150 × g, 10 min, 20–25 °C), and the pellet was resuspended and cultured in DMEM containing fetal calf serum (10%), L-glutamine (2 mM), penicillin (100 U/mL), streptomycin (100 mg/mL), neuregulin (10 nM), and forskolin (2 μM). Three days later, cytosine arabinoside (Ara-C, 10 mM) was added to remove the fibroblasts. Cells were cultured at 37 °C in 5% CO_2 and 95% O_2. The culture medium was replaced every 3 d, and the cells were used after 15 d of culture.

Primary culture of mouse DRG neurons

Mouse DRGs (combined cervical, thoracic, and lumbar) were bilaterally excised under a dissection microscope and enzymatically digested using or 2 mg/mL of collagenase type 1A and 1 mg/mL of papain, in HBSS for 35 min at 37 °C. Ganglia were disrupted by several passages using a series of syringe needles (23–25G). Neurons were then pelleted by centrifugation at 180 x g for 5 min at room temperature and resuspended in Ham's F12 supplemented with 10% heat inactivated horse serum, containing 10% heat-inactivated FBS, 100 U/mL of penicillin, 0.1 mg/mL streptomycin, and 2 mM L-glutamine added with 100 ng/mL nerve growth factor, and 2.5 mM cytosine-b-D-arabino-furanoside free base (ARA-C), and maintained at 37 °C in 5% CO_2 and 95% O_2 for 3 d before being used for Ca^{2+} imaging experiments.

Triple co-culture

Triple co-culture experiments were performed using OMEGA^{ACE} devices (#eN-oace-002; eNUVIO Inc., Montréal, Canada). Every device contained three chambers connected *via* a series of microfluidic channels. Chambers #1 and #3 (working volume: 30–140 μL and surface area: 29.6 mm^2) had identical dimensions, were not directly connected, and were each adjoined to chamber #2 (upper and lower well, working volume [combined]: 60–280 μL and combined surface area: 58.6 mm^2) *via* a series of microfluidic channels (number of interfaces per device: 2, number of microchannels per interface: 70, microchannel length: >630 μm, microchannel width: 10 μm). The upper and lower wells that comprised chamber #2 were separated by a 250 μm-wide and 500 μm-high channel.

To mimic the *in vivo* mechanism, different experiments were performed using human and mouse breast cancer cells (MDA-MB-231 and E0771 GFP^+, respectively), osteoclasts (U937 and RAW267.4, respectively), HSC, and MSC. Briefly, MDA-MB-231 or E0771 cells were plated in chamber #1, U937 or RAW267.4 osteoclasts induced cells in the upper and lower wells of chamber #2, and HSC or primary MSC in chamber #3. The three different combinations in which one of the cell types was absent (medium only) were tested. Cells were seeded at a density of 3×10^4 cells/cm^2. The direction of fluid flow across the high-resistance microchannels was determined by asymmetrical volume loading contained within each of the chambers, and the volumes were as follows: 130 μL in chamber #1, 200 μL in chamber #2 (100 μL/each well), and 80 μL in chamber #3. In a set of experiments, PPP (10 nM), L-NAME (10 μM), Akti-1/2 (100 nM), NT157 (3 μM), cPTIO (50 μM), PBN (50 μM) or A967079 (50 μM) were added to chamber #3. In a different set of experiments, RAW264.7 osteoclast induced cells were treated with neutralizing anti-CXCR2/IL-8RB antibody (50 μg/mL; #MAB2164; R&D Systems, Minneapolis, MN, USA), reparixin L-lysine salt (10–100 nM; #6957; Tocris, Bristol, UK), neutralizing anti-TNF-α (100 ng/mL; #AF-410-NA; R&D Systems), and anti-IL-11 (2 μg/mL) (#AF-418-NA; R&D Systems) antibodies or their vehicle (0.0001% DMSO). Cells were incubated at 37 °C in 5% CO_2 and 95% O_2 for 24 h. To minimize evaporation from the chambers during incubation steps, ~500 μL of sterile water was added to the circular track of the evaporation minimizer.

Ca^{2+} imaging

Cells were plated on poly L-lysine-coated (8.3 μM) 35-mm glass coverslips and maintained at 37 °C in 5% CO_2 and 95% O_2 for 24 h. Cells were loaded for 40 min with Fura-2, AM-ester (5 μM) added to the buffer solution (37 °C) containing (in mM) 2 $CaCl_2$; 5.4 KCl; 0.4 MgSO4; 135 NaCl, 10 D-glucose, 10 HEPES, and 0.1% bovine serum albumin (BSA). Cells were washed and transferred to a chamber on the stage of a fluorescent microscope for recording (Axio Observer 7; with a fast filter wheel and Digi-4 lens to record excitations ZEISS). Cells were exposed to human IGF-1 (100 nM) or its vehicle (0.9% NaCl), and the Ca^{2+} response was monitored for approximately 1 h. The Ca^{2+} response to IGF-1 (100 nM) was also monitored in the presence of PPP (10 nM), L-NAME (10 μM), Akti-1/2 (100 nM), NT157 (3 μM), cPTIO (50 μM), and A967079 (50 μM) or their vehicle (0.1% DMSO). In some experiments, a Ca^{2+}-free buffer solution containing EDTA (1 mM) was used. In other experiments, HSC were exposed to MDA-

MB-231/osteoclasts (differentiated U937) conditioned medium in the presence of PPP (10 nM) or a non-conditioned medium for 1 h. To obtain the conditioned medium, MDA-MB-231 cells were incubated at 37 °C in 5% CO_2 and 95% O_2 for 24 h and the day after the medium was collected and used to incubate osteoclasts (differentiated U937) for 24 h, then the medium was used to stimulate the HSC. Conditioned medium was collected from MDA-MB-231 cells (24 h) without osteoclast stimulation. Results are expressed as the percentage increase in $ratio_{340/380}$ over the baseline normalized to the maximum effect, induced by ionomycin (5 μM) added at the end of each experiment. A high concentration (50 mM) of KCl, which depolarizes functional DRG neurons causing Ca^{2+} influx, was used to exclude non-neuronal cells.

Nitric oxide *in vitro* imaging

A fluorescence probe for NO imaging (FP-NO) in live cells was synthesized as reported previously [233, 234]. In a set of experiments, HSC and mouse DRG neurons were plated on poly-L-lysine-coated (8.3 μM) 35-mm glass coverslips and maintained at 37 °C in 5% CO_2 and 95% O_2 for 24 h. Cells were loaded for 30 min with FP-NO (5 μM) and added to Hank's balanced salt solution (HBSS) at pH 7.4. Cells were washed and transferred to a chamber on the stage of a fluorescent microscope for recording (Axio Observer 7; with a fast filterwheel and Digi-4 lens to record excitations; ZEISS, Stuttgart, Germany) and were exposed to human or mouse IGF-1 (100 nM) or its vehicle (0.9% NaCl) for 0.5 h. HSC were exposed to human IGF-1 also in the presence of PPP (10 nM) or its vehicle (0.0005% DMSO). The ΔF/F0 ratio was calculated for each experiment and the results were expressed as the area under the curve (AUC).

In another set of experiments, HSC cells were plated in 96-well black wall clear bottom plates (5×10^5 cells/well; Corning Life Sciences, Tewksbury, MA, USA) and maintained in 5% CO_2 and 95% O_2 (24 h, 37 °C). The cells were incubated for 30 min with FP-NO (5 μM). The culture medium was replaced with HBSS supplemented with NT157 (3 μM), Akti-1/2 (100 nM), and L-NAME (10 μM) or their vehicle (0.1% DMSO) for 20 min at 20–25 °C, and then stimulated with human IGF1 (100 nM) or its vehicle (0.9% NaCl) for 0.5 h. Diethylamine NONOate (2-[N,N-diethylamino]-diazenolate 2-oxide sodium salt hydrate) (10 μM) was used as a positive control. The measurements were performed using a fluorescence plate reader (FlexStation 3 Multi-Mode Microplate Reader; Molecular Devices, San Jose, CA, USA) with SoftMax® Pro 7 software (Molecular Devices) with

the following settings: λ excitation, 436 nM and λ emission, 475 nM. The results are expressed as arbitrary units (A.U.).

Synthesis of fluorescence probe for NO imaging (FP-NO)

The 7-diethylamino-3-hydrazide-coumarin was obtained, under an argon atmosphere, from the reaction of ethyl 7-(diethylamino)-2-oxo-2H-chromene-3-carboxylate (1 mmol; BLDpharm, Shanghai, China) and hydrazine monohydrate (5 mmol) in absolute ethanol (5 mL) at room temperature. The reaction mixture was then stirred for 30 min. After completion, it was cooled to 0 °C, providing an orange precipitate that was filtered, washed with cold ethanol (3 × 15 mL), and dried under a vacuum (59% yield). Then, a solution of 4-nitrophenyl isothiocyanate (1 mmol) in acetonitrile (5 mL) was slowly added to a stirred solution of 7-diethylamino-3-hydrazide-coumarin (1 mmol) in acetonitrile (15 mL) under an argon atmosphere. The mixture was refluxed for 6 h, after which it was cooled to RT. The solvent was removed under vacuum, and the residue was purified via flash column chromatography using petroleum ether and ethyl acetate as the eluents. The probe FP-NO was obtained as an orange solid with 90% yield. The purity of the probe was assessed by analytical high-performance liquid chromatography showing a degree of purity >95%. ^{1}H and ^{13}C NMR characterizations of both 7-diethylamino-3-hydrazide-coumarin and FP-NO matched the data reported in the literature[233, 234] . All the solvents were used without further purification. The reaction progress and product mixtures were monitored by thin-layer chromatography on precoated plates of silica gel F254 (Merck Millipore). The compounds were purified by silica gel flash chromatography (silica gel 60, 40–63 μm) using the opportune eluent. Analytical high-performance liquid chromatography analyses were performed using a Beckman 116 liquid chromatograph equipped with a Beckman 166 diode array detector (Beckman Coulter). Analytical purity of the final compound FP-NO was assessed using an XBridge BEH C18 column (4.6 × 150 mm, 5 μm particle size; Waters, Milford, MA, USA) at a flow rate of 0.7 mL/min with a linear gradient of acetonitrile (0.1% TFA) in water (0.1% TFA) over 25 min. The mass spectra were recorded using a Micromass ZMD 2000 instrument (Waters) by dissolving the samples in a solution of H_2O/CH_3CN/TFA (40:60:0.1). ^{1}H NMR and ^{13}C NMR were recorded on a Varian 400 spectrometer (Agilent technologies, Santa Clara, CA, USA) and were referenced to the residual ^{1}H signals of the deuterated solvents (δ ^{1}H 7.26 for $CDCl_3$, δ ^{1}H 2.50 for DMSO-d_6).

H_2O_2 *in vitro* imaging

A genetically encoded probe for H_2O_2-HyPer [HyPer7.2 [235], kindly donated by Dr. Emrah Eroglu, Harvard Medical School, Boston, US] was used on live cells. HSC were plated on poly-L-lysine-coated (8.3 μM) 35-mm glass coverslips and transfected with DNA (2 μg) of HyPer7.2 using jetOPTIMUS® DNA transfection reagent (#55-250; Polyplus, Lexington, MA, USA). After 24–48 h, the HSC were washed and transferred to a chamber on the stage of a fluorescent microscope for recording (Axio Observer 7; with a fast filterwheel and Digi-4 lens to record excitations; ZEISS, Stuttgart, Germany). Cells were exposed to IGF-1 (1 μM) or its vehicle (0.9% NaCl) and H_2O_2 variations were monitored for approximately 1 h in the presence of PPP (10 nM), Akti-1/2 (100 nM), or A967079 (50 μM). Results were expressed as the percentage increase in the $ratio_{408/455}$ over the baseline normalized to the maximum effect, induced by H_2O_2 (10 μM) added at the end of each experiment.

Protein extraction and western immunoblot assay

HSC were plated on 60 mm culture dishes and maintained at 37 °C in 5% CO_2 and 95% O_2 until 90% confluence. The cells were serum-starved for 4 h in Schwann cell medium without FBS and then treated with IGF-1 (100 nM) for 10 min. Cells were collected and homogenized in RIPA buffer [NaCl (150 mM), Tris-base (50 mM), EGTA (5 mM), Triton X-100 (1%), sodium deoxycholate (0.5%), sodium dodecyl sulfate (0.1%)] containing dithiothreitol (1 mM) and complete protease inhibitor cocktail. Lysates were centrifuged at 1800 x g at 4 °C for 10 min. The protein concentration in the supernatants was determined using a BCA protein assay (Thermo Fisher Scientific). Samples containing equal amounts of proteins (30 μg) were then separated by NuPAGE 4%–12% Bis-Tris gel electrophoresis (Life Technologies, Carlsbad, CA, USA), and the proteins were transferred to nitrocellulose (Bio-Rad, Hercules, CA, USA). Membranes were incubated with BSA (5%) in Tris buffer [TBST; Tris (20 mM) at pH 7.5, NaCl (150 mM)] containing Tween 20 (0.1%) for the phosphorylated proteins and with dry milk (5%) in TBST for 1 h at room temperature, and incubated with the following primary antibodies: phospho-IGF-1 Receptor β (Tyr1131)/Insulin Receptor β (Tyr1146) (#3021, rabbit polyclonal, 1:1000; Cell Signaling, Danvers, MA, USA), IGF-I Receptor β (D23H3) XP (#9750, mouse monoclonal, 1:1000; Cell Signaling), Phospho-IRS1 (Tyr612) (#44-816G, rabbit polyclonal, 1:1000; Thermo Fisher Scientific), IRS-1 (#2382, rabbit polyclonal, 1:1000; Cell Signaling), Phospho-Akt (Ser473) (D9E) XP (#4060,

rabbit monoclonal, 1:2000; Cell Signaling), Akt (pan) (40D4) (#2920, mouse monoclonal, 1:2000; Cell Signaling), Phospho-eNOS (Ser1177) (C9C3) (#2920, rabbit monoclonal, 1:1000; Cell Signaling) or eNOS (D9A5L) (#32027, rabbit monoclonal, 1:1000; Cell Signaling) at 4 °C overnight. The membranes were then probed with goat anti-mouse or donkey anti-rabbit IgG conjugated with horseradish peroxidase (1:10,000; Bethyl Laboratories Inc., Montgomery, TX, USA) for 2 h at RT. Finally, membranes were washed three times with TBST, and bound antibodies were detected using chemiluminescence reagents (Pierce™ ECL; Thermo Fisher Scientific) and revealed using an imaging system (ChemiDoc; Bio-Rad). The density of specific bands was measured using ImageJ (v.1.53t; National Institutes of Health, Bethesda, MD, USA) and normalized to β-actin.

Immunofluorescence

The mouse femurs were fixed in 4% paraformaldehyde overnight at 4 °C, followed by decalcification in 0.5 M EDTA solution at pH 8.0 for 14 d at RT. They were then cryoprotected in 30% sucrose and cryosectioned at 10 μm for immunostaining. The metastatic tumor mass was calculated as GFP^+ area in the femur head expressed as $\mu m^2 x 10^3$.

HSC and primary MSC cells were plated on poly-L-lysine (8.3 μM)-and laminin (5 μM) coated 35-mm glass coverslips (Thermo Fisher Scientific) and maintained at 37 °C in 5% CO_2 and 95% O_2 for 24 h. Cells were washed in PBS and fixed with 4% paraformaldehyde, followed by permeabilization with 0.5% Triton X-100. Blocking was performed using normal goat serum (NGS, 5%) for 1 h and incubated with anti-IGF-1R (#BS-0227R, rabbit polyclonal, 1:250; Thermo Fisher Scientific) for 1 h. The cells were washed and incubated with the fluorescent polyclonal secondary antibody Alexa Fluor 488 (#A32731, goat polyclonal, 1:600; Thermo Fisher Scientific). After incubation with the secondary antibody, the cells were incubated for 1 h with recombinant Alexa Fluor 647 Anti-S100 beta [EP1576Y] (#ab196175, rabbit monoclonal, 1:50; Abcam). Sections were coverslipped using a water-based mounting medium containing DAPI (#ab104139; Abcam).

Mouse sciatic nerve, DRG, and human cutaneous formalin-fixed paraffin-embedded tissue sections (5 μm) were deparaffinized and incubated in Tris-EDTA (pH 9) buffer for antibody retrieval. The slides were incubated with primary antibodies: IGF-1R (#BS-0227R, rabbit polyclonal, 1:250; Thermo Fisher Scientific), recombinant Alexa Fluor 647

Anti-S100 beta [EP1576Y] (#ab196175, rabbit monoclonal, 1:50; Abcam, Cambridge, UK), NeuN (#MAB377, mouse monoclonal, 1:250; Merck Life Science SRL, Milan, Italy), diluted in the blocking solution (NGS 5%). Tissues were incubated (2 h, RT) with Alexa Fluor 488 (#A32731, goat polyclonal, 1:600; Thermo Fisher Scientific) and Alexa Fluor 594 (#A11005, goat polyclonal, 1:600; Thermo Fisher Scientific) secondary antibodies, washed, and coverslipped with mounting medium containing DAPI (#ab104139; Abcam).

For macrophages analysis mouse sciatic nerve were cryoprotected overnight at 4 °C in 30% sucrose until cryosectioning. Slides containing cryosections (10 μm) were incubated with F4/80 [1:50, MA516624, rat monoclonal (Cl:A3-1), RRID:AB_2538120 Thermo Fisher Scientific] diluted in the blocking solution (PBS, pH 7.4, Triton-X 0.3%, NGS 5%). Followed by an Alexa Fluor 488 (#A21208, donkey polyclonal, 1:600; Thermo Fisher Scientific) secondary antibody incubation, washed, and coverslipped with mounting medium containing DAPI (#ab104139; Abcam). Negative controls (non-immune serum) were simultaneously analyzed to exclude the presence of non-specific immunofluorescence staining, cross-immunostaining, or fluorescence bleed-through. All slides were visualized and analyzed using a Zeiss Axio Imager 2 microscope with Z-stacks in the Apotome mode (ZEISS). The number of $F4/80^+$ cells was counted in $4.5x10^5$ μm^2 boxes in the sciatic nerve trunk.

RNAscope

Frozen tissue sections (10 μm) of mouse DRG were washed with 1× PBS, baked for 30 min at 60 °C, post-fixed with 4% paraformaldehyde in 1× PBS at 4 °C, and dehydrated. Frozen tissue sections of the mouse sciatic nerve (10 μm) were baked for 30 min at 60 °C and washed with 1× PBS. DRG and sciatic nerve tissues were treated with hydrogen peroxide (#322335; Advanced Cell Diagnostics, Newark, CA, USA) for 10 min at RT. Target retrieval was performed for 5 min at 99–100 °C, followed by Protease Plus (#322331; Advanced Cell Diagnostics) pre-treatment for 30 min at 40 °C. Samples were subsequently hybridized with a probe specific to mouse TRPA1 (#400211; Advanced Cell Diagnostics) and a negative (#310043; Advanced Cell Diagnostics) control probe for 2 h at 40 °C. Sequential signal amplification and red chromogenic detection was performed. Sciatic nerve slides were subjected to immunofluorescence labeling using Alexa Fluor® 488 anti-S100 beta antibody [EP1576Y] (#ab196442; monoclonal rabbit, 1:100; Abcam, Cambridge, UK) overnight at 4 °C. Both DRG and sciatic nerve sections were coverslipped using a mounting medium with an aqueous Fluoroshield with 4′6′-diamidino-2-

phenylindole (DAPI; #ab104139; Abcam). Fluorescent images were acquired using a Zeiss Axio Imager 2 (ZEISS).

Plasma Ca^{2+} level

The total plasma Ca^{2+} content was measured at 20 d after cancer cell inoculation using a colorimetric Ca^{2+}assay kit (#ab102505; Abcam, Cambridge, UK), according to the manufacturer's protocol.

IGF-1, IL-6, TGF-b, M-CSF assays

The IGF-1 contents were assayed in the bone and sciatic nerve tissue homogenates at 20 d after cancer cell inoculation and in the cultured medium using a single-analyte enzyme-linked immunosorbent assay kit (#ab100695 and #ab100545, Abcam, Cambridge, UK) according to the manufacturer's protocol. Data are expressed as pg/mg of protein and pg/mL. IL-6 and TGF-b levels were assayed in the bone and sciatic nerve tissue homogenates at 20 d after cancer cell inoculation using a single-analyte enzyme-linked immunosorbent assay kit (#ab100713 and #ab119557, respectively, Abcam) according to the manufacturer's protocol. The samples were assayed in triplicate. Data are expressed as pg/mg of protein. M-CSF content was assayed in the sciatic nerve tissue homogenates at 20 d after cancer cell inoculation and in the cultured medium using a single-analyte enzyme-linked immunosorbent assay kit (#ab199084 ad #ab245714 Abcam) according to the manufacturer's protocol. Data are expressed as pg/mg of protein and pg/mL.

H_2O_2 assay

H_2O_2 levels were assessed in sciatic nerve tissue homogenates and cultured medium using the Amplex Red® assay (Invitrogen, Waltham, MA, USA), according to the manufacturer's protocol. Fluorescence excitation and emission were measured at 540 and 590 nm, respectively. H_2O_2 production was calculated using the H_2O_2 standard and expressed as nmol/mg protein or μmol/L.

Nitric oxide assay

The NO content was determined in sciatic nerve tissue homogenates at 20 d after cancer cell inoculation and in the cultured medium using a colorimetric assay kit (#ab272517; Abcam, Cambridge, UK) according to the manufacturer's protocol. Data are expressed as μmol/L/mg of protein or μmol/L.

RT-qPCR

Total RNA was extracted from HSC, primary MSC, mice sciatic nerves, and DRGs using the RNeasy Mini Kit (Qiagen SpA, Hilden, Germany), according to the manufacturer's protocol. RNA concentration and purity were assessed spectrophotometrically by measuring the absorbance at 260 and 280 nm. RNA was reverse transcribed using the Qiagen QuantiTect Reverse Transcription Kit (Qiagen SpA, Hilden, Germany) following the manufacturer's protocol. For relative mRNA quantification, RT-PCR was performed using Rotor Gene® Q software (v.2.3.1.49; Qiagen SpA). The relative abundance of mRNA transcripts was calculated using the Δ^{CT} method and normalized to glyceraldehyde-3-phosphate dehydrogenase (GAPDH) levels.

Statistical analysis

The results are expressed as the mean ± SEM. For multiple comparisons, a one-way ANOVA followed by a post-hoc Bonferroni's test or Dunnett's test was used. The two groups were compared using Student's *t*-test. For behavioral experiments with repeated measures, a two-way mixed-model ANOVA followed by a post-hoc Bonferroni's test was used. Statistical analyses were performed on raw data using GraphPad Prism 8 (GraphPad Software Inc., San Diego, CA, USA). *P*-values less than 0.05 ($P < 0.05$) were considered significant. The statistical tests used and sample size for each analysis are shown in the Fig. legends.

6.2 Results

6.2.1 IGF-1 in metastatic bone cancer pain

Inoculation of E0771 breast carcinoma cells into the mammary gland (intramammary) of C57BL/6J female mice (C57) (**Fig. 25a**) induced a time-dependent increase in mammary tumor mass, mainly due to tumor growth (**Fig. 25b**). Tumor evolution was associated with a progressive increase in hind paw mechanical/cold hypersensitivity and a reduction in spontaneous locomotor activity (cumulative distance traveled) and thigmotaxis behavior (time spent in the inner zone), two indices of non-stimulus-evoked pain-like behavior [148, 228, 236, 237] (**Fig. 25c–f**). Hereafter, these behaviors are collectively defined as pain-like behaviors. No impairment in motor coordination was observed in E0771 cell-inoculated mice (E0771-mice) compared to control mice (**Fig. 26a**). Control mice, inoculated with E0771-killed cells, showed no

increase in mammary thickness, nor in measurable pain-like behaviors (**Fig. 25b–f).** As pain-like behaviors plateaued between 16–20 d after E0771 cell inoculation, if not otherwise specified, all outcome measures reported hereafter were assessed 20 d after inoculation. Unless otherwise specified, all experiments were conducted in C57 mice. Body weight of E0771- or control mice at the beginning and end of the protocol was similar (**Fig. 26b**)

Mice inoculated with E0771-green fluorescent protein (GFP) cells showed a time-dependent increase in the fluorescent metastatic mass in the femoral head (**Fig. 25g**). The presence of bone metastasis in E0771-mice was further supported by increased plasma Ca^{2+} levels (**Fig. 25h**). To verify that the source of pain-like behaviors was the metastasis and not the primary tumor, poor-metastatic melanoma cells (B16-F0) [238] were inoculated in the C57 fat pad. Twenty days after cell inoculation, primary tumor masses of E0771 and B16-F0 mice were comparable (**Fig. 25b** and **Fig. 26c**). However, B16-F0-mice did not show any pain-like behaviors or increased plasma Ca^{2+} levels (**Fig. 26d-h**). This data confirms that the primary tumor in the fat pad is not *per se* sufficient to induce pain-like behaviors in C57 mice. In E0771-mice, the development of pain-like behaviors was associated with increased levels of osteolysis biomarkers, including IGF-1, IL-6, and TGF-b, in both bone and sciatic nerve tissue homogenates (**Fig. 25i** and **Fig. 26i** and **26j**). We then explored which of these mediators were implicated in pain-like behaviors. Repeated administration of the IGF-1 receptor (IGF-1R) inhibitor, picropodophyllin (PPP), attenuated E0771 cell-evoked pain-like behaviors (**Fig. 25j-m**), without affecting the growth of the primary tumor size (**Fig 25n**) or femur metastasis (**Fig. 25o**). Furthermore, repeated administration of IL-6 or TGF-b neutralizing antibodies (from days 10 to 20) had no effect on pain-like behaviors or primary tumor growth (**Fig. 26k-t**). To test the effect of IL-6 or TGF-b in the initial development of pain-like behaviors, we administered the neutralizing antibodies from day 2 to day 10 in E0771- mice. No significant difference was observed in paw mechanical/thermal hypersensitivity after these treatments compared to control (**Fig.26u-x**). The results suggest that pain-like behaviors depend solely on increased IGF-1 levels and are unrelated to the expansion of femur metastases.

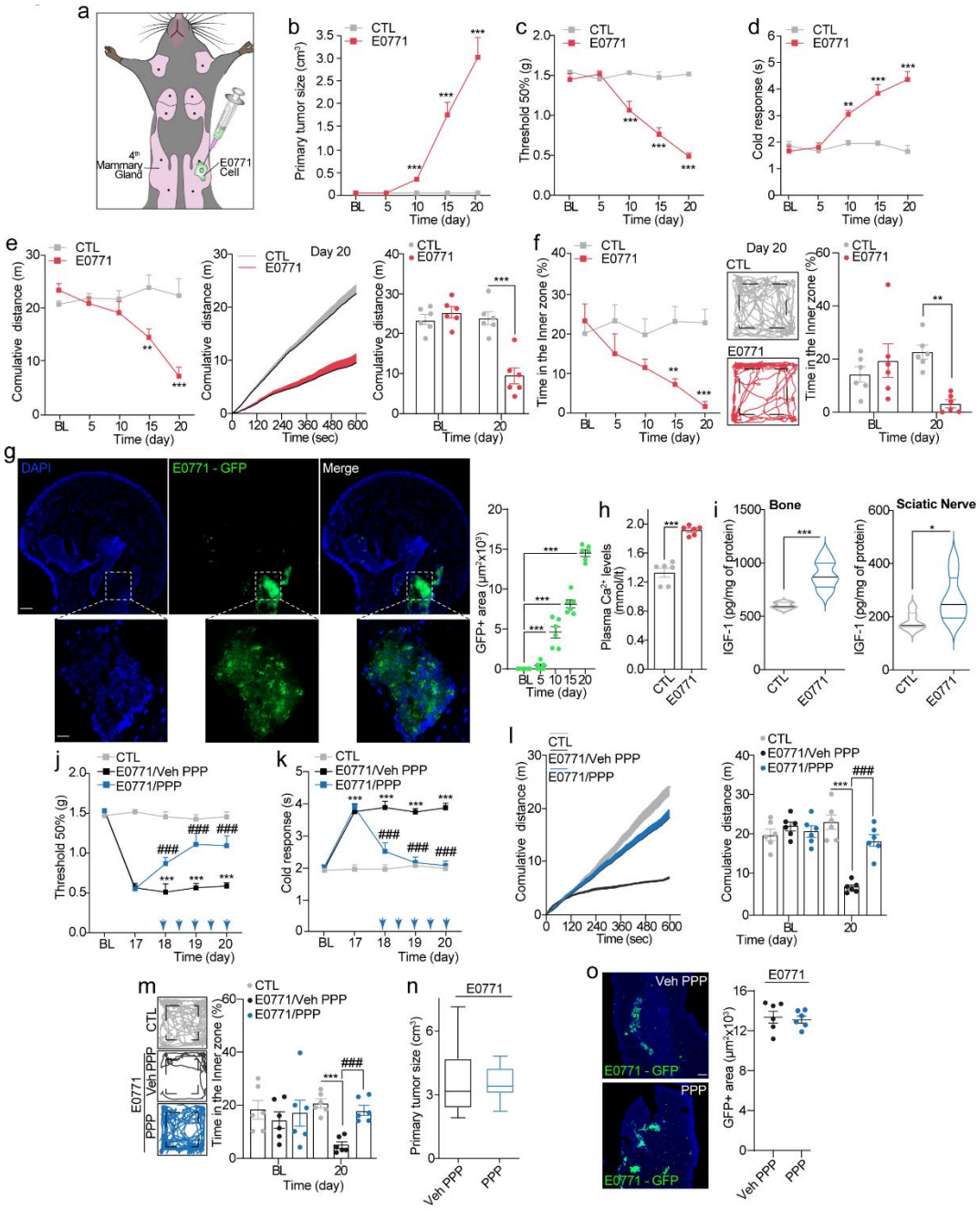

Figure 25. E0771 cells intramammary inoculation induces bone metastatic cancer pain mediated by IGF-1 (**a**) Graphical illustration of intramammary E0771 cell inoculation. (**b**) Time-dependent increase in primary tumor size and (**c**) mechanical and (**d**) cold allodynia after E0771 cell intramammary inoculation or control (CTL) in C57BL/6J mice. (**e**) Cumulative distance and (**f**) time spent in the inner zone after E0771 cell inoculation or CTL in C57BL/6J mice (n=6 mice per group). (**g**) Whole slide images of E0771-GFP^{+} cells in the femur head 20 d after E0771 cell inoculation in C57BL/6J mice (Scale bar: 50 µm, inset 20 µm) and time-dependent increase of the bone metastasis tumor mass (GFP^{+}area µm^{2}x10^{3}). (**h**) Plasma Ca^{2+} levels and (**i**) bone and sciatic nerve tissue homogenate IGF-1 content 20 d after E0771 cell inoculation or CTL in C57BL/6J mice. (**j**) Mechanical and (**k**) cold allodynia, (**l**) cumulative distance, (**m**) time spent in the inner zone, (**n**) primary tumor size and (o) representative images and bone metastasis tumor mass (GFP^{+}area µm^{2}x10^{3}) after E0771 cell inoculation or CTL in C57BL/6J mice

treated with PPP/vehicle (i.p.). (Scale bar: 50 µm) (n=6 mice per group). Mean ± SEM. **P*<0.05, ***P*<0.01, ****P*<0.001 vs. CTL, BL; ###*P*<0.001 vs. E0771, E077/vehicle PPP.

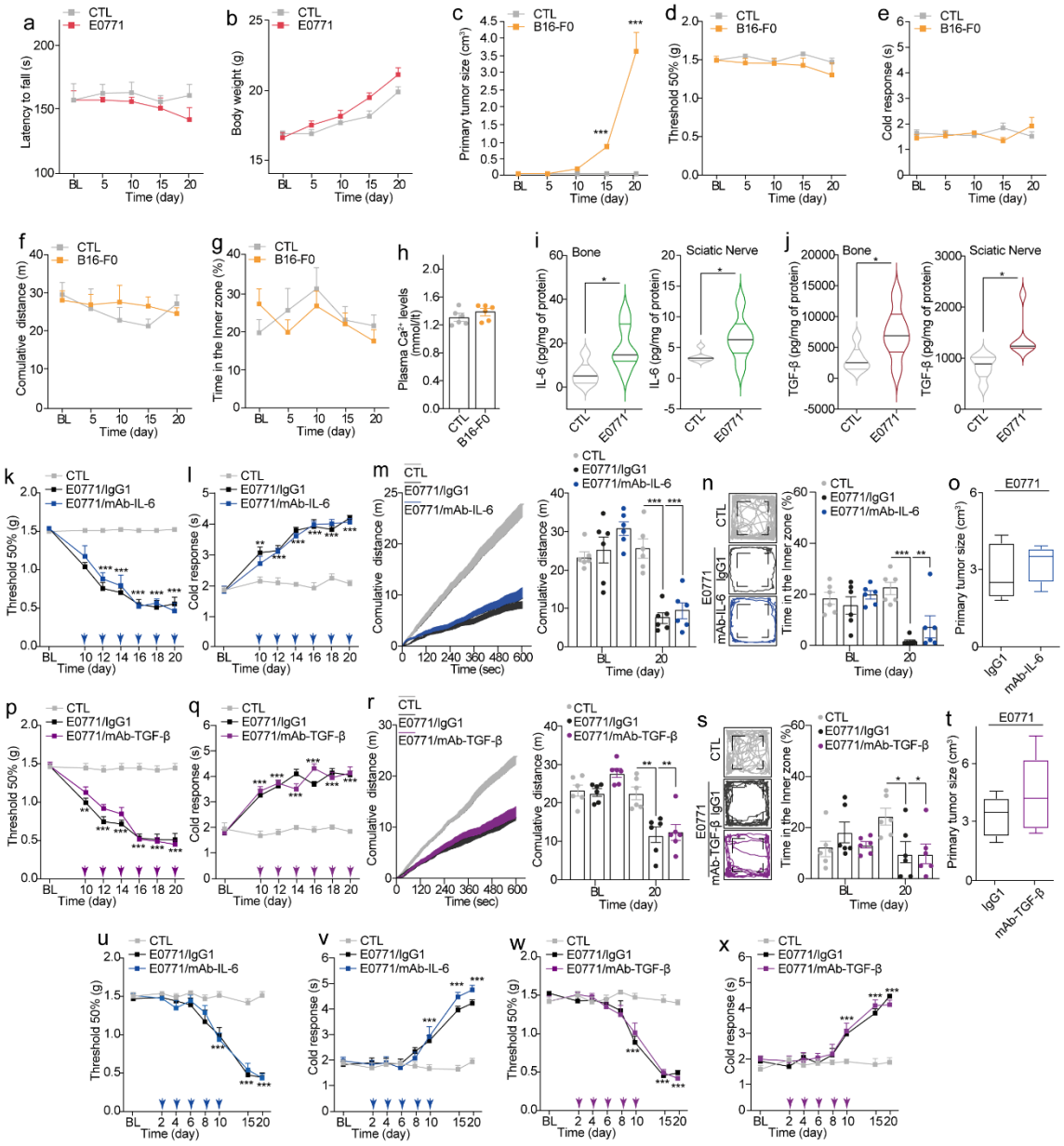

<u>Figure 26</u>. TGF-β and IL-6 do not contribute to E0771 bone metastatic cancer pain. **(a)** Time-dependent motor coordination on rotarod performance and (**b**) body weight measurement after E0771 cell inoculation or control (CTL) in C57BL/6J mice. (**c**) Time-dependent increase in tumor size and (**d**) mechanical, (**e**) cold allodynia, (**f**) cumulative distance and (**g**) time spent in the inner zone and (**h**) plasma Ca^{2+} levels after B16-F0 cell inoculation or CTL in the fat pad of C57BL/6J mice. (**i**) TGF-β and (**j**) IL-6 content in bone and sciatic nerve tissue homogenates 20 d after E0771 cell inoculation or CTL in C57BL/6J mice. (**k, p, u, w**) Mechanical/(**l, q, v, x)** cold allodynia, (**m, r**) cumulative distance, (**n, s)** time spent in the inner zone and (**o, t**) tumor size after E0771 cell inoculation or CTL in C57BL/6J mice treated with an anti-IL-6 mAb, anti-TGF-β mAb or IgG1 control (n = 6 mice per group). Mean ± SEM. **P* < 0.05, ***P* < 0.01, ****P* < 0.001 vs. CTL.

6.2.2 IGF-1-induced hypersensitivity is mediated by Schwann cell IGF-1R

IGF-1 has been reported to contribute in various rodent pain models [239-243], including bone pain induced by the inoculation of mammary carcinoma cells into the tibial cavity [244]. The proalgesic action of IGF-1 has been proposed to have a direct action on nociceptors [239]. However, the pathways by which IGF-1 signals pain remain unknown. Owing to the emerging critical role of Schwann cells in sustaining mechanical hypersensitivity in different chronic pain models in mice [51, 67, 177, 227], and the presence of IGF-1R in Schwann cells [245], we hypothesized that Schwann cells encode the IGF-1 signal that elicits pain-like behaviors in the present metastatic bone cancer pain (MBCP) mouse model.

First, we showed the proalgesic activity of IGF-1 in the peripheral and not in the central nervous system in E0771-mice. Repeated perineural (p.n.), but not intrathecal (i.th.), administration of an IGF-1-neutralizing antibody reduced pain-like behaviors in E0771-mice (**Fig. 27a–d** and **27f–i**), while tumor growth was unaffected by both treatments (**Fig. 27e** and **27j**). These findings indicate the peripheral nervous system as the primary site of IGF-1 proalgesic action. Second, to identify the cell(s) responsible for cancer-evoked and IGF-1-mediated pain-like behaviors, we confirmed the expression of IGF-1R mRNA and protein in human and mouse cultured Schwann cells and in *ex-vivo* nerve trunks and mouse DRGs (**Fig. 28a–e**). Then, by using AAV-based Cre-dependent shRNA, we selectively silenced IGF-1R in mice expressing Cre recombinase, either in Schwann cells (Plp-Cre) or primary sensory neurons (Adv-Cre), thus generating Plp-Cre/ERT^{+}-shRNA(IGF-1R) and Adv-Cre-shRNA(IGF-1R) mice, respectively (**Fig. 28f and g** and **Fig. 27k**). IGF-1R silencing was confirmed by RT-qPCR (**Fig. 28g** and **Fig. 27k**). Intrasciatic (i.sc.) administration of AAV-shRNA(IGF-1R) in Plp-Cre mice, but not i.th. administration of AAV-shRNA(IGF-1R) in Adv-Cre mice, attenuated pain-like behaviors in E0771-mice (**Fig. 28h–k** and **Fig. 27l–o**). The growth of bone metastasis was unaffected by selective silencing of SC IGF-1R (**Fig. 28l**). These findings pointed to IGF-1R in Schwann cells, but not in nociceptors, as the mediator of pain-like behaviors.

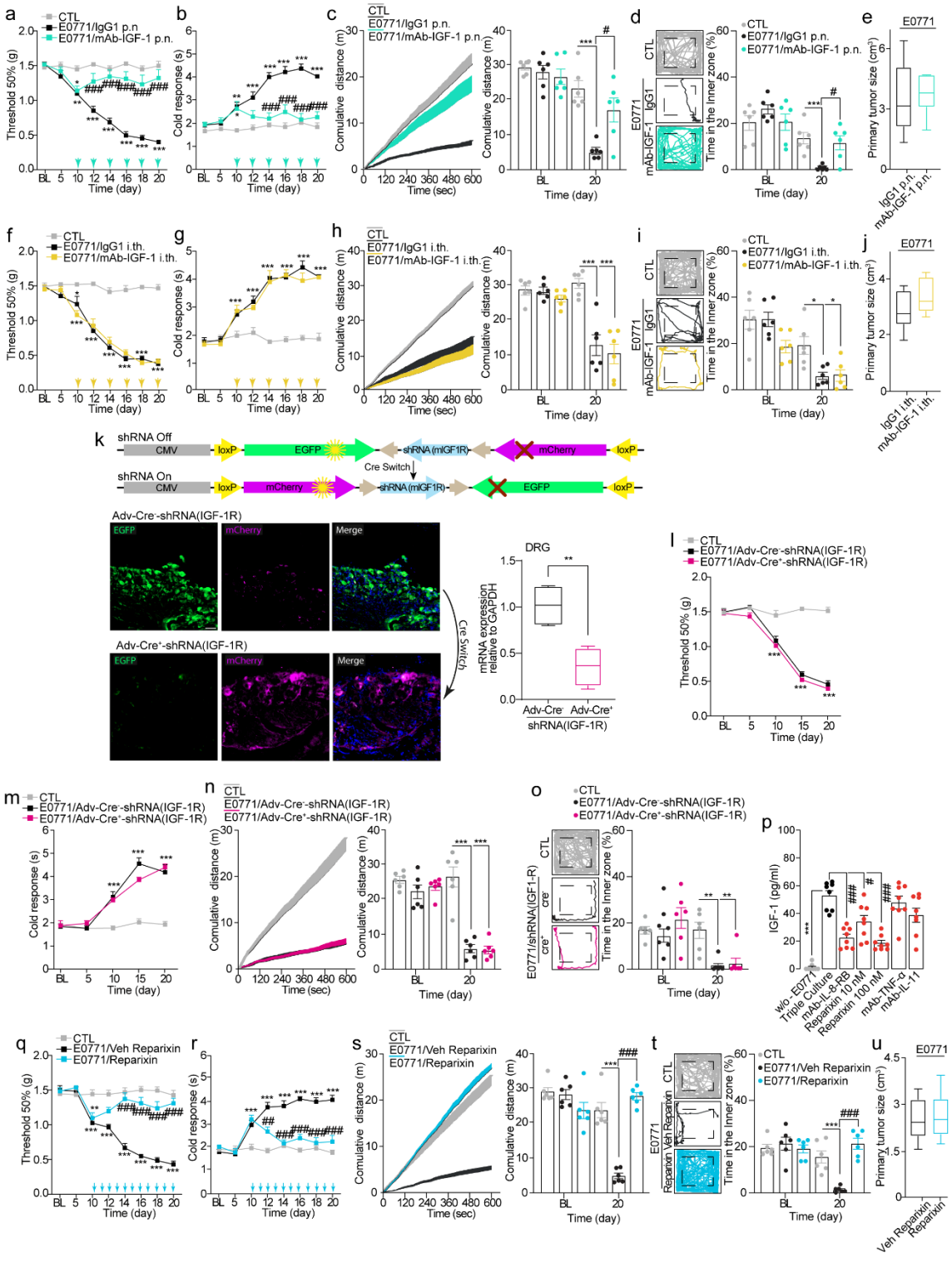

Figure 27. E0771 bone metastatic cancer pain is not mediated by neuronal IGF-1 receptor. (**a, f**) Mechanical/(**b, g**) cold allodynia, (**c, h**) cumulative distance, (**d, i**) time spent in the inner zone, and (**e, j**) tumor size after E0771 cell inoculation or control (CTL) in C57BL/6J mice treated with (**a–e**) perineural (p.n.) or (**f–j**) intrathecal (i.th.) anti-IGF-1 mAb or IgG1 control (n = 6 mice per group). (**k**) Diagram of AAV-(loxP-shRNA)IGF-1R vector pre- and post-Cre switch, representative images of Cre switch and IGF-1R mRNA relative expression in DRG of Adv-Cre^{-} and Adv-Cre^{+} mice infected with AAV-

(loxP-shRNA)IGF-1R viral vector [Adv-Cre^{-}-shRNA(IGF-1R) and Adv-Cre^{+}-shRNA(IGF-1R)] (Scale bar: 20 µm). (**l**) Mechanical/(**m**) cold allodynia, (**n**) cumulative distance, and (**o**) time spent in the inner zone after E0771 cell inoculation or CTL in Adv-Cre^{-}-shRNA(IGF-1R) and Adv-Cre^{+}-shRNA(IGF-1R)] (n = 6 mice per group) (**p**) IGF-1 content in mouse triple co-culture without E0771 cells or incubated with mAb-IL-8-RB, reparixin (10 and 100 µM), mAb-TNF-α, and mAb-IL-11 (n = 8 replicates) (**q**) Mechanical/(**r**) cold allodynia, (**s**) cumulative distance, (**t**) time spent in the inner zone and (**u**) tumor size after E0771 cell inoculation or CTL in C57BL/6J mice treated with reparixin /vehicle (i.p.) (n = 6 mice per group). Mean ± SEM. *P < 0.05, **P < 0.01, ***P < 0.001 vs. CTL, triple culture; $^{\#}P$ < 0.05, $^{\#\#\#}P$ < 0.001 vs. E0771/IgG1, E0771/vehicle reparixin, mAb-IL-8-RB, and reparixin.

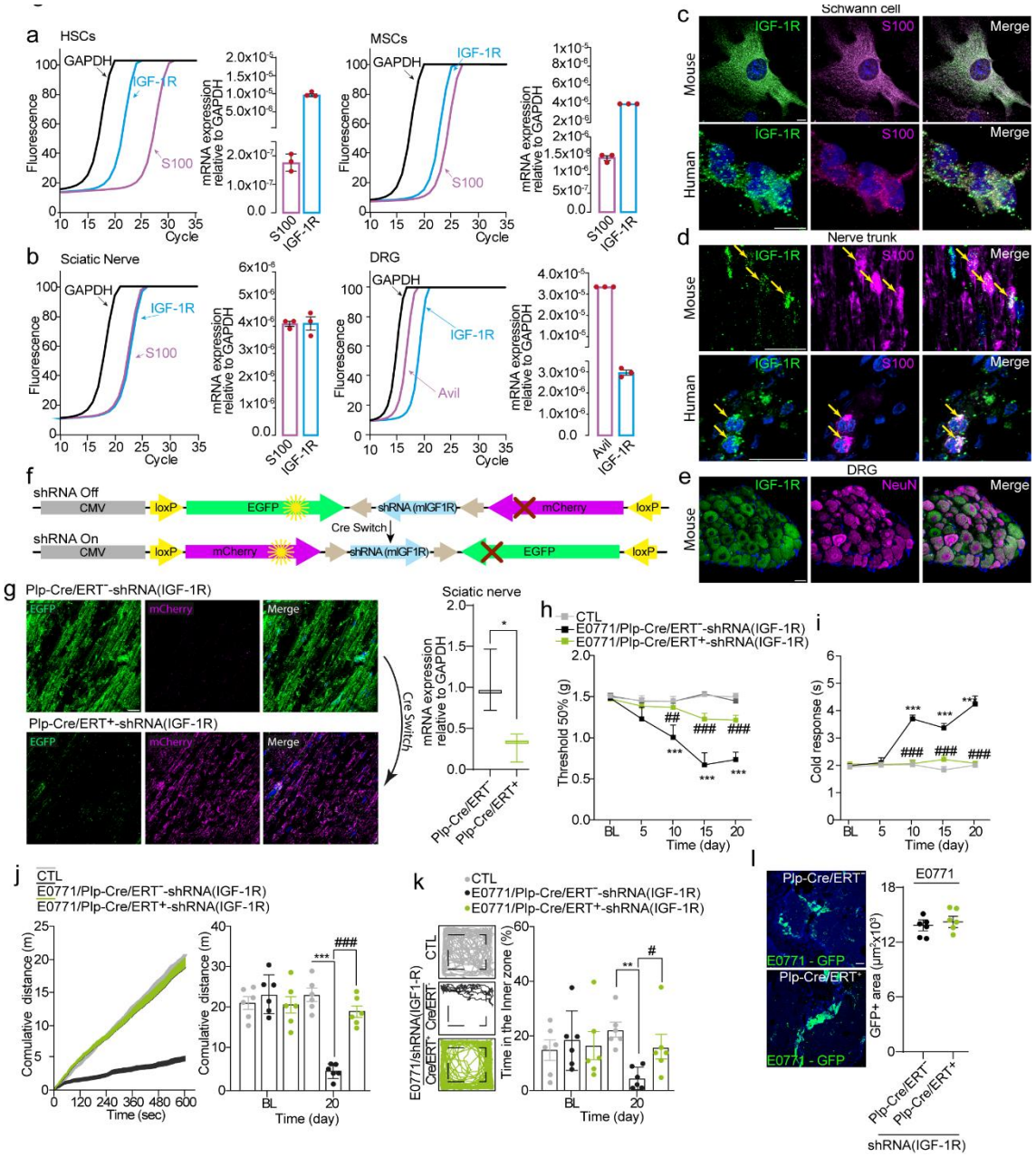

Fig. 28. SC IGF-1R modulates E0771 bone metastatic cancer pain (**a**) IGF-1R mRNA relative expression in primary HSC and MSC and (**b**) mouse sciatic nerve and dorsal root ganglia (DRG) tissue homogenates (n=3 replicates). (**c**) Immunocytochemistry of IGF-1R in primary HSC and MSC (Scale bar: 10 µm) (n=3 replicates). Images of IGF-1R expression in (**d**) human intraepidermal nerve and mouse sciatic nerve and (**e**) mouse DRGs (Scale bar: 20 µm) (n=3 subjects). (**f**) Diagram of AAV-(loxP-shRNA) IGF-1R vector pre- and post-Cre switch. (**g**) Representative images of Cre switch and IGF-1R mRNA relative expression in mouse sciatic nerve of Plp-Cre/ERT^{-} and Plp-Cre/ERT^{+} mice infected with AAV-(loxP-shRNA) IGF-1R viral vector (Scale bar: 20 µm). (**h**) Mechanical and (**i**) cold allodynia, (**j**) cumulative distance (**k**) time spent in the inner zone and (**l**) representative images and bone metastasis tumor mass (GFP^{+}area µm^{2}x10^{3}) after E0771 cell inoculation or control (CTL) in Plp-Cre/ERT^{-} and Plp-Cre/ERT^{+} infected with AAV-(loxP-shRNA) IGF-1R [E0771/Plp-Cre/ERT^{-}-shRNA(IGF-1R) and E0771/Plp-Cre/ERT^{+}-shRNA(IGF-1R)] (Scale bar: 50 µm) (n=6 mice per group). Mean ± SEM. **P*<0.05, ***P*<0.01, ****P*<0.001 vs. CTL; $^{\#}$*P*<0.05, $^{\#\#\#}$*P*<0.001 vs. E0771/Plp-Cre/ERT^{-}-shRNA(IGF-1R).

To identify the sequential events underlying pain-like behaviors, we set up a triple co-culture chamber containing mouse or human: breast cancer cells (E0771 or MDA-MB-231, respectively), osteoclasts (RAW 264.7 or U937, respectively), and Schwann cells. This setup allowed unidirectional flux from breast cancer cells to osteoclasts, and finally to Schwann cells (**Fig. 29a** and **29f**). The absence of cancer cells or osteoclasts, but not Schwann cells, attenuated IGF-1 release (**Fig. 29b** and **29g**). Previous evidence indicates that IL-8, IL-11, and TNF-a [246, 247] are released from cancer cells and might be responsible for IGF-1 release. In the triple chamber, IL-8, but not IL-11 or TNF-a, inhibition attenuated the increase in IGF-1 in the medium (**Fig. 27p**). *In vivo* findings strengthened the role of IL-8 as an antagonist of the IL-8 receptor (CXCR1/2), reparixin, reduced pain-like behaviors, and left unaffected primary tumor growth in E0771-mice (**Fig. 27q–u**), thus indicating that cancer cell-derived IL-8 releases IGF-1 from osteoclasts.

Recently, we reported the essential role of oxidative stress generated by Schwann cells in hypersensitivity in various mouse pain models [51, 227]. Using the triple chamber, we found that the removal of each cell type reduced the H_2O_2 increase (**Fig. 29c** and **29h**), leading us to conclude that Schwann cells, the last cell bathed by the fluid, generated an oxidative stress burst. The finding that treatment with the IGF-1R antagonist, PPP, prevented the release of H_2O_2, but not IGF-1 (**Fig. 29d** and **29e** and **29i and 29j**), suggests that osteoclast-derived IGF-1 increases oxidative stress by targeting Schwann cell IGF-1R. Our *in vivo* experiments corroborated these findings. Intraperitoneal (i.p.) administration of the antioxidant phenyl-alpha-tert-butyl nitrone (PBN) abated pain-like

behaviors in E0771-mice (**Fig. 29k–n**) by reducing H_2O_2 sciatic nerve content (**Fig. 29o**), without affecting IGF-1 increase in either bone or sciatic nerve tissue homogenates (**Fig. 29p**) and primary tumor growth (**Fig. 29q**).

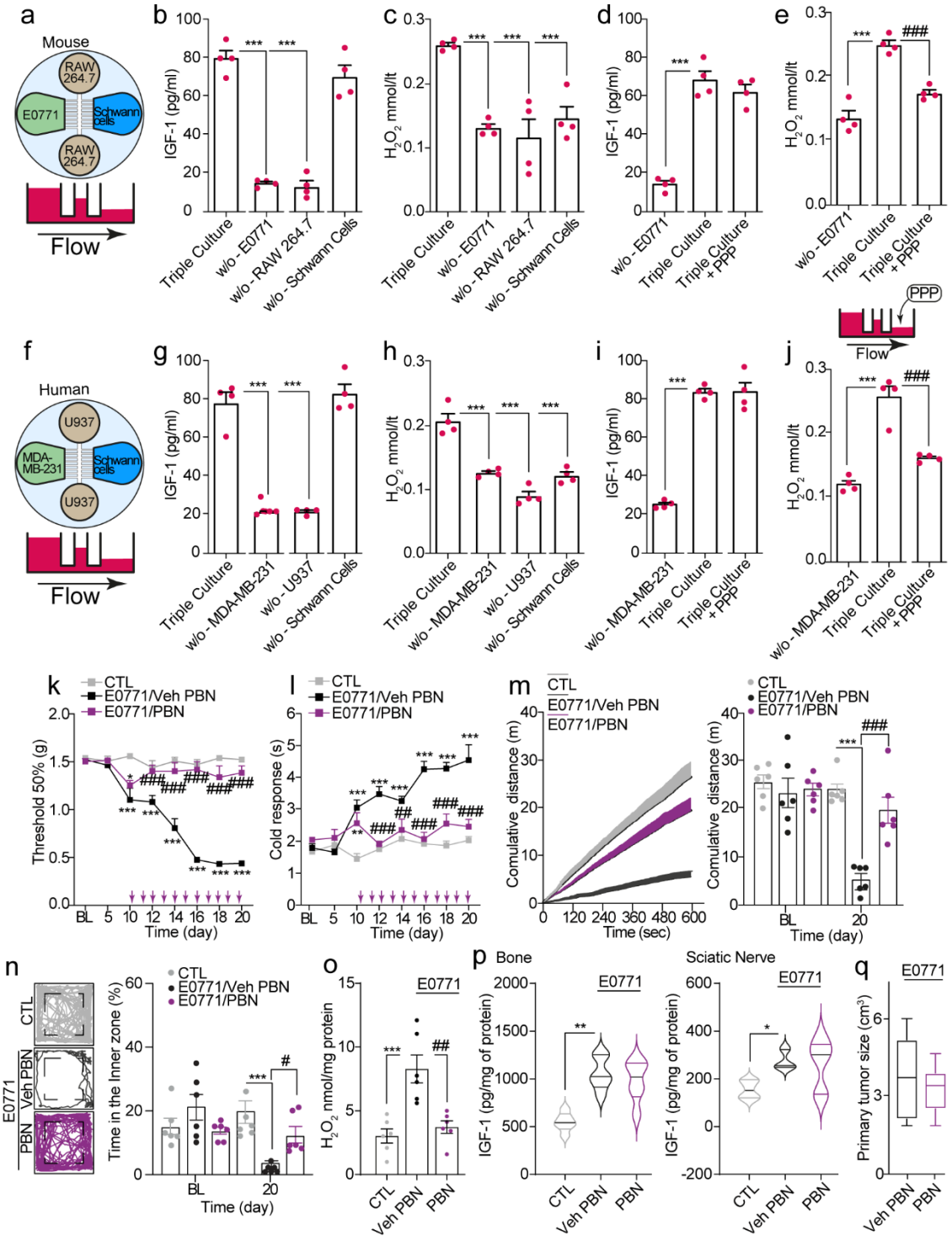

Fig. 29. IGF-1 from osteoclast induces Schwann cell H_2O_2 release (**a**) Diagram of the triple co-culture chamber with mouse (E0771, RAW264.7, and Schwann cells) and (**f**) human (MDA-MB-231, U937, and Schwann cells) cells. IGF-1 levels in (**b**) mouse and

(**g**) human triple co-culture without each of the three cell cultures. H_2O_2 levels in (**c**) mouse and (**h**) human triple co-culture without each of the three cell cultures. IGF-1 and H_2O_2 levels in (**d, e**) mouse and (**i, j**) human triple co-culture after Schwann cell treatment with PPP (n=4 replicates). (**k**) Mechanical/(**l**) cold allodynia, (**m**) cumulative distance, (**n**) time spent in the inner zone after E0771 cell inoculation or control (CTL) in C57BL/6J mice treated with PBN/vehicle (i.p.). (**o**) H_2O_2 levels in the sciatic nerve, (**p**) IGF-1 levels in bone and sciatic nerve tissue homogenates and (**q**) primary tumor size in C57BL/6J mice at 20 d after E0771 cell inoculation or CTL treated with PBN/vehicle (i.p.) (n=6 mice per group). Mean ± SEM. **P*<0.05, ***P*<0.01, ****P*<0.001 vs. CTL, Triple Culture; $^{\#}P$<0.05, $^{\#\#}P$<0.01, $^{\#\#\#}P$<0.001 vs. E0771/vehicle PBN.

6.2.3. Dichotomous proalgesic pathways of IGF-1R in DRG neurons (spontaneous nociception) and Schwann cells (mechanical/cold hypersensitivity).

To better delineate the IGF-1/ Schwann cell pathway, both *in vivo* and *in vitro* experiments were performed. As previously reported [248], we observed that IGF-1 stimulation of human Schwann cells induced IGF-1R trans-phosphorylation and the activation of insulin receptor substrate 1 (IRS-1) and serine/threonine kinase (Akt) (**Fig. 30a** and **30b**). We also found that IGF-1R activation in human Schwann cells caused endothelial nitric oxide synthase (eNOS) phosphorylation and the release of NO and H_2O_2 (**Fig. 30c–k**). Both NO and H_2O_2 release elicited by IGF-1 from human Schwann cells was attenuated in the presence of the IGF-1R antagonist, PPP, the IRS-1 inhibitor, NT157, the Akt inhibitor, Akti-1/2, and the eNOS inhibitor, L-NAME (**Fig. 30d–k**). It has been proposed that IGF-1R elicits nociception by activating protein kinase Ca (PKCa) in DRG neurons *via* phosphorylation of the voltage-gated T-type Ca^{2+}(CaV3) channels [239]. In our experiments, the PKC inhibitor, Ro32-0432, did not affect H_2O_2 generation induced by IGF-1 (**Fig. 30l**), indicating that a PKC-independent pathway mediates IGF-1 responses in Schwann cells. Conversely, we confirmed that IGF-1 induces a Ca^{2+}response in DRG neurons, which was abolished by PKC inhibition (**Fig. 30m**). IGF-1 stimulation was unable to induce a significant increase in NO and H_2O_2 in cultured DRG neurons (**Fig. 31a and 31b**).

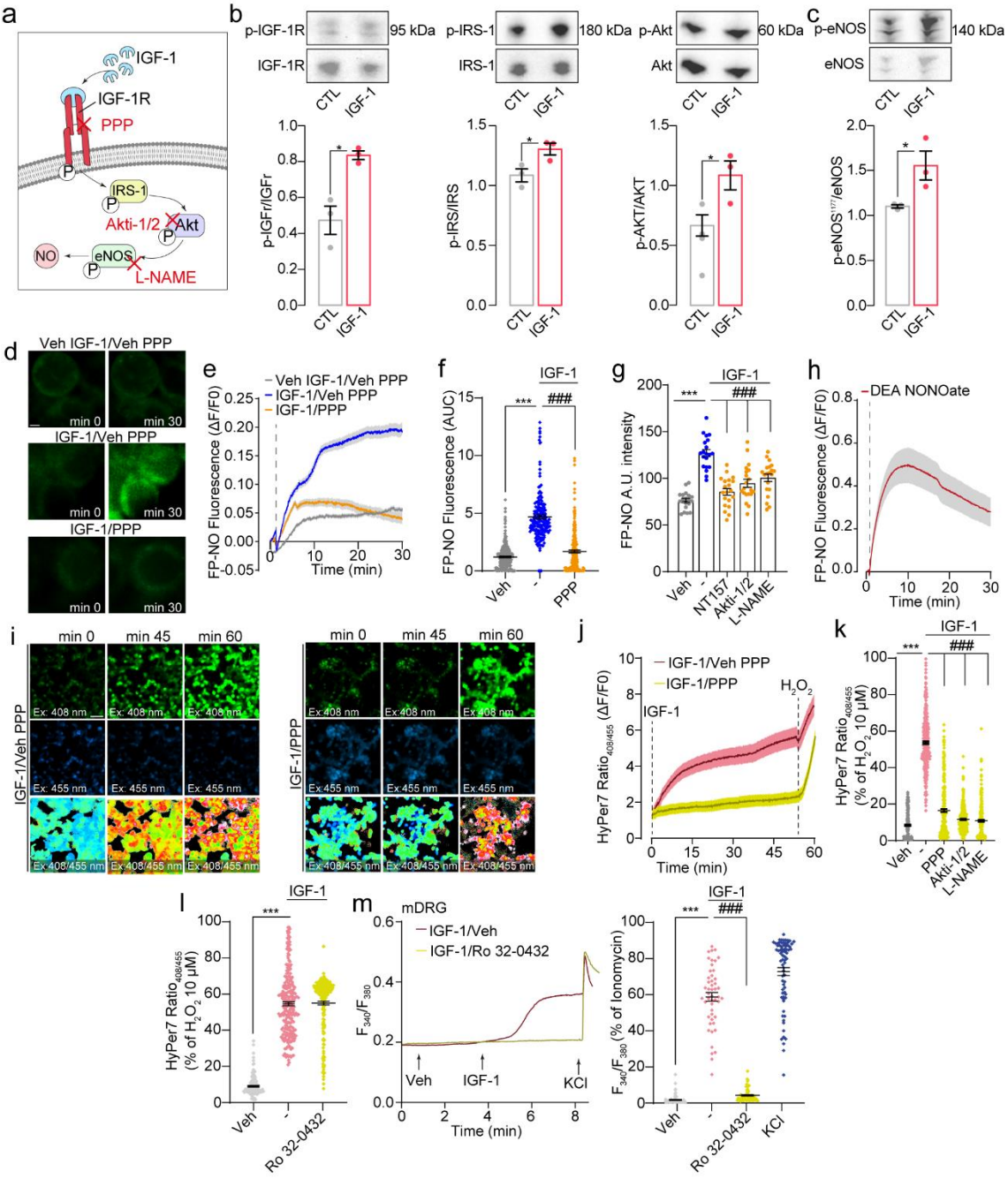

Figure 30. IGF-1R phosphorylation induces eNOS phosphorylation and NO release (**a**) Schematic illustration of IGF-1R signaling cascade. (**b**) Images and cumulative data of non-phosphorylated/phosphorylated ratio of IGF-1R, IRS-1, and Akt in HSC stimulated with IGF-1/vehicle (n=3 replicates). (**c**) Images and cumulative data of non-phosphorylated/phosphorylated ratio of eNOS in HSC stimulated with IGF-1/vehicle (n=3 replicates). (**d**) FP-NO (ΔF/F0) images, (**e**) traces, and (**f**) cumulative data of HSC stimulated with IGF-1/vehicle in the presence of PPP/vehicle (Scale bar: 20 μm) (cells number: IGF-1=207, vehicle=250, and PPP=220, n=3 independent experiments). (**g**) FP-NO (ΔF/F0) (arbitrary unit, A.U.) cumulative data of HSC stimulated with IGF-1/vehicle in the presence of NT157, Akt-1/2, or L-NAME/vehicles (n=20 replicates). (**h**) FP-NO (ΔF/F0) typical trace of DEA NONOate in HSC. (**i**) Images, (**j**) typical traces, and (**k**) cumulative data of HyPer7.2, in HSC, stimulated with IGF-1/vehicle in the presence of

PPP, Akti-1/2, or L-NAME/vehicles (Scale bar: 50 µm) (cells number: IGF-1=310, vehicles=237, PPP=280, Akti-1/2=227, L-NAME=236, n=3 independent experiments). (**l**) Cumulative data of HyPer7.2 in HSC stimulated with IGF-1/vehicle in the presence of Ro32-0432/vehicle (cells number: IGF-1=244, vehicle=140, and Ro32-04320=232, n=3 independent experiments). (**m**) Traces and cumulative data of Ca^{2+} influx (F_{340}/F_{380}) in DRG neurons stimulated with IGF-1/vehicle in the presence of Ro32-0432/vehicle (cells number: IGF-1=49, vehicle=74, Ro32-0432=62, and KCl=74, n=3 independent experiments). Mean ± SEM. **P*<0.05, ***P*<0.01, ****P*<0.001 vs. CTL, vehicle; ###*P*<0.001 vs. IGF-1/different treatments.

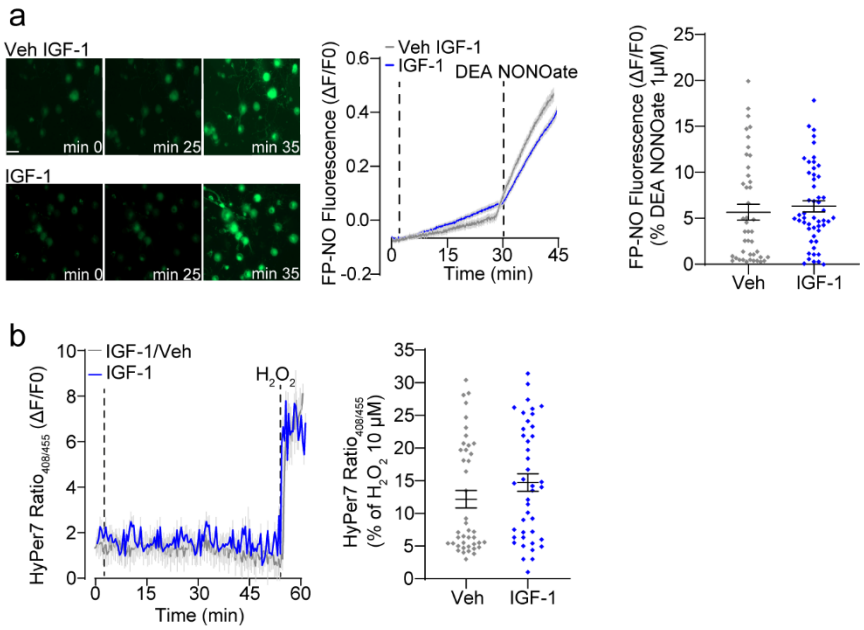

Figure 31. IGF-1 stimulation in DRG neurons does not evoke NO and H_2O_2 release. (**a**) FP-NO (ΔF/F0) representative images (Scale bar: 50 µm), typical trace and cumulative data of IGF-1/vehicle and DEA NONOate stimulation in DRG neurons (cells number: IGF-1= 43, vehicle=51, n=3 independent experiments). (**b**) Typical traces, and cumulative data of HyPer7.2 in DRG neurons stimulated with IGF-1/vehicle and H_2O_2 (cells number: IGF-1= 42, vehicle=42, n=3 independent experiments). Mean ± SEM.

Next, we explored the Schwann cell/IGF-1R pathway in mice. IGF-1 injection (i.pl.) dose-dependently produced an early and transient (10 min) spontaneous nociception, followed by a prolonged (~4 h) mechanical/cold hypersensitivity, which were attenuated by pretreatment with the IGF-1R inhibitor, PPP (**Fig. 32a–f**). IGF-1 (i.pl.) also increased NO and H_2O_2 levels in sciatic nerve homogenates, all effects reduced by PPP (**Fig. 32g and 32h**). A key result was obtained after IGF-1 (i.pl.) injection in mice with selective silencing of IGF-1R in Schwann cells (Plp-Cre/ERT$^+$-shRNA(IGF-1R)). Sustained mechanical/cold hypersensitivity, but not acute spontaneous nociception, evoked by IGF-1 was attenuated in these mice (**Fig. 32i–k).** Conversely, in mice with selective silencing

of IGF-1R in primary sensory neurons (Adv-Cre-shRNA(IGF-1R)), acute spontaneous nociception evoked by IGF-1 was attenuated, whereas mechanical/cold allodynia remained unaffected (**Fig. 33a–c**). In addition, pretreatment with Ro32-0432 attenuated spontaneous nociception without affecting mechanical/cold hypersensitivity (**Fig. 33d–f**).

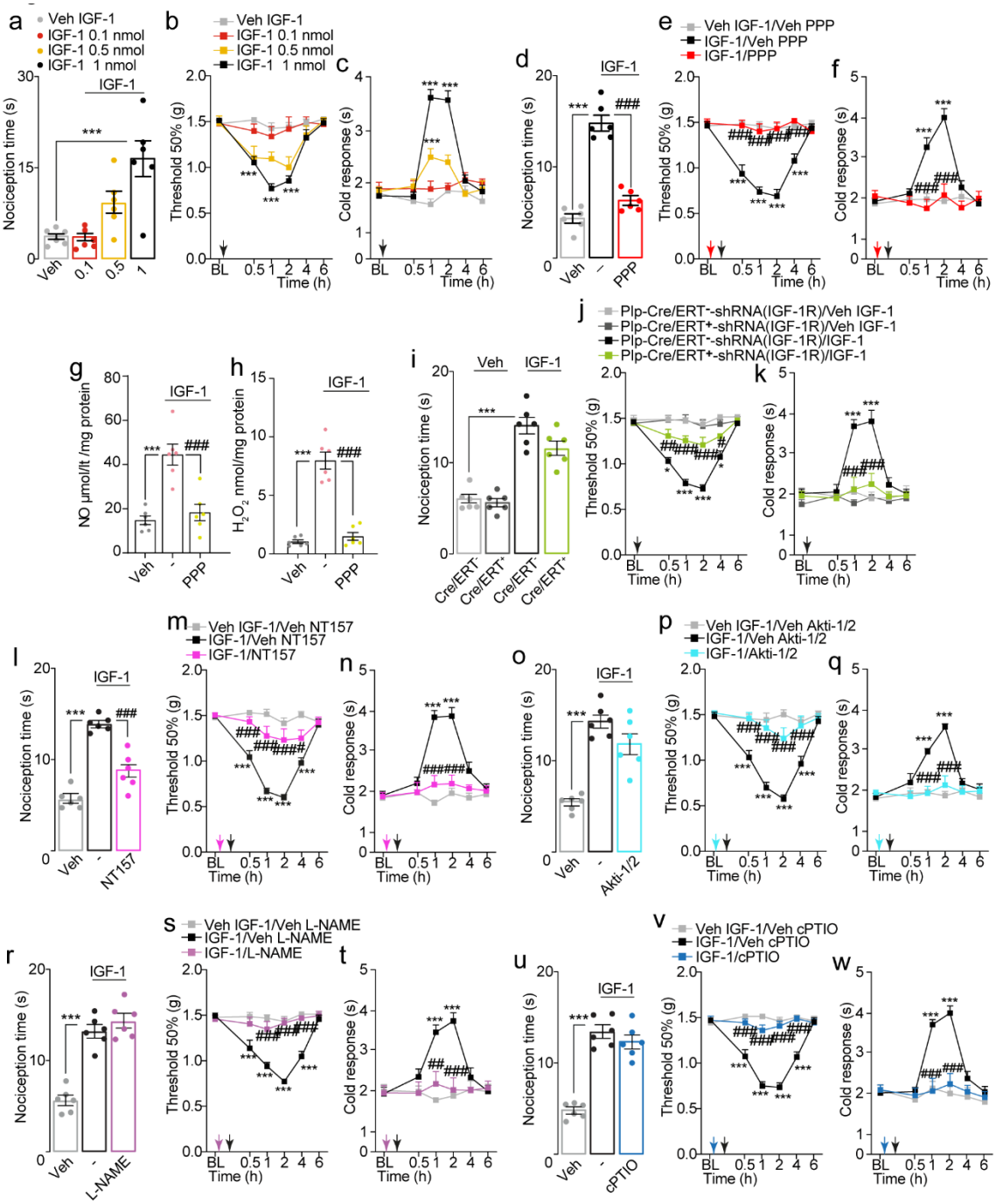

Figure 32. SC IGF-1R does not regulate IGF-1 induced acute nociception**.** Dose- and time-dependent (**a**) nociceptive response and (**b**) mechanical/(**c**) cold allodynia induced

by intraplantar (i.pl.) IGF-1/vehicle in C57BL/6J mice. (**d**) Nociceptive response and (**e**) mechanical/(**f**) cold allodynia induced by IGF-1 (1 nmol) /vehicle (i.pl.) in C57BL/6J mice after i.pl. PPP/vehicle (n=6 mice per group). (**g**) NO and (**h**) H_2O_2 content in sciatic nerve tissue homogenates of C57BL/6J mice treated with IGF-1 (1 nmol)/vehicle (i.pl.) and pretreated with PPP/vehicle (i.pl.). **(i)** Nociceptive response and (**j**) mechanical/(**k**) cold allodynia by IGF-1 (1 nmol)/vehicle (i.pl.) in Plp-Cre/ERT^{-} and Plp-Cre/ERT^{+} infected with AAV-(loxP-shRNA)IGF-1R [E0771/Plp-Cre/ERT^{-}-shRNA(IGF-1R) and E0771/Plp-Cre/ERT^{+}-shRNA(IGF-1R)]. **(l, i, r, u)** Nociceptive response and (**m, p, s, v**) mechanical/(**n, q, t, w**) cold allodynia induced by IGF-1 (1 nmol)/vehicle (i.pl.) in C57BL/6J mice pretreated with NT157 (**l–n**), Akti-1/2 (**o–q**), L-NAME (**r–t**), or cPTIO (**u–w**) (n=6 mice per group). Mean ± SEM. (-) represents the combination of various vehicles ***P<0.001 vs. vehicle, Cre/ERT^{-}/vehicle, vehicle IGF-1/vehicle NT157, vehicle IGF-1/vehicle Akti-1/2, vehicle IGF-1/vehicle L-NAME, vehicle IGF-1/vehicle cPTIO; $^{\#\#}P$<0.01, $^{\#\#\#}P$<0.001 vs. Cre/ERT^{+}/IGF-1, IGF-1/vehicle NT157, IGF-1/vehicle Akti-1/2, IGF-1/vehicle L-NAME, and IGF-1/vehicle cPTIO.

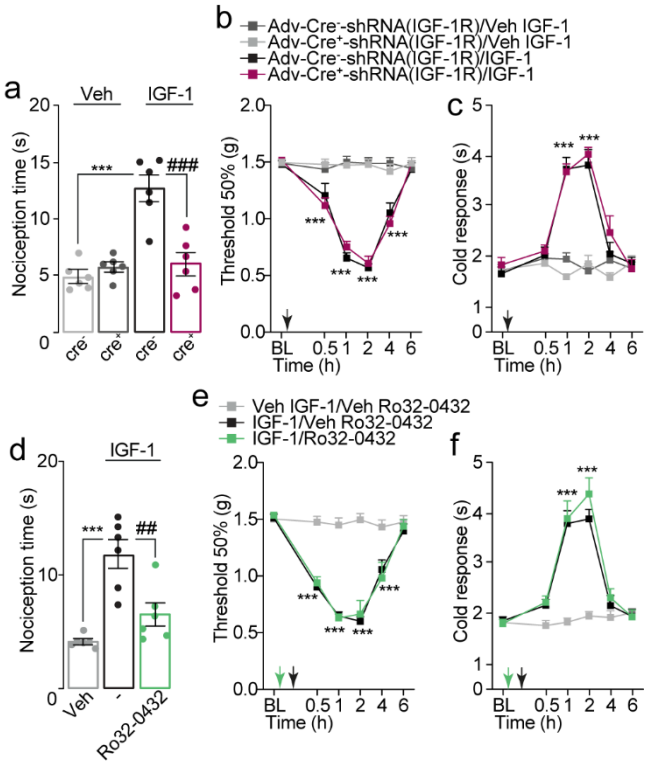

<u>Figure 33</u>. PKC is involved in IGF-1 induced acute nociception but not mechanical and cold allodynia **(a**) Nociceptive response and (**b**) mechanical/(**c**) cold allodynia induced by intraplantar (i.pl.) injection of IGF-1 (1 nmol)/vehicle in Adv-Cre^{-} and Adv-Cre^{+} infected with AAV-(loxP-shRNA)IGF-1R [Adv-Cre^{-}-shRNA(IGF-1R) and Adv-Cre^{+}-shRNA(IGF-1R)]. (**d**) Nociceptive response and (**e**) mechanical/(**f**) cold allodynia induced by injection of IGF-1(1 nmol)/vehicle (i.pl.) in C57BL/6J mice treated with Ro32-0342/vehicle (n = 6 mice per group). Mean ± SEM. ***P < 0.001 vs. vehicle; $^{\#\#}P$ < 0.01, $^{\#\#\#}P$ < 0.001 vs. Adv-Cre^{-}/IGF-1 and IGF-1/vehicle Ro32-0432.

Pretreatment with the IRS-1 inhibitor, NT157, reduced both spontaneous nociception and mechanical/cold hypersensitivity, whereas Akti-1/2, L-NAME, and cPTIO only reduced mechanical/cold hypersensitivity, but not spontaneous nociception, evoked by IGF-1 (i.pl.) in mice (**Fig. 32l–w**). IRS-1 is known to inhibit IGF-1R internalization in endosomes by suppressing IGF-1R recruitment in clathrin structure, thus prolonging the permanence of activated IGF-1R to the cell surface [249, 250], a phenomenon likely associated with mechanical/cold hypersensitivity. In agreement with these findings, pretreatment with the clathrin-dependent endocytosis inhibitor, Pitstop2, did not affect spontaneous IGF-1-evoked nociception nor mechanical/cold hypersensitivity (**Fig. 34a–c**). NT157, which, by inhibiting IRS-1, promotes IGF-1R internalization, reduced both spontaneous nociception and mechanical/cold hypersensitivity. However, Pitstop2 restored only spontaneous nociception and failed to restore mechanical/cold hypersensitivity (**Fig. 34d–f**). This data supports the role of IGF-1R clathrin-dependent endocytosis, and the canonical PKC-dependent pathway encoded by neuronal IGF-1R solely in spontaneous nociception. In the triple chamber, NT157, Akti-1/2, L-NAME, and cPTIO attenuated the increase in NO and H_2O_2, while the increase in IGF-1 was not affected (**Fig. 35a–g**). NT157, Akti-1/2, L-NAME, and cPTIO reduced NO and H_2O_2 levels *in vivo* in sciatic nerve homogenates (**Fig. 34g** and **34h**) and attenuated all pain-like responses observed in E0771-mice (**Fig. 34i–x**). Altogether, present data highlight a novel pathway resulting from IGF-1R activation in Schwann cells, which promotes mechanical/cold hypersensitivity by Akt and eNOS phosphorylation and NO and ROS release.

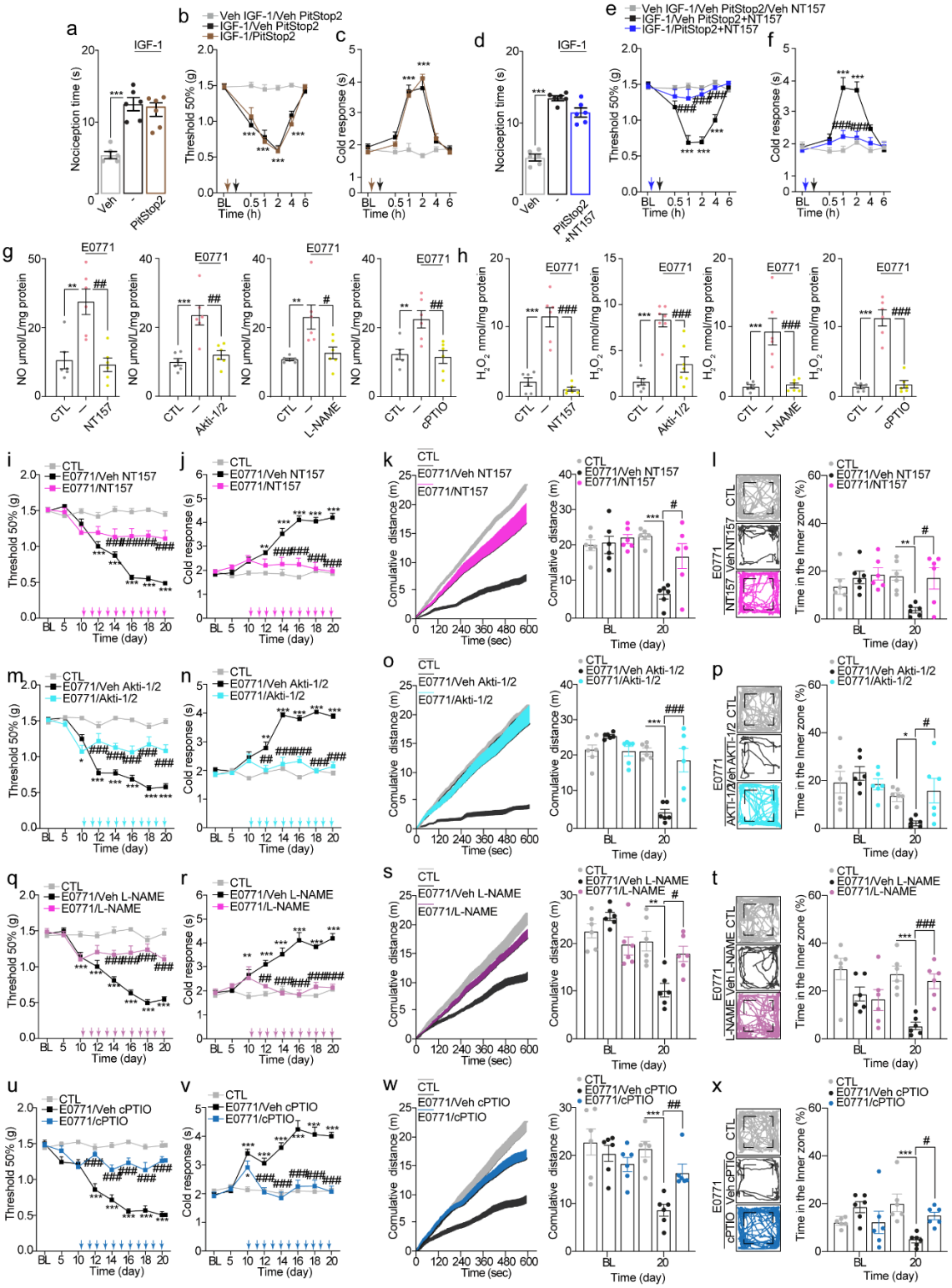

Figure 34. IGF-1 mediates E0771 bone metastatic cancer pain by NO release. (**a, d**) Nociceptive response, (**b, e**) mechanical/(**c, f**) cold allodynia induced by intraplantar (i.pl.) injection of IGF-1 (1 nmol)/vehicle in C57BL/6J mice treated with Pitstop2 (**a–c**) or NT157 + Pitstop2 (**d–f**)/vehicle (n = 6 mice per group). (**g**) NO and (**h**) H_2O_2 contents in sciatic nerve tissue homogenates at 20 d after E0771 cell inoculation or control (CTL) in C57BL/6J mice treated with NT157, Akti-1/2, L-NAME, cPTIO/vehicles intraperitoneal (i.p.) (n = 6 replicates). (**i, m, q, u**) Mechanical/(**j, n, r, v**) cold allodynia,

(**k, o, s, w**) cumulative distance, and (**i, p, t, x**) time spent in the inner zone after E0771 cell inoculation or control (CTL) in C57BL/6J mice treated with (**i–l**) NT157, (**m–p**) Akti-1/2, (**q–t**) L-NAME, (**u–x**) cPTIO/vehicles (i.p.) (n = 6 mice per group). Mean ± SEM. (-) represents different vehicles. **P* < 0.05, ***P* < 0.01, ****P* < 0.001 vs. vehicle, CTL; $^{\#}P$ < 0.05, $^{\#\#}P$ < 0.01, $^{\#\#\#}P$ < 0.001 vs. IGF-1/vehicle PitStop2+NT157, (-)E0771, E0771/vehicle NT157, E0771/vehicle Akti-1/2, E0771/vehicle L-NAME, and E0771/vehicle cPTIO.

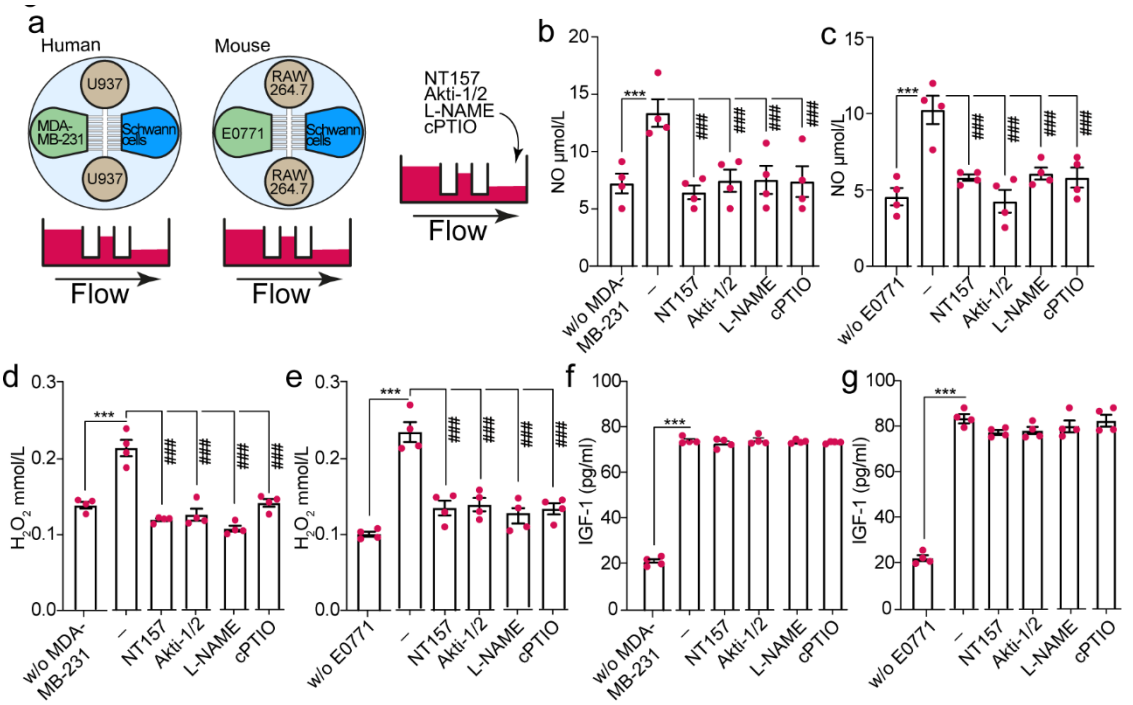

Figure 35. Osteoclast activation by tumor cells induces NO release by Schwann cells (**a**) Diagram of the triple co-culture chamber with the mouse (E0771, RAW264.7, and Schwann cells) and human (MDA-MB-231, U937, and Schwann cells). (**b, c**) NO, (**d, e**) H_2O_2, and (**f, g**) IGF-1 levels in human and mouse triple co-culture with or without human or mouse breast cancer cells and in the presence of NT157, Akti-1/2, L-NAME, or cPTIO in HSC and MSC chamber (n=4 replicates). Mean ± SEM. (-) represents the combination of different vehicles, ****P*<0.001 vs. triple co-culture without cancer cells; $^{\#\#\#}P$<0.001 vs. triple co-cultures.

6.2.4 NO release by IGF-1 in Schwann cells activates TRPA1 to generate oxidative stress.

The final step of the IGF-1R/Schwann cell pathway involves the release of H_2O_2. Recently, we showed that eNOS activation in Schwann cells, elicited by calcitonin gene-related peptide (CGRP), releases NO. NO directly, or *via* reactive nitrogen species [251], stimulates Schwann cell TRPA1, which amplifies the oxidative stress signal to sustain periorbital mechanical allodynia [67]. RNAscope analysis provided further evidence of TRPA1 mRNA expression in Schwann cells of mouse sciatic nerve and DRG neurons

(**Fig. 36a**). Stimulation of human Schwann cells with breast cancer cell/osteoclast-conditioned medium elicited a delayed TRPA1-mediated Ca^{2+} response that was inhibited by PPP, NT157, Akti-1/2, L-NAME, cPTIO, and in a Ca^{2+}-free medium, thus recapitulating results obtained by IGF-1R activation (**Fig. 36b–f**). Stimulation of human Schwann cells with IGF-1 produced an increase in H_2O_2, which was prevented by the TRPA1 selective antagonist, A967079 (**Fig. 36g**). In the triple chamber, A967079 attenuated the release of H_2O_2, but not that of IGF-1 or NO (**Fig. 36h**), suggesting that TRPA1 activation and oxidative stress generation are downstream of IGF-1R. *In vivo* studies supported this hypothesis, as mechanical/cold hypersensitivity, but not spontaneous nociception induced by IGF-1 (i.pl.), was attenuated in mice with selective deletion of *Trpa1* in Schwann cells (Plp-Cre/ERT^{+};*Trpa1*$^{fl/fl}$) and in *Trpa1*$^{-/-}$ mice (**Fig. 36i–k** and **Fig. 37a–c**). Pain-like behaviors observed in control mice were attenuated in Plp-Cre/ERT^{+};*Trpa1*$^{fl/fl}$ and *Trpa1*$^{-/-}$ mice inoculated with E0771 cells (**Fig. 36l–o** and **Fig. 37d–g**).

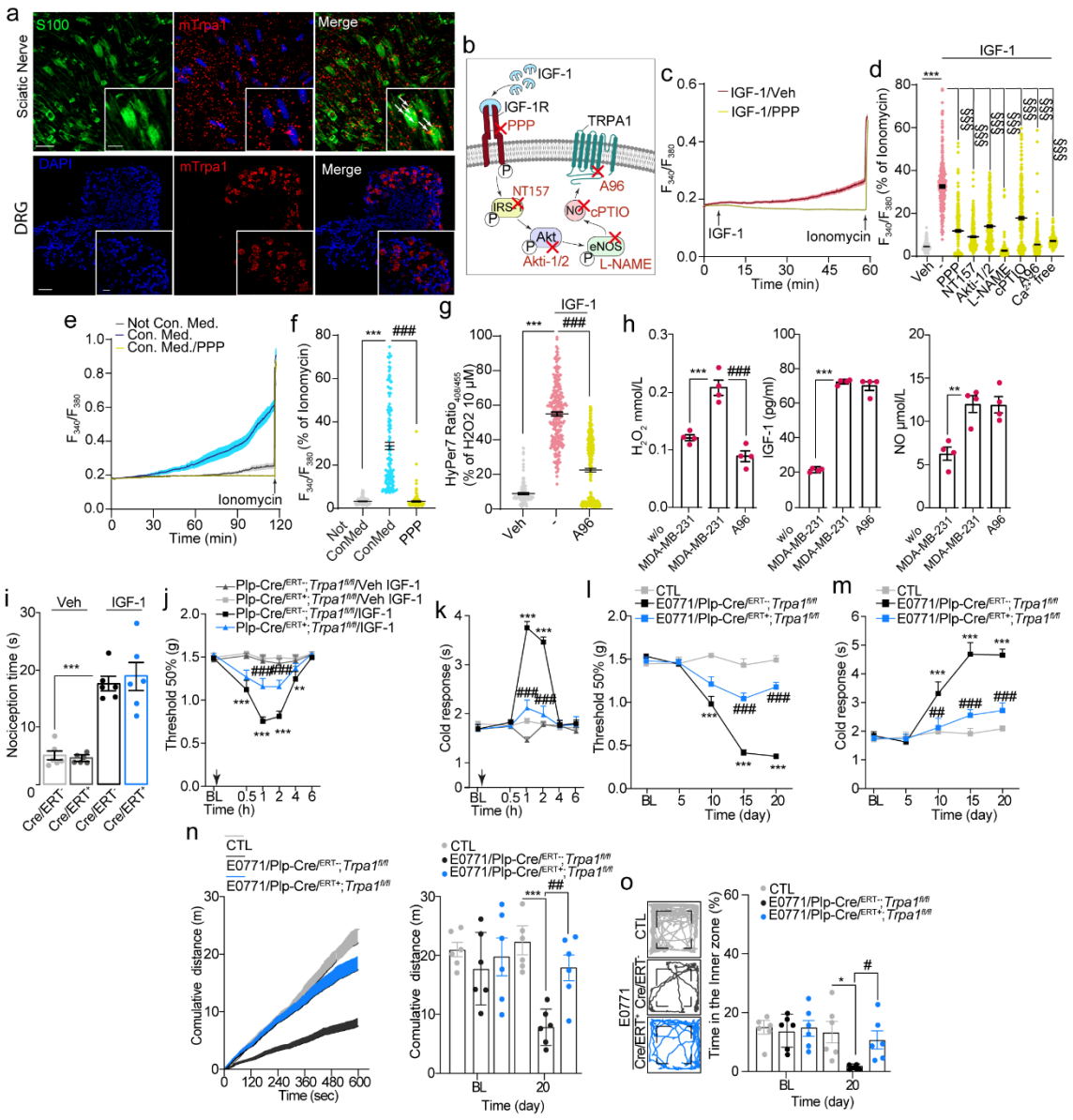

Figure 36. SC TRPA1 mediates bone metastatic cancer pain by IGF-1 (**a**) Images of IGF-1R RNA scope in mouse sciatic nerve and dorsal root ganglia (DRG) (Scale bar: 20 µm, inset 10 µm) (n=3 subjects). (**b**) Schematic representation of the TRPA1 activation pathway after IGF-1R activation. (**c**) Traces and (**b**) cumulative data of Ca^{2+} influx (F_{340}/F_{380}) in HSC stimulated with IGF-1/vehicle in Ca^{2+}-free medium (Ca^{2+} free) or in the presence of PPP, NT157, Akt-1/2, L-NAME, cPTIO, or A967079 (A96)/vehicles (cells number: IGF-1=310, vehicles= 233, PPP=344, NT157=348, Akt-1/2=323, L-NAME=316, cPTIO=333, A96=407, and Ca^{2+}free=233, n=3 independent experiments). (**e**) Traces and (**f**) cumulative data of Ca^{2+} influx (F_{340}/F_{380}) in HSC stimulated with breast cancer cells/osteoclast conditioned medium (ConMed) or normal medium (NotConMed) in the presence of PPP/vehicle (cells number: ConMed=139, NotConMed=166, PPP/vehicle=152, n=3 independent experiments). (**g**) HyPer7.2 in HSC stimulated with IGF-1/vehicle in the presence of A96/vehicle (cells number: IGF-1=234, vehicles=129, A96=316, n=3 independent experiments). (**h**) H_2O_2, IGF-1, and NO levels in human triple co-culture (MDA-MB-231, U937 and Schwann cells) and without MDA-MB-231 or in the presence of A96/vehicle in Schwann cells (n=4 replicates). (**i**) Nociceptive response

and (**j**) mechanical/(**k**) cold allodynia induced by IGF-1 (1 nmol)/vehicle (i.pl.) in Plp-Cre/ERT^{-}-*Trpa1*$^{fl/fl}$ Plp-Cre/ERT^{+}-*Trpa1*$^{fl/fl}$ mice. (**l**) Mechanical (**m**)/cold allodynia, (**n**) cumulative distance, and (**o**) time spent in the inner zone after E0771 cell inoculation in Plp-Cre/ERT^{-}-*Trpa1*$^{fl/fl}$, Plp-Cre/ERT^{+}-*Trpa1*$^{fl/fl}$ or control (CTL) mice (n=6 mice per group). Mean ± SEM. (-) represents the combination of different vehicles. **P*<0.05, ***P*<0.01, ****P*<0.001 vs. vehicle, CTL, NotConMed, Cre/ERT^{-}/vehicle, $^{\#}$*P*<0.05, $^{\#\#}$*P*<0.01, $^{\#\#\#}$*P*<0.001 vs. ConMed, MDA-MB-231, Cre/ERT^{-}/IGF-1, Cre^{-}/IGF-1.

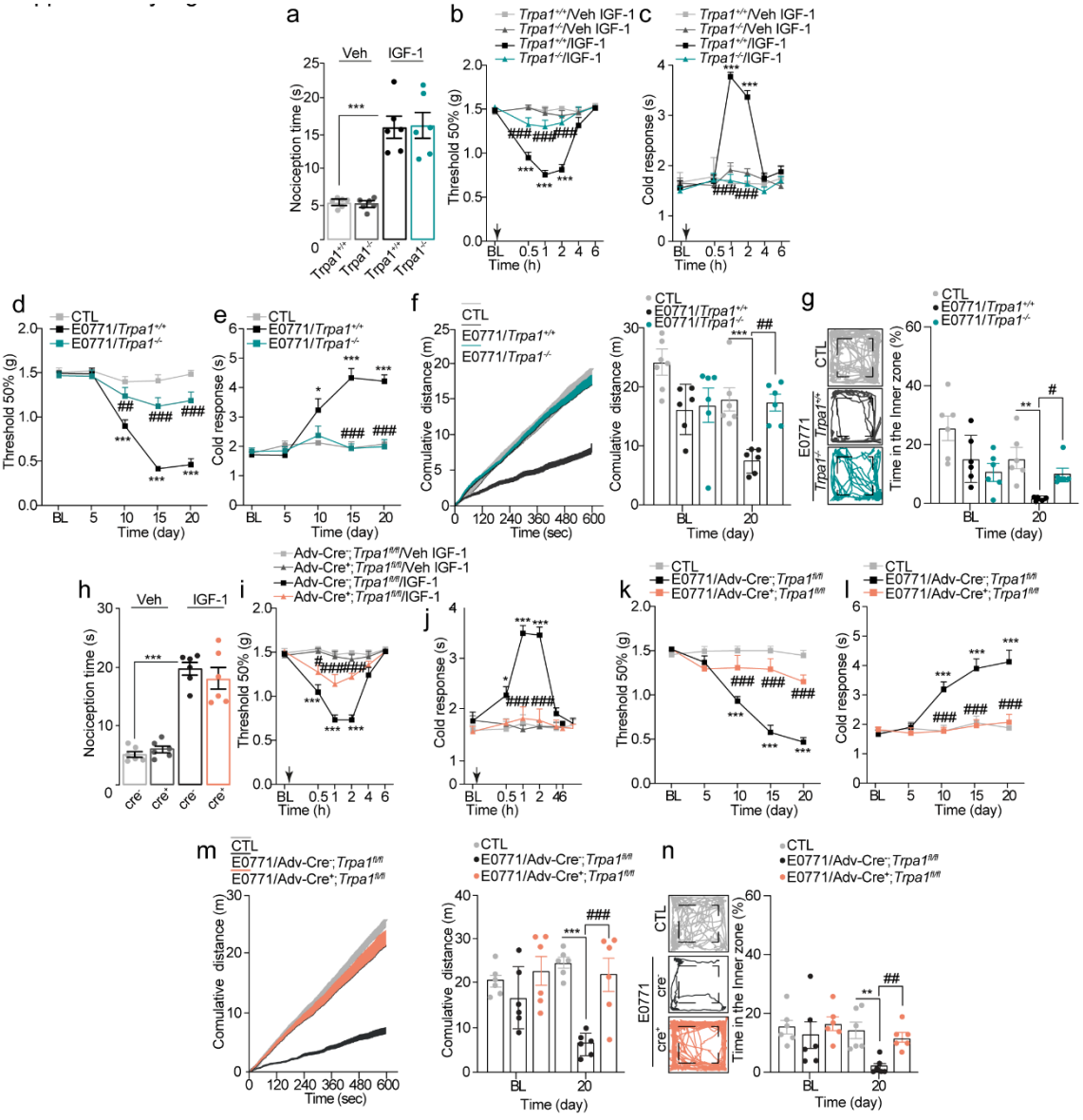

<u>Figure 37.</u> TRPA1 mediates E0771 bone metastatic cancer pain. (**a**) Nociceptive response and (**b**) mechanical/(**c**) cold allodynia induced by intraplantar (i.pl.) injection of IGF-1 (1 nmol)/vehicle in *Trpa1*$^{+/+}$ or *Trpa1*$^{-/-}$ mice. (**d**) Mechanical/(**e**) cold allodynia, (**f**) cumulative distance, and (**g**) time spent in the inner zone after E0771 cell inoculation or control (CTL) in *Trpa1*$^{+/+}$ or *Trpa1*$^{-/-}$ mice (n = 6 mice per group). (**h**) Nociceptive response and (**i**) mechanical/(**j**) cold allodynia induced by intraplantar (i.pl.) injection of IGF-1 (1 nmol)/vehicle in Adv-Cre^{-} and Adv-Cre^{+}/Trpa1$^{fl/fl}$ mice. (**k**) Mechanical/(**l**)cold allodynia, (**m**) cumulative distance, and (**n**) time spent in the inner zone after E0771 cell

inoculation or control (CTL) in Adv-Cre^{-} and Adv-Cre^{+}/Trpa1$^{fl/fl}$ mice (n = 6 mice per group). Mean ± SEM. (-) represents different vehicles. *P < 0.05, **P < 0.01, ***P < 0.001 vs. vehicle, CTL, Cre^{-}/vehicle; $^{\#}P$ < 0.05, $^{\#\#}P$ < 0.01, $^{\#\#\#}P$ < 0.001 vs. *Trpa1*$^{+/+}$/IGF-1, and E0771/*Trpa1*$^{+/+}$, E0771/Cre^{-}.

6.2.5 IGF-1 in Schwann cells activates TRPA1 to expand endoneurial macrophages (MΦs).

Recently, in a model of cancer pain, we reported that TRPA1 activation by oxidative stress induced the release of M-CSF from Schwann cells, which expanded endoneurial resident MΦs (rMΦs), thus sustaining mechanical allodynia [227]. An increased number of F4/80^{+} (a MΦ biomarker) cells was also observed in the sciatic nerve of E0771-mice (**Fig. 38a**). To explore the MΦ role in pain-like behaviors, E0771 cells were inoculated in MΦ Fas-Induced Apoptosis (MaFIA) mice, which exhibit a typical and marked reduction in the number of F4/80^{+} cells when injected with the apoptosis inducer, AP20187 [222]. E0771 inoculation in MaFIA mice induced tumor growth and pain-like behaviors, like in C57 mice (**Fig. 38b–f**). AP20187 injections (2 mg/kg, i.p., once a day from day 10 to 20) in E0771-MaFIA mice markedly reduced the increase in sciatic nerve F4/80^{+} cells and pain-like behaviors, but not tumor growth (**Fig 38b–g**). Then, we investigated whether M-CSF was involved in E0771-evoked MΦ expansion. M-CSF level was increased in sciatic nerve of E0771-mice (**Fig. 38h**). The M-CSF receptor inhibitor, PLX-3397, attenuated pain-like behaviors, without affecting tumor growth (**Fig.38i–m**). In the triple chamber, the absence of cancer cells, osteoclasts, or Schwann cells, or treatment with PPP, PBN, or A967079, reduced M-CSF levels (**Fig.38n** and **38o**), thus confirming the role of Schwann cell TRPA1 in the cytokine release. It has been reported that activated MΦs release IGF-1, which is implicated in hyperalgesia in a mouse model of endometriosis [241]. Here, we show that human and murine MΦs (U937 and Raw264.7 cells, respectively) exposed to H_2O_2 release IGF-1 (**Fig. 38p** and **38q**). MΦ depletion in MaFIA mice significantly attenuated, but did not abolish, IGF-1 levels in sciatic nerve homogenates (**Fig. 38r**). Osteoclast derived IGF-1 may provide a major contribution to the cancer-dependent proalgesic pathway, including MΦ expansion, but an additional contribution by IGF-1 released from expanded MΦs cannot be excluded.

Finally, the role of neuronal TRPA1 for signaling pain-like behaviors was investigated in E0771 inoculated mice with sensory neuron-specific deletion of TRPA1 (Adv-Cre^{+};*Trpa1*$^{fl/fl}$). In these mice, mechanical/cold hypersensitivity induced by IGF-1 (i.pl.) and pain-like behaviors induced by E0771 cell inoculation were attenuated (**Fig.**

37i–n). In contrast, spontaneous nociceptive behavior induced by IGF-1 (i.p.l.), presumably mediated by a direct action on neuronal IGF-1R, was unaffected (**Fig. 37h**), thus confirming the dichotomous proalgesic pathway elicited by i.pl. IGF-1. As previously reported in another model of cancer pain [227], the present results strengthen the hypothesis that Schwann cell TRPA1 activated by IGF-1R amplifies the oxidative stress that sustains pain-like behaviors in the present mouse model of breast cancer cell bone metastases.

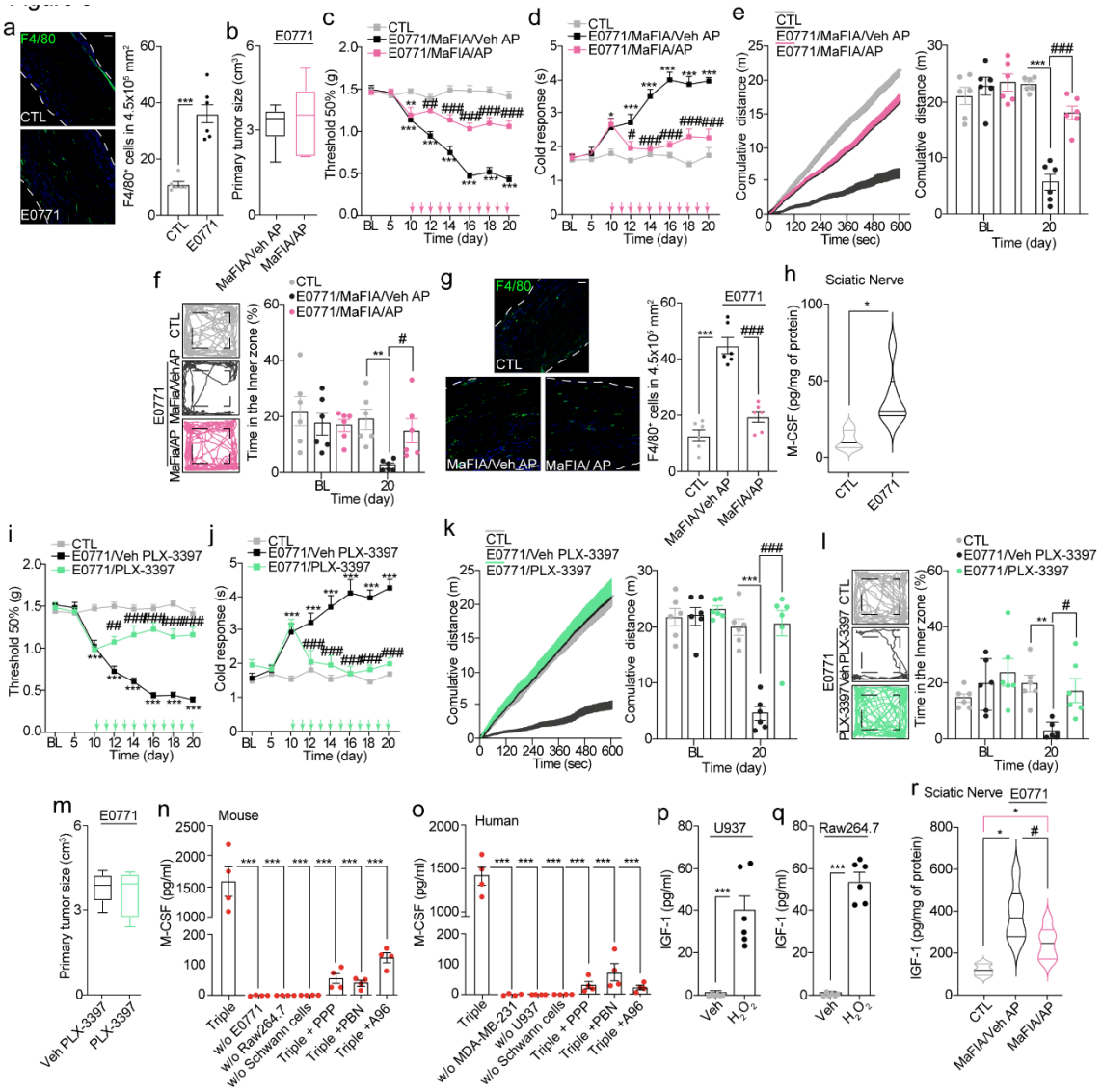

Figure 38. IGF-1 in Schwann cells activates TRPA1 to expand endoneurial macrophages (MΦs). (**a**) Number of F4/80^{+} cells inside the sciatic nerve trunk after E0771 cell inoculation or control (CTL) in C57BL/6J mice (Scale bar: 50 µm) (n=6 mice per group). (**b**) Tumor size, (**c**) mechanical (**d**)/cold allodynia, (**e**) cumulative distance (**f**), and time spent in the inner zone and (**g**) number of sciatic nerve F4/80^{+} cells after E0771 cell inoculation in MaFIA/Veh AP, MaFIA/AP or CTL mice. (**h**) M-CSF levels sciatic nerve tissue homogenates after E0771 cell inoculation or CTL in C57BL/6J mice (Scale bar: 50

µm) (n=6 mice per group). (**i**) Mechanical (**j**)/cold allodynia, (**k**) cumulative distance, (**l**) time spent in the inner zone, and (**m**) primary tumor size after E0771 cell inoculation or CTL in C57BL/6J mice treated with PLX-3397/vehicle (i.p.) (n=6 mice per group). (**n-o)** M-CSF levels in human and mouse triple co-culture with or without osteoclasts, cancer cells and Schwann cells, or in the presence of PPP, PBN or A967079 (A96) in Schwann cells (n=4 replicates). (**p-q**) IGF-1 levels in human and mouse MΦs (U937 and Raw264.7 cells respectively) exposed to H_2O_2 (100 mM) or vehicle (Veh). (**r**) IGF-1 levels in sciatic nerve tissue homogenates after E0771 cell inoculation in MaFIA/Veh AP, MaFIA/AP or CTL mice (n=6 mice per group). Mean ± SEM. **P*<0.05, ***P*<0.01, ****P*<0.001 vs. CTL, Veh $^{\#}P$<0.05, $^{\#\#}P$<0.01, $^{\#\#\#}P$<0.001 vs. E0771/MaFIA/Veh AP, E0771/Veh PLX-3397, MaFIA/Veh AP.

DISCUSSION

In the first part of the PhD project, we examined the pain mechanisms associated with CIPN. Thalidomide, an old sedative and antiemetic drug banned for causing birth defects in humans, has been repurposed for the treatment of leprosy and several types of cancer [252], including multiple myeloma, myelodysplastic syndrome, and several solid cancers [253]. Thalidomide derivatives, pomalidomide and lenalidomide, also exhibit anticancer activity in multiple myeloma patients who relapse or are refractory to other anticancer treatments. Unfortunately, as with other chemically unrelated chemotherapeutic agents (platinum-based drugs, taxanes, and bortezomib), thalidomide and its derivatives cause a painful peripheral polyneuropathy that often results in severe discomfort or even drug discontinuation [254]. Despite its clinical relevance, the underlying mechanism of the neuropathy and the associated pain symptoms caused by thalidomide and its derivatives remains poorly known.

Several studies have investigated the ability of thalidomide to attenuate inflammatory and neuropathic pain in rodent models presumably by interacting with indirect mechanisms dependent on the inhibition of proalgesic cytokines, such as TNF-a and NF-kB [255-257]. Surprisingly, to the best of our knowledge, no study has investigated the ability of thalidomide or related drugs to elicit pain-like responses in animal models so far. Only one study has shown that thalidomide increased electrophysiological responses in rat sensory nerve fibers [258], reminiscent of a sensory neuropathy. Thus, our study shows for the first time that thalidomide, pomalidomide and lenalidomide evoke mechanical and cold hypersensitivity in mice. Although the chemotherapeutic drugs failed to evoke heat hypersensitivity, as cold and mechanical allodynia are the major and most debilitating symptoms of thalidomide-evoked CIPN [259, 260], the present model seems to satisfactorily replicate the human pain condition. A series of previous investigations have highlighted the ability of thalidomide to produce beneficial and toxic effects, including its anticancer action and severe teratogenic effects, *via* the generation of oxidative stress [195, 196]. In particular, it has been reported that the bioactivation of thalidomide from horseradish peroxidase to free-radical intermediates produces ROS, which cause oxidative damage to DNA and other cellular macromolecules, apparently responsible for the anticancer effect, but also for the teratogenic action [196].

Our data show that oxidative stress byproducts, such as H_2O_2, and 4-HNE, are generated both at the peripheral (hind paw and sciatic nerve) and central (spinal cord) levels, after thalidomide systemic injection. Thus, thalidomide generates oxidative stress along the entire pain pathway, which encompasses the entire anatomical route that conveys the pain signal from the hind paw to the lumbar spinal cord. The observation that increased H_2O_2 and 4-HNE levels and mechanical and cold allodynia were reduced by systemic treatment with the antioxidant, PBN, further supports the hypothesis that oxidative stress is essential for the pain-like symptoms evoked by thalidomide. We also revealed that TRPA1 and TRPV4 channels mediate mechanical and cold allodynia evoked by thalidomide and related drugs. However, as reported for other anticancer drugs, including oxaliplatin/cisplatin, paclitaxel and bortezomib [117, 261, 262], the observation that thalidomide and its derivatives failed to evoke any excitatory effect in cultured TRPA1 and TRPV4-expressing neurons excludes the possibility that their proalgesic effect depends on a direct action on these channels, and suggests the implication of indirect mechanisms, including oxidative stress generation.

Whereas the role of TRPA1 as a sensor of oxidative stress has been extensively investigated and recognized, a similar function of TRPV4 has been poorly explored. Several studies have reported that TRPA1 is activated by an unprecedented series of reactive oxygen, nitrogen or carbonyl species [104, 197]. In particular, robust proof supports the hypothesis that H_2O_2 causes nociceptor stimulation *via* TRPA1 [211, 263]. In contrast, little evidence showing that H_2O_2 stimulates TRPV4 has been provided [198, 199]. TRPV4 carries cysteine residues, corresponding to those found in other redox-sensitive TRP channels [264], thus enabling their targeting through oxidation, which leads to channel activation [264]. Here, we report that H_2O_2 targets the recombinant and native TRPV4, although with a potency about 10 times lower than that exhibited toward TRPA1. The observation that two cysteine-reducing agents, DTT and β-ME [197, 265], abated the H_2O_2 evoked Ca^{2+}-response further supports the hypothesis that TRPV4 may be directly activated by oxidants.

Results obtained in cultured DRG neurons strengthen the findings obtained in recombinant systems. While the Ca^{2+}-response produced by a low H_2O_2 concentration was entirely abated in the presence of the TRPA1 antagonist, the response to a higher H_2O_2 concentration was blocked only when a TRPV4 antagonist was added. Importantly, the residual Ca^{2+}-response to a high H_2O_2 concentration observed in DRG neurons from *Trpa1*$^{-/-}$ mice was completely attenuated by a TRPV4 antagonist. Thus, it may be concluded that,

provided a sufficiently elevated burden is present, oxidative stress may engage not only TRPA1 but also TRPV4.

A peculiar difference of the two channels regarding their roles in thalidomide-evoked hypersensitivities is that, as shown by genetic or pharmacological studies, mechanical allodynia was partially attenuated by these interventions, and abolition was attained only by a combination of peripheral TRPA1 and central TRPV4 blockade. Various anticancer drugs, including platinum-derived drugs or the proteasome inhibitor, bortezomib, promote mechanical allodynia exclusively *via* oxidative stress and the ensuing TRPA1 activation [117, 262]. The partial contribution of TRPV4 to mechanical hypersensitivity has been previously reported in the CIPN model produced by the taxane derivative, paclitaxel [261]. Notably, as shown in the paclitaxel-evoked model [261], cold allodynia elicited by thalidomide, lenalidomide and pomalidomide was entirely TRPA1-dependent. However, the reason why cold hypersensitivity is solely dependent on TRPA1, whereas mechanical allodynia requires the contribution of both TRPA1 and TRPV4, remains unknown.

We previously found that local (intraplantar) administration of an oxidative stress scavenger or a TRPA1 antagonist completely reversed mechanical and cold allodynia evoked by bortezomib and oxaliplatin [117], suggesting that TRPA1 sensitization/activation may occur in terminal nerve fibers of the hind paw. To understand more precisely where TRPV4 and TRPA1 act to mediate thalidomide-evoked mechanical and cold allodynia, site-specific strategies of drug administration were used. Results show that peripheral (intraplantar) antagonism of TRPA1 in the mouse paw provided complete reversal of cold allodynia, but only partial attenuation of mechanical allodynia. If central (intrathecal) antagonism of TRPV4 was added to the peripheral TRPA1 blockade, thalidomide-evoked mechanical allodynia was completely inhibited.

Evidence of a differential contribution of peripheral *vs.* central oxidative stress has been reported in cisplatin- and paclitaxel-evoked mechanical hypersensitivity [200]. Oxidative stress manipulation experiments strengthen the conclusion deriving from channel pharmacological antagonism. In fact, whereas local oxidative stress inhibition either in the hind paw or CNS provided only partial attenuation, a combination of central and peripheral oxidative stress blockade completely reversed allodynia. Final proof that mechanical allodynia was mediated by oxidative stress activation of both peripheral TRPA1 and central TRPV4 was derived from experiments with genetic channel deletion. Elimination of

oxidative stress by an intrathecal antioxidant, while not further inhibiting thalidomide-evoked mechanical allodynia in *Trpv4*$^{-/-}$ mice, completely reversed the residual response observed in *Trpa1*$^{-/-}$ mice. These data further confirmed that full protection from thalidomide-induced mechanical allodynia can be attained by attenuating oxidative stress at both peripheral and central sites of action.

Although we have identified the role of oxidative stress, peripheral TRPA1 and central TRPV4 in mechanical and cold hypersensitivity elicited by thalidomide and related drugs in mice, several questions remain for further studies to investigate. These include the cell types that express peripheral TRPA1 and central TRPV4 that, engaged by oxidative stress, signal allodynia. Although TRPA1 is abundantly found in nociceptive C-fiber neurons [70], there is proof that the channel expressed in Schwann cells contributes to mechanical allodynia [263]. TRPV4 seems poorly expressed in nociceptors [47], while it may be present in satellite glial cells [266] and CNS astrocytes [267]. Furthermore, although H_2O_2 levels and 4-HNE staining were higher in the spinal cord than in the paw, it is not clear if these differences may explain the differential ability of oxidative stress to target TRPA1 in the periphery and TRPV4 in the CNS. From a therapeutic standpoint, the present results indicate the need of peripheral acting TRPA1 antagonists and blood brain barrier-penetrating TRPV4 antagonists to treat the pain symptoms associated to CIPN evoked by thalidomide and related drugs.

In the second part of this PhD project, we demonstrated that MΦs, in particular rMΦs, play a critical role in maintaining mechanical/cold hypersensitivity and spontaneous nociception in mice models of cancer pain.

A series of findings support this conclusion. Melanoma B16-F10 cell growth in the mouse hindpaw was associated with a time-dependent and parallel increase in mechanical allodynia and in the number of tMΦs and rMΦs. Depletion of the two MΦ populations by the homodimerizer agent, AP20187, in MaFIA mice abolished the allodynia. In neuropathic pain models, including partial nerve injury [51, 268], constriction of the infraorbital nerve [211], and diabetic neuropathy [269], clodronate, which depletes circulating monocytes, simultaneously removed MΦs and abated mechanical allodynia. In contrast, in the present cancer pain model, clodronate markedly reduced tMΦs, but affected neither rMΦ expansion nor allodynia. Additional evidence that cancer-evoked allodynia is solely dependent on rMΦs was obtained in MΦ-depleted MaFIA mice, whose tumor microenvironment, but not the nerve bundle, was replenished with peritoneal MΦs from

donor mice. While in these mice allodynia was not restored, in mice depleted of tMΦs, but not rMΦs, by treatment with AP20187 in the hindpaw, allodynia was maintained. Thus, mechanical allodynia is elicited by the expansion of rMΦs, whereas tMΦs, which are recruited from the blood circulation and rapidly depleted by clodronate, are not relevant. In this respect, the present cancer pain model shows some similarity with certain models of neuropathic pain, such as those produced by the spared nerve injury and the spinal nerve transection, where rMΦs have been identified as the proinflammatory cellular component responsible for allodynia [270, 271]. Elimination of mechanical allodynia in MΦ-depleted MaFIA mice with LLC supports the hypothesis that the role of MΦs in cancer pain is not unique to the B16-F10 melanoma model, but is essential in various types of murine tumors. The analysis of a proinflammatory cytokine panel in melanoma homogenates showed a pronounced increase in CCL2 and M-CSF levels, whereas a more diffuse augmentation of most cytokines, including CCL2 and M-CSF, was observed in sciatic nerve homogenates. While an anti-CCL2 mAb did not affect allodynia, both a M-CSFR antagonist and an anti-M-CSF mAb robustly attenuated allodynia. Targeting the M-CSF signaling not only reduced pain, but also inhibited neuroinflammation, as after immunological or pharmacological blockade of the M-CSF signal both MΦ expansion and increased oxidative stress (H_2O_2 levels) in the sciatic nerve homogenates were attenuated. M-CSF has been shown to induce mechanical allodynia after intrathecal administration [212]. We showed that intraplantar M-CSF elicits mechanical allodynia in mice. Although the entire family of CSF chemokines exhibits a similar proalgesic activity [272-274], only M-CSF, and not G-CSF or MG-CSF, produced MΦ-dependent allodynia. Together, these findings support the role of M-CSF in cancer pain and indicate another common feature between the present cancer pain model and certain [202, 214, 270], but not other [51, 207, 211], neuropathic pain models where MΦ chemoattraction was driven by CCL2.

We recently reported a major role for TRPA1 in mechanical allodynia evoked by melanoma in mice [148]. Thus, we hypothesized that TRPA1 is implicated in the rMΦs/M-CSF-mediated pro-allodynic pathway. After confirming that *Trpa1*$^{-/-}$ mice did not develop mechanical hypersensitivity after B16-F10 melanoma cell inoculation, we found that TRPA1 deletion abolished allodynia evoked by (intraplantar) M-CSF, but not by G-CSF or MG-CSF. These results reveal a cause and effect relationship between M-CSF and TRPA1 in pain. Therefore, we investigated how M-CSF elicits TRPA1-dependent allodynia. The inability of M-CSF to evoke allodynia in *Trpa1*$^{-/-}$ mice was associated with failure to expand rMΦs and to increase H_2O_2 levels in the sciatic nerve. Thus, elimination

of TRPA1 blunted the neuroinflammatory response evoked by M-CSF. The observation that rMΦ expansion was attenuated by TRPA1 deletion implies that channel activation is required to increase rMΦ number. This finding was unexpected, as MΦs express M-CSFR [275, 276]{Antoniazzi, 2019 #78}, and therefore, in principle, M-CSF, might increase their number by direct activation of its cognate receptor on rMΦs, without the involvement of TRPA1. This apparent contradictory finding was addressed by using multiple tools, including MaFIA mice, cultured human and mouse Schwann cells, and an *ex vivo* sciatic nerve mouse explant culture.

Cancer cells [277], monocytes [216], DRG neurons [270, 278], and Schwann cells [279] can all express and release M-CSF. The increased M-CSF levels evoked by cancer growth were not reduced in either the mouse hindpaw or sciatic nerve in MΦ-depleted MaFIA mice, indicating that MΦs are not involved in cancer-associated secretion of the chemokine. We corroborated the previous findings [279], showing that M-CSF is expressed by either mouse or human Schwann cells in culture. We also demonstrated that the TRPA1 agonist H_2O_2, which is increased in the sciatic nerve of mice with cancer, elicited a TRPA1-dependent release of M-CSF from cultured Schwann cells. Furthermore, in an *ex vivo* sciatic nerve explant culture, rMΦ expansion elicited by H_2O_2 was attenuated by a M-CSFR antagonist, a TRPA1 antagonist and an antioxidant. As H_2O_2 increases MΦs at sites of injury [51, 280], the inhibitory action of the antioxidant on rMΦ expansion was expected. However, the ability of M-CSFR and TRPA1 antagonists to similarly attenuate rMΦ expansion and M-CSF release from Schwann cells suggests a feed-forward mechanism, which entails the following steps: an oxidative stress burst from expanded rMΦs activates Schwann cells TRPA1 which releases M-CSF to sustain further rMΦ expansion (**Figure 39**). Direct assay of M-CSF in the hindpaw and sciatic nerve provides support to this hypothesis. In mice with a Cre-mediated deletion of *Trpa1* in the Schwann cell/oligodendrocyte lineage (*Plp1-Cre*$^{ERT+}$*/Trpa1*$^{fl/fl}$), cancer-evoked increase in tumor M-CSF was unchanged, whereas a marked reduction in the M-CSF levels was observed in the ipsilateral sciatic nerve. Thus, while M-CSF of the tumor microenvironment does not contribute to the proalgesic rMΦ expansion, the Schwann cell-mediated M-CSF release in the ipsilateral sciatic nerve is essential for the cancer-evoked allodynia.

The proalgesic pathways that include glial cell activation, inflammatory cell expansion, and increased proinflammatory mediators in the central and peripheral nervous systems, collectively referred to as neuroinflammation, have been extensively characterized as a major underlying mechanism of neuropathic pain associated with a variety of

neuropathological conditions [51, 202, 205, 207, 211, 270]. Although several cell types and proalgesic mediators have been proposed, the neuroinflammatory pathways that drive cancer pain remains uncertain [281-283]. Here, we identified the key role of M-CSF, released following Schwann cellTRPA1 activation, in sustaining cancer-evoked rMΦ expansion and the ensuing mechanical allodynia. Supporting evidence derives from the observation that deletion of TRPA1 in Schwann cell/oligodendrocyte lineage (*Plp1-Cre^{ERT+}/Trpa1$^{fl/fl}$*) attenuates neuroinflammation and mechanical allodynia in the melanoma mouse model of cancer pain. In contrast, deletion of TRPA1 in primary sensory neurons (*Adv-Cre^{+};Trpa1$^{fl/fl}$*) attenuates mechanical allodynia but not neuroinflammation. Thus, we hypothesize that, although neural TRPA1 is the final target of the proalgesic signaling pathway, the feed-forward mechanism that encompasses M-CSF, rMΦs oxidative stress, and Schwann cell/TRPA1 is needed to chronically sustain mechanical allodynia (Figure 8). The essential role of rMΦs and Schwann cell TRPA1 in cancer pain was further shown in the murine LLC, as allodynia and expansion in rMΦs evoked by this type of cancer were attenuated in both *Trpa1$^{-/-}$* and *Plp1-Cre^{ERT+}/Trpa1$^{fl/fl}$* mice. The selective elimination of rMΦs in mice with a Cre-mediated Schwann cell deletion of *Trpa1*, associated with eradication of allodynia, supports the crucial role of the Schwann cellchannel in orchestrating neuroinflammation and pain not only in melanoma but also in LLC.

However, there are two additional findings of our study that are difficult to interpret. The first relates to the different effects produced by TRPA1 pharmacological antagonism *vs.* those elicited by TRPA1 genetic deletion. While *Trpa1$^{-/-}$* mice showed a marked attenuation of both mechanical allodynia and neuroinflammation, systemic exposure to a TRPA1 antagonist efficiently abrogated allodynia, but did not affect rMΦ expansion. To explain this apparent contradiction, the different time courses of these interventions should be considered. In fact, *Trpa1$^{-/-}$* mice harbor a permanent channel deletion, whereas the short half-life of the TRPA1 antagonist, A967079, provides brief channel inhibition. Thus, the transient (a few hours) blockade of the neuronal channel is sufficient to shortly reverse allodynia, but cannot provide the prolonged inhibition (some days) of the Schwann cell TRPA1, which is necessary to attenuate the rMΦ expansion and the ensuing allodynia. This interpretation is further supported by the observation that treatment of MaFIA mice with AP20187, which depletes MΦs for several days, elicits a prolonged attenuation of allodynia, probably because the rMΦ/Schwann cell TRPA1 feed-forward mechanism is switched off for a prolonged period of time.

The second unsettled finding relates to the anatomical site of action where expanded rMΦs sustain allodynia. In models of MΦ-dependent neuropathic pain, MΦ depletion at the site of nerve injury efficiently attenuated allodynia [51, 211, 271]. However, in other models, a series of direct and indirect evidence showed that selective elimination of rMΦs at the site of the damaged nerve did not affect allodynia, which suggested that rMΦ expansion in the DRG was required [268, 270]. In the present model of cancer pain, we asked which was the anatomical site where the M-CSF/rMΦ/Schwann cell TRPA1 pathway must operate to sustain allodynia. Because of the technical complications inherent to the elimination of DRG rMΦs, we chose to examine this issue by depleting rMΦs in an anatomically well-identified segment of the sciatic nerve. The observation that a selective rMΦ depletion in a ~4 mm portion of the sciatic nerve trunk abrogated mechanical allodynia proposes a spatial constraint in the neuroinflammatory mechanism that sustains allodynia. As rMΦ expansion was unaltered in the proximal and distal untreated segments, the amplification loop consisting of rMΦs and Schwann cell TRPA1 that communicates *via* M-CSF and oxidative stress must function by contiguity throughout the entire sciatic nerve to warrant that the mechanical stimulus applied to the mouse paw is conveyed centrally as an allodynic signal.

The soma of DRG neurons does not participate in the central conduction of action potentials [284]. Instead, sensory impulses from peripheral terminals continue directly into the spinal cord and do not depolarize the soma [285]. However, the present findings do not exclude the possibility that DRG cells, with the cooperation of surrounding satellite cells and local expanded rMΦs, are implicated in magnifying the sensory impulse that conveys mechanical allodynia. Nevertheless, the present discovery of the role of the neuroinflammatory and proalgesic pathway that entails M-CSF, rMΦs, oxidative stress and Schwann cell TRPA1 in two different types of murine cancer offers novel targets for the identification of better and safer treatments for cancer pain.

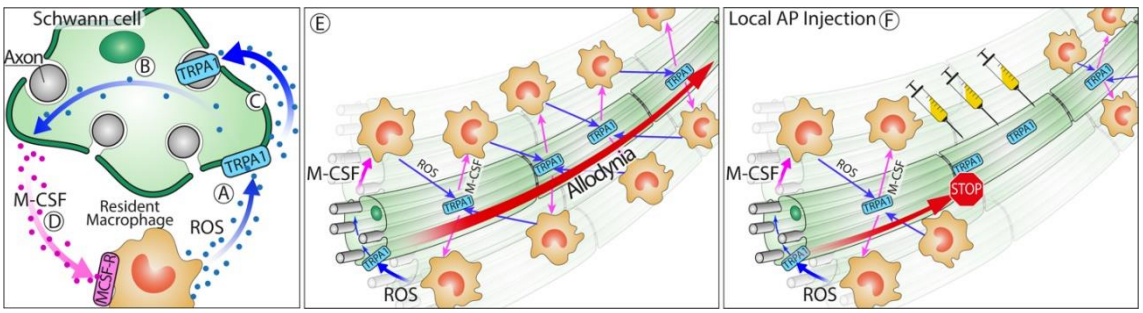

Figure 39. Feed-forward mechanism that sustains cancer pain**.** We propose a feed-forward mechanism that, to sustain cancer pain, encompasses the following steps: (**A**) expanded sciatic nerve resident macrophages (rMΦs) by their own oxidative burst target Schwann cell TRPA1; (**B**) Schwann cellTRPA1 amplifies the oxidative burst; (**C**) to release M-CSF which sustains further rMΦ expansion, and; (**D**) to target neuronal TRPA1 which signals allodynia. The paracrine pathway, which entails Schwann cellTRPA1 activation, M-CSF release and signaling and rMΦ expansion, and Schwann cell- and rMΦs-dependent oxidative burst (**E**) must be present along the entire sciatic nerve to sustain mechanical allodynia, as (**F**) the disruption of the feed-forward mechanism by segmental depletion of rMΦs switches off the pain-like response.

In the last part of the PhD project, we deciphered the mechanisms underlying pain due to metastasis in a MBCP mouse model. E0771 breast cancer cells were inoculated into the mouse mammary gland metastasize to the femur head and, *via* IL-8, subjugate osteoclasts to release osteolytic biomarkers, including IGF-1. The unexpected and major finding of the study is that the entire panel of pain-like behaviors evoked by bone metastasis depends on osteoclast-derived IGF-1, which, targeting the Schwann cell IGF-1R, converts the glial cell into an active proalgesic phenotype. IGF-1R activation in Schwann cells *via* a series of intracellular mediators and TRPA1 releases M-CSF that, promoting endoneurial rMΦs expansion, sustains pain-like behaviors.

Tumor-activated osteoclasts are known to release a series of osteolytic biomarkers, including TGF-b, IL-6, and IGF-1 [286-288]. Results obtained with inhibition of IGF-1 signaling by an IGF-1R antagonist and anti-IGF-1 neutralizing antibodies disclosed the critical role of IGF-1 in generating pain-like behaviors. IGF-1 has been implicated in various mouse pain models, including chronic constriction injury [289], carrageenan-induced inflammation [290], and type 2 diabetic neuropathy [291]. Although previous [292, 293] and recent [243] studies have suggested that IGF-1 exerts analgesic effects in the CNS, general consensus indicates that its peripheral administration elicits acute nociceptive response and prolonged mechanical and thermal hypersensitivity [239, 291]. This conclusion is strengthened by present observations that perineural, but not central, administration of a neutralizing antibody against IGF-1 reverted pain-like behaviors, thus excluding the contribution of central IGF-1 in our model of MBCP.

The proalgesic effects of IGF-1 peripheral administration have been ascribed to a direct action on IGF-1R expressed by DRG neurons [239]. The present data obtained by IGF-1R cell-selective silencing confirm the role of neuronal IGF-1R in acute nociception. However, they reveal an unforeseen role of SC IGF-1R in sustaining mechanical/cold hypersensitivity evoked by i.pl. IGF-1 injection, thus highlighting a dichotomous action of

IGF-1 in DRG neurons and peripheral glial cells. IGF-1 injection (i.pl.) elicits two distinct types of responses: an early and transient acute nociception and a delayed and persistent mechanical/cold hypersensitivity. Silencing of IGF-1R in DRG neurons attenuated acute nociception, leaving sustained mechanical/cold hypersensitivity unaffected. *Vice versa*, silencing IGF-1R in Schwann cells inhibited mechanical/cold hypersensitivity without affecting acute nociception. These findings have major pathophysiological consequences as selective silencing of IGF-1R in DRG neurons failed to attenuate pain-like behaviors evoked by E0771 cell inoculation, which, in contrast, were inhibited in mice with selective silencing of IGF-1R in Schwann cells.

IGF binding proteins (IGFBPs) can affect the extent of IGF-1 signaling [294]. In particular, the interaction of IGFBP-4, which is abundantly expressed in bone tissue, with IGF-1, has been shown to prevent IGF-1R activation [295, 296]. However, there is no evidence that increased levels of IGFBP-4, or other IGFBPs modulating IGF-1R signaling, reduce MBCP. Some promiscuity in IGF-1R signaling has been reported. In fact, IGF-2 and insulin have been shown to promote the same intracellular pathway, *via* the activation of hybrid receptors *via* insulin half receptors [297]. However, if and how this non-canonical signaling pathway might trigger a response implicated in the Schwann cell algesic pathway is currently unknown.

The divergent proalgesic responses to IGF-1 in DRG neurons and Schwann cells are encoded by distinct intracellular pathways recruited by IGF-1R activation in the two cell types (**Fig. 40**) IGF-1R activation in cultured mouse DRG neurons promotes a PKCa-dependent T-type channel Ca^{2+} influx, which has been associated with peripheral pain [239].

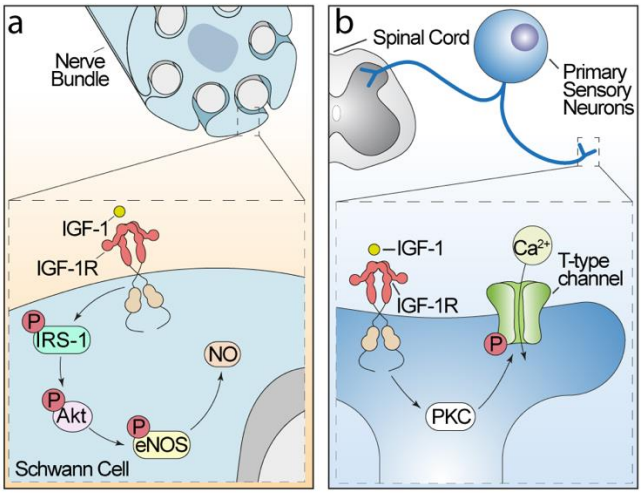

Figure 40. IGF-1R signaling cascade in Schwann cells and dorsal root ganglion (DRG) neurons. Schematic representation of the IGF-1 intracellular pathway in (**a**) Schwann cells and (**b**) DRG neurons after IGF-1 stimulation.

However, the PKC inhibitor, Ro32-0432, attenuated acute nociception but failed to inhibit prolonged mechanical/cold hypersensitivity evoked by i.pl. IGF-1 injection. In Schwann cells, IGF-1R trans-phosphorylation did not activate PKC, but stimulated IRS-1 and the AKT-dependent cascade that promotes eNOS phosphorylation. Activated IRS-1 interacts with the clathrin adaptor protein complex (AP2) to prevent IGF-1R clathrin-mediated endocytosis, thereby prolonging receptor activity [250]. Here, we show that an IRS-1 inhibitor (NT157) prevented mechanical/cold hypersensitivity induced by i.pl. IGF-1 injection. Notably, mechanical/cold hypersensitivity and pain-like behaviors were not apparently due to endosome internalization, as the combination of an IRS-1 inhibitor and a clathrin-mediated endocytosis inhibitor (PitStop2) failed to restore sustained mechanical/cold hypersensitivity and pain-like behaviors. In contrast, acute nociception produced by i.pl. IGF-1 injection, reduced by IRS-1 inhibition, was restored by the clathrin inhibitor, thus supporting the existence of two distinct and cell-specific IGF-1 signaling pathways. In DRG neurons, permanence of IGF-1R to the plasma membrane mediated by IRS-1 and PKC activation encodes the acute nociception response induced by IGF-1, attenuated by the clathrin-dependent internalization. In contrast, IRS-1 elicits sustained mechanical/cold hypersensitivity *via* a different pathway in Schwann cells, which is independent of PKC and clathrin-mediated endocytosis, is mediated by eNOS phosphorylation, and is the sole mechanism implicated in pain-like behaviors observed in the current model of MBCP.

IGF-1 stimulation of cultured Schwann cells resulted in eNOS phosphorylation and the ensuing NO release. Inoculation of osteosarcoma cells in the femurs of C3H/HeJ mice induces pain-like behaviors through the activation of neuronal and inducible NOS isoforms (nNOS and iNOS, respectively) in the spinal cord [298]. Here, we show that administration of the NO scavenger, cPTIO, or the NOS inhibitor, L-NAME, attenuated pain-like behaviors in mice inoculated with E0771 cells and sustained mechanical/cold hypersensitivity elicited by i.pl. IGF-1. Failure of cPTIO and L-NAME to reduce acute nociception induced by i.pl. IGF-1 strengthens the hypothesis that NO released by Schwann cell eNOS is necessary and sufficient for generating prolonged proalgesic responses, including mechanical/cold hypersensitivity by IGF-1 and cancer-evoked pain-

like behaviors, as previously proposed in a model of CGRP-evoked periorbital mechanical allodynia [67].

Inoculation of melanoma cancer cells in mouse hind paw was shown to cause M-CSF release from Schwann cells, which promotes the expansion of endoneurial rMΦs [227]. The resulting oxidative stress targets neuronal TRPA1 to signal mechanical hypersensitivity [227]. In the present MBCP model, E0771 breast carcinoma cells growing in the femur metastasis release IL-8, which stimulates osteoclasts to liberate IGF-1. The ensuing IGF-1R activation in Schwann cells results in NO production that targets Schwann cell TRPA1. Activated TRPA1 releases M-CSF that promotes endoneurial rMΦ expansion and the ensuing ROS generation sustains mechanical allodynia by targeting neuronal TRPA1. Therefore, we propose that the humoral communication between osteoclasts and Schwann cells converges in a final common pathway implicating a role of NO/TRPA1/oxidative stress that is observed in different mouse models of cancer or neuropathic pain. However, this conclusion does not implicate that different proalgesic pathways contribute to MBCP. Glial cell-selective targeting of the various mediators that sustain proalgesic signals initiated by Schwann cell IGF-1R activation could be a promising area for future treatments against MBCP.

The major conclusion of this three-year project is that TRPA1 channel expressed by Schwann cell is a crucial mediator in cancer-related pain models. We also revealed a role of TRPV4 in thalidomide-induced neuropathic pain.

Targeting these channels may be a promising therapeutic method for the treatment of pain symptoms associated with cancer. TRPA1 and TRPV4 antagonists, as well as TRPA1/TRPV4-desensitizing medicines, may significantly improve pain therapy.

In perspective, we propose to test the novel therapeutic strategies that, acting on the various targetable steps (endoneurial MΦs/microglia, Schwann cells/oligodendrocytes, M-CSF, TRPA1/NOX1/oxidative stress and SP/CGRP receptors) of the proalgesic pathway activated by various types of cancer, that may provide relief from cancer pain, and to explore the efficacy of therapeutic strategies directed to affect the selected targets, including TRPA1 antagonists, by local administration of the new compounds in order to maximize the analgesic potential and minimize the adverse effects.

REFERENCES

1. Nilius, B., et al., *Transient receptor potential cation channels in disease.* Physiol Rev, 2007. **87**(1): p. 165-217.
2. Samanta, A., T.E.T. Hughes, and V.Y. Moiseenkova-Bell, *Transient Receptor Potential (TRP) Channels.* Subcell Biochem, 2018. **87**: p. 141-165.
3. Cosens, D.J. and A. Manning, *Abnormal electroretinogram from a Drosophila mutant.* Nature, 1969. **224**(5216): p. 285-7.
4. Minke, B., *The history of the Drosophila TRP channel: the birth of a new channel superfamily.* J Neurogenet, 2010. **24**(4): p. 216-33.
5. Zhang, M., et al., *TRP (transient receptor potential) ion channel family: structures, biological functions and therapeutic interventions for diseases.* Signal Transduct Target Ther, 2023. **8**(1): p. 261.
6. Montell, C., *The history of TRP channels, a commentary and reflection.* Pflugers Arch, 2011. **461**(5): p. 499-506.
7. Zhu, X., et al., *Molecular cloning of a widely expressed human homologue for the Drosophila trp gene.* FEBS Lett, 1995. **373**(3): p. 193-8.
8. Suss-Toby, E., Z. Selinger, and B. Minke, *Lanthanum reduces the excitation efficiency in fly photoreceptors.* J Gen Physiol, 1991. **98**(4): p. 849-68.
9. Liu, C.H., et al., *In vivo identification and manipulation of the Ca2+ selectivity filter in the Drosophila transient receptor potential channel.* J Neurosci, 2007. **27**(3): p. 604-15.
10. Gillo, B., et al., *Coexpression of Drosophila TRP and TRP-like proteins in Xenopus oocytes reconstitutes capacitative Ca2+ entry.* Proc Natl Acad Sci U S A, 1996. **93**(24): p. 14146-51.
11. Xu, X.Z., et al., *Coassembly of TRP and TRPL produces a distinct store-operated conductance.* Cell, 1997. **89**(7): p. 1155-64.
12. Wes, P.D., et al., *TRPC1, a human homolog of a Drosophila store-operated channel.* Proc Natl Acad Sci U S A, 1995. **92**(21): p. 9652-6.
13. Caterina, M.J., et al., *The capsaicin receptor: a heat-activated ion channel in the pain pathway.* Nature, 1997. **389**(6653): p. 816-24.
14. Li, H., *TRP Channel Classification.* Adv Exp Med Biol, 2017. **976**: p. 1-8.
15. Venkatachalam, K. and C. Montell, *TRP channels.* Annu Rev Biochem, 2007. **76**: p. 387-417.
16. Souza Monteiro de Araujo, D., et al., *TRPA1 as a therapeutic target for nociceptive pain.* Expert Opin Ther Targets, 2020. **24**(10): p. 997-1008.
17. Pedersen, S.F., G. Owsianik, and B. Nilius, *TRP channels: an overview.* Cell Calcium, 2005. **38**(3-4): p. 233-52.
18. Cao, E., *Structural mechanisms of transient receptor potential ion channels.* J Gen Physiol, 2020. **152**(3).
19. Yu, F.H. and W.A. Catterall, *The VGL-chanome: a protein superfamily specialized for electrical signaling and ionic homeostasis.* Sci STKE, 2004. **2004**(253): p. re15.
20. Huffer, K.E., et al., *Global alignment and assessment of TRP channel transmembrane domain structures to explore functional mechanisms.* Elife, 2020. **9**.
21. Ramsey, I.S., M. Delling, and D.E. Clapham, *An introduction to TRP channels.* Annu Rev Physiol, 2006. **68**: p. 619-47.

22. Bork, P., *Hundreds of ankyrin-like repeats in functionally diverse proteins: mobile modules that cross phyla horizontally?* Proteins, 1993. **17**(4): p. 363-74.
23. Cao, E., et al., *TRPV1 structures in distinct conformations reveal activation mechanisms.* Nature, 2013. **504**(7478): p. 113-8.
24. Paulsen, C.E., et al., *Structure of the TRPA1 ion channel suggests regulatory mechanisms.* Nature, 2015. **520**(7548): p. 511-7.
25. Erler, I., et al., *Ca2+-selective transient receptor potential V channel architecture and function require a specific ankyrin repeat.* J Biol Chem, 2004. **279**(33): p. 34456-63.
26. Liao, M., et al., *Structure of the TRPV1 ion channel determined by electron cryo-microscopy.* Nature, 2013. **504**(7478): p. 107-12.
27. Clapham, D.E., *TRP channels as cellular sensors.* Nature, 2003. **426**(6966): p. 517-24.
28. Schaeffer, C., et al., *Calcitonin gene-related peptide partly protects cultured smooth muscle cells from apoptosis induced by an oxidative stress via activation of ERK1/2 MAPK.* Biochim Biophys Acta, 2003. **1643**(1-3): p. 65-73.
29. Hoffmann, J. and P.J. Goadsby, *Emerging targets in migraine.* CNS Drugs, 2014. **28**(1): p. 11-7.
30. Vriens, J., G. Appendino, and B. Nilius, *Pharmacology of vanilloid transient receptor potential cation channels.* Mol Pharmacol, 2009. **75**(6): p. 1262-79.
31. Benemei, S., et al., *TRPA1 and other TRP channels in migraine.* J Headache Pain, 2013. **14**(1): p. 71.
32. Nilius, B. and G. Owsianik, *Transient receptor potential channelopathies.* Pflugers Arch, 2010. **460**(2): p. 437-50.
33. Mickle, A.D., A.J. Shepherd, and D.P. Mohapatra, *Sensory TRP channels: the key transducers of nociception and pain.* Prog Mol Biol Transl Sci, 2015. **131**: p. 73-118.
34. Patapoutian, A., S. Tate, and C.J. Woolf, *Transient receptor potential channels: targeting pain at the source.* Nat Rev Drug Discov, 2009. **8**(1): p. 55-68.
35. Vriens, J., et al., *Modulation of the Ca2 permeable cation channel TRPV4 by cytochrome P450 epoxygenases in vascular endothelium.* Circ Res, 2005. **97**(9): p. 908-15.
36. Vennekens, R., et al., *Permeation and gating properties of the novel epithelial Ca(2+) channel.* J Biol Chem, 2000. **275**(6): p. 3963-9.
37. den Dekker, E., et al., *The epithelial calcium channels, TRPV5 & TRPV6: from identification towards regulation.* Cell Calcium, 2003. **33**(5-6): p. 497-507.
38. Macpherson, L.J., et al., *The pungency of garlic: activation of TRPA1 and TRPV1 in response to allicin.* Curr Biol, 2005. **15**(10): p. 929-34.
39. Siemens, J., et al., *Spider toxins activate the capsaicin receptor to produce inflammatory pain.* Nature, 2006. **444**(7116): p. 208-12.
40. Ahern, G.P., et al., *Extracellular cations sensitize and gate capsaicin receptor TRPV1 modulating pain signaling.* J Neurosci, 2005. **25**(21): p. 5109-16.
41. Zhang, X., J. Huang, and P.A. McNaughton, *NGF rapidly increases membrane expression of TRPV1 heat-gated ion channels.* EMBO J, 2005. **24**(24): p. 4211-23.
42. Ji, R.R., et al., *p38 MAPK activation by NGF in primary sensory neurons after inflammation increases TRPV1 levels and maintains heat hyperalgesia.* Neuron, 2002. **36**(1): p. 57-68.
43. Suzuki, M., et al., *Impaired pressure sensation in mice lacking TRPV4.* J Biol Chem, 2003. **278**(25): p. 22664-8.

44. Chuang, H.H., et al., *Bradykinin and nerve growth factor release the capsaicin receptor from PtdIns(4,5)P2-mediated inhibition.* Nature, 2001. **411**(6840): p. 957-62.
45. Liedtke, W., et al., *Vanilloid receptor-related osmotically activated channel (VR-OAC), a candidate vertebrate osmoreceptor.* Cell, 2000. **103**(3): p. 525-35.
46. Wissenbach, U., et al., *Trp12, a novel Trp related protein from kidney.* FEBS Lett, 2000. **485**(2-3): p. 127-34.
47. Grant, A.D., et al., *Protease-activated receptor 2 sensitizes the transient receptor potential vanilloid 4 ion channel to cause mechanical hyperalgesia in mice.* J Physiol, 2007. **578**(Pt 3): p. 715-33.
48. Watanabe, H., et al., *Heat-evoked activation of TRPV4 channels in a HEK293 cell expression system and in native mouse aorta endothelial cells.* J Biol Chem, 2002. **277**(49): p. 47044-51.
49. O'Neil, R.G. and L. Leng, *Osmo-mechanically sensitive phosphatidylinositol signaling regulates a Ca2+ influx channel in renal epithelial cells.* Am J Physiol, 1997. **273**(1 Pt 2): p. F120-8.
50. Jaquemar, D., T. Schenker, and B. Trueb, *An ankyrin-like protein with transmembrane domains is specifically lost after oncogenic transformation of human fibroblasts.* J Biol Chem, 1999. **274**(11): p. 7325-33.
51. De Logu, F., et al., *Schwann cell TRPA1 mediates neuroinflammation that sustains macrophage-dependent neuropathic pain in mice.* Nat Commun, 2017. **8**(1): p. 1887.
52. Meens, M.J., et al., *Calcitonin gene-related peptide selectively relaxes contractile responses to endothelin-1 in rat mesenteric resistance arteries.* J Pharmacol Exp Ther, 2009. **331**(1): p. 87-95.
53. Talavera, K., et al., *Mammalian Transient Receptor Potential TRPA1 Channels: From Structure to Disease.* Physiol Rev, 2020. **100**(2): p. 725-803.
54. Banke, T.G., S.R. Chaplan, and A.D. Wickenden, *Dynamic changes in the TRPA1 selectivity filter lead to progressive but reversible pore dilation.* Am J Physiol Cell Physiol, 2010. **298**(6): p. C1457-68.
55. Sinharoy, P., et al., *TRPA1 and TRPV1 contribute to propofol-mediated antagonism of U46619-induced constriction in murine coronary arteries.* PLoS One, 2017. **12**(6): p. e0180106.
56. Meents, J.E., C.I. Ciotu, and M.J.M. Fischer, *TRPA1: a molecular view.* J Neurophysiol, 2019. **121**(2): p. 427-443.
57. Hasan, R., et al., *Calmodulin is responsible for Ca(2+)-dependent regulation of TRPA1 Channels.* Sci Rep, 2017. **7**: p. 45098.
58. Bhattacharya, M.R., et al., *Radial stretch reveals distinct populations of mechanosensitive mammalian somatosensory neurons.* Proc Natl Acad Sci U S A, 2008. **105**(50): p. 20015-20.
59. Latorre, R., et al., *ThermoTRP channels as modular proteins with allosteric gating.* Cell Calcium, 2007. **42**(4-5): p. 427-38.
60. Taylor-Clark, T.E., et al., *Prostaglandin-induced activation of nociceptive neurons via direct interaction with transient receptor potential A1 (TRPA1).* Mol Pharmacol, 2008. **73**(2): p. 274-81.
61. Andrade, E.L., F.C. Meotti, and J.B. Calixto, *TRPA1 antagonists as potential analgesic drugs.* Pharmacol Ther, 2012. **133**(2): p. 189-204.
62. Wang, Y.Y., R.B. Chang, and E.R. Liman, *TRPA1 is a component of the nociceptive response to CO2.* J Neurosci, 2010. **30**(39): p. 12958-63.

63. Miyamoto, T., et al., *TRPV1 and TRPA1 mediate peripheral nitric oxide-induced nociception in mice.* PLoS One, 2009. **4**(10): p. e7596.
64. Xiao, B., et al., *Identification of transmembrane domain 5 as a critical molecular determinant of menthol sensitivity in mammalian TRPA1 channels.* J Neurosci, 2008. **28**(39): p. 9640-51.
65. Karashima, Y., et al., *Bimodal action of menthol on the transient receptor potential channel TRPA1.* J Neurosci, 2007. **27**(37): p. 9874-84.
66. Moparthi, L., et al., *Human TRPA1 is intrinsically cold- and chemosensitive with and without its N-terminal ankyrin repeat domain.* Proc Natl Acad Sci U S A, 2014. **111**(47): p. 16901-6.
67. De Logu, F., et al., *Schwann cell endosome CGRP signals elicit periorbital mechanical allodynia in mice.* Nat Commun, 2022. **13**(1): p. 646.
68. Schmidt, M., et al., *Nociceptive signals induce trafficking of TRPA1 to the plasma membrane.* Neuron, 2009. **64**(4): p. 498-509.
69. Meents, J.E., M.J. Fischer, and P.A. McNaughton, *Sensitization of TRPA1 by Protein Kinase A.* PLoS One, 2017. **12**(1): p. e0170097.
70. Story, G.M., et al., *ANKTM1, a TRP-like channel expressed in nociceptive neurons, is activated by cold temperatures.* Cell, 2003. **112**(6): p. 819-29.
71. Akopian, A.N., et al., *Transient receptor potential TRPA1 channel desensitization in sensory neurons is agonist dependent and regulated by TRPV1-directed internalization.* J Physiol, 2007. **583**(Pt 1): p. 175-93.
72. Gaudet, R., *A primer on ankyrin repeat function in TRP channels and beyond.* Mol Biosyst, 2008. **4**(5): p. 372-9.
73. Logashina, Y.A., et al., *TRPA1 Channel as a Regulator of Neurogenic Inflammation and Pain: Structure, Function, Role in Pathophysiology, and Therapeutic Potential of Ligands.* Biochemistry (Mosc), 2019. **84**(2): p. 101-118.
74. Petrus, M., et al., *A role of TRPA1 in mechanical hyperalgesia is revealed by pharmacological inhibition.* Mol Pain, 2007. **3**: p. 40.
75. Kwan, K.Y., et al., *TRPA1 modulates mechanotransduction in cutaneous sensory neurons.* J Neurosci, 2009. **29**(15): p. 4808-19.
76. Meents, J.E., M.J. Fischer, and P.A. McNaughton, *Agonist-induced sensitisation of the irritant receptor ion channel TRPA1.* J Physiol, 2016. **594**(22): p. 6643-6660.
77. Baraldi, P.G., et al., *Transient receptor potential ankyrin 1 (TRPA1) channel as emerging target for novel analgesics and anti-inflammatory agents.* J Med Chem, 2010. **53**(14): p. 5085-107.
78. McNamara, C.R., et al., *TRPA1 mediates formalin-induced pain.* Proc Natl Acad Sci U S A, 2007. **104**(33): p. 13525-30.
79. Wei, H., et al., *Transient receptor potential ankyrin 1 ion channel contributes to guarding pain and mechanical hypersensitivity in a rat model of postoperative pain.* Anesthesiology, 2012. **117**(1): p. 137-48.
80. Chen, S.P., E.A. Tolner, and K. Eikermann-Haerter, *Animal models of monogenic migraine.* Cephalalgia, 2016. **36**(7): p. 704-21.
81. Wei, H., et al., *Attenuation of mechanical hypersensitivity by an antagonist of the TRPA1 ion channel in diabetic animals.* Anesthesiology, 2009. **111**(1): p. 147-54.
82. Koivisto, A., et al., *TRPA1 Antagonists for Pain Relief.* Pharmaceuticals (Basel), 2018. **11**(4).
83. Klionsky, L., et al., *Species-specific pharmacology of Trichloro(sulfanyl)ethyl benzamides as transient receptor potential ankyrin 1 (TRPA1) antagonists.* Mol Pain, 2007. **3**: p. 39.

84. Nassini, R., et al., *The TRPA1 channel in inflammatory and neuropathic pain and migraine.* Rev Physiol Biochem Pharmacol, 2014. **167**: p. 1-43.
85. Materazzi, S., et al., *Parthenolide inhibits nociception and neurogenic vasodilatation in the trigeminovascular system by targeting the TRPA1 channel.* Pain, 2013. **154**(12): p. 2750-2758.
86. Nassini, R., et al., *Acetaminophen, via its reactive metabolite N-acetyl-p-benzo-quinoneimine and transient receptor potential ankyrin-1 stimulation, causes neurogenic inflammation in the airways and other tissues in rodents.* FASEB J, 2010. **24**(12): p. 4904-16.
87. Nassini, R., et al., *The TRPA1 channel mediates the analgesic action of dipyrone and pyrazolone derivatives.* Br J Pharmacol, 2015. **172**(13): p. 3397-411.
88. Woolf, T., *Surviving brain surgery.* Seizure, 2010. **19**(10): p. 656-7.
89. Woolf, A.D., T. Vos, and L. March, *How to measure the impact of musculoskeletal conditions.* Best Pract Res Clin Rheumatol, 2010. **24**(6): p. 723-32.
90. Abd-Elsayed, A., et al., *Neuropathic pain and Kv7 voltage-gated potassium channels: The potential role of Kv7 activators in the treatment of neuropathic pain.* Mol Pain, 2019. **15**: p. 1744806919864256.
91. Dubin, A.E. and A. Patapoutian, *Nociceptors: the sensors of the pain pathway.* J Clin Invest, 2010. **120**(11): p. 3760-72.
92. Bandell, M., et al., *Noxious cold ion channel TRPA1 is activated by pungent compounds and bradykinin.* Neuron, 2004. **41**(6): p. 849-57.
93. Bautista, D.M., et al., *TRPA1 mediates the inflammatory actions of environmental irritants and proalgesic agents.* Cell, 2006. **124**(6): p. 1269-82.
94. Obata, K., et al., *Overexpression of calmodulin induces cardiac hypertrophy by a calcineurin-dependent pathway.* Biochem Biophys Res Commun, 2005. **338**(2): p. 1299-305.
95. Dunham, J.P., S. Kelly, and L.F. Donaldson, *Inflammation reduces mechanical thresholds in a population of transient receptor potential channel A1-expressing nociceptors in the rat.* Eur J Neurosci, 2008. **27**(12): p. 3151-60.
96. da Costa, D.S., et al., *Dissecting cardosin B trafficking pathways in heterologous systems.* Planta, 2010. **232**(6): p. 1517-30.
97. McGaraughty, S., et al., *TRPA1 modulation of spontaneous and mechanically evoked firing of spinal neurons in uninjured, osteoarthritic, and inflamed rats.* Mol Pain, 2010. **6**: p. 14.
98. Bonet, I., et al., *Classifier ensemble based on feature selection and diversity measures for predicting the affinity of A(2B) adenosine receptor antagonists.* J Chem Inf Model, 2013. **53**(12): p. 3140-55.
99. Murnion, B.P., *Neuropathic pain: current definition and review of drug treatment.* Aust Prescr, 2018. **41**(3): p. 60-63.
100. Campbell, C.Y., et al., *Role of atherosclerosis assessment and other novel markers in the metabolic syndrome.* Metab Syndr Relat Disord, 2006. **4**(4): p. 261-9.
101. Caspani, O., et al., *The contribution of TRPM8 and TRPA1 channels to cold allodynia and neuropathic pain.* PLoS One, 2009. **4**(10): p. e7383.
102. Eid, S.R., et al., *HC-030031, a TRPA1 selective antagonist, attenuates inflammatory- and neuropathy-induced mechanical hypersensitivity.* Mol Pain, 2008. **4**: p. 48.
103. Kerstein, S.J., *Autonomy, moral constraints, and markets in kidneys.* J Med Philos, 2009. **34**(6): p. 573-85.

104. Trevisani, M., et al., *4-Hydroxynonenal, an endogenous aldehyde, causes pain and neurogenic inflammation through activation of the irritant receptor TRPA1*. Proc Natl Acad Sci U S A, 2007. **104**(33): p. 13519-24.
105. Koivisto, A., et al., *Inhibiting TRPA1 ion channel reduces loss of cutaneous nerve fiber function in diabetic animals: sustained activation of the TRPA1 channel contributes to the pathogenesis of peripheral diabetic neuropathy.* Pharmacol Res, 2012. **65**(1): p. 149-58.
106. Koivisto, A., *Sustained TRPA1 activation in vivo.* Acta Physiol (Oxf), 2012. **204**(2): p. 248-54.
107. Cavaletti, G. and P. Marmiroli, *Chemotherapy-induced peripheral neurotoxicity.* Nat Rev Neurol, 2010. **6**(12): p. 657-66.
108. Joseph, S. and R. Kamble, *Current trends in endovascular management of intracranial aneurysms (including posterior fossa aneurysms and multiple aneurysms).* Indian J Radiol Imaging, 2008. **18**(3): p. 256-63.
109. Bolcskei, K., et al., *Investigation of the role of TRPV1 receptors in acute and chronic nociceptive processes using gene-deficient mice.* Pain, 2005. **117**(3): p. 368-376.
110. Bessac, B.F. and S.E. Jordt, *Breathtaking TRP channels: TRPA1 and TRPV1 in airway chemosensation and reflex control.* Physiology (Bethesda), 2008. **23**: p. 360-70.
111. Nassini, R., et al., *Oxaliplatin elicits mechanical and cold allodynia in rodents via TRPA1 receptor stimulation.* Pain, 2011. **152**(7): p. 1621-1631.
112. Trevisan, G., et al., *Transient receptor potential ankyrin 1 receptor stimulation by hydrogen peroxide is critical to trigger pain during monosodium urate-induced inflammation in rodents.* Arthritis Rheum, 2013. **65**(11): p. 2984-95.
113. Alessandri-Haber, N., et al., *Interaction of transient receptor potential vanilloid 4, integrin, and SRC tyrosine kinase in mechanical hyperalgesia.* J Neurosci, 2008. **28**(5): p. 1046-57.
114. Materazzi, S., S. Canepari, and S. Aquili, *Monitoring heavy metal pollution by aquatic plants: a systematic study of copper uptake.* Environ Sci Pollut Res Int, 2012. **19**(8): p. 3292-8.
115. Barriere, D.A., et al., *Paclitaxel therapy potentiates cold hyperalgesia in streptozotocin-induced diabetic rats through enhanced mitochondrial reactive oxygen species production and TRPA1 sensitization.* Pain, 2012. **153**(3): p. 553-561.
116. Materazzi, S., et al., *TRPA1 and TRPV4 mediate paclitaxel-induced peripheral neuropathy in mice via a glutathione-sensitive mechanism.* Pflugers Arch, 2012. **463**(4): p. 561-9.
117. Trevisan, G., et al., *Novel therapeutic strategy to prevent chemotherapy-induced persistent sensory neuropathy by TRPA1 blockade.* Cancer Res, 2013. **73**(10): p. 3120-31.
118. De Logu, F., et al., *Migraine-provoking substances evoke periorbital allodynia in mice.* J Headache Pain, 2019. **20**(1): p. 18.
119. Benemei, S., et al., *The TRPA1 channel in migraine mechanism and treatment.* Br J Pharmacol, 2014. **171**(10): p. 2552-67.
120. Kunkler, P.E., et al., *TRPA1 receptors mediate environmental irritant-induced meningeal vasodilatation.* Pain, 2011. **152**(1): p. 38-44.
121. Nassini, R., et al., *Transient receptor potential ankyrin 1 channel localized to non-neuronal airway cells promotes non-neurogenic inflammation.* PLoS One, 2012. **7**(8): p. e42454.

122. Andre, E., et al., *Cigarette smoke-induced neurogenic inflammation is mediated by alpha,beta-unsaturated aldehydes and the TRPA1 receptor in rodents.* J Clin Invest, 2008. **118**(7): p. 2574-82.
123. Wang, S., et al., *Roles of TRPV1 and TRPA1 in Spontaneous Pain from Inflamed Masseter Muscle.* Neuroscience, 2018. **384**: p. 290-299.
124. Amin, F.M., et al., *The effect of sumatriptan on cephalic arteries: A 3T MR-angiography study in healthy volunteers.* Cephalalgia, 2013. **33**(12): p. 1009-16.
125. Wei, E.P., et al., *Calcitonin gene-related peptide mediates nitroglycerin and sodium nitroprusside-induced vasodilation in feline cerebral arterioles.* Circ Res, 1992. **70**(6): p. 1313-9.
126. Fanciullacci, M., et al., *Increase in plasma calcitonin gene-related peptide from the extracerebral circulation during nitroglycerin-induced cluster headache attack.* Pain, 1995. **60**(2): p. 119-123.
127. Nassini, R., et al., *The 'headache tree' via umbellulone and TRPA1 activates the trigeminovascular system.* Brain, 2012. **135**(Pt 2): p. 376-90.
128. Benemei, S., et al., *CGRP receptors in the control of pain and inflammation.* Curr Opin Pharmacol, 2009. **9**(1): p. 9-14.
129. Benemei, S., et al., *The anti-migraine component of butterbur extracts, isopetasin, desensitizes peptidergic nociceptors by acting on TRPA1 cation channel.* Br J Pharmacol, 2017. **174**(17): p. 2897-2911.
130. Marshall, J.L., et al., *Implementation of a performance improvement initiative in colorectal cancer care.* J Oncol Pract, 2012. **8**(5): p. 309-14.
131. Breivik, H., et al., *Cancer-related pain: a pan-European survey of prevalence, treatment, and patient attitudes.* Ann Oncol, 2009. **20**(8): p. 1420-33.
132. Simone, C.B., 2nd, et al., *Cancer patient attitudes toward analgesic usage and pain intervention.* Clin J Pain, 2012. **28**(2): p. 157-62.
133. Lema, M.J., K.M. Foley, and F.H. Hausheer, *Types and epidemiology of cancer-related neuropathic pain: the intersection of cancer pain and neuropathic pain.* Oncologist, 2010. **15 Suppl 2**: p. 3-8.
134. Raphael, J., et al., *Cancer pain: part 2: physical, interventional and complimentary therapies; management in the community; acute, treatment-related and complex cancer pain: a perspective from the British Pain Society endorsed by the UK Association of Palliative Medicine and the Royal College of General Practitioners.* Pain Med, 2010. **11**(6): p. 872-96.
135. Pergolizzi, J.V., C. Gharibo, and K.Y. Ho, *Treatment Considerations for Cancer Pain: A Global Perspective.* Pain Pract, 2015. **15**(8): p. 778-92.
136. Marcus, D.A., *Epidemiology of cancer pain.* Curr Pain Headache Rep, 2011. **15**(4): p. 231-4.
137. Kroenke, K., et al., *The association of depression and pain with health-related quality of life, disability, and health care use in cancer patients.* J Pain Symptom Manage, 2010. **40**(3): p. 327-41.
138. Deandrea, S., et al., *Prevalence of undertreatment in cancer pain. A review of published literature.* Ann Oncol, 2008. **19**(12): p. 1985-91.
139. McGuire, D.B., *Occurrence of cancer pain.* J Natl Cancer Inst Monogr, 2004(32): p. 51-6.
140. Bennett, R.M., *The rational management of fibromyalgia patients.* Rheum Dis Clin North Am, 2002. **28**(2): p. 181-99, v.
141. Swarm, R.A., et al., *Adult Cancer Pain, Version 3.2019, NCCN Clinical Practice Guidelines in Oncology.* J Natl Compr Canc Netw, 2019. **17**(8): p. 977-1007.

142. Prieto-Fernandez, E., et al., *Hypoxia Promotes Syndecan-3 Expression in the Tumor Microenvironment.* Front Immunol, 2020. **11**: p. 586977.
143. Kaplan, S., et al., *Chapter 2: Development of the peripheral nerve.* Int Rev Neurobiol, 2009. **87**: p. 9-26.
144. Liu, Q., et al., *The TRPA1 Channel Mediates Mechanical Allodynia and Thermal Hyperalgesia in a Rat Bone Cancer Pain Model.* Front Pain Res (Lausanne), 2021. **2**: p. 638620.
145. Currie, G.L., et al., *Animal models of bone cancer pain: systematic review and meta-analyses.* Pain, 2013. **154**(6): p. 917-26.
146. Slosky, L.M., T.M. Largent-Milnes, and T.W. Vanderah, *Use of Animal Models in Understanding Cancer-induced Bone Pain.* Cancer Growth Metastasis, 2015. **8**(Suppl 1): p. 47-62.
147. Colvin, L. and M. Fallon, *Challenges in cancer pain management--bone pain.* Eur J Cancer, 2008. **44**(8): p. 1083-90.
148. Antoniazzi, C.T.D., et al., *Transient receptor potential ankyrin 1 (TRPA1) plays a critical role in a mouse model of cancer pain.* Int J Cancer, 2019. **144**(2): p. 355-365.
149. Engel, M.A., et al., *TRPA1 and substance P mediate colitis in mice.* Gastroenterology, 2011. **141**(4): p. 1346-58.
150. Jain, P., et al., *Transient receptor potential ankyrin 1 contributes to somatic pain hypersensitivity in experimental colitis.* Sci Rep, 2020. **10**(1): p. 8632.
151. Cattaruzza, F., et al., *Transient receptor potential ankyrin 1 mediates chronic pancreatitis pain in mice.* Am J Physiol Gastrointest Liver Physiol, 2013. **304**(11): p. G1002-12.
152. Moilanen, L.J., et al., *Monosodium iodoacetate-induced inflammation and joint pain are reduced in TRPA1 deficient mice--potential role of TRPA1 in osteoarthritis.* Osteoarthritis Cartilage, 2015. **23**(11): p. 2017-26.
153. Jessen, K.R., *Glial cells.* Int J Biochem Cell Biol, 2004. **36**(10): p. 1861-7.
154. Chen, C.Z., et al., *Schwann cell remyelination of the central nervous system: why does it happen and what are the benefits?* Open Biol, 2021. **11**(1): p. 200352.
155. Sardella-Silva, G., B.S. Mietto, and V.T. Ribeiro-Resende, *Four Seasons for Schwann Cell Biology, Revisiting Key Periods: Development, Homeostasis, Repair, and Aging.* Biomolecules, 2021. **11**(12).
156. Reynolds, M.L. and C.J. Woolf, *Reciprocal Schwann cell-axon interactions.* Curr Opin Neurobiol, 1993. **3**(5): p. 683-93.
157. Griffin, J.W. and W.J. Thompson, *Biology and pathology of nonmyelinating Schwann cells.* Glia, 2008. **56**(14): p. 1518-1531.
158. Ndubaku, U. and M.E. de Bellard, *Glial cells: old cells with new twists.* Acta Histochem, 2008. **110**(3): p. 182-95.
159. Wei, Z., et al., *Emerging Role of Schwann Cells in Neuropathic Pain: Receptors, Glial Mediators and Myelination.* Front Cell Neurosci, 2019. **13**: p. 116.
160. Nave, K.A., M.W. Sereda, and H. Ehrenreich, *Mechanisms of disease: inherited demyelinating neuropathies--from basic to clinical research.* Nat Clin Pract Neurol, 2007. **3**(8): p. 453-64.
161. Arthur-Farraj, P.J., et al., *c-Jun reprograms Schwann cells of injured nerves to generate a repair cell essential for regeneration.* Neuron, 2012. **75**(4): p. 633-47.
162. Ji, R.R., A. Chamessian, and Y.Q. Zhang, *Pain regulation by non-neuronal cells and inflammation.* Science, 2016. **354**(6312): p. 572-577.
163. Lee, H., et al., *Toll-like receptors: sensor molecules for detecting damage to the nervous system.* Curr Protein Pept Sci, 2013. **14**(1): p. 33-42.

164. Campana, W.M., *Schwann cells: activated peripheral glia and their role in neuropathic pain.* Brain Behav Immun, 2007. **21**(5): p. 522-7.
165. Inoue, M., et al., *Initiation of neuropathic pain requires lysophosphatidic acid receptor signaling.* Nat Med, 2004. **10**(7): p. 712-8.
166. Meyer zu Horste, G., et al., *Mouse Schwann cells activate MHC class I and II restricted T-cell responses, but require external peptide processing for MHC class II presentation.* Neurobiol Dis, 2010. **37**(2): p. 483-90.
167. Keswani, S.C., et al., *A novel endogenous erythropoietin mediated pathway prevents axonal degeneration.* Ann Neurol, 2004. **56**(6): p. 815-26.
168. Kobayashi, K., et al., *Distinct expression of TRPM8, TRPA1, and TRPV1 mRNAs in rat primary afferent neurons with adelta/c-fibers and colocalization with trk receptors.* J Comp Neurol, 2005. **493**(4): p. 596-606.
169. Morelli, M.B., et al., *TRP channels: new potential therapeutic approaches in CNS neuropathies.* CNS Neurol Disord Drug Targets, 2013. **12**(2): p. 274-93.
170. Kheradpezhouh, E., et al., *TRPA1 expression and its functional activation in rodent cortex.* Open Biol, 2017. **7**(4).
171. Hamilton, N.B., et al., *Proton-gated Ca(2+)-permeable TRP channels damage myelin in conditions mimicking ischaemia.* Nature, 2016. **529**(7587): p. 523-7.
172. Takizawa, M., et al., *Transient receptor potential ankyrin 1 channels are involved in spontaneous peptide hormone release from astrocytes.* Biochem Biophys Res Commun, 2018. **501**(4): p. 988-995.
173. Cao, H., et al., *Activation of extracellular signal-regulated kinase in the anterior cingulate cortex contributes to the induction and expression of affective pain.* J Neurosci, 2009. **29**(10): p. 3307-21.
174. Woolf, C.J., *Evidence for a central component of post-injury pain hypersensitivity.* Nature, 1983. **306**(5944): p. 686-8.
175. De Logu, F., et al., *Macrophages and Schwann cell TRPA1 mediate chronic allodynia in a mouse model of complex regional pain syndrome type I.* Brain Behav Immun, 2020. **88**: p. 535-546.
176. Basbaum, A.I., et al., *Cellular and molecular mechanisms of pain.* Cell, 2009. **139**(2): p. 267-84.
177. De Logu, F., et al., *Schwann cells expressing nociceptive channel TRPA1 orchestrate ethanol-evoked neuropathic pain in mice.* J Clin Invest, 2019. **129**(12): p. 5424-5441.
178. Rades, D., S.E. Schild, and J.L. Abrahm, *Treatment of painful bone metastases.* Nat Rev Clin Oncol, 2010. **7**(4): p. 220-9.
179. Hiraga, T. and T. Ninomiya, *Establishment and characterization of a C57BL/6 mouse model of bone metastasis of breast cancer.* J Bone Miner Metab, 2019. **37**(2): p. 235-242.
180. Ewens, A., E. Mihich, and M.J. Ehrke, *Distant metastasis from subcutaneously grown E0771 medullary breast adenocarcinoma.* Anticancer Res, 2005. **25**(6b): p. 3905-15.
181. Andriessen, A.S., C.R. Donnelly, and R.R. Ji, *Reciprocal interactions between osteoclasts and nociceptive sensory neurons in bone cancer pain.* Pain Rep, 2021. **6**(1): p. e867.
182. Zajaczkowska, R., et al., *Bone Pain in Cancer Patients: Mechanisms and Current Treatment.* Int J Mol Sci, 2019. **20**(23).
183. Mantyh, P.W., *Bone cancer pain: from mechanism to therapy.* Curr Opin Support Palliat Care, 2014. **8**(2): p. 83-90.

184. Kwan, K.Y., et al., *TRPA1 contributes to cold, mechanical, and chemical nociception but is not essential for hair-cell transduction.* Neuron, 2006. **50**(2): p. 277-89.
185. Liedtke, W. and J.M. Friedman, *Abnormal osmotic regulation in trpv4-/- mice.* Proc Natl Acad Sci U S A, 2003. **100**(23): p. 13698-703.
186. Faul, F., et al., *Statistical power analyses using G*Power 3.1: tests for correlation and regression analyses.* Behav Res Methods, 2009. **41**(4): p. 1149-60.
187. Chaplan, S.R., et al., *Quantitative assessment of tactile allodynia in the rat paw.* J Neurosci Methods, 1994. **53**(1): p. 55-63.
188. De Logu, F., et al., *TRPA1 Mediates Aromatase Inhibitor-Evoked Pain by the Aromatase Substrate Androstenedione.* Cancer Res, 2016. **76**(23): p. 7024-7035.
189. Reagan-Shaw, S., M. Nihal, and N. Ahmad, *Dose translation from animal to human studies revisited.* Faseb j, 2008. **22**(3): p. 659-61.
190. Glasmacher, A., et al., *A systematic review of phase-II trials of thalidomide monotherapy in patients with relapsed or refractory multiple myeloma.* Br J Haematol, 2006. **132**(5): p. 584-93.
191. Everaerts, W., et al., *Inhibition of the cation channel TRPV4 improves bladder function in mice and rats with cyclophosphamide-induced cystitis.* Proc Natl Acad Sci U S A, 2010. **107**(44): p. 19084-9.
192. Goldschmidt, H., et al., *Navigating the treatment landscape in multiple myeloma: which combinations to use and when?* Ann Hematol, 2019. **98**(1): p. 1-18.
193. Luo, J., et al., *Comparative effectiveness and safety of thalidomide and lenalidomide in patients with multiple myeloma in the United States of America: A population-based cohort study.* Eur J Cancer, 2017. **70**: p. 22-33.
194. Dimopoulos, M.A., et al., *Expert panel consensus statement on the optimal use of pomalidomide in relapsed and refractory multiple myeloma.* Leukemia, 2014. **28**(8): p. 1573-85.
195. Kumar, N., et al., *Thalidomide: chemistry, therapeutic potential and oxidative stress induced teratogenicity.* Curr Top Med Chem, 2012. **12**(13): p. 1436-55.
196. Parman, T., M.J. Wiley, and P.G. Wells, *Free radical-mediated oxidative DNA damage in the mechanism of thalidomide teratogenicity.* Nat Med, 1999. **5**(5): p. 582-5.
197. Andersson, D.A., et al., *Transient receptor potential A1 is a sensory receptor for multiple products of oxidative stress.* J Neurosci, 2008. **28**(10): p. 2485-94.
198. Suresh, K., et al., *Hydrogen peroxide-induced calcium influx in lung microvascular endothelial cells involves TRPV4.* Am J Physiol Lung Cell Mol Physiol, 2015. **309**(12): p. L1467-77.
199. Bai, J.Z. and J. Lipski, *Differential expression of TRPM2 and TRPV4 channels and their potential role in oxidative stress-induced cell death in organotypic hippocampal culture.* Neurotoxicology, 2010. **31**(2): p. 204-14.
200. Shim, H.S., et al., *Peripheral and central oxidative stress in chemotherapy-induced neuropathic pain.* Mol Pain, 2019. **15**: p. 1744806919840098.
201. Faul, F., et al., *G*Power 3: a flexible statistical power analysis program for the social, behavioral, and biomedical sciences.* Behav Res Methods, 2007. **39**(2): p. 175-91.
202. Guan, Z., et al., *Injured sensory neuron-derived CSF1 induces microglial proliferation and DAP12-dependent pain.* Nat Neurosci, 2016. **19**(1): p. 94-101.
203. Zurborg, S., et al., *Generation and characterization of an Advillin-Cre driver mouse line.* Mol Pain, 2011. **7**: p. 66.

204. Selvaraj, D., et al., *A Functional Role for VEGFR1 Expressed in Peripheral Sensory Neurons in Cancer Pain.* Cancer Cell, 2015. **27**(6): p. 780-96.
205. Shepherd, A.J., et al., *Angiotensin II Triggers Peripheral Macrophage-to-Sensory Neuron Redox Crosstalk to Elicit Pain.* J Neurosci, 2018. **38**(32): p. 7032-7057.
206. Bailey, K.N., et al., *Intra-articular depletion of macrophages increases acute synovitis and alters macrophage polarity in the injured mouse knee.* Osteoarthritis and Cartilage, 2020.
207. Abbadie, C., et al., *Impaired neuropathic pain responses in mice lacking the chemokine receptor CCR2.* Proc Natl Acad Sci U S A, 2003. **100**(13): p. 7947-52.
208. Van Steenwinckel, J., et al., *Stromal cell-derived CCL2 drives neuropathic pain states through myeloid cell infiltration in injured nerve.* Brain Behav Immun, 2015. **45**: p. 198-210.
209. Kim, C.F. and G. Moalem-Taylor, *Detailed characterization of neuro-immune responses following neuropathic injury in mice.* Brain Res, 2011. **1405**: p. 95-108.
210. Gray, M., et al., *Macrophage depletion alters the blood-nerve barrier without affecting Schwann cell function after neural injury.* J Neurosci Res, 2007. **85**(4): p. 766-77.
211. Trevisan, G., et al., *TRPA1 mediates trigeminal neuropathic pain in mice downstream of monocytes/macrophages and oxidative stress.* Brain, 2016. **139**(Pt 5): p. 1361-77.
212. Okubo, M., et al., *Macrophage-Colony Stimulating Factor Derived from Injured Primary Afferent Induces Proliferation of Spinal Microglia and Neuropathic Pain in Rats.* PLoS One, 2016. **11**(4): p. e0153375.
213. Saleh, R., et al., *CSF-1 in Inflammatory and Arthritic Pain Development.* J Immunol, 2018. **201**(7): p. 2042-2053.
214. Lee, S., et al., *Targeting macrophage and microglia activation with colony stimulating factor 1 receptor inhibitor is an effective strategy to treat injury-triggered neuropathic pain.* Mol Pain, 2018. **14**: p. 1744806918764979.
215. Schweizerhof, M., et al., *Hematopoietic colony-stimulating factors mediate tumor-nerve interactions and bone cancer pain.* Nat Med, 2009. **15**(7): p. 802-7.
216. Oster, W., et al., *Production of macrophage-, granulocyte-, granulocyte-macrophage- and multi-colony-stimulating factor by peripheral blood cells.* Eur J Immunol, 1989. **19**(3): p. 543-7.
217. Goudot, C., et al., *Aryl Hydrocarbon Receptor Controls Monocyte Differentiation into Dendritic Cells versus Macrophages.* Immunity, 2017. **47**(3): p. 582-596 e6.
218. Groh, J., et al., *Cell-Surface and Secreted Isoforms of CSF-1 Exert Opposing Roles in Macrophage-Mediated Neural Damage in Cx32-Deficient Mice.* J Neurosci, 2016. **36**(6): p. 1890-901.
219. Martini, R., et al., *Interactions between Schwann cells and macrophages in injury and inherited demyelinating disease.* Glia, 2008. **56**(14): p. 1566-77.
220. Lin, A.H., et al., *Lung Epithelial TRPA1 Transduces the Extracellular ROS into Transcriptional Regulation of Lung Inflammation Induced by Cigarette Smoke: The Role of Influxed Ca^{2+}.* Mediators Inflamm, 2015. **2015**: p. 148367.
221. Sturrock, A., et al., *Key role of microRNA in the regulation of granulocyte macrophage colony-stimulating factor expression in murine alveolar epithelial cells during oxidative stress.* J Biol Chem, 2014. **289**(7): p. 4095-105.
222. Burnett, S.H., et al., *Conditional macrophage ablation in transgenic mice expressing a Fas-based suicide gene.* J Leukoc Biol, 2004. **75**(4): p. 612-23.

223. McGrath, J.C. and E. Lilley, *Implementing guidelines on reporting research using animals (ARRIVE etc.): new requirements for publication in BJP*. Br J Pharmacol, 2015. **172**(13): p. 3189-93.
224. Islam, S., et al., *Bacterial lipopolysaccharide induces osteoclast formation in RAW 264.7 macrophage cells.* Biochem Biophys Res Commun, 2007. **360**(2): p. 346-51.
225. Amoui, M., et al., *An osteoclastic protein-tyrosine phosphatase may play a role in differentiation and activity of human monocytic U-937 cell-derived, osteoclast-like cells.* Am J Physiol Cell Physiol, 2004. **287**(4): p. C874-84.
226. Nachat-Kappes, R., et al., *Effects of enriched environment on COX-2, leptin and eicosanoids in a mouse model of breast cancer.* PLoS One, 2012. **7**(12): p. e51525.
227. De Logu, F., et al., *Peripheral Nerve Resident Macrophages and Schwann Cells Mediate Cancer-Induced Pain.* Cancer Res, 2021. **81**(12): p. 3387-3401.
228. Zhang, C., H. Li, and R. Han, *An open-source video tracking system for mouse locomotor activity analysis.* BMC Res Notes, 2020. **13**(1): p. 48.
229. Schnütgen, F., et al., *A directional strategy for monitoring Cre-mediated recombination at the cellular level in the mouse.* Nat Biotechnol, 2003. **21**(5): p. 562-5.
230. Homs, J., et al., *Schwann cell targeting via intrasciatic injection of AAV8 as gene therapy strategy for peripheral nerve regeneration.* Gene Ther, 2011. **18**(6): p. 622-30.
231. Skorput, A.G.J., et al., *Targeting the somatosensory system with AAV9 and AAV2retro viral vectors.* PLoS One, 2022. **17**(3): p. e0264938.
232. Strobel, B., et al., *Comparative Analysis of Cesium Chloride- and Iodixanol-Based Purification of Recombinant Adeno-Associated Viral Vectors for Preclinical Applications.* Hum Gene Ther Methods, 2015. **26**(4): p. 147-57.
233. Long, L., et al., *A fluorescent probe for hypochlorite based on the modulation of the unique rotation of the N-N single bond in acetohydrazide.* Chem Commun (Camb), 2015. **51**(52): p. 10435-8.
234. Han, Q., et al., *Turn-On Fluorescence Probe for Nitric Oxide Detection and Bioimaging in Live Cells and Zebrafish.* ACS Sens, 2019. **4**(2): p. 309-316.
235. Pak, V.V., et al., *Ultrasensitive Genetically Encoded Indicator for Hydrogen Peroxide Identifies Roles for the Oxidant in Cell Migration and Mitochondrial Function.* Cell Metab, 2020. **31**(3): p. 642-653.e6.
236. Deuis, J.R., L.S. Dvorakova, and I. Vetter, *Methods Used to Evaluate Pain Behaviors in Rodents.* Front Mol Neurosci, 2017. **10**: p. 284.
237. Huang, W., et al., *A clinically relevant rodent model of the HIV antiretroviral drug stavudine induced painful peripheral neuropathy.* Pain, 2013. **154**(4): p. 560-575.
238. Nicolson, G.L., K.W. Brunson, and I.J. Fidler, *Specificity of arrest, survival, and growth of selected metastatic variant cell lines.* Cancer Res, 1978. **38**(11 Pt 2): p. 4105-11.
239. Zhang, Y., et al., *Peripheral pain is enhanced by insulin-like growth factor 1 through a G protein-mediated stimulation of T-type calcium channels.* Sci Signal, 2014. **7**(346): p. ra94.
240. Sugawara, S., et al., *Increase in IGF-1 Expression in the Injured Infraorbital Nerve and Possible Implications for Orofacial Neuropathic Pain.* Int J Mol Sci, 2019. **20**(24).

241. Forster, R., et al., *Macrophage-derived insulin-like growth factor-1 is a key neurotrophic and nerve-sensitizing factor in pain associated with endometriosis.* FASEB J, 2019. **33**(10): p. 11210-11222.
242. Takayama, B., et al., *Localization and function of insulin-like growth factor 1 in dorsal root ganglia in a rat disc herniation model.* Spine (Phila Pa 1976), 2011. **36**(2): p. E75-9.
243. Kohno, K., et al., *A spinal microglia population involved in remitting and relapsing neuropathic pain.* Science, 2022. **376**(6588): p. 86-90.
244. Li, Y., et al., *Enhanced function of TRPV1 via up-regulation by insulin-like growth factor-1 in a rat model of bone cancer pain.* Eur J Pain, 2014. **18**(6): p. 774-84.
245. Syroid, D.E., et al., *A role for insulin-like growth factor-I in the regulation of Schwann cell survival.* J Neurosci, 1999. **19**(6): p. 2059-68.
246. Le Pape, F., G. Vargas, and P. Clézardin, *The role of osteoclasts in breast cancer bone metastasis.* J Bone Oncol, 2016. **5**(3): p. 93-95.
247. Weilbaecher, K.N., T.A. Guise, and L.K. McCauley, *Cancer to bone: a fatal attraction.* Nat Rev Cancer, 2011. **11**(6): p. 411-25.
248. Kavran, J.M., et al., *How IGF-1 activates its receptor.* Elife, 2014. **3**.
249. Dam, D.H.M., et al., *Flotillin and AP2A1/2 Promote IGF-1 Receptor Association with Clathrin and Internalization in Primary Human Keratinocytes.* J Invest Dermatol, 2020. **140**(9): p. 1743-1752 e4.
250. Yoneyama, Y., et al., *IRS-1 acts as an endocytic regulator of IGF-I receptor to facilitate sustained IGF signaling.* Elife, 2018. **7**.
251. Eberhardt, M., et al., *H2S and NO cooperatively regulate vascular tone by activating a neuroendocrine HNO-TRPA1-CGRP signalling pathway.* Nat Commun, 2014. **5**: p. 4381.
252. Sheskin, J., *THALIDOMIDE IN THE TREATMENT OF LEPRA REACTIONS.* Clin Pharmacol Ther, 1965. **6**: p. 303-6.
253. Grisold, W., G. Cavaletti, and A.J. Windebank, *Peripheral neuropathies from chemotherapeutics and targeted agents: diagnosis, treatment, and prevention.* Neuro Oncol, 2012. **14 Suppl 4**: p. iv45-54.
254. Chaudhry, V., et al., *Thalidomide-induced neuropathy.* Neurology, 2002. **59**(12): p. 1872-5.
255. Ribeiro, R.A., et al., *Analgesic effect of thalidomide on inflammatory pain.* Eur J Pharmacol, 2000. **391**(1-2): p. 97-103.
256. Tian, J., et al., *Thalidomide alleviates bone cancer pain by down-regulating expressions of NF-kappaB and GFAP in spinal astrocytes in a mouse model.* Int J Neurosci, 2019. **129**(9): p. 896-903.
257. Xu, H., et al., *Systemic Injection of Thalidomide Prevent and Attenuate Neuropathic Pain and Alleviate Neuroinflammatory Response in the Spinal Dorsal Horn.* J Pain Res, 2019. **12**: p. 3221-3230.
258. Kirchmair, R., et al., *Therapeutic angiogenesis inhibits or rescues chemotherapy-induced peripheral neuropathy: taxol- and thalidomide-induced injury of vasa nervorum is ameliorated by VEGF.* Mol Ther, 2007. **15**(1): p. 69-75.
259. Han, Y. and M.T. Smith, *Pathobiology of cancer chemotherapy-induced peripheral neuropathy (CIPN).* Front Pharmacol, 2013. **4**: p. 156.
260. Cata, J.P., et al., *Clinical and experimental findings in humans and animals with chemotherapy-induced peripheral neuropathy.* Minerva Anestesiol, 2006. **72**(3): p. 151-69.

261. Materazzi, S., et al., *TRPA1 and TRPV4 mediate paclitaxel-induced peripheral neuropathy in mice via a glutathione-sensitive mechanism.* Pflügers Archiv - European Journal of Physiology, 2012. **463**(4): p. 561-569.
262. Nassini, R., et al., *Oxaliplatin elicits mechanical and cold allodynia in rodents via TRPA1 receptor stimulation.* Pain, 2011. **152**(7): p. 1621-31.
263. De Logu, F., et al., *Schwann cell TRPA1 mediates neuroinflammation that sustains macrophage-dependent neuropathic pain in mice.* Nature Communications, 2017. **8**(1): p. 1887.
264. Mori, Y., et al., *Redox-sensitive transient receptor potential channels in oxygen sensing and adaptation.* Pflugers Arch, 2016. **468**(1): p. 85-97.
265. Lauriault, V.V. and P.J. O'Brien, *Molecular mechanism for prevention of N-acetyl-p-benzoquinoneimine cytotoxicity by the permeable thiol drugs diethyldithiocarbamate and dithiothreitol.* Mol Pharmacol, 1991. **40**(1): p. 125-34.
266. Rajasekhar, P., et al., *P2Y1 Receptor Activation of the TRPV4 Ion Channel Enhances Purinergic Signaling in Satellite Glial Cells.* J Biol Chem, 2015. **290**(48): p. 29051-62.
267. Benfenati, V., et al., *Expression and functional characterization of transient receptor potential vanilloid-related channel 4 (TRPV4) in rat cortical astrocytes.* Neuroscience, 2007. **148**(4): p. 876-92.
268. Cobos, E.J., et al., *Mechanistic Differences in Neuropathic Pain Modalities Revealed by Correlating Behavior with Global Expression Profiling.* Cell Rep, 2018. **22**(5): p. 1301-1312.
269. Sun, J.J., et al., *Infiltration of Blood-Derived Macrophages Contributes to the Development of Diabetic Neuropathy.* J Immunol Res, 2019. **2019**: p. 7597382.
270. Yu, X., et al., *Dorsal root ganglion macrophages contribute to both the initiation and persistence of neuropathic pain.* Nat Commun, 2020. **11**(1): p. 264.
271. Peng, J., et al., *Microglia and monocytes synergistically promote the transition from acute to chronic pain after nerve injury.* Nat Commun, 2016. **7**: p. 12029.
272. Carvalho, T.T., et al., *Granulocyte-colony stimulating factor (G-CSF)-induced mechanical hyperalgesia in mice: Role for peripheral TNFalpha, IL-1beta and IL-10.* Eur J Pharmacol, 2015. **749**: p. 62-72.
273. Zhang, F., et al., *Transcriptional Regulation of Voltage-Gated Sodium Channels Contributes to GM-CSF-Induced Pain.* J Neurosci, 2019. **39**(26): p. 5222-5233.
274. Nicol, L.S.C., et al., *Central inhibition of granulocyte-macrophage colony-stimulating factor is analgesic in experimental neuropathic pain.* Pain, 2018. **159**(3): p. 550-559.
275. Van Overmeire, E., et al., *M-CSF and GM-CSF Receptor Signaling Differentially Regulate Monocyte Maturation and Macrophage Polarization in the Tumor Microenvironment.* Cancer Res, 2016. **76**(1): p. 35-42.
276. MacDonald, K.P., et al., *An antibody against the colony-stimulating factor 1 receptor depletes the resident subset of monocytes and tissue- and tumor-associated macrophages but does not inhibit inflammation.* Blood, 2010. **116**(19): p. 3955-63.
277. Park, J., et al., *M-CSF from Cancer Cells Induces Fatty Acid Synthase and PPARbeta/delta Activation in Tumor Myeloid Cells, Leading to Tumor Progression.* Cell Rep, 2015. **10**(9): p. 1614-1625.
278. Yang, G., et al., *Implication of microglia activation and CSF-1/CSF-1Rpathway in lumbar disc degeneration-related back pain.* Mol Pain, 2018. **14**: p. 1744806918811238.

279. Trias, E., et al., *Schwann cells orchestrate peripheral nerve inflammation through the expression of CSF1, IL-34, and SCF in amyotrophic lateral sclerosis.* Glia, 2020. **68**(6): p. 1165-1181.
280. Moreira, S., et al., *Prioritization of competing damage and developmental signals by migrating macrophages in the Drosophila embryo.* Curr Biol, 2010. **20**(5): p. 464-70.
281. Zhu, Y.F., et al., *Cancer pain and neuropathic pain are associated with A beta sensory neuronal plasticity in dorsal root ganglia and abnormal sprouting in lumbar spinal cord.* Mol Pain, 2018. **14**: p. 1744806918810099.
282. Liu, S., et al., *IL-18 Contributes to Bone Cancer Pain by Regulating Glia Cells and Neuron Interaction.* J Pain, 2018. **19**(2): p. 186-195.
283. Lindsay, T.H., et al., *Pancreatic cancer pain and its correlation with changes in tumor vasculature, macrophage infiltration, neuronal innervation, body weight and disease progression.* Pain, 2005. **119**(1-3): p. 233-46.
284. Devor, M., *Unexplained peculiarities of the dorsal root ganglion.* Pain, 1999. **Suppl 6**: p. S27-35.
285. Marani, E. and E.A.J.F. Lakke, *Peripheral Nervous System Topics*, in *The Human Nervous System*. 2012. p. 82-140.
286. Chen, Y.C., D.M. Sosnoski, and A.M. Mastro, *Breast cancer metastasis to the bone: mechanisms of bone loss.* Breast Cancer Res, 2010. **12**(6): p. 215.
287. Breuksch, I., M. Weinert, and W. Brenner, *The role of extracellular calcium in bone metastasis.* J Bone Oncol, 2016. **5**(3): p. 143-145.
288. Hiraga, T., et al., *Bone-derived IGF mediates crosstalk between bone and breast cancer cells in bony metastases.* Cancer Res, 2012. **72**(16): p. 4238-49.
289. Chen, X., et al., *Abnormal Insulin-like Growth Factor 1 Signaling Regulates Neuropathic Pain by Mediating the Mechanistic Target of Rapamycin-Related Autophagy and Neuroinflammation in Mice.* ACS Chem Neurosci, 2021. **12**(15): p. 2917-2928.
290. Manzano-Garcia, A. and M. Gamal-Eltrabily, *A new role of growth hormone and insulin growth factor receptor type 1 in neonatal inflammatory nociception.* Pain Rep, 2017. **2**(4): p. e608.
291. Tang, Z., et al., *Peripheral pain is enhanced by insulin-like growth factor 1 and its receptors in a mouse model of type 2 diabetes mellitus.* J Diabetes, 2019. **11**(4): p. 309-315.
292. Bitar, M.S., et al., *Antinociceptive action of intrathecally administered IGF-I and the expression of its receptor in rat spinal cord.* Brain Res, 1996. **737**(1-2): p. 292-4.
293. Bonnefont, J., et al., *Acetaminophen recruits spinal p42/p44 MAPKs and GH/IGF-1 receptors to produce analgesia via the serotonergic system.* Mol Pharmacol, 2007. **71**(2): p. 407-15.
294. Zhou, R., et al., *IGF-binding protein-4: biochemical characteristics and functional consequences.* J Endocrinol, 2003. **178**(2): p. 177-93.
295. Schiltz, P.M., S. Mohan, and D.J. Baylink, *Insulin-like growth factor binding protein-4 inhibits both basal and IGF-mediated chick pelvic cartilage growth in vitro.* J Bone Miner Res, 1993. **8**(4): p. 391-6.
296. Mohan, S., et al., *Studies on the mechanisms by which insulin-like growth factor (IGF) binding protein-4 (IGFBP-4) and IGFBP-5 modulate IGF actions in bone cells.* J Biol Chem, 1995. **270**(35): p. 20424-31.
297. Benyoucef, S., et al., *Characterization of insulin/IGF hybrid receptors: contributions of the insulin receptor L2 and Fn1 domains and the alternatively*

spliced exon 11 sequence to ligand binding and receptor activation. Biochem J, 2007. **403**(3): p. 603-13.
298. Yang, Y., et al., *Role of nitric oxide synthase in the development of bone cancer pain and effect of L-NMMA.* Mol Med Rep, 2016. **13**(2): p. 1220-6.